KERNFORSCHUNGSANLAGE JÜLICH GmbH
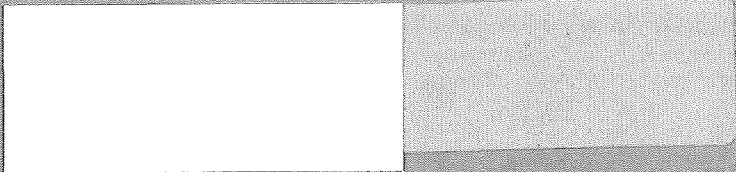
Implementing Agreement
for Co-Operation in the Development
of Large Scale
Wind Energy Conversion Systems

**First Meeting of Experts –
Seminar on Structural Dynamics
Munich, October 12, 1978**

Organised by
Project Management for Energy Research (PLE)
of the Nuclear Research Establishment Jülich (KFA)
on behalf of the
Federal Minister of Research and Technology

Implementing Agreement
for Co-Operation in the Development
of Large Scale
Wind Energy Conversion Systems

First Meeting of Experts -
Seminar on Structural Dynamics
Munich, October 12, 1978

Organised by
Project Management for Energy Research (PLE)
of the Nuclear Research Establishment Jülich (KFA)
on behalf of the
Federal Minister of Research and Technology

Scientific Coordination:
R. Cuntze (MAN München) and R. Windheim (PLE KFA)

C O N T E N T S

Investigations af structural dynamics on

the Gedser WTG and on new Danish wind turbines

by

P. Lundsager and C.J. Christensen

Risø National Laboratory, DK 4000 Roskilde

Denmark

Presented at the 1.st meeting of experts - structural dynamics -
IEA-Implementary Agreement for co-operation in the development
of Large-Scale Wind Energy Conversion Systems.

Abstract

A survey is given of activities on Risø National Laboratory rela-
ted to structural dynamics of large WTG's. Since only few of the
activities have yet been completed, the presentation is a review
of status, preliminary conclusions and experience. The topics dealt
with in the presentation are:

- Analysis of prototype WTG rotors
- Analysis of the Gedser WTG rotor
- Measurements on the Gedser WTG

Investigations being made of the power train oscillations in the
Gedser WTG are dealt with in some detail.

Introduction

The present paper is a written, extended version of the presentation at the meeting. The paper includes some figures that were not shown at the meeting due to time limitations.

Risø National Laboratory participates in the activities shown in fig. 1. Items 1 and 2 are parts of the wind power program of the Ministry of Commerce and the Electric Utilities in Denmark. Item 1 is handled in cooperation with two other Danish institutions, Danish Ship Research Laboratory and Structural Research Laboratory of the Technical University of Denmark.

The topics dealt with in the presentation are listed in fig. 2. Key-words are added to some of the topics.

The present period of Danish wind power related activities have started recently, about 2 years ago. Therefore only few of the activities have been completed and thus the presentation is a review of status and preliminary conclusions and experience. The Gedser WTG, having operated during the years 1958-1968 represents the connection to the preceeding period of Danish wind power activities.

1. Prototype windmill computations

Two prototype windmills are being designed and built as part of the Danish wind power program. Both mills have 3 bladed upwind located rotors with a diameter of 40 m, and both have an induction generator of 630 kW installed. The difference between the rotors is shown in fig. 3. Rotor A is a stayed rotor with stall control while rotor B is a cantilevered rotor with full blade pitch control.

Risø is consultant on the rotor design, and as part of the design calculations the eigenfrequencies of single blades and of the total rotor A have been calculated in addition to static analysis.

The blades have an inner part with a tu bular steel beam with GRP shells, while the outer part is made of a spun GRP main spar with GRP shells as shown in fig. 4. The blades and the rotor have been modelled by beam elements and the response calculations are made

using the general purpose finite element program SAP IV [1].

The beam cross section properties of the actual blade cross section fig. 4 are computed by a special purpose program SECTIO [2], developed at Risø. In this program the cross sections are idealized as shown in fig. 5, where each element may have independently specified material properties. The only anisotropy considered is that the shear and youngs moduli are independently prescribed.

In addition to the necessary average cross sectional properties SECTIO computes the locations of the shear centre (SC), elastic center (EC) and mass center (TP) indicated on fig. 5. The program then establishes a SAP IV beam model and punches the input cards for SAP IV.

When representing a structure of this kind by a conventional beam model some decisions must be taken since not all features can be represented at the same time. Fig 6 indicates the principle of the beam model applied here. The radial beams, having properties associated with the elastic centers, connect the shear centers. The mass centers are connected to the shear centers by rigid beams, and the principal directions for a specific shear beam are averages of those of the adjacent cross sections. Thus the pretwist and the dynamic coupling between bending and torsion are taken into account, while several other features are taken into account only partial (e.g. influence on bending of centrifugal forces) or not at all (e.g. static coupling bending/torsion).

This results in a beam model as shown scematically in fig. 6. The chosen principle may of course be subject to discussion, and the calculated results will be checked with measurements on both the Gedser WTG and the prototype WTGs.

In order to avoid the inherent difficulties in representing correctly the different section centres using conventional FEM beam elements as described above, a computer program is presently being developed at Risø, which is based on a consistent generalization of the work of Houbolt and Brooks [10] to include the effects of cross sectional warping.

The program is developed for static analysis of tapered, pretwisted thin walled beams but will later be extended to cover dynamic analysis also.

Applied to WTG's this program will supplement and in certain contexts replace the SECTIO/FEM approach.

The results shown in figs. 8-11 are based on calculations on rotor A, but most of the conclusions in fig. 12 are valid for model B as well.

Fig. 8 shows some results from calculations on a single blade. Due to uncertainties in material properties in general and especially the youngs modulus Ew for the web the results obtained cover rather wide ranges. The ranges for the shear center position x_s, the mass center position x_M and the 1.st flap-and edgewise eigenfrequencies are shown in the figure. All results come from calculations based on seriously proposed material data, made on a 206 DOF beam model. The rotational frequencies are shown for comparison. By comparison with a simpler model with no mass center offset the influence of the offset on the lowest eigenfrequencies is found to be low, of the order 1%. The coupling between bending and torsion seems to be weak for the lowest eigenfrequencies, but a simple quantitative measure for the importance of the coupling has not been found.

However, the material investigation program (fig. 1) resulted in more well defined material properties, and fig. 9 shows representative eigenfrequencies and eigenmodes computed for material properties that are believed to be realistic.

Fig. 10 shows some results for the total model A rotor, using material data that differ slightly from those of fig. 9. It is seen that the coupling between the blades due to the stays is very small, changing the eigenfrequency by 1% only. The stiffening due to centrifugal forces cannot be accounted for by the program SAP IV, but using the type of expression shown in fig. 10 [3] the rise in fundamental eigenfrequency ω_0 due to the rotational frequency Ω is estimated to be of order 6%.

Fig. 11 shows a Campbell diagram based on the values of fig. 10. From such diagrams the needs for improvements in design are indentified, and this type of computations are currently repeated with updated models as the fabrication of the blades proceeds. These design computations will be repeated as proof computations when the blades are fabricated and their final form is known in detail. The results then will be compared with laboratory tests on full blades to be performed by Structural Research Laboratory, and finally the results from the updated beam model will be compared with field measurements on the mills.

Analysis of dynamic stability of rotor A has been made by SAAB-SCANIA, using cross section data from the program SECTIO. The analysis showed the rotor to be dynamically stable under all possible operating conditions. The same type of analysis of rotor B is being performed by Paragon Pacific Inc. as a part of an analysis of the entire system.

Although the work is not completed yet, some conclusions may be drawn on basis of the work done so far. The conclusions are summarized in fig. 12. The most important conclusion is that reliable data for GRP materials in this context seem difficult to obtain. This is partly because of difficulties in predicting the overall behaviour of the material, but also the prediction of the actual material configuration in the blades seems difficult. This considerably influences the accuracy of the predicted eigenfrequencies.

2. Gedser WTG rotor computations

In order to check the analysis procedure dealt with in chapter 1 as soon as possible - and before experimental data were available for the prototype WTG's - analysis has been made of the rotor and blades of the Gedser WTG. These results have been compared with experimental data from laboratory and field tests on the rotor of the Gedser WTG (see chapter 3).

The main characteristics of the Gedser WTG are listed in fig. 13, and the blade design is shown in fig. 14. Fig. 15 shows a typical blade cross section together with the beam model used for a single blade. The beam model is established as described in chapter 1, with the exception that the mass center offset is not modelled as a consequence

of its small influence on the eigenfrequencies, cf. fig. 12.

Results for a single blade with zero stay stiffnesses are shown in
fig. 16 and compared with values measured during laboratory tests [4].
The blade stifnesses have been checked with the measured ones, and the
masses have been adjusted in accordance with the measured mass, cf.
[5]. The eigenfrequencies agree well.

The single blade model has been combined into a total rotor model.
The point where the stays join together, cf. fig. 17, is not clamped
and thus the blades are coupled. Various boundary conditions have been
imposed on the blade roots, which have been clamped in radius 1 m or
joined together at the centre. In some cases a spring stiffness has
been added at radius 1 m. This is done in order to estimate the
influence of the hub stiffnes.

Computed eigenfrequencies are shown in fig. 18. In addition to the
boundary conditions mentioned above also the pretwist and the coupling
of the blade tips to each other by means of wires have been varied.
Model 6 is the model believed to represent the actual rotor best.
In addition results computed for a single blade are shown together
with preliminary results obtained by WEPO [6] for a total rotor model.

The fundamental eigenfrequencies computed vary considerably with the
parameters. The hub stiffness has a large influence on the frequencies,
and the coupling between the blades is strong as can be seen from
the values for the 1st assymetric flatwise mode. The results do not
agree too well with those of WEPO.

Since the blade model itself agrees well with the laboratory measurements,
the deviations may arise from inadequate modelling of the boundary
conditions and perhaps the modelling of the stays.

Also shown in fig. 18 are frequencies extracted from frequency spectra,
cf. chapter 4. They fall within the ranges of the computed values, but
being preliminary values they do not clarify the problem further.

The conclusions drawn from this investigation are summarized in fig.
19. The beam model for a single blade without stays, established by
the program SECTIO, agreed well with the laboratory tests during which
the blade was rigidly clamped at the roof. This gives some confidence

in the results for the prototype blades, cf. chapter 1, that have
well defined boundary conditions. For the Gedser WTG rotor, however,
the boundary conditions are not well defined - mainly due to the
hub design - and this is reflected in eigenfrequencies computed.

3. Measurements on the Gedser WTG

Together with two other Danish institutes, Danish Ship Research Labora-
tory and Structural Research Laboratory of the Technical University
of Denmark, Risø performs a series of measurements on the 20 year old
Gedser WTG.

The measurement program is carried out during 1977-1978 under contract
with the Research Association of the Danish Electricity Supply Under-
takings (DEFU) in cooperation with US Energy Research and Development
administration (US ERDA). The work done so far has been reported in
[7] and presented at the 2nd BHRA Wind Energy Conference [8] .

Fig. 20 contains keyword information on the measurement programm and
its purpose. The Gedser WTG is one of the very few large WTG's from
the 50's that have avoided major mechanical troubles, and it was
in automatic operation during the years 1958 through 1967. The
main characteristics of the WTG are listed in fig. 13 and they deviate
from most modern designs in 3 points: The rotor is upwind located,
stall regulated and heavily stiffened by stays. Furthermore the genera-
tor installed is an induction generator. The design was to some extent
documented in [9] , but the renewed interest in large WTG's have made
a more extensive documentation desirable, especially concerning the
dynamic behaviour of the WTG. This includes detailed measurements of
the structural response of the rotor assembly. The power performance
is investigated, and special attention is payed to power fluctuations as
an extension of investigations reported in [9] . The ongoing study of
power train oscillations is further described in chapter 4.

At present the contract does not include data evaluation beyond consist-
ency checks etc., but the whole instrumentation setup aims at the
collection of data that may be used for the evaluation of models for
the analysis of large WTG's. Evidently not all features of modern WTG's
can be verified by these data, which pertain to an alternative design
that due to its good record may have some influence on future designs.

Still referring to fig. 20 the measurement program is divided in a
long term part, during which continuous meteorological background
measurements are made, and a short term part. These latter are
made in runs with a duration of 40 minutes, during which the data
are stored on tape for later processing.

In order to account for drift and offset of the strain gauge instru-
mentation, each short term run is preceded by a zero run during
which the signals are recorded while the WTG is in some well defined,
stationary condition. This zero run is repeated after the actual
run, and the values recorded are corrected by the zero values. This
leads to some problems which will be discussed later.

Fig. 21 shows the data flow during short term runs, and the numbers
of channels in each group are indicated. The digital telemetry unit
triggers the recording, which is made on two tape recorders. During
the commissioning of the instrumentation the telemetry systems posed
by far the largest problems, and until now only the digital teleme-
try system has been operating.

Fig. 22 scematically shows blade 3, and the channels mounted for
recording are indicated. The symbols used for denoting the measured
moments (M) and forces (N) in the tables shown later are introduced.

Fig. 23 shows full resolution plots of some of the rotor channels.
On the right hand side are indicated instrument indentification,
scale, i.e. range from top to bottom of each single strip in physical
units, and either the zero level or the level at the bottom of the
strip. The two arrows indicate common time on this figure and fig.
24. The limiting frequency due to averaging is 12.5 Hz, and the
figure indicate the type and quality of the rotor channel records.
The gravity loads are seen to be predominant in most edgewise
bending moments and forces, while also higher frequencies contibute
significantly to flatwise bending moments and forces. The resolution
of the records allow for frequency analysis in addition to the more
common time history approach as will be dealt with in chapter 4.

Fig. 24 shows the channels of fig. 23 averaged to a limiting frequency of 2.5 Hz. The figure shows a full short run at an average wind speed of approx. 12 m/s including start and stop of the mill. While the records of fig. 23 are scaled to give maximum information on each channel, the records of fig. 24 are shown with common scales in order to indicate the orders of magnitude of associated channels. The figure gives a visual impression of the zero offset, corresponding to the average loads, and the amplitudes.

For the particular run shown in figs. 23 and 24, some representative forces and stresses in the rotor assembly are given in figs. 25 and 26. The stays (channels 14-21) do carry considerable loads and thus play an important part in the distribution of forces in the rotor assembly. Except for the blade root driving moment M21 the stresses in the blade channels 1-13 are very low compared to the design stress 59 MN/m^2, and this of course is one of the reasons why this particular WTG has performed well during 10 years of operation.

For the same run some additional representative values are given in fig. 27. The yaw rate and accellerations of the nacelle have moderate levels, reflecting the smooth run of this WTG. During normal operation the yaw movements are within the slack of the yaw drive and therefore do not cause significant accellerations. The values of the channels 37 and 44 are 10% too high because of problems in the recording of pulse type signals.

Finally fig. 28 shows power and efficiency curves recorded for wind speeds below 14 m/s. The curves are based on 10 min. averages, and although they are not directly related to structural dynamics they may be of some interest since they describe the performance of an alternative design. At these windspeeds the stall regulation do not show very much on the power curve. However, the efficiency curve shows a reasonably high peak value in spite of the large number of stays that play a significant role in the dynamic behaviour of the WTG.

The measurement program is not concluded at present. The interim report [7] is based on a measurement campaign carried through in the spring 1978, but additional measurements will be made during another campaign in late 1978. As the data evaluation in excess of what is listed in fig. 20 is at present not included in the con-

tract, the preliminary conclusions indicated as keywords in fig. 28 are based mainly on a number of spot checks reported in [7]. A more detailed summary of preliminary conclusions is given in [8].

The records are almost free of noise and seem generally to be sufficiently detailed for a meaningful frequency analysis.

The interpretation of the results are in many ways straightforward. However, problems were encountered during the interpretation of the blade channel signals, i.e. the main spar moments. There seems to be two reasons for this:

- The influence of unknown external forces on the blades during zero run is difficult to account for, partly because the blades are statically indeterminate due to the stays. This influences the zero reference for the measurements.

- The determination of external forces actually experienced by the blades during operation is rendered difficult by the loads being very sensitive to correct modelling of the blade.

This seems to imply that the determination of absolute values on basis of the measurements demands a rather high level of modelling.

The behaviour of the mill is characterized by the absence of extremes. The force and stress levels/amplitudes are generally low, cf. figs. 25 and 26, and the run is smooth. The primary loads edgewise and flatwise appear to be gravity and wind loads, respectively, and gyral effects as well as tower shadowing effects have at present not been traced in the records. During assembly the rotor was given geometric symmetry by prestressing the stay assembly with an unsymmetric internal force system. This may contribute significantly to the smooth run that is characterized by stiff rotor behaviour. These features have so far been recorded for wind speeds up to approx. 15 m/s only, but the mill has been operated at considerably higher windspeeds during the test period, and the impression was that no drastic change in behaviour takes place during such operation in fully stalled condition. The autumn campaign aims at the recording during high windspeeds.

4. Power fluctuations

It is well known that the power quality of wind mills, especially when using induction generators, is mated by sizable fluctuations. We are looking into this problem and will discuss a few aspects of it, although we have so far not identified the sources of the fluctuations.

Fig. 29 shows the kind of fluctuations that is seen. We observe fluctuations up to 40-50 kW peak to peak around 150 kW. In order to study these fluctuations we calculate the fourier transformed variance spectra. As examples of these spectra fig. 30 shows the variance (power) spectrum of the electrical power output whereas fig. 31 shows the power spectrum of the torque in the generator shaft. A general feature of these spectra is a host of sharp, dominant peaks (contain more than 90% of the variance). The important question is, what is the source of the peaks. To begin with we set up the differential equation for the power-train, rotor, shaft and generator.

Fig. 32 defines the various elements of the system.

The governing equations are

rotor acceleration: $\qquad M_v = I\ddot{\phi}_r + M_r$ $\qquad\qquad$ (1)

shaft torsion: $\qquad\qquad M_r = k(\phi_r - \phi_g)$ $\qquad\qquad$ (2)

generator torque: $\qquad M_r = A_c \cdot S_g$ $\qquad\qquad$ (3)

where k is shaft stiffness, S_r and S_g are the slips of the rotor and generator, respectively, i.e.

$$S_r = \frac{\dot{\phi}_r - \omega_r^o}{\omega_r^o} \quad \text{and} \quad S_g = \frac{\dot{\phi}_g - \omega_g^o}{\omega_g^o} \qquad\qquad (4)$$

with $\omega_r^o = \omega_g^o = \omega^o$ as the zero slip frequency of the system.

A_c is a complex constant, which as an oversimplified model of the generator describes a linear relation between torque and slip, yet possibly with a phase shift.

Eq. 2 yields

$$\frac{\dot{M}_r}{\omega_o} = k(S_r - S_g) \quad \text{and} \quad S_r = \frac{1}{k}\frac{\dot{M}_r}{\omega_o} + S_g \qquad\qquad (5)$$

and using this S_r in 1 yields

$$\ddot{S}_g + \frac{k\omega_o}{A_c} \dot{S}_g + \frac{k}{I} S_g - M_v \frac{k}{IA_c} = o$$

In order to find the transfer function for pure oscillations of cyclic frequency ω from the forcing function M_v to the generator slip S_g let

$$M_v = e^{i\omega t} \quad \text{and assume} \quad S_g = A\, e^{i\omega t}$$

then

$$(-A\omega^2 + \frac{k\omega_o}{A_c} A\omega i + \frac{k}{I} A - \frac{k}{IA_c}) \times e^{i\omega t} = 0$$

or

$$H(\omega) = A = \frac{1/A_c}{(1-\frac{\omega^2}{\omega_r^2}) + i \frac{I\omega_o}{A_c}\omega} \qquad (\omega_r = \frac{k}{I})$$

The very simplest expression for M_r (does not take into account transient phenomena of the generator) is the steady S_g expression (constant power E):

$$M_r = \frac{E}{\omega_o} = \frac{C}{\omega_o} S_g = \frac{E_S}{S_g^S \omega_o} \cdot S_g$$

where E_S is nominal effect at nominal slip S_g^S (from generator specifications). Inserting this, we find the transfer function

$$H(\omega) = \frac{S_g^S \omega_o / E_S}{(1 - \frac{\omega^2}{\omega_r^2}) + \frac{\sqrt{KI}}{E_S} S_g^S \omega_o^2 \frac{\omega}{\omega_r} i}$$

This resonance line has its max-value at a frequency ω_r (here $\sim$ o.5-1 Hz) and a peak width (at $1/\sqrt{2}$ × max heigth) of $\sim \frac{2\Delta\omega}{\omega_r} \cong 0.7$, for our system, that is a broad peak.

In this model the energy that the generator delivers to the network provides the damping.

Therefore, the sharp peaks in the spectrum fig. 30 (widths $\sim$ 1-2%) can not originate in this overall drive train model. A more complicated expression for A_c taking account of transient phenomena has been given by H.W. Lorenzen (Brown-Boveri Mitt. p. 650, vol. 55, 1968):

$$M_r = S_g (m_s + j(- m_c + \omega_o I_g \omega)) (= A_c S_g)$$

which gives for $H(\omega)$

$$H(\omega) = \frac{1/m_s}{(1 - \frac{\omega^2}{\omega_r^2}) + i \left[\frac{\sqrt{kI}}{m_s} \omega_o \frac{\omega}{\omega_r} + (- \frac{m_c}{m_s} + \frac{\omega_o I_g \omega}{m_s})(1 - \frac{\omega^2}{\omega_r^2}) \right]}$$

which does keep the same mechanical resonance frequency but will change the damping. But evaluating the constants does not show any appreciable sharpening of the peak.

Now it should be kept in mind that sharp peaks can develop other places. Assume that the forcing function M_v into our model equation has a spectrum $S_{Mv}(\omega)$. Then the spectrum of S_g will look like

$$S_{sg}(\omega) = H(\omega) S_{Mv}(\omega)$$

(although this assumes linear behaviour!). This does allow for putting sharp resonances into the system, in such a way, that sharp peaks (from S_{Mv}) could ride on top of a broad resonance from the model equation. This would be a possible solution. Also the chain drive can be shown to be able to produce sharp peaks in the same way.

Finally as indicated in fig. 30 (el-power spectra) many higher harmonics of the prominent peaks are present here, but not in the shaft moment, which suggests nonlinear behaviour of the induction generator.

Figs. 33-34 illustrates a different use of fourier analysis for describing the dynamic behaviour of the blades. Fig. 33 is the edgewise driving moment in the wing base. Fig. 34 is the force in one of the wires connecting the tips of two neighbouring blades. The 0.51 Hz rotor revolution frequency dominates these two spectra but are strongly suppressed in the shaft moment (fig. 31). This suggests the rotating gravity influence on the blade to cause strong

internal forces in the rotor, but to be balanced out fairly well on the hub and shaft because of the rotor symmetries. The 0.78 Hz resonance, on the other hand, must be a common mode movement of the three blades, as it does not balance out onto the shaft.

Finally a remark about the simultaneous measurements of wind speed and electric power, which is a fundamental problem because of the turbulent character of the wind. The lack of coherence between wind fluctuations as seen in different points is often expressed in an approximate way as

$$\mathrm{coh}(u_1, u_2) = \exp(-\gamma \frac{\Delta u}{\bar{u}}),$$

where Δ is the separation between the points (here the distance 30 m between anemometer and windmill), u is the frequency of a disturbance in the wind and $\bar{u}$ the the mean windspeed. γ is an experimental constant ranging from 3-20 depending on the relative directions of $\vec{u}$ and $\overrightarrow{P_1 P_2}$ (anemometer to mill). Even with $\gamma = 3$ (wind directly going from P_1 to P_2), n must be smaller than $\frac{\bar{u}}{\gamma \Delta} \sim \frac{1}{10}$ Hz at $\bar{u} = 10$ m/s. This does make it difficult to measure simultaneous values the two places this is illustrated in fig. 29 , where wind speed and electric power are plotted, on top with high time resolution, at bottom with a long averaging time (2.5 secs). It is seen that the longer averaging does make the two measured parameters look more alike, but still not completely. Another way of illustrating this is via the coherence spectra in fig. 35 (shaft torque el-power) and fig. 36 (wind velocity-el-power). It is seen that the coherence in the wind-power (one dies out already at $\sim 1/100$ Hz) in contrast to the torque-power coherence that extends to ~ 100 times higher frequency. This warrants more discussions of the power curve measurements.

References

[1]   SAP IV: A structural Analysis Program for Static and Dynamic Response
      of Linear Systems. ASEA-ATOM Computer Program Ro 1058, 1976.

[2]   P. Lundsager: SECTIO: A Program for Determination of Cross Sectional
      Properties of Thin Walled Beams. (To appear)

[3]   S. Putter, H. Manor: Natural Frequencies of Radial Rotating Beams.
      Journal of Sound and Vibration (1978) 56(2) 175-185.

[4]   V. Askegaard, C. Dyrbye, S. Gravesen: Laboratory Tests on Gedser Wind
      Turbine's Blades.
      The Wind Power Program of the Ministry of Commerce and the Electric
      Utilities in Denmark, November 1977.

[5]   J. Bjørnbale-Hansen, P. Mossing: Weighing and Determination of Centre
      of Gravity of Gedser Wind Turbin's Blades.
      Structural Research Laboratory, Technical University of Denmark,
      Report S28/77 1977.

[6]   T. Sullivan, D. Miller: Determination of Gedser Mill Free Vibration
      Frequencies and Mode Shapes.
      WEPO Preliminary Internal Report PIR No. 35, Dec. 77.

[7]   P. Lundsager, C. J. Christensen, S. Frandsen (Ed.):Interim Report on the
      Measurements on the Gedser Windmill.
      Report GTG 771.105- 1. September 1978.

[8]   P. Lundsager, V. Askegaard, E. Bjerregaard: Measurements of Performance
      and Structural Response of the Danish 200 kW Gedser Windmill.
      Paper D2 presented at the 2nd International Symposium on Wind Energy
      Systems, Amsterdam, Netherlands, October 1978. Also available as Report
      GTG 771.105-2, September 1978.

[9]   Report from the Wind Power Committee (Vindkraftudvalgets betænkning)
      (In Danish)
      Union of Danish Electric Utilities 1962.

[10] J. C. Houbolt, G. W. Brooks: Differential Equations of Motion for
      Combined Flapwise Bending, Chordwise bending and Torsion of Twisted
      Nonuniform Rotor Blades.
      NASA Report 1346, Langley, 1958.

ROTOR STRUCTURAL DYNAMICS

MEASUREMENTS GEDSER WINDMILL
      DOCUMENTATION OF DESIGN
      DATA FOR MODEL VERIFICATION
      ANALYSIS
      STATUS: INTERMEDIATE REPORT ISSUED

PROTOTYPE WINDMILL COMPUTATIONS
      DESIGN COMPUTATIONS
      PROOF COMPUTATIONS
      STATUS: INTERMEDIATE REPORT UNDER PREP.

DEVELOPMENT WORK
      MATERIAL INVESTIGATIONS (GRP)
      STATUS: LAB TESTS BEING MADE
      BEAM MODEL DEVELOPMENT
      STATUS: PROGRAM DEVELOPED AND IN USE
              REFINED PGM UNDER DEVELOPMENT

Fig. 1.

TOPICS

PROTOTYPE WINDMILL COMPUTATIONS
    DESIGN (TYPE A AND B)
    COMPUTATION OF BEAM PROPERTIES OF BLADES
    BEAM MODELS (SINGLE BLADE/ROTOR)
    RESULTS   (COUPLINGS)
    CONCLUSIONS

GEDSER ROTOR COMPUTATIONS
    DESIGN
    SINGLE BLADE (LAB TESTS)
    TOTAL ROTOR (COUPLINGS, BOUNDARY COND.)
    COMPARISON WITH MEASURED SPECTRA
    CONCLUSIONS

MEASUREMENTS ON THE GEDSER WINDMILL
    PURPOSE   (OPERATION, DESIGN)
    TECHNIQUE   (LONG/SHORT TERM)
    RESULTS   (RECORDS)
    EXPERIENCE   (MILL CHARACTERISTICS)
    VARIOUS SPECTRA
    POWER FLUCTUATIONS (GENERATOR)
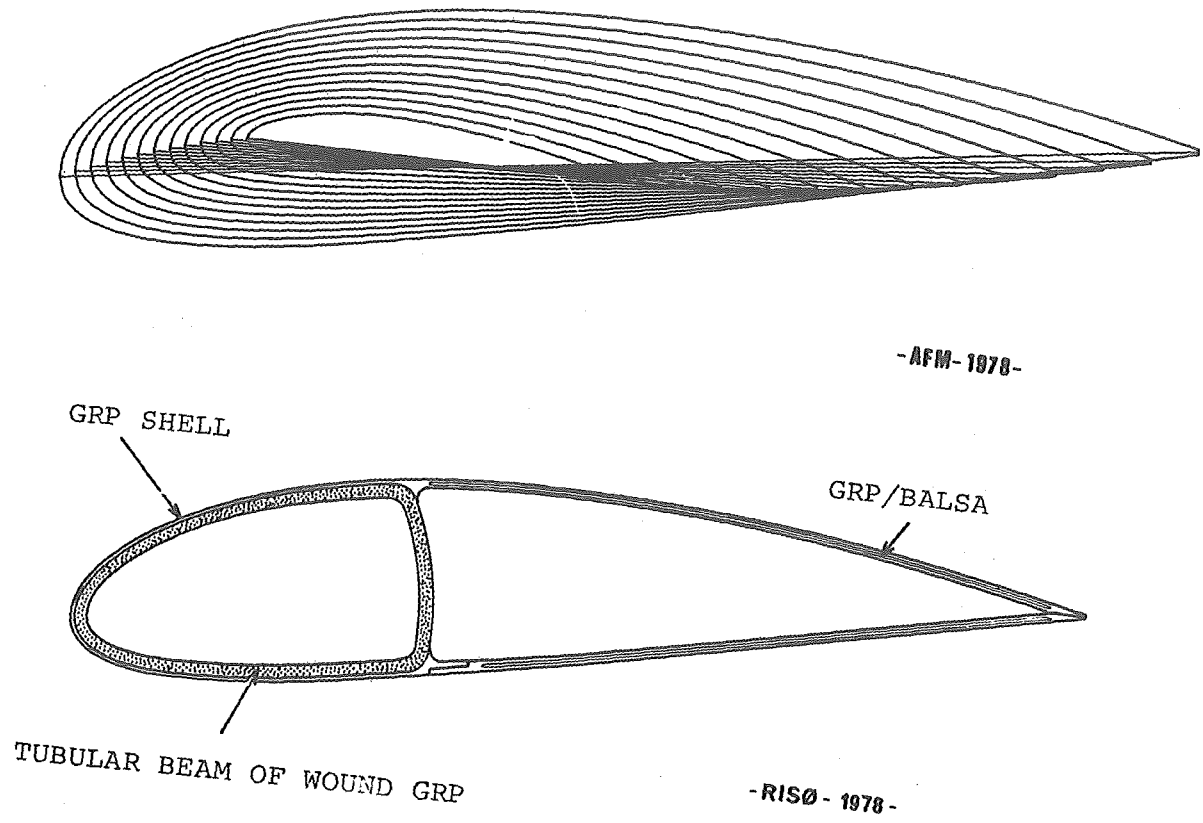   CONCLUSIONS
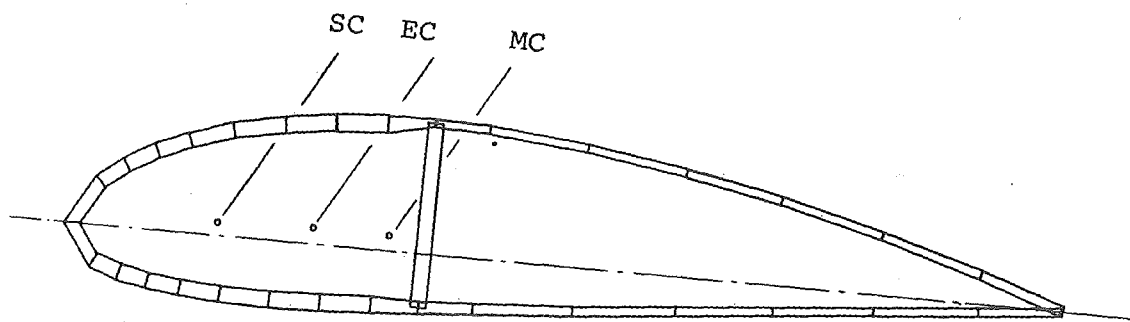

Fig. 2

Fig. 3.

-AFM-1978-

GRP SHELL

GRP/BALSA

TUBULAR BEAM OF WOUND GRP

-RISØ-1978-

Fig. 4.

SC   EC   MC
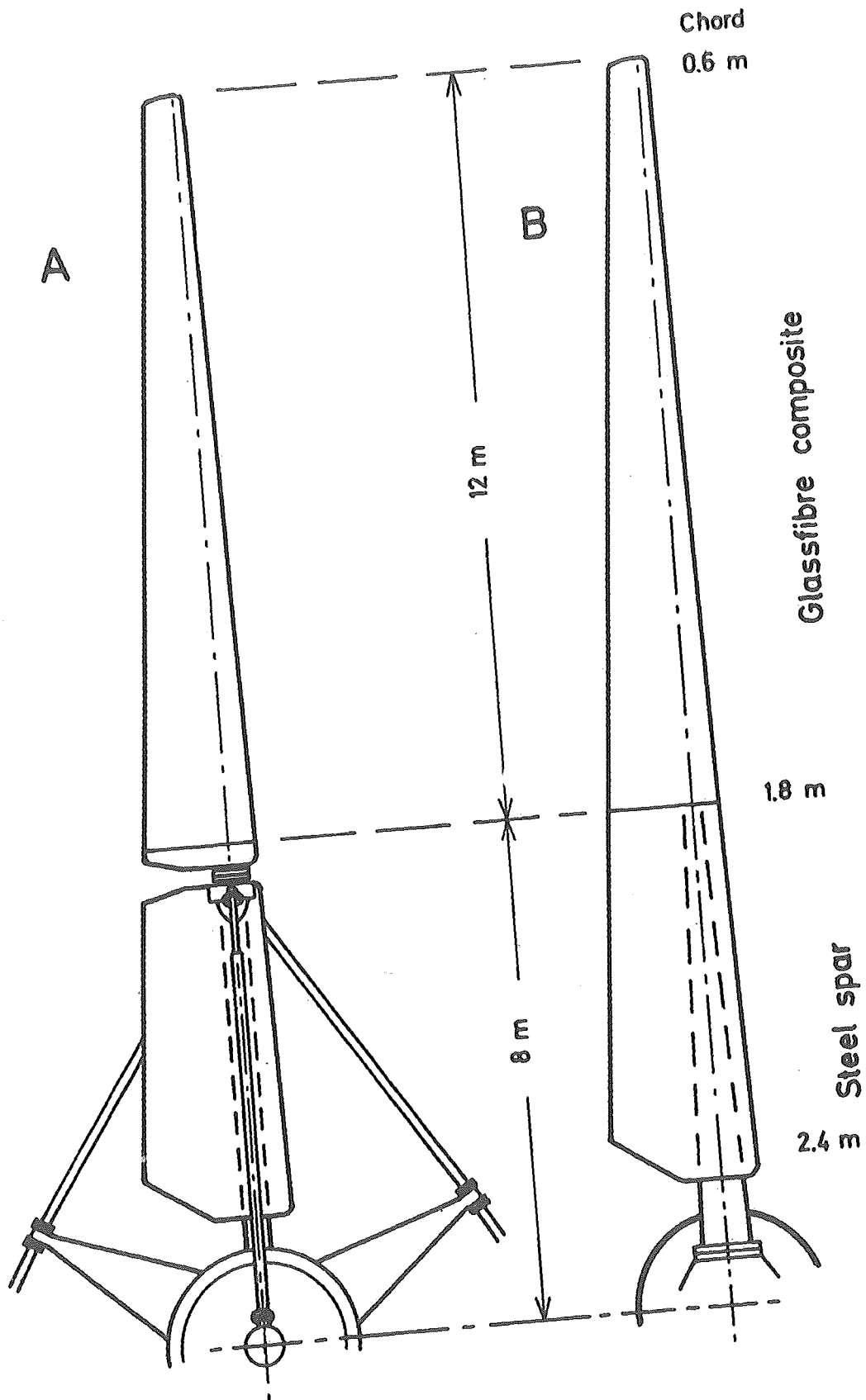
Fig. 5.

BEAM MODEL, PRINCIPLE

SHEAR CENTERS
MASS CENTERS
POINTS DEFINING PRINCIPAL
DIRECTIONS FOR EACH SHEAR
BEAM

ROTOR AXIS

Fig. 6.

8 m

12 m

STAYS

MASSES

BEAMS

Fig. 7.

PROTOTYPE   GRP BEAM
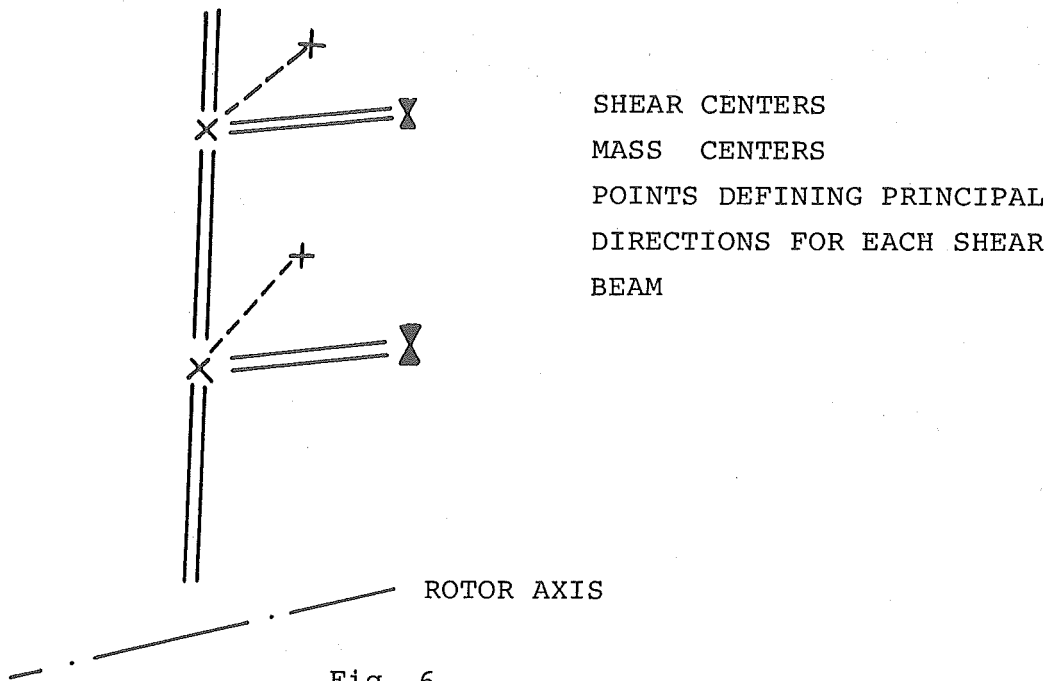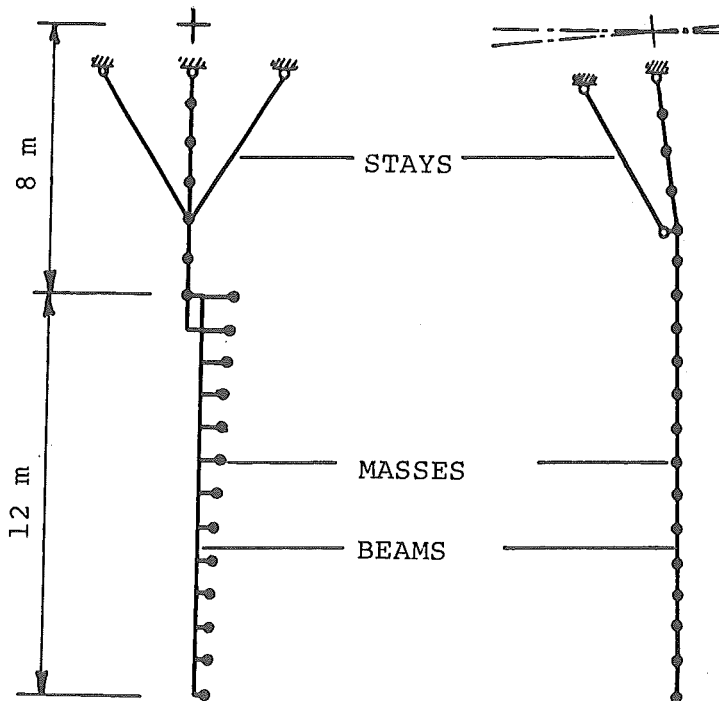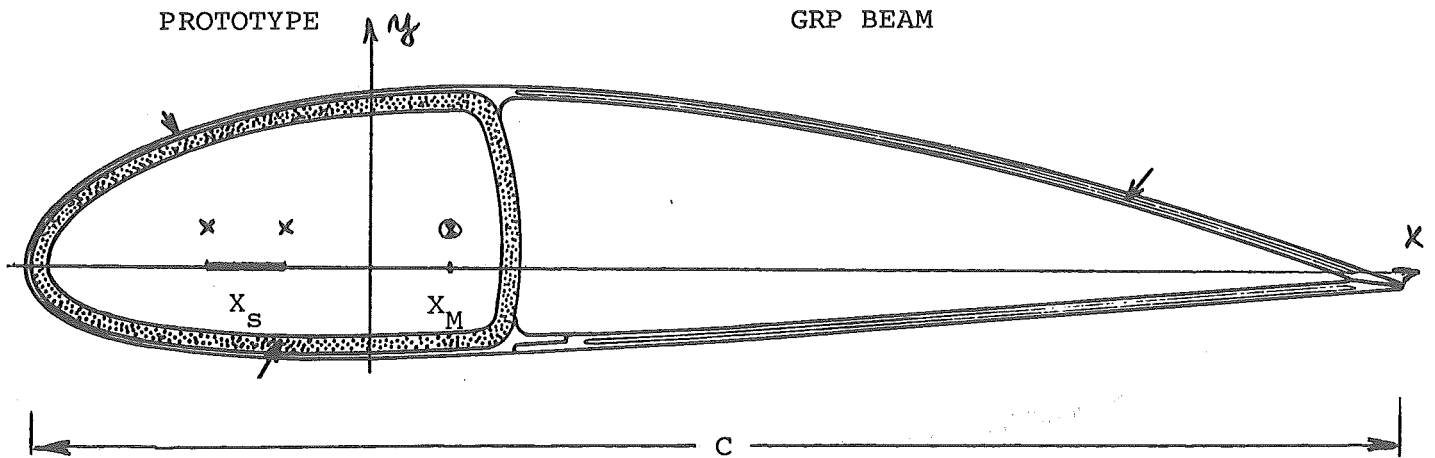
| UNCERTAINCY MAT. DATA | E, ς, G |
| UNCERTAINCY PROD. TECH. | E_ω |

| X_S IN THE RANGE | $-0.11/-.06 * C$ |
| $X_M - X_S$ IN THE RANGE | $0.17/0.11 * C$ |

| 1ST FLAP. IN THE RANGE | $1.87 - 2.69$ Hz |
| 1ST EDGE. IN THE RANGE | $3.09 - 3.92$ Hz |

INFLUENCE OF $X_M - X_S$ ON FREQUENCY $\sim$ 1%

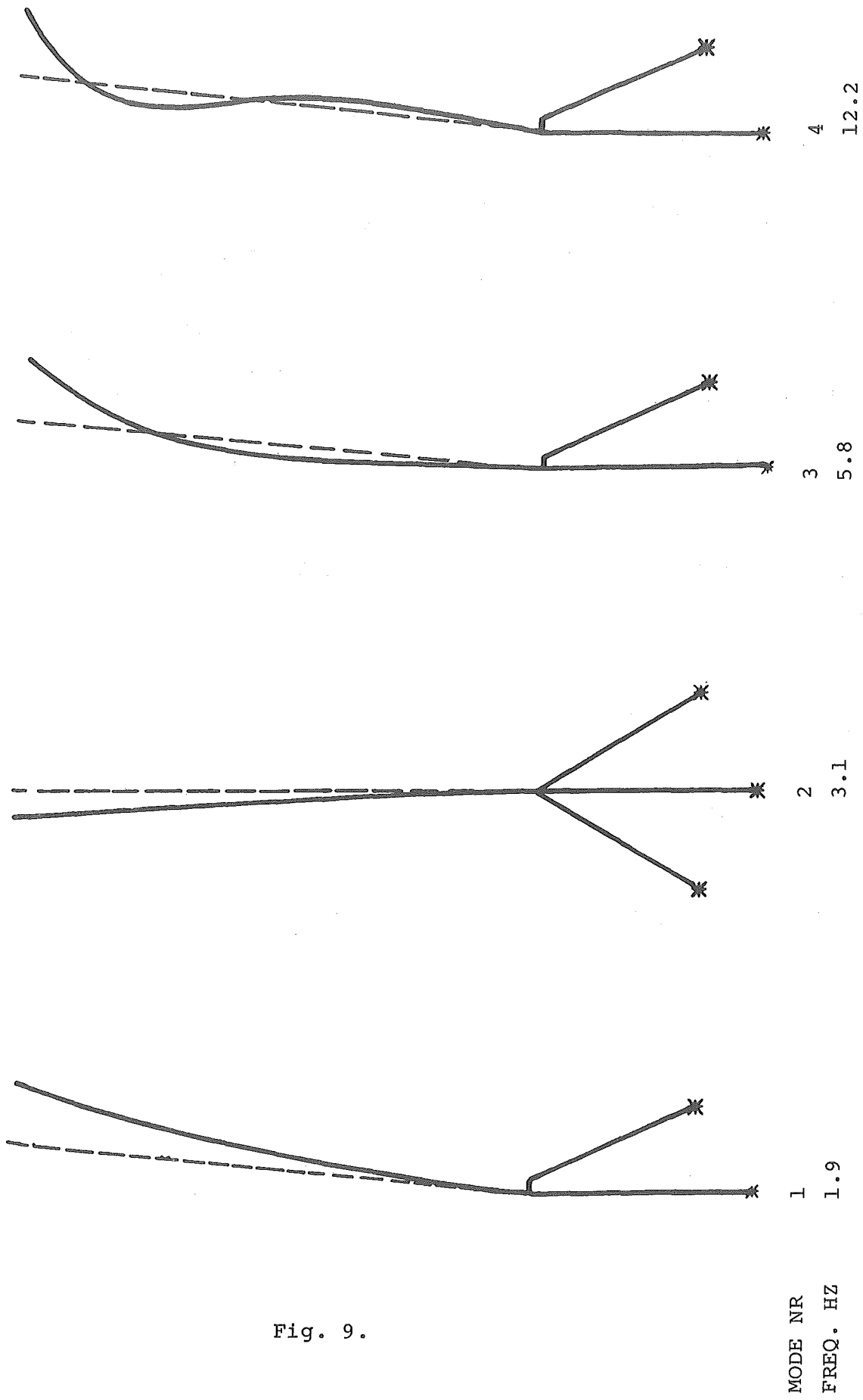| ROTATIONAL FREQUENCY | ROTOR | 0.56 Hz |
| | BLADE | 1.68 HZ |

BEAM MODEL: 200 DOF.

Fig. 8.

Fig. 9.

MODE NR	1	2	3	4
FREQ. HZ	1.9	3.1	5.8	12.2

PROTOTYPE

TOTAL ROTOR MODEL: 420 DOF
(SIMPLIFIED BLADE MODEL)

FREQUENCIES:

1ST ASSYM. FLAPW. (DEGENERATE)	1.96	HZ
2ND — —	1.97	Hz
1ST SYMM. FLAPW.	1.983	Hz
SINGLE BLADE	1.981	Hz
1ST — 3RD EDGEWISE	3.63 — 3.66	Hz

STIFFENING DUE TO CENTRIFUGAL FORCES ~ 6%
ESTIMATED FROM
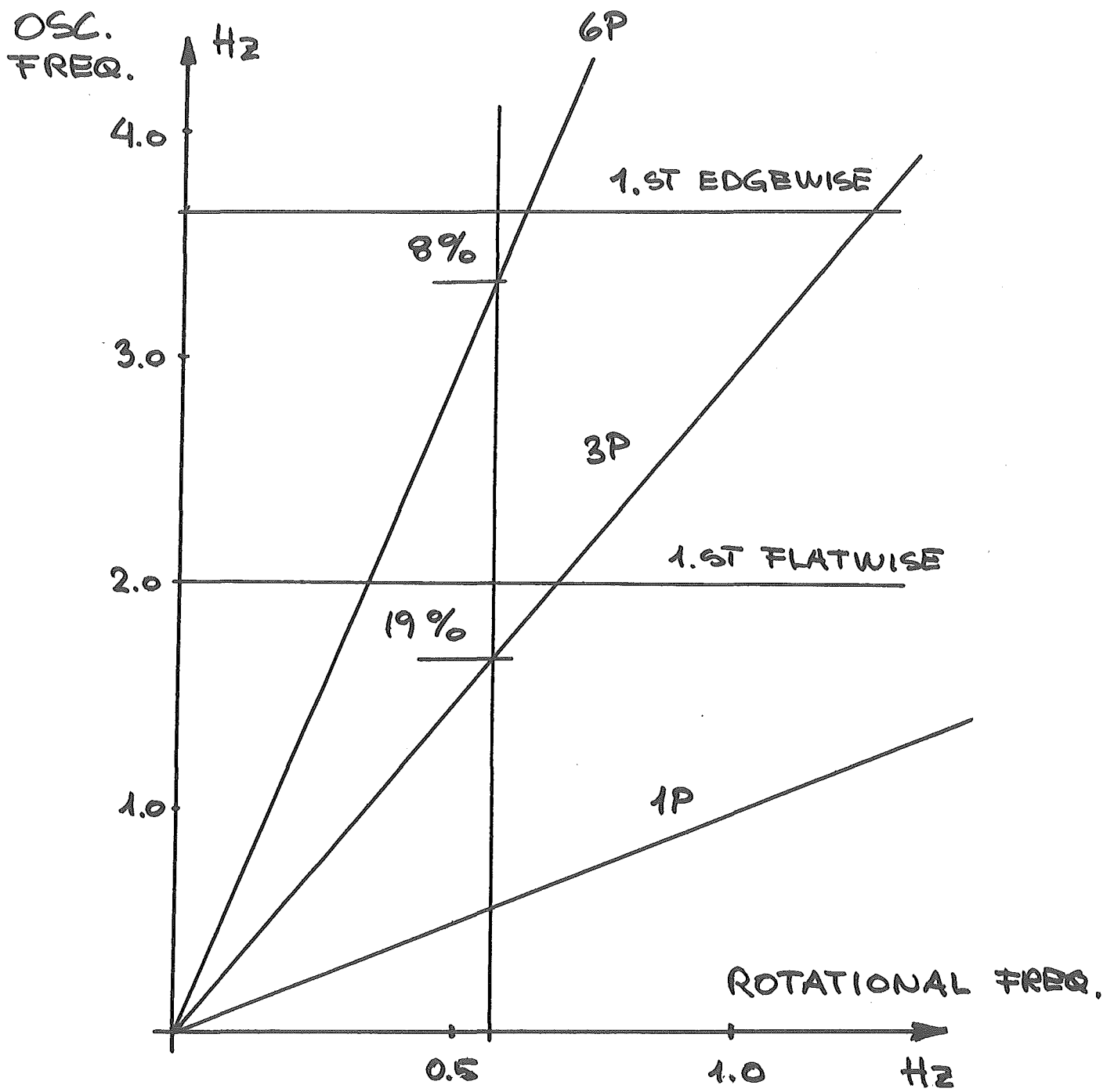
$$\omega = \omega_o + \phi \, \Omega^2$$

Fig. 10.

Fig. 11.

PROTOTYPE

CONCLUSIONS ROTOR COMPUTATION:

GRP MATERIAL MODELS NEEDED

CHECKS ON STRUCTURAL MODEL AWAIT LAB TESTS

SMALL COUPLING BETWEEN BLADES DUE TO STAYS
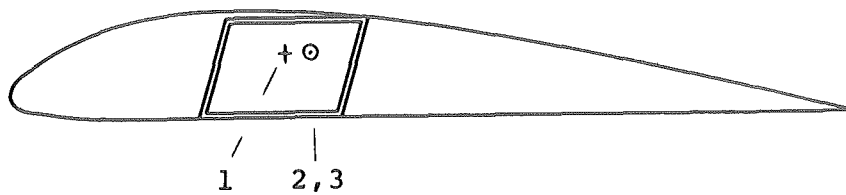
DEPENDENCY OF EIGENFREQUENCIES ON:

- DISTANCE MASS-SHEAR CENTRES	LOW
- CENTRIFUGAL FORCE	MEDIUM
- MATERIAL PROPERTIES AVAILABLE	HIGH
- PRETWIST	LOW
- ANGLE OF REGULATION	(LOW)
- HUB FLEXIBILITY	-
- BOUNDARY CONDITIONS	LOW

Fig. 12.

MAIN CHARACTERISTICS OF THE GEDSER WINDMILL

|	
Rotor location	Upwind
Rotor diameter	24 m
Number of blades	3
Blade tip velocity	38 m/s
Rotational velocity	30 rpm
Rotor area	450 m^2
Blade construction	Steel, main spar, wooden webs, aluminium skin. Heavily stayed. Braking flaps in blade tips (cf. fig. 2)
Regulation	Stall regulated, no pitch control
Generator	Asyncroneous 200 kW, 750 rpm
Transmission	Double chain 1:25
Tower	Stiffened concrete cylinder, hub height 24 m
Performance	Selfstarting at 5 m/s
	200 kW at 15 m/s
	Typical annual production 350.000 kWh/yr

Fig. 13.

Calculated positions of 1. Shear center,
2. Elastic center and 3. Mass center in
the blades.
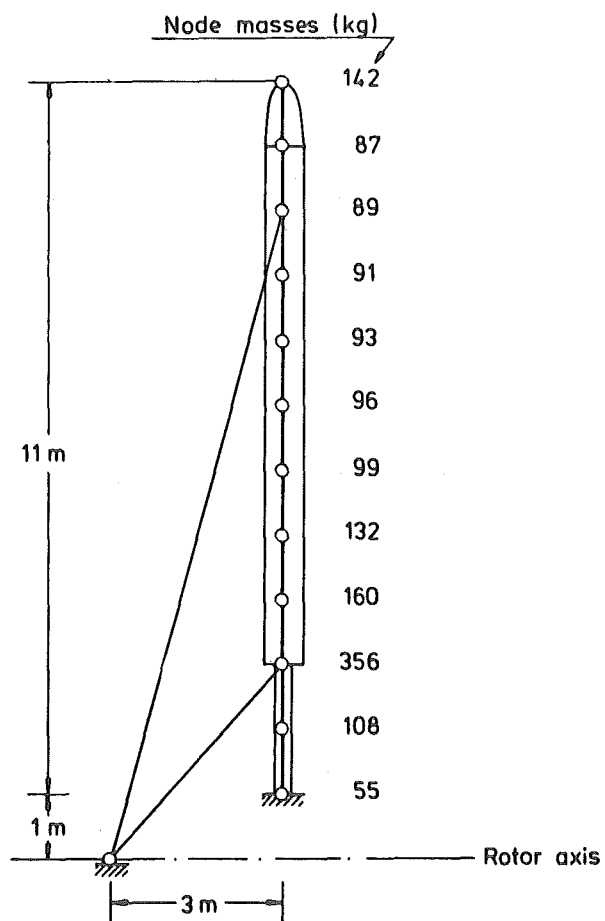
The beam model used for the computation
of blade overall response.

Fig. 14.
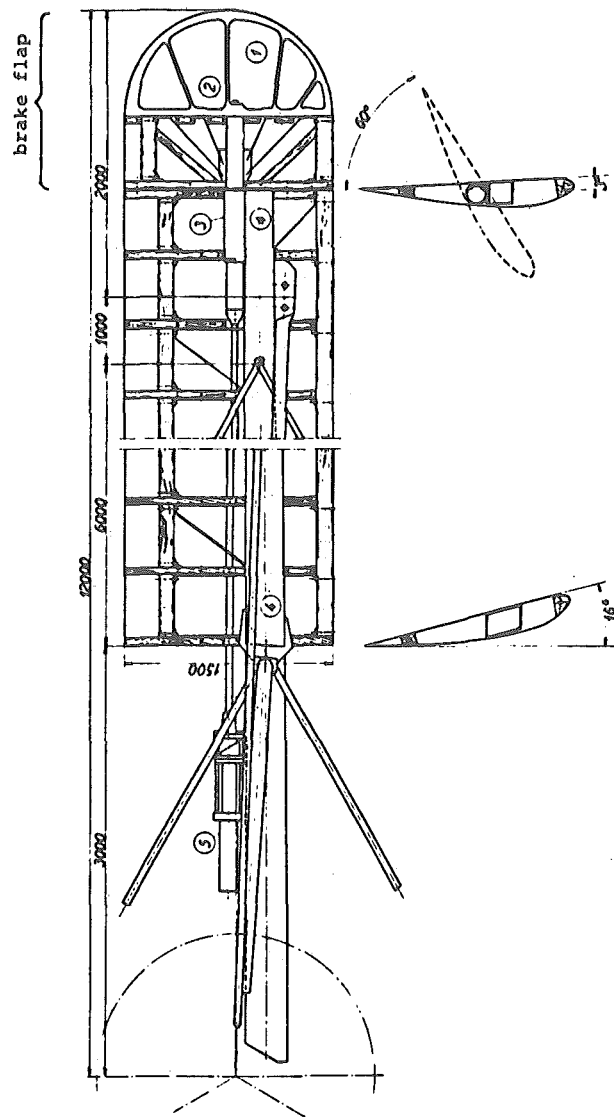
Blade design

1 Brake flap
2 Rod for brake flap
3 Link motion
4 Steel main spar
5 Hydraulic cylinder.

Fig. 15.

GEDSER

SINGLE BLADE WITHOUT STAYS:

	LABTEST	SAP IV
1ST FLAPW.	1.57 Hz	1.56 Hz
1ST EDGEW.	2.35 Hz	2.51 Hz

DEFLECTION PATTERN CHEKED WITH LAB TESTS

Fig. 16.
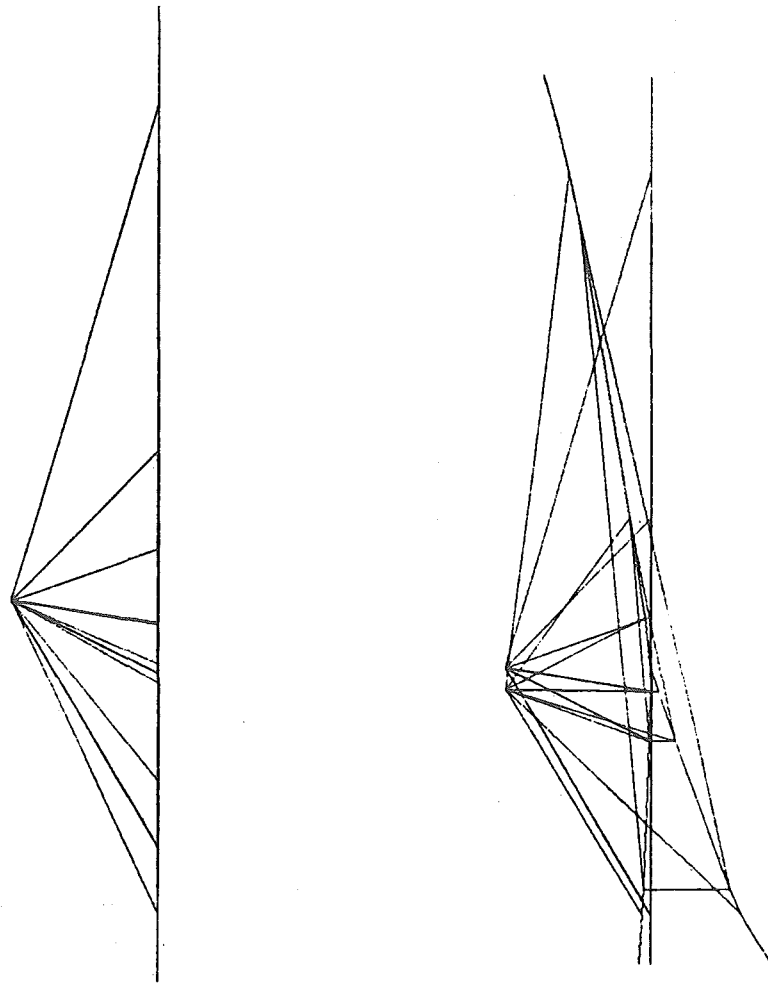
GEDSER MODEL 3 COMPLETE ROTOR DYNAMIC ANALYSIS

GEDSER ROTOR SIDE VIEW MODE I + II

Fig. 17.

GEDSER

COMPUTED:		PRETWIST	CLAMP. RADIUS	SPRING RADIUS	COUPLING	1ST EDGEW.	1ST ASSYM. FLAP	1ST SYMM. FLAP	2ND ASSYM. FLAP
ROTOR	1	+	1	–	+	2.48	7.06	8.16	
	2	+	0	–	+	2.05	3.69	8.10	9.62
	3	–	0	–	+	2.09	3.66	8.10	9.65
	4	+	0	–	–	2.06	–	8.12	
	5	–	0	1	+	2.54	3.66	8.10	
	6	+	0	1	+	2.48	3.70	8.10	9.62
BLADE		+	1	–	–	2.48	–	8.14	
ROTOR (WEPO)						2.25	4.62	9.91	

MEASURED:

SHAFT MOMENT	2.4	
DRIVING MOMENT (EDGE)	2.4	
BENDING MOMENT (FLAP)	(2.4)	
WIRE FORCE (3 PEAKS)	2.2-2.4	
STAY FORCE	2.0-2.2	8.6

Fig. 18.

GEDSER

CONCLUSIONS ROTOR COMPUTATIONS:

SINGLE BEAM (BLADE):
GOOD AGREEMENT WITH LAB TESTS   (BEAM)

ROTOR:

STRONG COUPLING OF BLADES THROUGH STAYS DEPENDENCY OF
EIGENFREQUENCIES ON:

    - DISTANCE MASS-SHEAR CENTRES: NEGLIGIBLE
    - CENTRIFIGAL FORCE ON BLADE :   NEGLIGIBLE
    - CENTRIFUGAL FORCE ON STAYS :   -
    - MATERIAL PROPERTIES   :   NEGLIGIBLE
    - PRETWIST   :   LOW
    - HUB FLEXIBILITY (MODELLING):   HIGH

SOME DISAGREEMENT WITH WEPO RESULTS
SOME DISAGREEMENT WITH MEASURED SPECTRA

Fig. 19

GEDSER MEASUREMENTS

PURPOSE

1 DOCUMENTATION OF DESIGN

2 STRUCTURAL RESPONSE

3 POWER PERFORMANCE

4 DATA FOR MODEL VERIFIKATION

BACKGROUND MEASUREMENTS: 10 MIN AVERAGES

- METEOROLOGICAL DATA
- POWER OUTPUT   16 CHANNELS

SHORT TERM MEASUREMENTS: 50 CPS   40 MIN
- SIMULTANEOUS MEAS.   60 - 80 CHANNELS
- 25-45 ROTOR CHANNELS
- 30   TOWER CHANNELS (POWER, ACC. etc.)
- 14   MET. CHANNELS

PROCEDURE:

- ZERO RUN
- MEASUREMENTS AUTOMATIC OPERATION
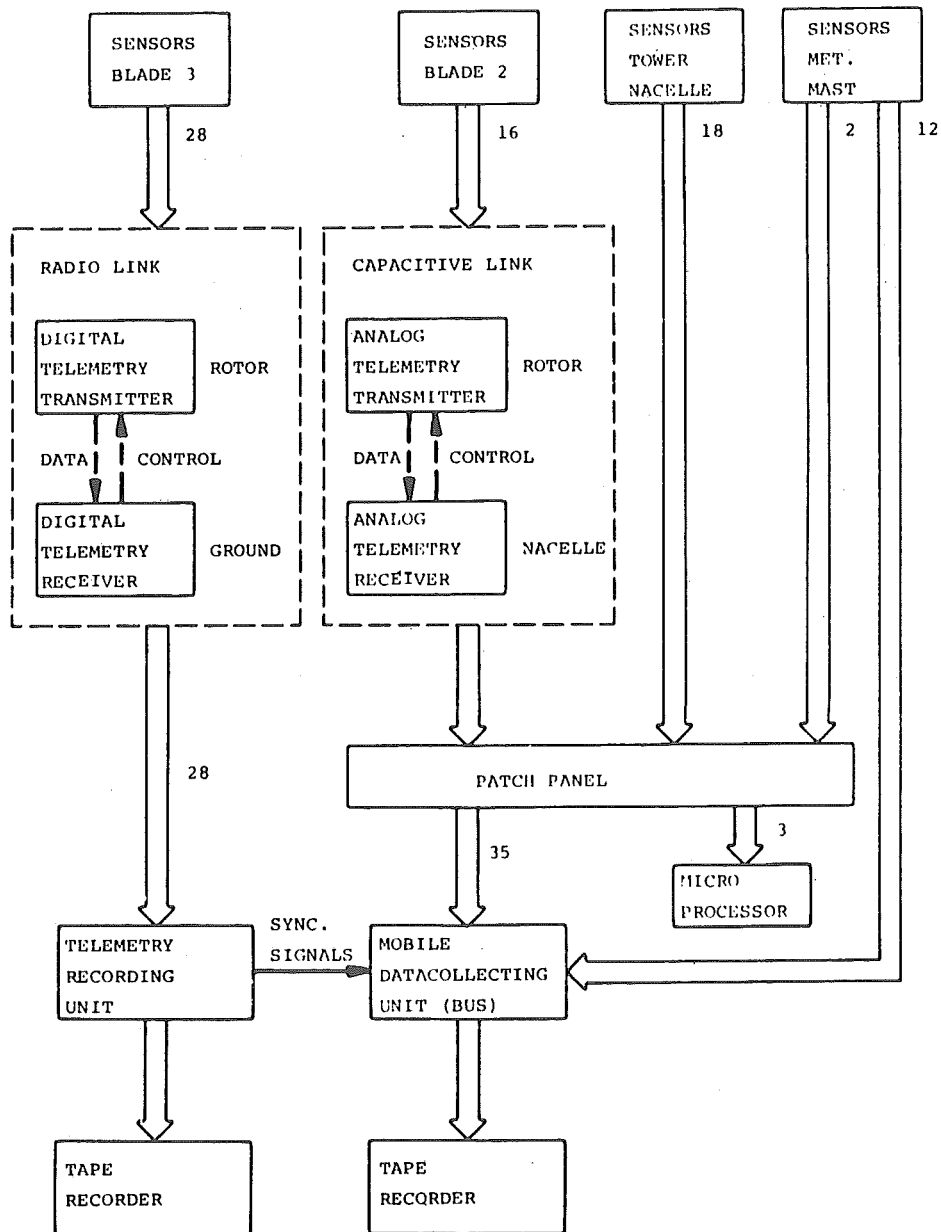- ZERO RUN
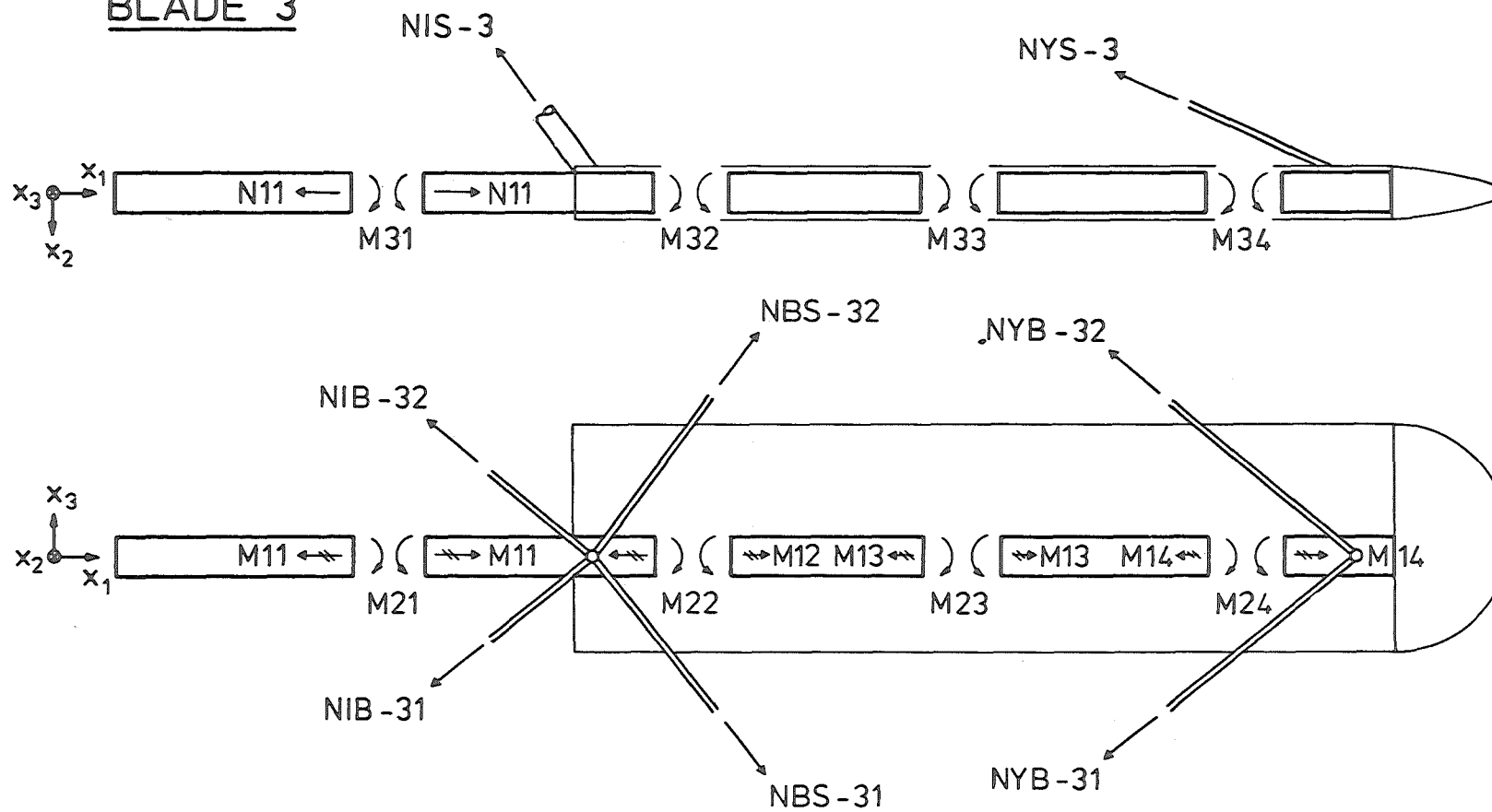- NO ON THE SPOT DATA PROCESSING

Fig. 20.

Fig. 21.

BLADE 3

NIS-3

NYS-3

x_1 x_3 x_2

N11 ←) (→ N11

M31   M32   M33   M34

NBS-32   NYB-32

NIB-32

x_3 x_2 x_1

M11 ←) (→ M11   ←) (→ M12 M13 ←) (→ M13 M14 ←) (→ M 14

M21   M22   M23   M24

NIB-31

NBS-31   NYB-31

Fig. 22.

GEDSER TELE2157.28-4-78.1 SEC PR. DELING.2 SC/BL..

Fig. 23.

13 kNm	M31/3
1.4 kNm	M32/3
3.7 kNm	M33/3
1.6 kNm	M34/3
10.3 kN	N15
17.8 kN	N45
FAST TIMER 50 c/s	
12.9 kNm	M21/3
3.3 kNm	M22/3
1.8 kNm	M23/3
35 kNm	M24/3
6.5 KN	N1B32
2.2 kN	N1B31
25.4 KN	N4B32
24.8 kN	N4B31
SLOW TIMER 50/256 c/s	

→ 1 s/div

- 35 -
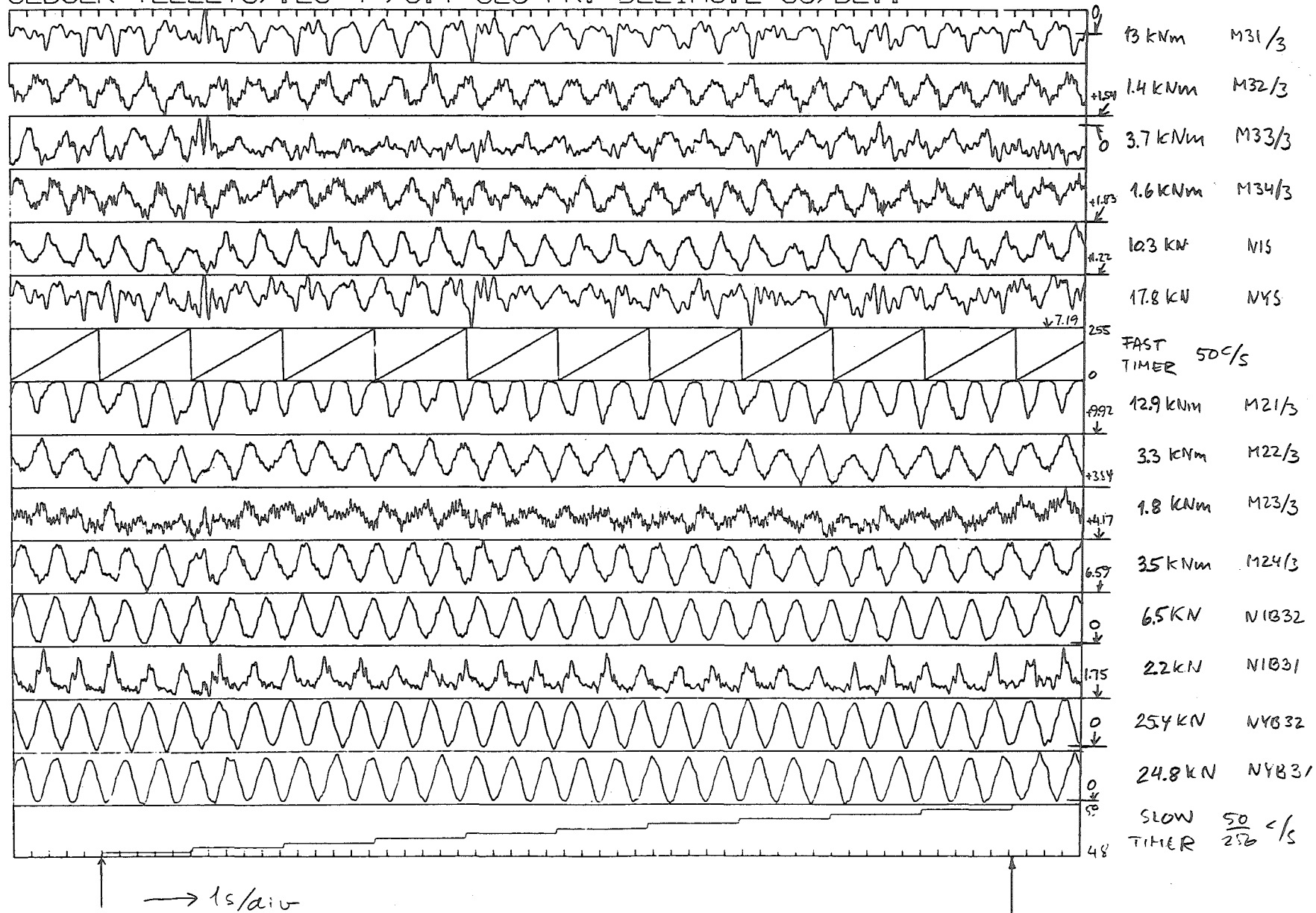
GEDSER2157.28-4-78; NY FORST;
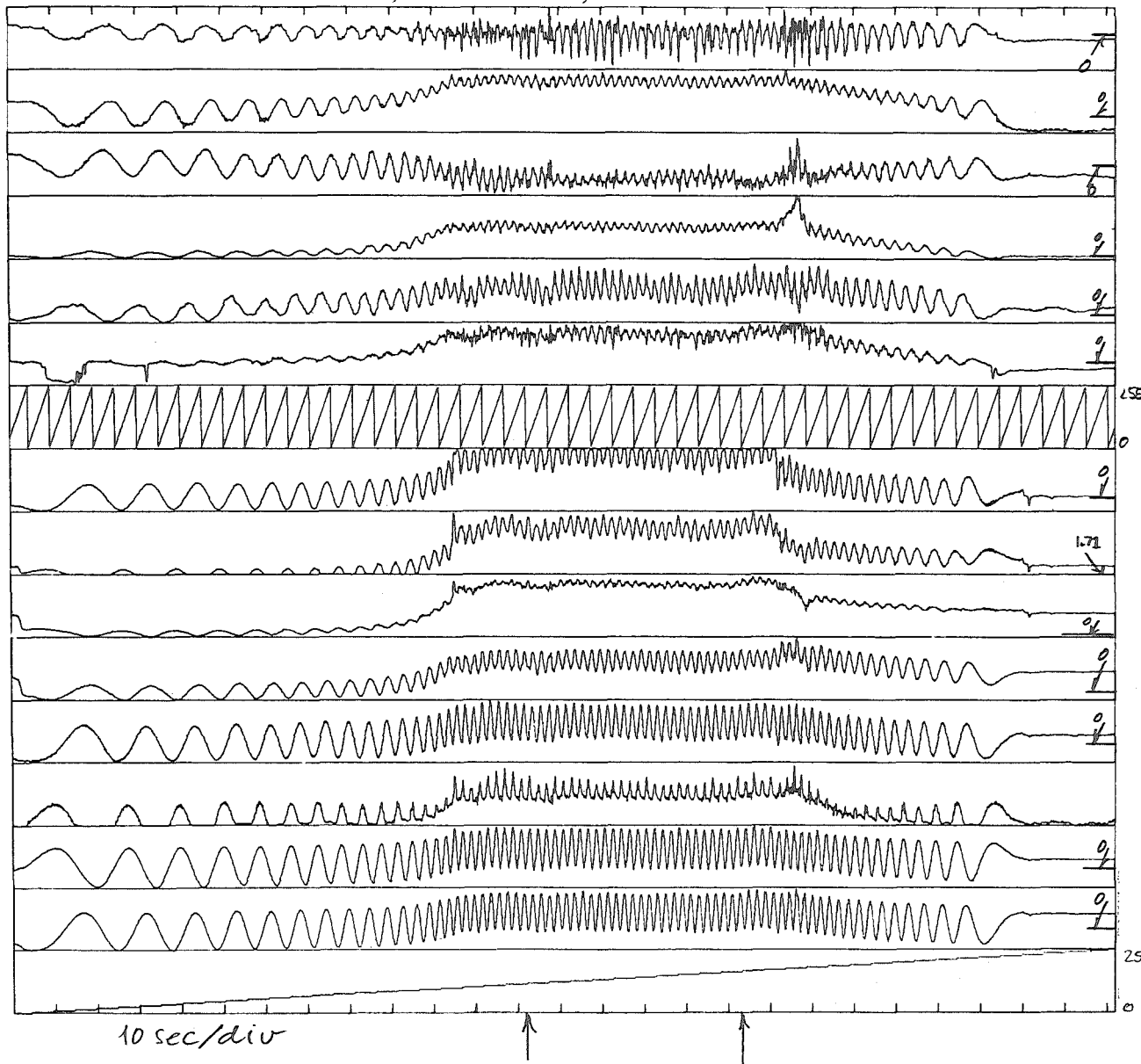
13.9 kNm	M31/3
4.1 kNm	M32/3
5.7 kNm	M33/3
5.8 kNm	M34/3
13.8 kN	NIS
39.5 kN	NYS
	FASTTIMER 50 c/s
30 kNm	M21/3
12.3 kNm	M22/3
6.2 kNm	M23/3
7.3 kNm	M24/3
9.1 kN	NIB32
3.9 kN	NIB31
34.3 kN	NYB32
33.6 kN	NYB31
	SLOW TIMER $\frac{50}{256}$ c/s

10 sec/div

Fig. 24.

- 36 -

Representative forces in blade 3

Channel no.	Sensor	Zero run ΔF_0	F_0	Run ΔF	F	Unit
1	N11	53.6	$\pm$ 26.8	52.8	26.9 $\pm$ 26.4	kN
2	M11	1.02	$\pm$ 0.51	1.02	- 0.57 $\pm$ 0.51	kNm
3	M21	13.5	$\pm$ 6.75	8.36	19.9 $\pm$ 9.95	kNm
4	M31	3.88	$\pm$ 1.94	7.39	- 3.10 $\pm$ 3.70	kNm
5	M12	1.64	$\pm$ 0.82	1.89	0.13 $\pm$ 0.95	kNm
6	M22	1.96	$\pm$ 0.98	3.92	9.45 $\pm$ 1.96	kNm
7	M32	1.64	$\pm$ 0.82	1.31	0.57 $\pm$ 0.66	kNm
8	M13	1.66	$\pm$ 0.83	1.79	- 0.32 $\pm$ 0.90	kNm
9	M23	0.62	$\pm$ 0.31	0.87	4.61 $\pm$ 0.44	kNm
10	M33	2.28	$\pm$ 1.14	1.82	- 2.07 $\pm$ 0.91	kNm
11	M14	0.66	$\pm$ 0.33	0.64	- 0.46 $\pm$ 0.32	kNm
12	M24	1.93	$\pm$ 0.97	2.42	3.43 $\pm$ 1.21	kNm
13	M34	0.77	$\pm$ 0.39	1.16	2.36 $\pm$ 0.58	kNm
14	NIS	4.40	$\pm$ 2.20	7.16	6.40 $\pm$ 3.58	kN
15	NYS	3.17	$\pm$ 1.59	11.1	19.2 $\pm$ 5.55	kN
16	NYB-31	20.2	$\pm$ 10.1	19.7	13.5 $\pm$ 9.85	kN
17	NYB-32	21.1	$\pm$ 10.6	21.1	11.3 $\pm$ 10.6	kN
18	NIB-31	2.60	$\pm$ 1.30	1.43	2.32 $\pm$ 0.72	kN
19	NIB-32	5.17	$\pm$ 2.59	4.87	3.04 $\pm$ 2.44	kN
20	NBS-31	0.25	$\pm$ 0.13	0.25	1.00 $\pm$ 0.13	kN
21	NBS-32	1.75	$\pm$ 0.88	1.75	1.16 $\pm$ 0.88	kN
22	PA	-	-	-	-	kN/m^2
23	PB	0.068	$\pm$ 0.034	0.077	- .119 $\pm$ .039	kN/m^2
24	PC	0.064	$\pm$ 0.032	0.319	- .576 $\pm$ .160	kN/m^2
25	PD	0.165	$\pm$ 0.083	0.297	- .614 $\pm$ .149	kN/m^2
26	PE	-	-	-	-	kN/m^2

Fig. 25.

Representative stresses, blade 3

Channel no	Sensor	A/I (m²) (m⁴)	e m	Zero run $\pm \Delta\sigma_o$ MN/m²	Run $\sigma \pm \Delta\sigma$ MN/m²
1	N11	1.43E-2	-	$\pm$ 1.87	1.88 $\pm$ 1.85
2	M11	-			
3	M21	1.52E-4	.137	$\pm$ 6.08	$\pm$ 17.9 $\pm$ 8.97
4	M31	7.62E-5	.085	$\pm$ 2.16	$\pm$ 3.46 $\pm$ 4.13
5	M12				
6	M22	2.49E-4	.122	$\pm$ 0.48	$\pm$ 4.63 $\pm$ 0.96
7	M23	7.09E-5	.085	$\pm$ 0.98	$\pm$ 0.68 $\pm$ 0.79
8	M13				
9	M23	1.79E-4	.109	$\pm$ 0.19	$\pm$ 2.81 $\pm$ 0.27
10	M33	4.04E-5	.085	$\pm$ 2.40	$\pm$ 4.36 $\pm$ 1.91
11	M14				
12	M24	1.51E-4	.101	$\pm$ 0.65	$\pm$ 2.29 $\pm$ 0.81
13	M34	3.69E-5	.085	$\pm$ 2.30	$\pm$ 1.58 $\pm$ 0.39
14	NIS	1.31E-3	-	$\pm$ 1.68	4.89 $\pm$ 2.73
15	NYS	1.61E-3	-	$\pm$ 0.99	11.9 $\pm$ 3.45
16	NYB-31	1.39E-3	-	$\pm$ 7.27	9.71 $\pm$ 7.09
17	NYB-32	1.40E-3	-	$\pm$ 7.57	8.07 $\pm$ 7.57
18	NIB-31	2.45E-4	-	$\pm$ 5.31	9.47 $\pm$ 2.94
19	NIB-32	3.05E-4	-	$\pm$ 8.49	9.97 $\pm$ 8.00
20	NBS-31	2.55E-4	-	$\pm$ 0.51	3.92 $\pm$ 0.51
21	NBS-32	2.30E-4	-	$\pm$ 3.83	5.04 $\pm$ 3.82

1 MN/m² = 9.81 kp/cm²

Fig. 26.

Representative values, bus channels

Channel no	Sensor		Repr. value		Comment
32	Yawrate	Y	$-$ 0.013	rad/s	Yaw motor on
			$\pm$ 0.014	rad/s	Max during stop
33	x-acc.	$\ddot{x}$	$\pm$ 0.93	m/s^2	$-$ $-$ $-$
34	y-acc.	$\ddot{y}$	$\pm$ 0.33	m/s^2	$-$ $-$ $-$
35	ϕ-acc.	$\ddot{\phi}$	$\pm$ 0.12	rad/s^2	Start of yaw motor
36	Rotorpos. 1/360°		3.19	rad/s	30.46 rpm.
37	Rotorpos 1/1°		3.56	rad/s	34.0 rpm.
38	Azimuth	ϕ	89/71	deg	
39	Torque	Mg	$-$		
40	Torque	M_s	2.62	kNm	Low wind (A)
		M_s	11.2	kNm	High wind (B)
	Power	W_s	39.4	kW	(A)
		W_s	168.3	kW	(B)
41	KVAR	$-$	30.4	kVAr	Max value
42	KWATT	W	39.3	kW	(A)
		W	157.1	kW	(B)
43	VOLT	$-$	407	volt	operating
		$-$	410	volt	stopped
44	Windspeed	V	9.4	m/s	Minimum
		V	13.8	m/s	Mean
		V	18.9	m/s	Maximum
45	Winddirection	Θ	69	deg	Mean

Fig. 27.
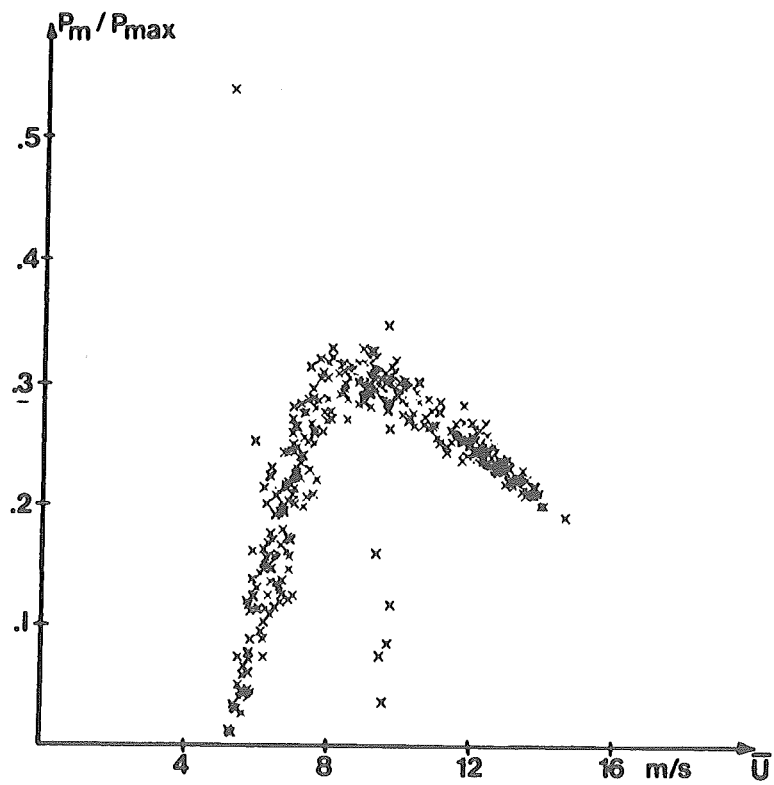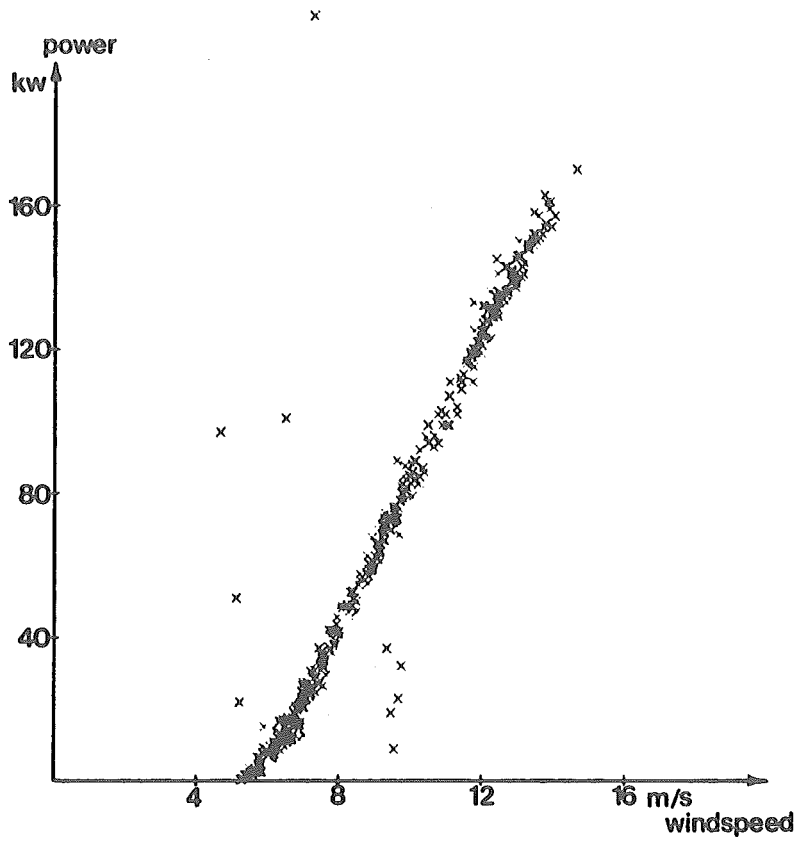
Fig. 28.

GEDSER MEASUREMENTS

PRELIMINARY CONCLUSIONS:

ROTOR:

LOW STRESS LEVELS/AMPLITUDES, EXEPTIONS:

- BLADE ROOT DRIVING MOMENT   MEDIUM STRESS
- STAYS TO BLADE TIPS   MEDIUM STRESS

FORCE LEVELS/AMPLITUDES INDICATE:

- PRIMARY LOAD. GRAVITY/WIND FORCES
- STAY SYSTEM ESSENTIAL IN THE INTERNAL
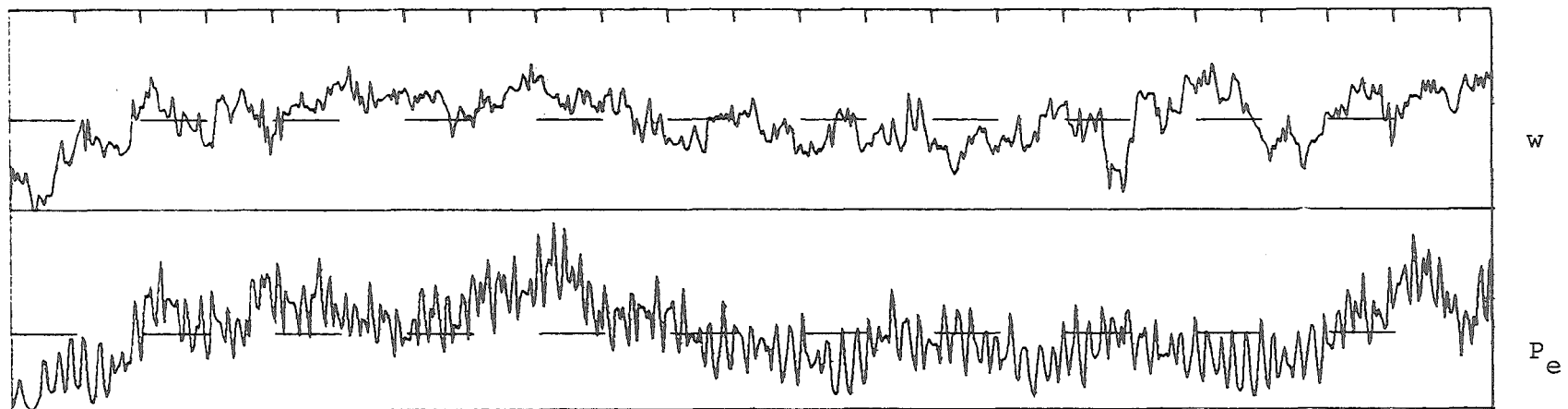 DISTRIBUTION OF FORCES, CAUSING STIFF
  ROTOR BEHAVIOUR.

TOWER

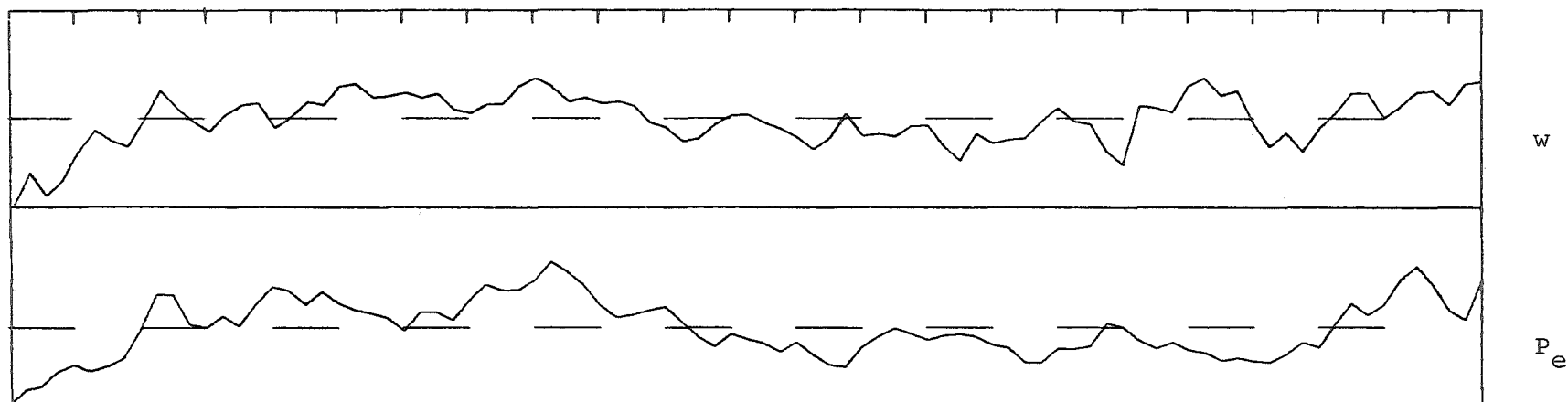LOW ACC. AND YAW RATE   LEVELS/AMPLITUDES
LOW GYRAL FORCES

DATA CONVERSION

UNKNOWN EXTERNAL FORCES DURING ZERO RUN GIVE
PROBLEMS IN THE ABSOLUTE DETERMINATION OF EX-
TERNAL FORCES DURING OPERATION

Fig. 28 a

Averaging time 0.4 sec

1o sec/div.

Averagint time 2.5 sec.

Fig. 29 Wind speed (w) and electric power (P_e)
showing a) power fluctuations and b) eff averaging
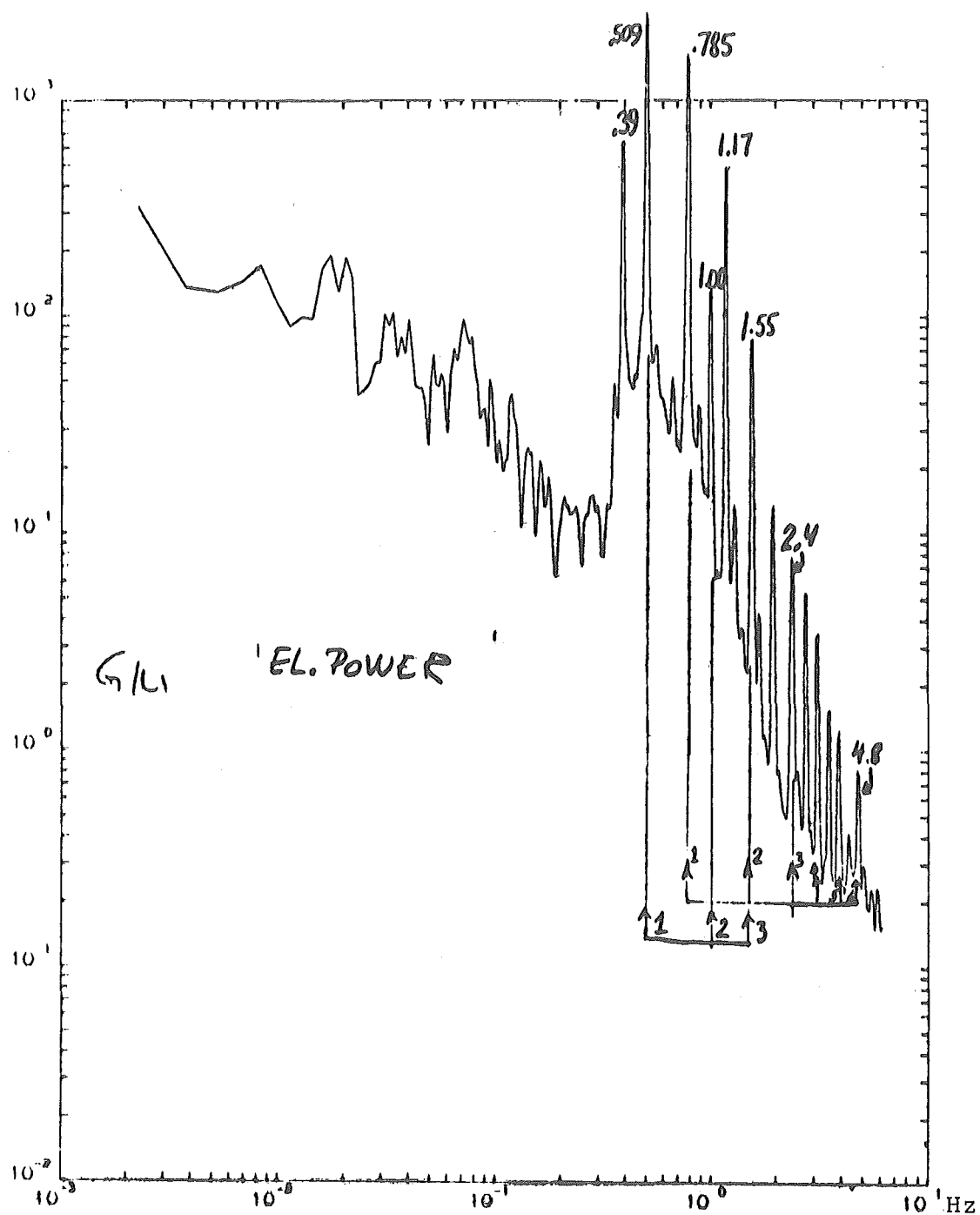
Fig. 30   Variance spectrum of electric power
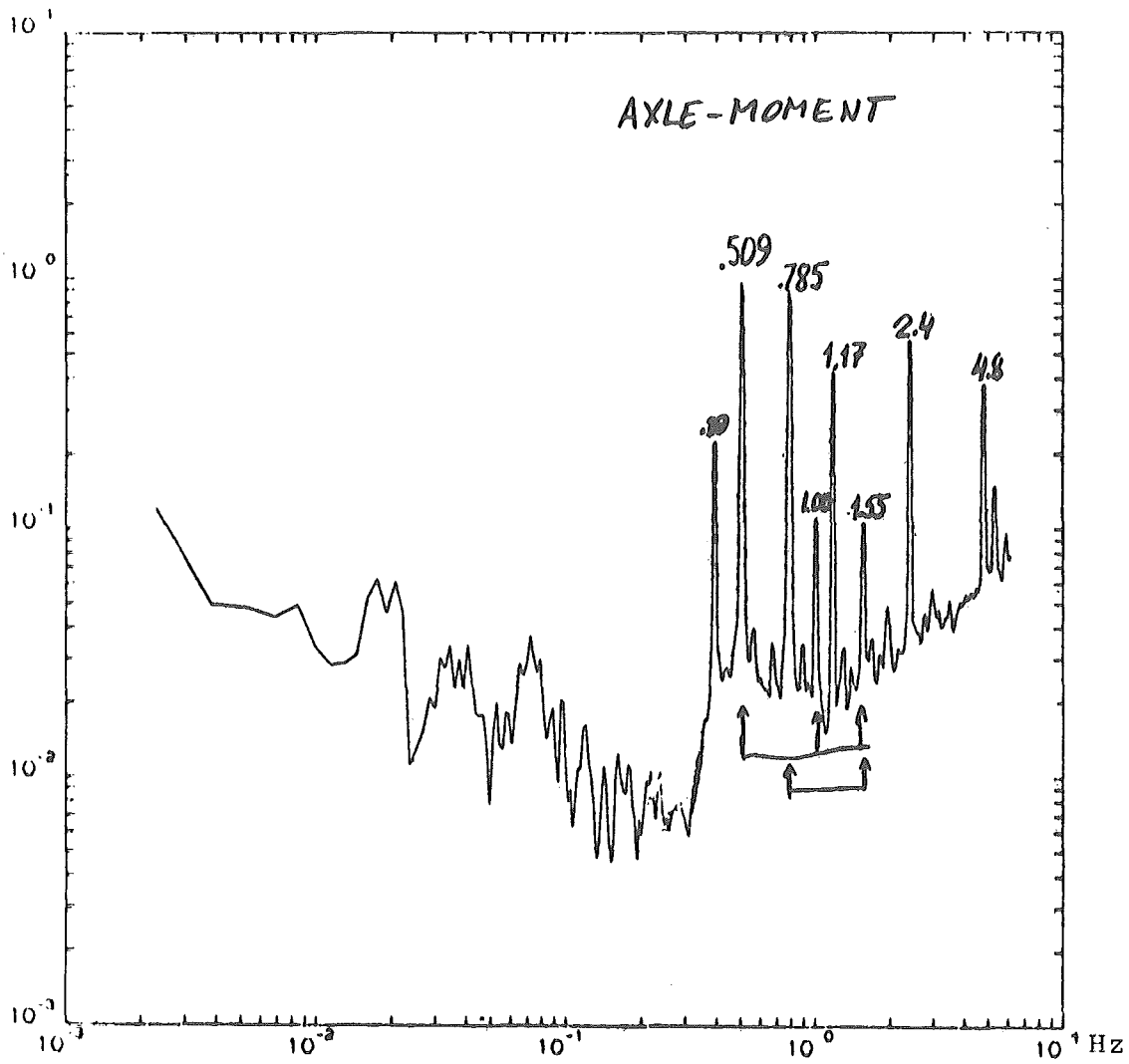
Fig. 31   Variance spectrum of shaft moment
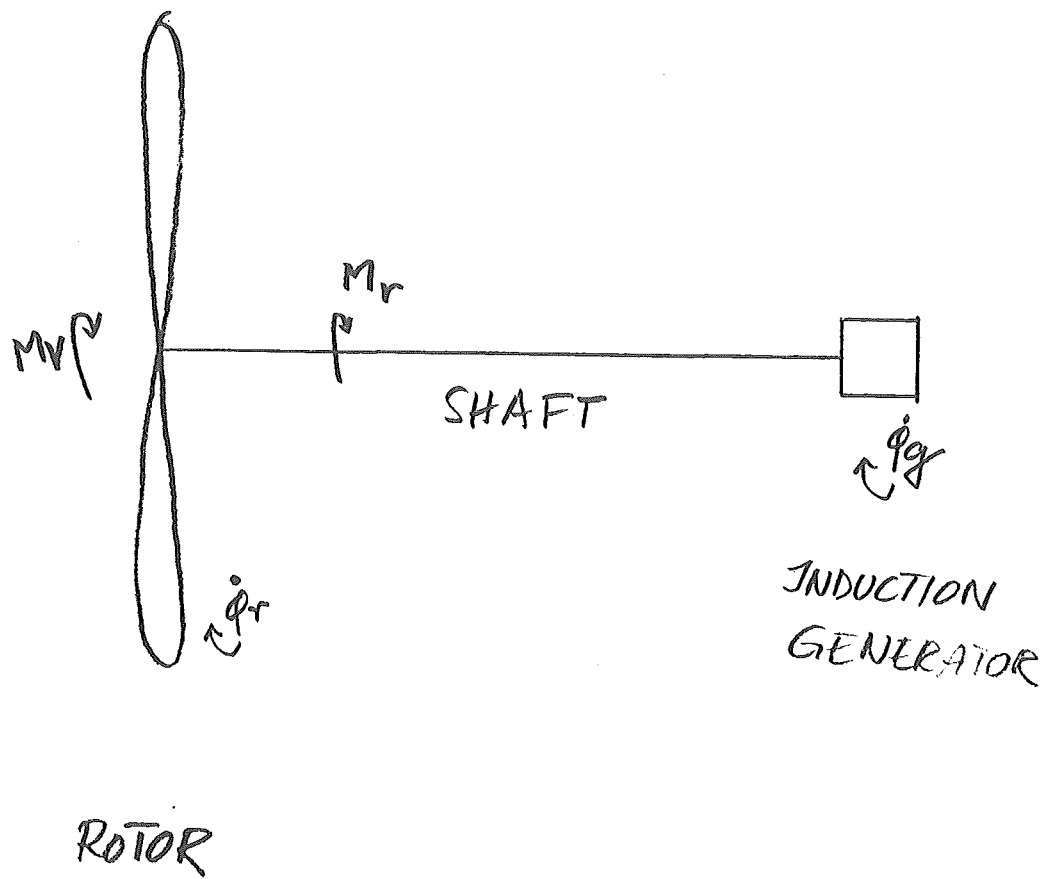
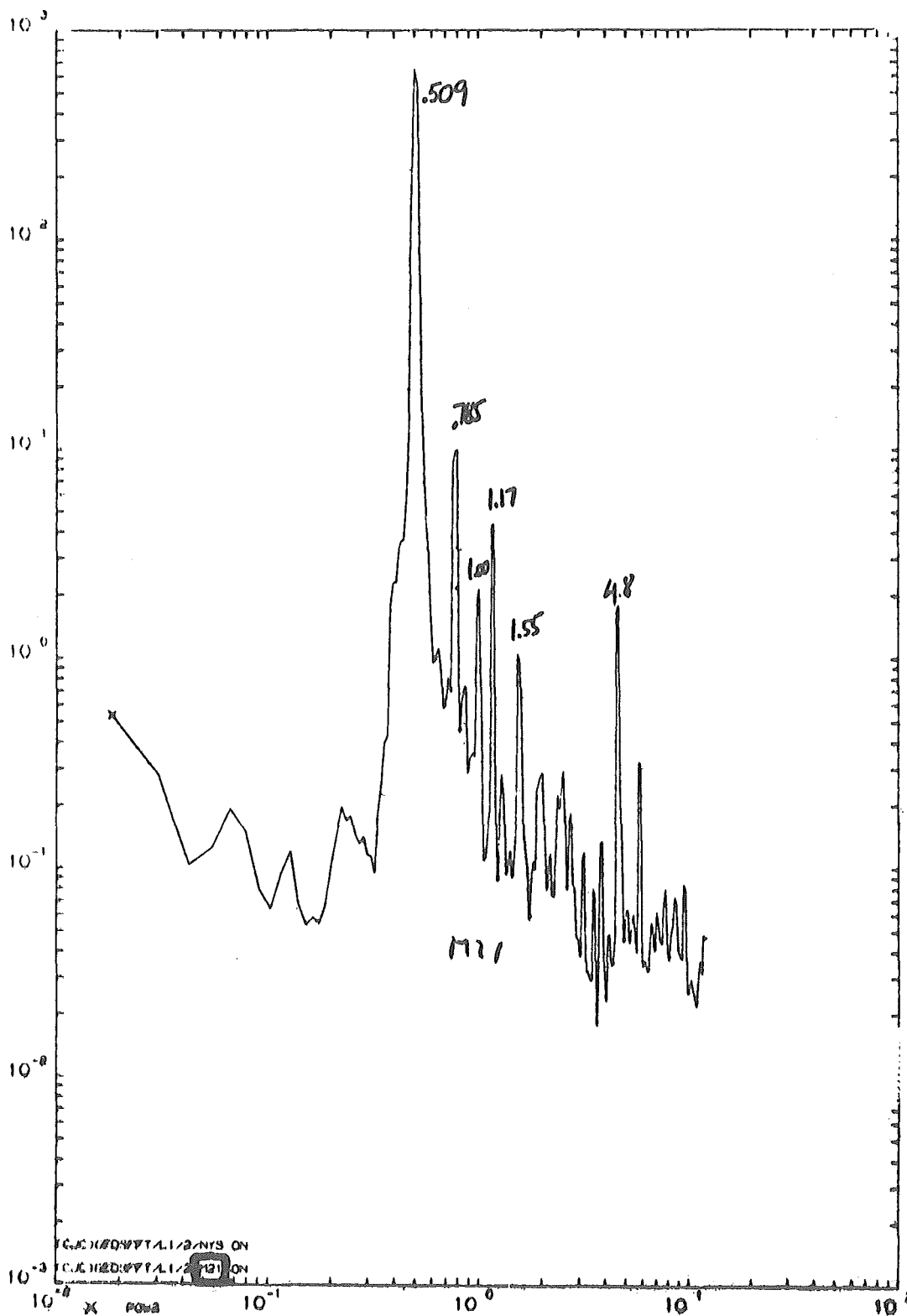Fig. 32   Power train components for simple model

FIG. NR. 1

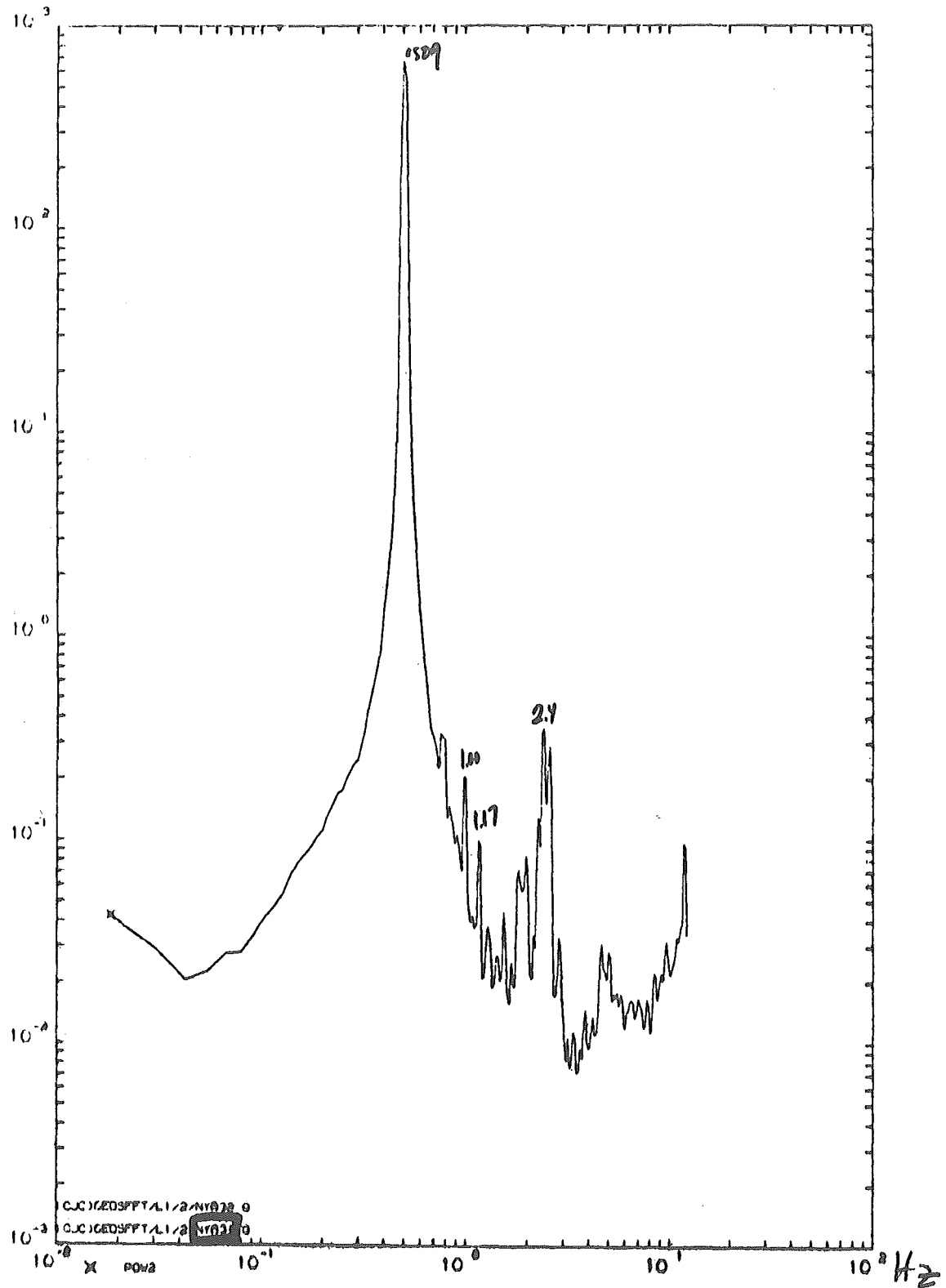Fig. 33   Variance spectrum wing base
flapwise moment

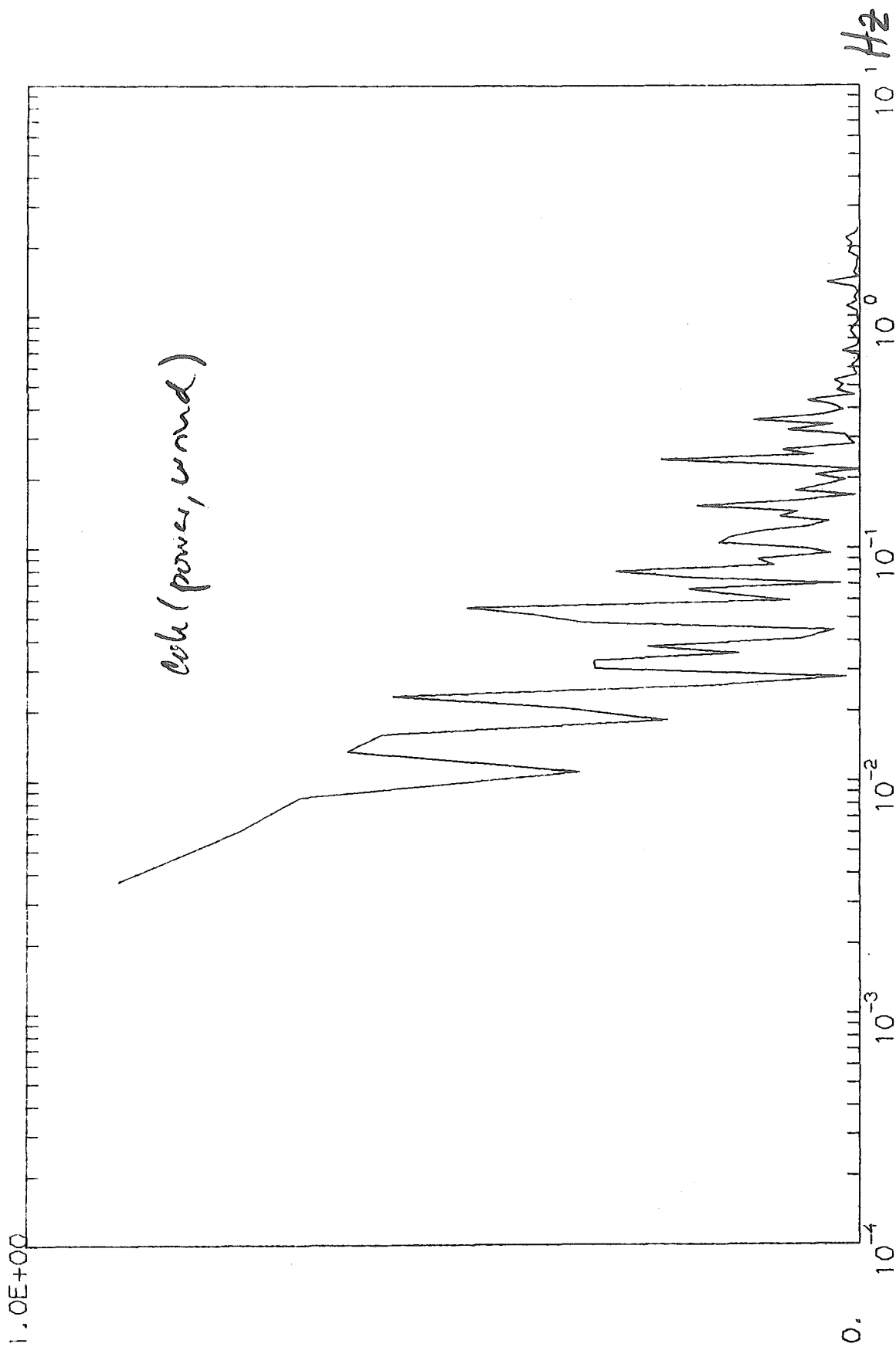Fig. 34   Variance spectrum of force in
          outer stay

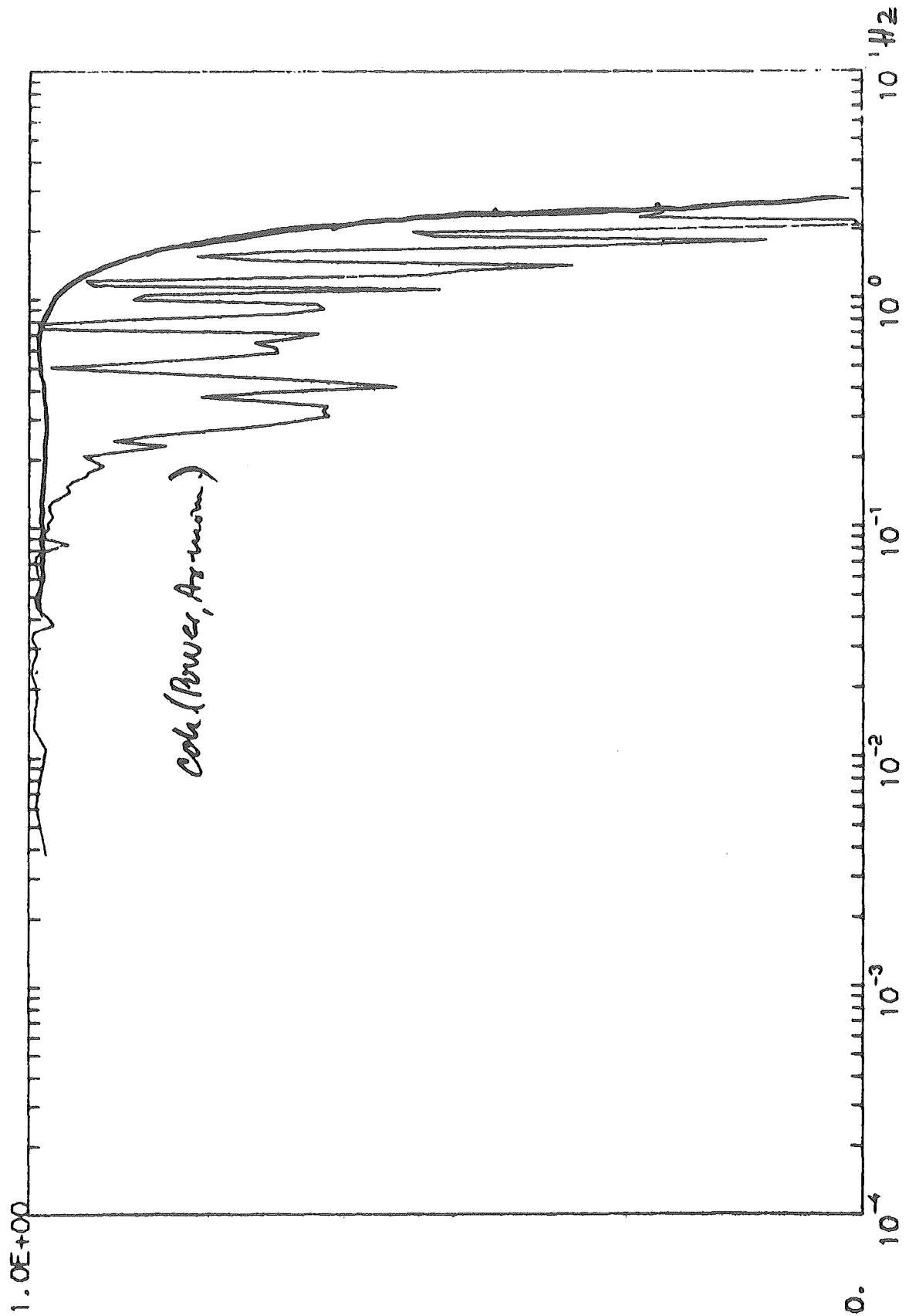Fig. 35   Coherence between electric power
          and wind speed spectra

Fig. 36 Coherence between shaft moment and electric power

Gedser Test Group

MEASUREMENTS OF PERFORMANCE AND STRUCTURAL RESPONSE

OF THE DANISH 200 KW GEDSER WINDMILL

by

P. Lundsager

Risø National Laboratory
DK 4000 Roskilde, Denmark

V. Askegaard

Structural Research Laboratory
Technical University of Denmark
DK 2800 Lyngby, Denmark

E. Bjerregaard

Danish Ship Research Laboratory
DK 2800 Lyngby, Denmark

Measurements of Performance and Structural Response
of the Danish 200 kW Gedser Windmill

by

P. Lundsager, Risø National Laboratory, DK 4000, Roskilde, Denmark

V. Askegaard, Structural Research Laboratory, Technical University
of Denmark, DK 2800, Lyngby, Denmark

E. Bjerregaard, Danish Ship Research Institute, DK 2800, Lyngby, Denmark

The paper deals with a series of static and dynamic measurements being performed on the 20 year old Danish Gedser windmill as a part of the Danish government and utility sponsored wind power program. The design of the mill, which in several points differ essentially from most modern designs, is still of interest since the mill has been in operation during a 10 year period without major mechanical troubles. The main objectives of the measurements are the determination of the power curve, the structural response especially of the rotor and the power quality, but the instrumentation lay-out also aims at obtaining results which should be useful in the verification of models for windmill analysis.

In the paper a technical description of the instrumentation is given. A total of 84 channels has been installed, 46 of which are telemetered from the rotor. The rotor instrumentation lay-out has been determined from laboratory tests on single blades, during which the final instrumentation was installed and calibrated.

During field tests short term measurements will be performed during automatic operation as well as forces maneuvres using scanning frequencies up to 50 cps. Furthermore long term power/wind measurements will be carried out. Examples of records will be presented and discussed together with experience with the equipment applied.

According to plans the measurement program will be finished in 1978.

1. INTRODUCTION   2.

The Danish Wind Power Program is being undertaken by the ministry of commerce in colla-
boration with the electric utility companies. The program incorporates the following
three main projects:

a) Restoring the Gedser windmill for suosequent measurements and analysis.

b) Construction of 2 major prototype WTG's.

c) Wind measurements and determination of sites for research WTG's.

The present paper deals with project a) exclusively.

The Gedser windmill, fig. 1, is the last and largest of 3 research windmills built
in the 1950's by SEAS (Sealand Electricity Ltd.). Table 1 shows a summary of the cha-
racteristics of the mill, which deviates from the majority of new designs in that the
rotor is 3 bladed, upwind located and stall regulated. The blades are stiffened by a
number of stays. (Fig. 2)

The mill was in continuous automatic operation during the years 1958-1968 without major
mechanical troubles and was taken out of operation mainly due to regular costs of opera-
tion being too high. The mill has been restored by SEAS during 1977 and is now being o-
perated for test purposes.

The purpose of the present paper is to give a technical description of the measurement
program sceduled to be carried out during 1977-78 under contract with the Danish Wind
Power Program as a joint venture by Risø National Laboratories, Structural Research
Laboratory of the Technical University of Denmark and Danish Ship Research Laboratory.
The measurement program is described more detailed in refs 1, 2 and 6.

2. THE MEASUREMENT PROGRAM

The main objectives for the measuring program, as stated by the contractor, are the
determination of

a) The power curve of the mill.

b) The loads on certain parts of the structure, especially the rotor, and their structu-
   ral response under various conditions.

c) The power quality. During the years of operation, power fluctuations were observed,
   (ref. 4).

3.

The layout of the instrumentation aims at obtaining results that may be useful in the evaluation and development of models for windmill design and analysis. Furthermore the results will be of interest in a comparison with later designs of USA and Sweden, which have several essentially different design features.

The measuring program comprises both laboratory and field tests. During laboratory tests the structural characteristics of single blades were investigated by means of provisional gauges, and the field instrumentation was mounted and calibrated. During the field tests long term measurements of wind and electric power are carried out, but the main effort is concentrated on short term measurements of wind conditions and structural response, performed during short sessions using high scanning frequencies.

3. LABORATORY TESTS

3.1. Preliminary static tests

Static laboratory tests have been performed on two of the rotor blades, shown in fig. 2, to create knowledge of the interaction between main spar and blade cladding in the distribution of forces. This was necessary in order to be able to place strain gauges such that combinations of these gauges could be expected to give a reasonably unique determination of the internal forces in the blade.

The results of the tests have been used for final instrumentation with strain gauges of these blades in order to determine certain of the internal forces in four sections of the main spar of the blade under operating conditions to enable specification of the external load on the blade.

The displacement pattern for the blade was determined by levelling to rods mounted on the blade.

The following six loading tests were performed:

1) torsional moment M_1 (about x_1 axis, see fig. 2)
   cladding removed at measuring section 3

2) as 1) with cladding in place

3) torsional moment M_1 plus force P_2 (x_2 direction)

4) force P_2

5) force P_1 (x_1 direction)

6) force P_3 (x_3 direction).

The test set up for loading case 1 and 2 can be seen in fig. 3. In all cases, the blade

was restrained at its root, with the x_1 direction horizontal. The air-brake was removed, and the load was applied at the tip of the blade in all tests.

From these tests it could be concluded that the strain gauge combinations formed only by gauges mounted on the main spar could be expected to give a reasonably accurate determination of the internal forces in the blade, since the main spar is responsible for the major part of the blade stiffness (about 90% in torsion).

It was further found that the signals from the combinations for determination of the shear forces N_2 and N_3 were so small that the accuracy on their determination did not warrant registration of these internal forces under working conditions.

3.2. Dynamic tests

Dynamic tests were carried out with the blade acting as a cantilever restrained at the root. Signals from accelerometers showed the lowest eigenfrequency for vibration in the $x_1 x_2$-plane to be 1.57 Hz and indicated the damping to be a combination of viscous and friction damping.

The lowest eigenfrequency for the vibration of the blade in the x_1-x_3-plane was determined to be 2.3-2.4 Hz partly on the basis of observations from the deflection curves in the static tests.

The lowest eigenfrequency in the torsion mode was not measured but was considerably higher.

3.3. Field instrumentation of blades

Fig. 4 shows a general drawing of the rotor with stays. The numbered stays are instrumented with strain gauges (full bridge configuration) in order to determine the normal force.

The sketch in fig. 5 shows how the stays were connected to blade No. 3 and the placing of the measuring sections in the main spar of the blade.

The internal forces M_1, M_2 and M_3 are measured in the sections 2-4, and the same internal forces plus N_1 are measured in section 1.

The gauge positions in the measuring sections is also shown in fig. 4, and information about gaugetype, cement and moisture protection is given, as well as the combination of gauges in Wheatstone bridges are shown.

The instrumentation of blade No. 2 is similar.

3.4. Static calibration tests

The same loading cases, 2-6, were used as in the introductory tests. Levelling was not performed, but the displacement of the point of application of the force was measured.

Good linearity between external load and measured signal for an internal force has been observed in the expected loading range for all loading cases as demonstrated in fig. 6.

Owing to minor deviations from the assumptions (deviation from linearity, eccentricities etc.) the individual signal combinations must be expected to be a function of all the internal forces in the section in question and not of a single one.

We have sought to determine this function on the basis of the results from loading cases 2 to 6, and for this purpose, the following assumptions have been made:

1) The function sought is linear.

2) The contribution of the shear forces N_2 and N_3 to the reading of the other signal combinations is neglected.

3) The internal forces M_1, M_2 and M_3 in sections 2-4 are independent of the normal force N_1 in the sections in question.

The loading cases 2, 3, 5 and 6 are used for determining the coefficients in the linear expressions for N_1, M_1, M_2, M_3 in section 1, while loading case 3 is used as control.

In the determination of the coefficients for the three internal forces M_1, M_2 and M_3 in sections 2-4, use is made of loading cases 2, 4 and 6, while, here too, loading case 3 is used as control.

The accuracy on the coefficients has been determined on the basis of an estimate of the accuracy on the measured signals and the internal forces.

A loading case which is thought to represent a realistic operating situation of the blade at wind velocities of about 12 m/sec. has been considered. It was found that in this example the standard deviation on N_1 in section 1 corresponded to about 7% of the magnitude of the internal force.

For M_1, the standard deviation corresponded to about 5-10% of the biggest internal force along the blade. For M_2 and M_3, the corresponding figures were about 4% and 5%.

A complete description of the laboratory tests is given in ref. 3.

4. FIELD MEASUREMENTS

4.1. General remarks

The content of the field program is outlined in table 3. As already mentioned in chapter 2 the field measurements aim at a description of the characteristics of the Gedser windmill as well as the collection of data that may be used in the evaluation of models for windmill analysis.

The measurements are performed both as continuous long term measurements and as short term measurements. The long term measurements are carried out for a limited number of parameters (electric power output and parameters describing the climatological wind data) and they aim at the investigation of the long term performance of the windmill. The short term measurements comprise in principle all the parameters involved. The measurements are carried out in sessions of runs covering different relevant wind conditions. During these sessions a scanning rate of 50 scans/sec is used and the results are recorded on magnetic tape, the rotor signals being transferred by wireless telemetry.

The short term measurements provide data that can be applied for detailed investigation of the aerodynamics and the structural response of the rotor together with the dynamic behaviour and power performance of the system.

The instrumentation lay-out is slowly scematically in figs. 8 to 10 and consists of the instrument groups shown in tables 4 to 7. Fig. 11 shows a plan of the site.

4.2. Meteorological measurements

The aerodynamic performance of the windmill and the dynamic loading are strongly related to the structure of the windfield, whose most dominant features are the wind profile and the turbulence structure. The measurements consist of a long term part during which the wind and temperature profiles are determined, and a short term part during which the turbulence structure is determined.

The undestructed windfield is measured along a 48 m tower erected 25 m to the west of the mill (fig.12). The instrument groups 9 to 11 (tables 4 and 5) are mounted in heights varying from 12 to 36 m. During long term measurements results from instrument group 10 are stored in digital form on magnetic tapes as 10 min averages. During short term measurements results from the "sonic" anemometers group 9 are stored in digital form on magnetic tape together with results from group 11 instruments in hub height.

Besides characterizing the meteorology of the site these measurements provide input to aerodynamic models and together with power output recordings result in the power characteristic of the mill.

4.3. Power measurements

During the previous period of operation of the Gedser windmill the long term power pro-
duction versus long term wind energy flux was determined (ref. 4). It was also found
that the power output of the generator fluctuated at a frequency of approx. 0.7 cps.
The purpose of the present power performance investigation is to supplement these ear-
lier findings with more detailed data in an effort to find an explanation for the fluc-
tuations in power output.

Both the mechanical and electrical power output are measured. The transmission shaft
torque is measured by strain-gauges (group 7) and the actual rotor speed is obtained
by a pulse counter giving one pulse/degree (group 6). Both the active and reactiv po-
wer of the generator are recorded (group 8) and the power quality in terms of peaks
of voltage and current is investigated for different wind conditions.

Long term measurements of the electric power production versus wind speed are per-
formed using 10 min. averages (channel groups 8 and 10). During short term measure-
ments the power curve is determined by measuring short time average of wind speed
at hub height together with short time average of shaft power and electrical power
(channel groups 7 and 10). The averaging is performed on the spot by means of a
microprocessor specially designed for quick power curve determination. However, the
instantaneous values of wind speed and power measured by channel groups 7, 8, 9 and
10 are stored on tape so that the original data are available for later processing.
10 min. avarages of electric power are also collected by the Aanderaa recorder (table 6).

The measurements are made for various degrees of turbulence, and the sensitivity to
skew wind is estimated.

4.4. Aerodynamic load and structural response

The Gedser windmill has a fixed pitch rotor which operates at constant angular velocity.
At low wind speeds the blades are not stalled but as the wind speed increases, stall
progresses from the inward portion of the blades towards the tips. Since theory can on-
ly give very uncertain information about rotor efficienty and loading in this condition,
the extent of stall is measured by the differential pressure transducers group 2 distri-
buted along blade 3, cf. fig.10. On the same blade a number of wool strips have been
mounted on the leaward side also to indicate stall. These measurements provide data
that can be compared with results from aerodynamic models.

It seems reasonable to assume that the overall behaviour of the blades of a modern wind
generating turbine can be determined by a suitable beam model. The results of the mea-
surements therefore should be applicable in the selection of a proper beam model and
in the verification of its applicability. Therefore section forces are measured at sta-
tions where the assumptions of a beam model can be considered valid, i.e. in some dis-
tance from stays etc. Forces from stays etc. are measured directly in order to make

each blade statically determinate. Blade 3 has the full instrumentation (group 1 and 2 transducers) while the stand by instrumentation on blade 2 (group 3) does not include pressure transducers. A limited number of wireless telemetry channels being available it was considered necessary to concentrate the instrumentation on single blades in order to obtain reasonable detailed information on the blade behaviour.

Besides recording the stresses in the rotor these measurements provide data that can be compared with results from structural models. Furthermore aerodynamic load averages can be computed from the section forces.

While there are no accelerometers in the blades due to cross sensitivity to the centrifugal forces, yaw rate and accelerations of the nacelle are recorded by transducer group 4. These measurements indicate tower vibrations and gyro moments on the rotor.

Furthermore, the total forces and moments acting on the tower top are recorded by the strain gauge channels group 4, mounted on a thin walled steel cylinder connecting the nacelle and the tower top. This steel cylinder was also applied for measurements during the previous test period (ref. 4), so that the present measurements therefore will be supplementary.

4.5. System dynamic behaviour

For a few wind speeds the system dynamic behaviour is recorded. The measurements mainly consists in the recording of the effects of skew wind under two conditions. In the first condition the nacelle is forced out of the wind and set free to turn into it again while wind speed (group 10), yaw rate of the nacelle (group 5) and forces/moments of the measurement cylinder (group 4) are recorded. From these measurements data for the investigation of gyro moments etc. are obtained.

In the second condition the nacelle is fixed in various angles to the wind, and measurements are made of transmission shaft torque (group 7) and electric power (group 8) in addition to the quantities mentioned above. From these measurements data for the estimation of the influence of skew wind on the power curve are obtained in addition to information on possible special dynamic effects due to skew wind.

4.6. Instrumentation

The channel lay-out is shown in figs. 8 to 10, while table 5 contains data for the applied transducers. During short term measurements the instrumentation usually consists of the tower channels and the channels from blade 3. The tower channels (from tower and nacelle) are connected by cables to a mobile recording station (bus) collecting meteorological data also. Data from blade 3 (blade tensions and differential pressures) are

transmitted by a wireless digital telemetry system having its own separate tape recorder. Alternatively data from the stand-by instrumentation on blade.2 (blade tensions only) may be transmitted by a wireless analog telemetry system connected to the mobile station.

Both telemetry systems may operate simultaneously, and all data are stored in digital form on magnetic tape, analog data being digitized by the mobile recording system. Data available as pulse counts are stored as such. When all channels are in operation a typical run at approx. 50 scans/sec has a duration of approx. 40 min, so that four consecutive periods of 10 min may be recorded. Afterwards data tapes are edited on computer and data are converted to physical units.

During long term measurements 10 min averages of meteorological data are stored on a tape recorder together with generator power. Typical tape endurance is 1 month and the tapes are analyzed on computer.

As mentioned previously a microprocessor is applied for "on the spot" determination of power characteristics. The microprocessor can operate both in an automatic mode independent of the rest of the system and in a mode integrated in the total data aquisition system. The scanning rate is 4 Hz.

During commissioning tests of the entire system most transducers have shown satisfactory performance and the problems experienced with that part of the system have been rather trivial, while the telemetry systems have posed by far the largest problems. The radio links have shown to be extremely sensitive to reflection phenomena and shadowing effects of the large number of stays. The rough conditions on the rotor where the equipment is exposed to the weather to vibrations and to a rotating gravity field have caused several mechanical failures.

4.7. Calibration and short term measurement procedure

Calibration of transducers and equipment has when possible been performed as laboratory measurements. Shaft moment transducers were easily calibrated on site, while the calibration of the measurement cylinder transducers on site was more complicated due to inexpedient details in the design of the existing cylinder (ref. 5). The sonic anemometers are calibrated at the beginning of each measurement session.

Due to the long period of time covered by the measurement program it has been necessary to define specific conditions that define zero for strain gauge readings. The following conditions have been chosen:

- Measurement cylinder gauges: Rotor in upwind position
- Rotor gauges: Blades 2 and 3, respectively, in vertical downwards position
- Shaft gauges: Brake released.

The mill is stopped during zero readings. A normal run contains the following readings:

- Zero reading

- Span check for certain channels built in span check capability

- Zero reading

- Measurements with the mill in automatic operation

Zero and span readings are recorded on separate files on the tape and they are made once for each blade to be measured. In the subsequent data conversion results are referred to the measured zero, and initial stresses are therefore not taken into account.

5. STATUS MEDIO SEPTEMBER 1978

Table 2 contains the updated scedule for the measurement program. During the spring campaign 7 runs were made at average wind speeds up to 12 m/s and instantaneous wind speeds up to 18 m/s. During these runs a 95% availability of the sensors were obtained. During the summer, preliminary data processing was made, mainly consisting in the conversion of data from a selected run to physical units, and spot checks on these data were made. The work done so far is described in the interim report (ref. 6). The start of the autumn campaign have been postphoned by approx. 1½ month due to repair work on the transmission of the mill.

6. PRELIMINARY RESULTS

The preliminary results listed here are extracted from the interim report ref. 6. The plots figs. 13 - 17 show the records from a short run including start and stop of the mill. The symbols used refer to table 6 and fig. 20. This is the run used for spot checks. The average wind speed was approx. 12 m/s.

The most important results, based on the preliminary data processing, are listed below:

The quality of the records

- The records are generally sufficiently detailed for meaningful frequency analysis. Fig. 18 shows details of some of the records, and fig. 19 shows the result of a preliminary frequency analysis of the electric power output.

- The records are almost free of noise.

- The spot checks indicated very few channel malfunctions. However, a small number of channels suffer from calibration problems.

The interpretation of the records

- During spot checks some problems became apparent, primarily:

  - Unknown external forces during zero runs may cause problems in the interpretation of results from the rotor sens   (groups 1 and 3) and the measurement cylinder gauges (group 4).

  - The calculation of external forces from the measured data demands very detailed and accurate modelling of the structure. Direct measurements of the blade deflections would be of great help.

The behaviour of the mill

- Both average stresses and stress amplitudes in the rotor assembly are small, compared to the design stress 59 MN/m^2 (600 kp/cm^2). In table 8 representative values for $\sim$ 12 m/s are listed.

- The spot checks indicate that all three blades extract an equal amount of power from the wind. Due to internal stay forces, however, the amount of mechanical power delivered from each blade seem to deviate more than 30% from the aerodynamic power.

- Both average forces and force amplitudes in the rotor assembly are listed in table 9. The outer stay forces NYS carry most of the wind load, while the outer wire forces NYB-31 and NYB-32 carry most of the gravity loads on the blades. Thus the stays and wires actually play a significant role in the distribution of forces in the rotor assembly.

- The pressure transducers indicated a stall transition zone at radius 5 to 7 meters-

- Acceleration and yaw rate levels of the nacelle are low. Gyral forces seem to be low and the run of the mill is very smooth.

- Fig. 21 shows the power curve and efficiency of the mill as determined from 10 min. averages from the long term measurements. The windspeeds are too low to show the the power cutoff due to stall. The peak efficiency appears at 8-9 m/s.

- Fig. 19 shows that a pulsation frequency of about 0.7 Hz in the electric power output is still present. The phenomenon was detected early during the operation of the mill (ref. 4), and a study of the phenomenon is going on in order to supplement investigations described in ref. 4. The power fluctuations, having amplitudes up to $\sim$ 40 kW, most probably are due to torsional vibrations of the rotating parts excited by wind turbulence, and the coupling of the asyncroneous generator to the grid may be a significant parameter.

REFERENCES

Ref. 1:   Smitt, L.W. and Bjerregaard, E.:
           "A Tentative Test Programme for the Gedser Wind Mill".
           Danish Ship Research Laboratory, SL 1251.77058.00
           Report no. 2 (April 20th 1977)

Ref. 2:   Lundsager, P., Andersen, P.S. and Petersen, E.L.:
           "Comments on the Measuring Programs Proposed for the
           Gedser Windmill".
           Risø note (May 1977).

Ref. 3:   Askegaard, V., Dyrbye, C. and Gravesen, S.:
           "Laboratory Tests on Gedser Wind Turbine's Blades".
           Structural Research Laboratory,
           Technical University of Denmark, Report S 28/77.
           (November 1977).

Ref. 4:   Danish Electric Utilities:
           "Report from the Wind Power Committee",
           (Vindkraftudvalgets Betænkning)
           Union of Danish Electric Utilities. (1962) (In Danish).

Ref. 5:   Askegaard, V. and Mossing, P.:
           "Instrumentation and Calibration of Measuring Cylinder on
           Gedser Wind Turbine".
           Structural Research Laboratory, Technical University of Denmark.
           Report S 28/77 (1978)

Ref. 6:   Lundsager, P., Christensen, C.J., Frandsen, S. (ed.)
           Interim report on the Measurements on the Gedser Windmill.
           Report GTG 771.105-1 Sept. 1978.

Table 1 Main characteristics of the Gedser mill

Rotor location	Upwind
Rotor diameter	24 m
Number of blades	3
Blade tip velocity	38 m/s
Rotational velocity	30 rpm
Rotor area	450 m^2
Blade construction	Steel, main spar, wooden webs, aluminium skin. Heavily stayed. Braking flaps in blade tips (cf. fig. 2)
Regulation	Stall regulated, no pitch control
Generator	Asyncroneous 200 kW, 750 rpm
Transmission	Double chain 1:25
Tower	Stiffened concrete cylinder, hub height 24 m
Performance	Selfstarting at 5 m/s 200 kW at 15 m/s Typical annual production 350.000 kWh/yr

Table 2   Time table as of Sept. 1978

Contract signed	Sept 77
Laboratory tests on blades 2 and 3	
Preliminary measurements	July 77
Instrumentation and calibration	Aug-Sept 77
Commissioning tests of the field equipment	
Mounting of equipment	Nov 77
Tests and modifications of equipment	Dec 77-March 78
Field tests, spring campaign	Apr-May 78
Preliminary data processing	June-Aug 78
Interim report issued	Sept 78
Commissioning of the field equipment	Oct 78
Field tests, autumn campaign	Nov 78-Feb 79

Table 3 Field measuring program

1. Meterological measurements.
    a. Long term wind measurements. Continuous sampling of 10 min. averages of wind velocity, temperature and pressure recorded at various heights.
    b. Short term wind measurements. High speed sampling during runs of the wind rotor and temperature using ultrasonic anemometers at various heights.
2. Power measurements.
    a. Determination of the power characteristics by both long and short term sampling of wind speed and mechanical/electrical power output.
    b. Investigation of aerodynamic stall effects as observed on the power curve and pressure transducer readings.
    c. Investigation of power fluctuations observed in the previous test period.
3. Structural response measurements.
    a. Rotor blade assembly. Short term high speed sampling of blade section forces and stay forces together with rotor angular position.
    b. Short term high speed sampling of transmission shaft torque together with nacelle accellerations, yaw rate and forces between nacelle and tower top, using the restored measuring cylinder.
    c. Short term high speed sampling of electrical power output and nacelle azimuthal position.

4. Additional dynamic investigations
    a. Investigation of system dynamic behaviour by short term high speed sampling during nacelle maneuvres of parameters Such as wind speed and direction, nacelle position, yaw rate, electrical power etc.

15.

Table 4 Channel groups

Group	Number of Channels	Transducers	Quantities measured
1	21	Strain gauge channels on blade 3 and adjacent stays	Blade section forces and stay forces
2	5	Differential pressure transducers on blade 3	Differential pressures on blade 3
3	19	Strain gauge channels on blade 2 and adjacent stays	Blade section forces and stay forces
4	5	Strain gauge channels on measuring cylinder	Forces between nacelle and tower top
5	4	Accelerometers in nacelle	Linear and angular accelerations, yaw rate
6	3	Pulse counters and potentiometer in nacelle	Rotor positions ($1/1^{\circ}$ and $1/360^{\circ}$) and nacelle position
7	2	Strain gauge channels on transmission shafts	Transmission and generator shaft torque
8	3	Electrical power transducers	KWATT, KVAR and Volt
9	12	Ultrasonic anemometer channels	Wind vector and temperature at 3 levels
10	9	Various	Meterological wind condition data
11	2	Anemometer and wind vane	Wind speed and direction at hub heigth

Table 5 Instrument Specifications

Group	Quantity measured	Sensor	Manufacture	Range	Output	Operating Temp.range °C	Accuracy
Blade 3							
1	Blade section forces and stay forces	Strain gauge		$\pm$ 500μStr.	$\pm$ 1 V		
2	Differential pressure (stall)	Pressure transducer	Endevco	$\pm$ 0.2 psi $\pm$ 0.4 psi	$\pm$ 1 V	-15/+40	1%
Blade 2	Blade section forces and stay forces	Strain gauge		$\pm$ 500μStr.	$\pm$ 1 V		
3							
Tower	Forces between tower/nacelle (measuring cylinder)	Strain gauge	HBM		$\pm$ 5 V	-40/+50	$\pm$ 1 μStr.
4							
Nacelle							
5	Accelerations	Accelerometer	Schavitz	$\pm$ 1 g	$\pm$ 5 V	-40/+50	1%
5	Yaw rate	Gyro	Smiths	20 deg/sec	$\pm$ 5 V	-40/+50	1%
6	Rotor position	Photo cell count	FORT	1/1 deg	TTL Pulse	-15/+40	
				1/360 deg	TTL Pulse	-15/+40	
6	Nacelle position	Potentiometer	Bourns	10 turns	$\pm$ 10 V	-40/+50	1%
7	Transmission shaft torque	Strain gauge	HBM	$\pm$ 200 μStr.	$\pm$ 5 V FM	-40/+50	2%
Generator							
8	Voltage	Trafo	BBC	3 x 380 V	$\pm$ 5 V	-40/+50	1%
8	Active power	Trafo	BBC	200 kW	$\pm$ 5 V	-40/+50	1%
8	Reactive power	Trafo	BBC	200 KVAR	$\pm$ 5 V	-40/+50	1%
Met.mast							
9	Wind vector and temperature	Ultrasonic anemometer	Kaijo Denki		$\pm$ 1 V	-20/+50	$\pm$ 3%
10	Wind speed	Cup anemometer	Aanderaa 2219			-40/+50	$\pm$ 2%
10	Wind direction	Wind vane	Aanderaa 2053	0-360° dead angle 3.5°	Connected to Anderaa tape recorder	-40/+50	$\pm$ 5%
10	Air temperature	Pt-100	Aanderaa 1289	-44/+48°C			
10	Air pressure	Barometer	Yellow springs	914-1067 mb		-35/+83°C	0.3 mb
10	Air humidity	LiCl					
11	Wind speed	Cup anomometer	Risø 70				
11	Wind direction	Wind vane	Anderaa 2053	0-360° dead angle 3.5°			

TABLE 6 CHANNELS

SENSOR NO	SYMBOL	DESCRIPTION	SENSOR GROUP
1	N11	AXIAL FORCE SECT 1	1 (BLADE 3)
2	M11	TORSIONAL MOMENT R= 1.42 M	
3	M21	BENDING MOMENT, CHORDWISE	
4	M31	BENDING MOMENT, FLAPWISE	
5	M12	TORSIONAL MOMENT SECT 2	
6	M22	BENDING MOMENT, CHORDWISE R= 4.72 M	
7	M32	BENDING MOMENT, FLAPWISE	(MAY BE
8	M13	TORSIONAL MOMENT SECT 3	
9	M23	BENDING MOMENT, CHORDWISE R= 7.63 M	REPLACED
10	M33	BENDING MOMENT, FLAPWISE	BY GROUP
11	M14	TORSIONAL MOMENT SECT 4	
12	M24	BENDING MOMENT, CHORDWISE R= 9.56 M	3 BLADE 2)
13	M34	BENDING MOMENT, FLAPWISE	
14	NIS	FORCE, INNER STAY	
15	NYS	FORCE, OUTER STAY	
16	NYB-31	FORCE, OUTER STAY FROM BLADE 3 TO BLADE 1	
17	NYB-32	FORCE, OUTER STAY FROM BLADE 3 TO BLADE 2	
18	NIB-31	FORCE, INNER STAY FROM BLADE 3 TO BLADE 1	
19	NIB-32	FORCE, INNER STAY FROM BLADE 3 TO BLADE 2	
20	NBS-31	FORCE, WIRE TO OUTER STAY FROM BLADE 3 TO BLADE 1	
21	NBS-32	FORCE, WIRE TO OUTER STAY FROM BLADE 3 TO BLADE 2	
22	PA	DIFFERENTIAL PRESSURE R= 3.56 M	
23	PB	DIFFERENTIAL PRESSURE R= 5.02 M	2
24	PC	DIFFERENTIAL PRESSURE R= 6.85 M	
25	PD	DIFFERENTIAL PRESSURE R= 7.94 M	BLADE 3
26	PE	DIFFERENTIAL PRESSURE R= 10.35 M	
27	P1	HORIZONTAL FORCE X_1-DIRECTION	
28	P2	HORIZONTAL FORCE X_2-DIRECTION	4
29	M1	TILTING MOMENT X_1-DIRECTION	
30	M2	TILTING MOMENT X_2-DIRECTION	MEAS. CYL.
31	M3	TORSIONAL MOMENT X_3-DIRECTION	
32	Y	YAW RATE	
33	ẍ	ACCELLERATION X-DIRECTION	5
34	ÿ	ACCELLERATION Y-DIRECTION	NACELLE
35	φ̈	ACCELLERATION ω (ANGULAR)	
36	-	ROTORPOSITION 1 PULSE/360°	6
37	-	1 PULSE/1°	NACELLE
38	φ	NACELLE POSITION	
39	Mg	GENERATOR SHAFT TORQUE	7
40	Ms	SECONDARY SHAFT TORQUE	NACELLE
41	-	KVAR	8
42	W	KWATT	NACELLE
43	-	VOLT	
46	VA-12	X-COMPONENT WINDSPEED	
47	VB-12	Y-COMPONENT WINDSPEED 12 M	9
48	VC-12	Z-COMPONENT WINDSPEED	
49	T-12	TEMPERATURE	MET. TOWER
50	VA-24	X-COMPONENT WINDSPEED	
51	VB-24	Y-COMPONENT WINDSPEED 24 M	
52	VC-24	Z-COMPONENT WINDSPEED	
53	T-24	TEMPERATURE	
54	VA-36	X-COMPONENT WINDSPEED	
55	VB-36	Y-COMPONENT WINDSPEED 36 M	
56	VC-36	Z-COMPONENT WINDSPEED	
57	T-36	TEMPERATURE	
58		HORIZONTAL WINDSPEED 6 M	
59		HORIZONTAL WINDSPEED 12 M	10
60		HORIZONTAL WINDSPEED 24 M	
61		HORIZONTAL WINDSPEED 36 M	MET. TOWER
62		WIND DIRECTION 6 M	
63		WIND DIRECTION 12 M	
64		WIND DIRECTION 24 M	
65		WIND DIRECTION 36 M	
66		AIR TEMPERATURE 12 M	
67		AIR TEMPERATURE 36 M	
68		KWATT	NACELLE
44	V	HORIZONTAL WINDSPEED 24 M	11
45	0	WIND DIRECTION 24 M	MET. TOWER

TABLE 7 Backup channels

SENSOR NO	SYMBOL	DESCRIPTION		SENSOR GROUP
69	N11	AXIAL FORCE	SECT 1	3 (BLADE 2)
70	M11	TORSIONAL MOMENT	R= 1.42 M	
71	M21	BENDING MOMENT, CHORDWISE		
72	M31	BENDING MOMENT, FLAPWISE		
73	M12	TORSIONAL MOMENT	SECT 2	
74	M22	BENDING MOMENT, CHORDWISE	R= 4.72 M	
75	M32	BENDING MOMENT, FLAPWISE		
76	M13	TORSIONAL MOMENT	SECT 3	(MAY REPLACE GROUP 1 BLADE 3)
77	M23	BENDING MOMENT, CHORDWISE	R= 7.63 M	
78	M33	BENDING MOMENT, FLAPWISE		
79	M14	TORSIONAL MOMENT	SECT 4	
80	M24	BENDING MOMENT, CHORDWISE	R= 9.56 M	
81	M34	BENDING MOMENT, FLAPWISE		
82	NIS	FORCE, INNER STAY		
83	NYS	FORCE, OUTER STAY		
84	NYB-21	FORCE, OUTER STAY FROM BLADE 2 TO BLADE 1		
85	NIB-21	FORCE, INNER STAY FROM BLADE 2 TO BLADE 1		
86	NBS-21	FORCE, WIRE TO OUTER STAY FROM BLADE 2 TO BLADE 1		
87	NBS-23	FORCE, WIRE TO OUTER STAY FROM BLADE 2 TO BLADE 3		

Table 8   Representative stresses, blade 3

Channel no	Sensor	A/I (m^2) (m^4)	e m	Zero run $\pm \Delta\sigma_o$ MN/m^2	Run $\sigma \pm \Delta\sigma$ MN/m^2
1	N11	1.43E-2	–	$\pm$ 1.87	1.88 $\pm$ 1.85
2	M11	–			
3	M21	1.52E-4	.137	$\pm$ 6.08	$\pm$ 17.9 $\pm$ 8.97
4	M31	7.62E-5	.085	$\pm$ 2.16	$\pm$ 3.46 $\pm$ 4.13
5	M12				
6	M22	2.49E-4	.122	$\pm$ 0.48	$\pm$ 4.63 $\pm$ 0.96
7	M23	7.09E-5	.085	$\pm$ 0.98	$\pm$ 0.68 $\pm$ 0.79
8	M13				
9	M23	1.79E-4	.109	$\pm$ 0.19	$\pm$ 2.81 $\pm$ 0.27
10	M33	4.04E-5	.085	$\pm$ 2.40	$\pm$ 4.36 $\pm$ 1.91
11	M14				
12	M24	1.51E-4	.101	$\pm$ 0.65	$\pm$ 2.29 $\pm$ 0.81
13	M34	3.69E-5	.085	$\pm$ 2.30	$\pm$ 1.58 $\pm$ 0.39
14	NIS	1.31E-3	–	$\pm$ 1.68	4.89 $\pm$ 2.73
15	NYS	1.61E-3	–	$\pm$ 0.99	11.9 $\pm$ 3.45
16	NYB-31	1.39E-3	–	$\pm$ 7.27	9.71 $\pm$ 7.09
17	NYB-32	1.40E-3	–	$\pm$ 7.57	8.07 $\pm$ 7.57
18	NIB-31	2.45E-4	–	$\pm$ 5.31	9.47 $\pm$ 2.94
19	NIB-32	3.05E-4	–	$\pm$ 8.49	9.97 $\pm$ 8.00
20	NBS-31	2.55E-4	–	$\pm$ 0.51	3.92 $\pm$ 0.51
21	NBS-32	2.30E-4	–	$\pm$ 3.83	5.04 $\pm$ 3.82

1 MN/m^2 = 9.81 kp/cm^2

Table 9   Representative forces in blade 3

Channel no.	Sensor	Zero run ΔF_o	F_o	Run ΔF	F	Unit
1	N11	53.6	$\pm$ 26.8	52.8	26.9 $\pm$ 26.4	kN
2	M11	1.02	$\pm$ 0.51	1.02	- 0.57 $\pm$ 0.51	kNm
3	M21	13.5	$\pm$ 6.75	8.36	19.9 $\pm$ 9.95	kNm
4	M31	3.88	$\pm$ 1.94	7.39	- 3.10 $\pm$ 3.70	kNm
5	M12	1.64	$\pm$ 0.82	1.89	0.13 $\pm$ 0.95	kNm
6	M22	1.96	$\pm$ 0.98	3.92	9.45 $\pm$ 1.96	kNm
7	M32	1.64	$\pm$ 0.82	1.31	0.57 $\pm$ 0.66	kNm
8	M13	1.66	$\pm$ 0.83	1.79	- 0.32 $\pm$ 0.90	kNm
9	M23	0.62	$\pm$ 0.31	0.87	4.61 $\pm$ 0.44	kNm
10	M33	2.28	$\pm$ 1.14	1.82	- 2.07 $\pm$ 0.91	kNm
11	M14	0.66	$\pm$ 0.33	0.64	- 0.46 $\pm$ 0.32	kNm
12	M24	1.93	$\pm$ 0.97	2.42	3.43 $\pm$ 1.21	kNm
13	M34	0.77	$\pm$ 0.39	1.16	2.36 $\pm$ 0.58	kNm
14	NIS	4.40	$\pm$ 2.20	7.16	6.40 $\pm$ 3.58	kN
15	NYS	3.17	$\pm$ 1.59	11.1	19.2 $\pm$ 5.55	kN
16	NYB-31	20.2	$\pm$ 10.1	19.7	13.5 $\pm$ 9.85	kN
17	NYB-32	21.1	$\pm$ 10.6	21.1	11.3 $\pm$ 10.6	kN
18	NIB-31	2.60	$\pm$ 1.30	1.43	2.32 $\pm$ 0.72	kN
19	NIB-32	5.17	$\pm$ 2.59	4.87	3.04 $\pm$ 2.44	kN
20	NBS-31	0.25	$\pm$ 0.13	0.25	1.00 $\pm$ 0.13	kN
21	NBS-32	1.75	$\pm$ 0.88	1.75	1.16 $\pm$ 0.88	kN
22	PA	-	-	-	- -	kN/m^2
23	PB	0.068	$\pm$ 0.034	0.077	- .119 $\pm$ .039	kN/m^2
24	PC	0.064	$\pm$ 0.032	0.319	- .576 $\pm$ .160	kN/m^2
25	PD	0.165	$\pm$ 0.083	0.297	- .614 $\pm$ .149	kN/m^2
26	PE	-	-	-	- -	kN/m^2

Figure Captions

Fig. 1   The Gedser windmill

        1 Vertical tube of the tower

        2 Buttresses

        3 Foundation

        4 Measuring cylinder

        5 Service platform

        6 External ladder

        7 Transformer house

Fig. 2   The Gedser windmill rotor

Fig. 3   The blade design

        1 Brake flap

        2 Rod for brake flap

        3 Link motion

        4 Steel main spar

        5 Hydraulic cylinder

Fig. 4   The laboratory test setup

Fig. 5   Sketch of the rotor assembly. Channel numbers and symbols refer to tables 6 and 7

Fig. 6   Sketch of the blade 3 assembly showing coordinate system, instrumented cross sections and strain gauge combinations

        Gauge type: Hottinger 6-120 XY-21, XY-11 and LY-11

        Cement: Hottinger X60

        Moisture

        protection: Silicagel, Philips PR 9258/00

                    Neoprene foam rubber, glass fabric

Fig. 7   Calibration curves for blade gauges for the load P_2 at the tip

Fig. 8   Diagram for the data flow during short term measurements

Fig. 9   Diagram for the data flow during long term measurements

Fig. 10   Sensor locations for the entire instrumentation. Numbers refer to tables 6 and 7

Fig. 1   The Gedser windmill

1   Vertical tube of the tower
2   Buttresses
3   Foundation
4   Measuring cylinder
5   Service platform
6   External ladder
7   Transformer house.

Fig. 2 The Gedser windmill rotor

Fig. 3   Blade design

1   Brake flap
2   Rod for brake flap
3   Link motion
4   Steel main spar
5   Hydraulic cylinder.

Fig. 4.   The laboratory test setup

(n) measuring point number (stays)

BLADE 3 (Table 5.1)			BLADE 2 (Table 5.1a)		
(n)	Channel	Symbol	(n)	Channel	Symbol
1	14	HIS	9	02	HIS
2	19	HIB-32	10	05	HIB-21
3	21	HBS-32	11	06	HBS-21
4	20	HBS-31	12	07	HBS-23
5	18	HIB-31			
6	15	HYS	13	03	HYS
7	17	HYB-32	14	04	HYB-21
8	16	HYB-31			

Fig. 5   Sketch of the rotor assembly. Numbers
refer to the stay sensors. (Table 5.1)
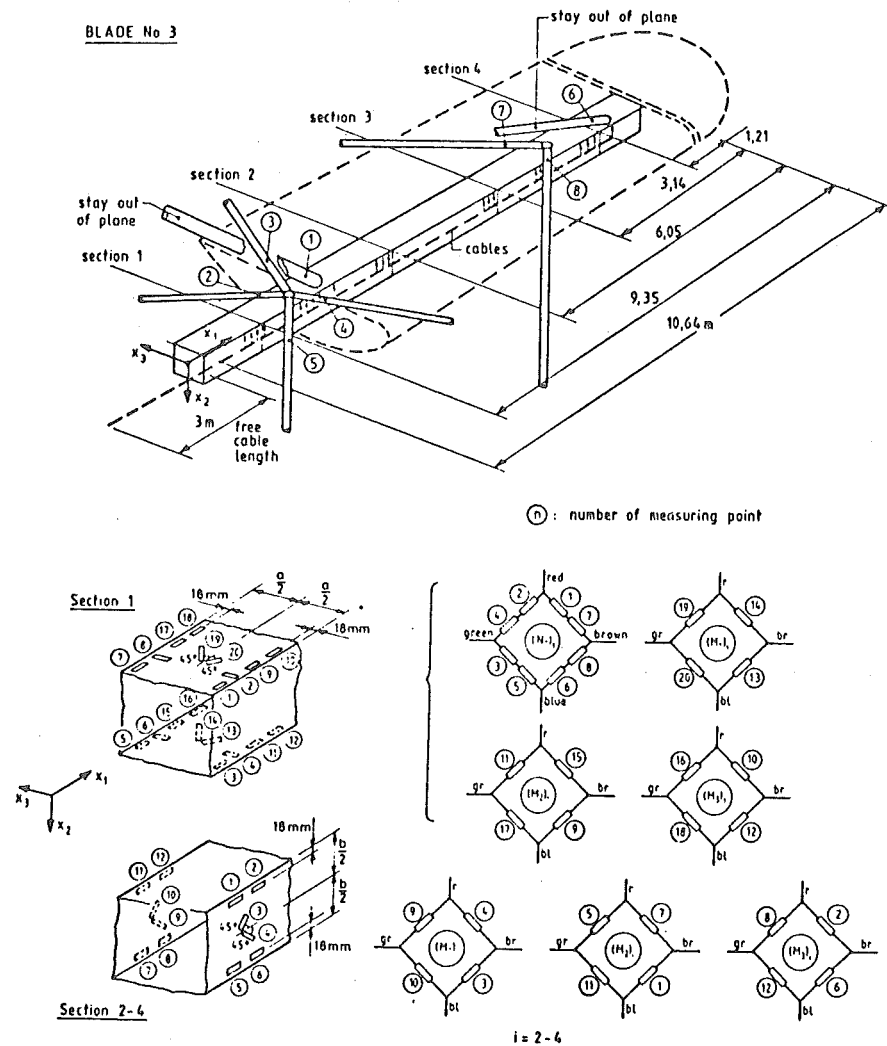
Fig. 6   Sketch of the blade 3 assembly showing coordinate system,
          instrumented cross sections and strain gauge combinations

          Gauge type: Hottinger 6-120 XY-21, XY-11 and LY-11

          Cement: Hottinger X60

          Moisture

          protection: Silicagel, Philips PR 9258/00

                      Neoprene foam rubber, glass fabric
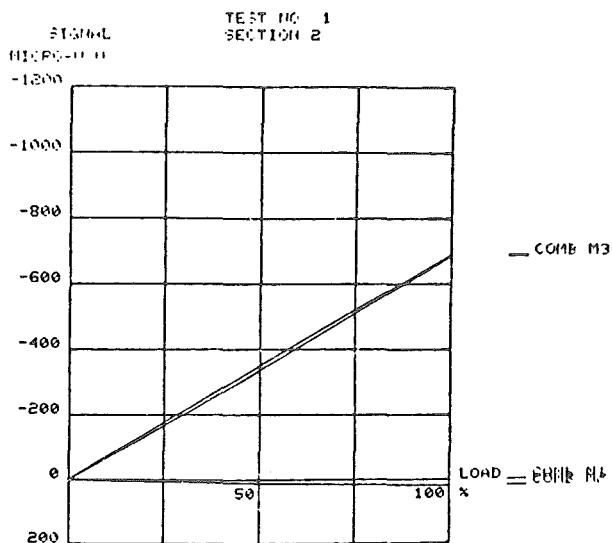
Fig. 7 Representative calibration curve for
gauge combination of blade·3.
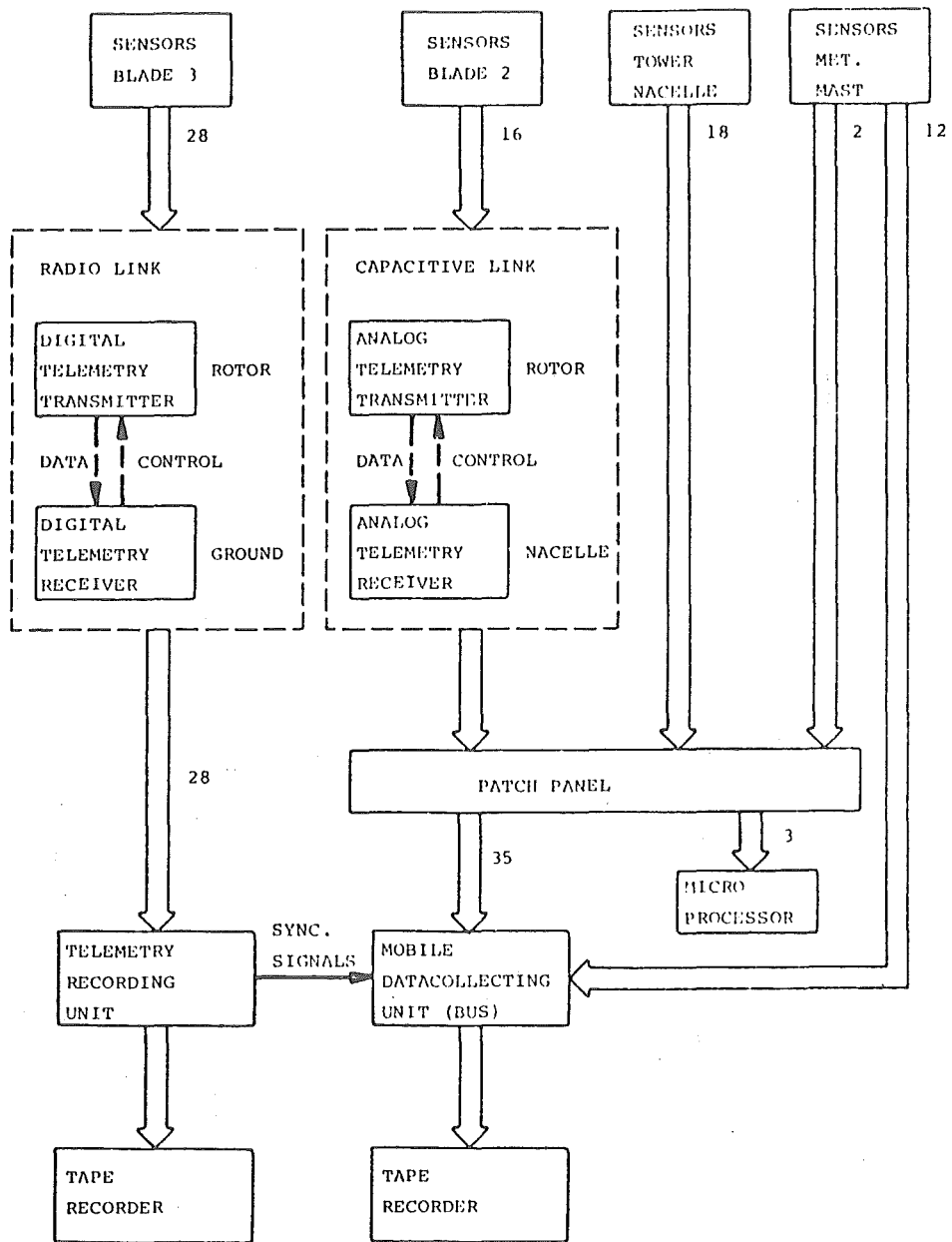
Fig. 8 Diagram for the data flow during
short term measurements.
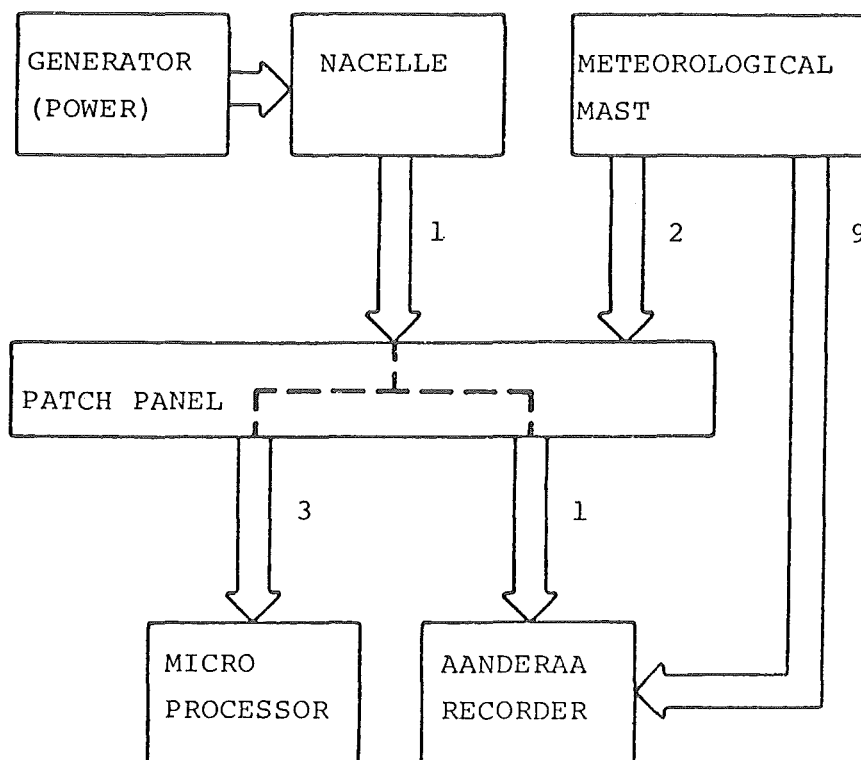
Fig. 9. Diagram for the data flow during
short term measurements
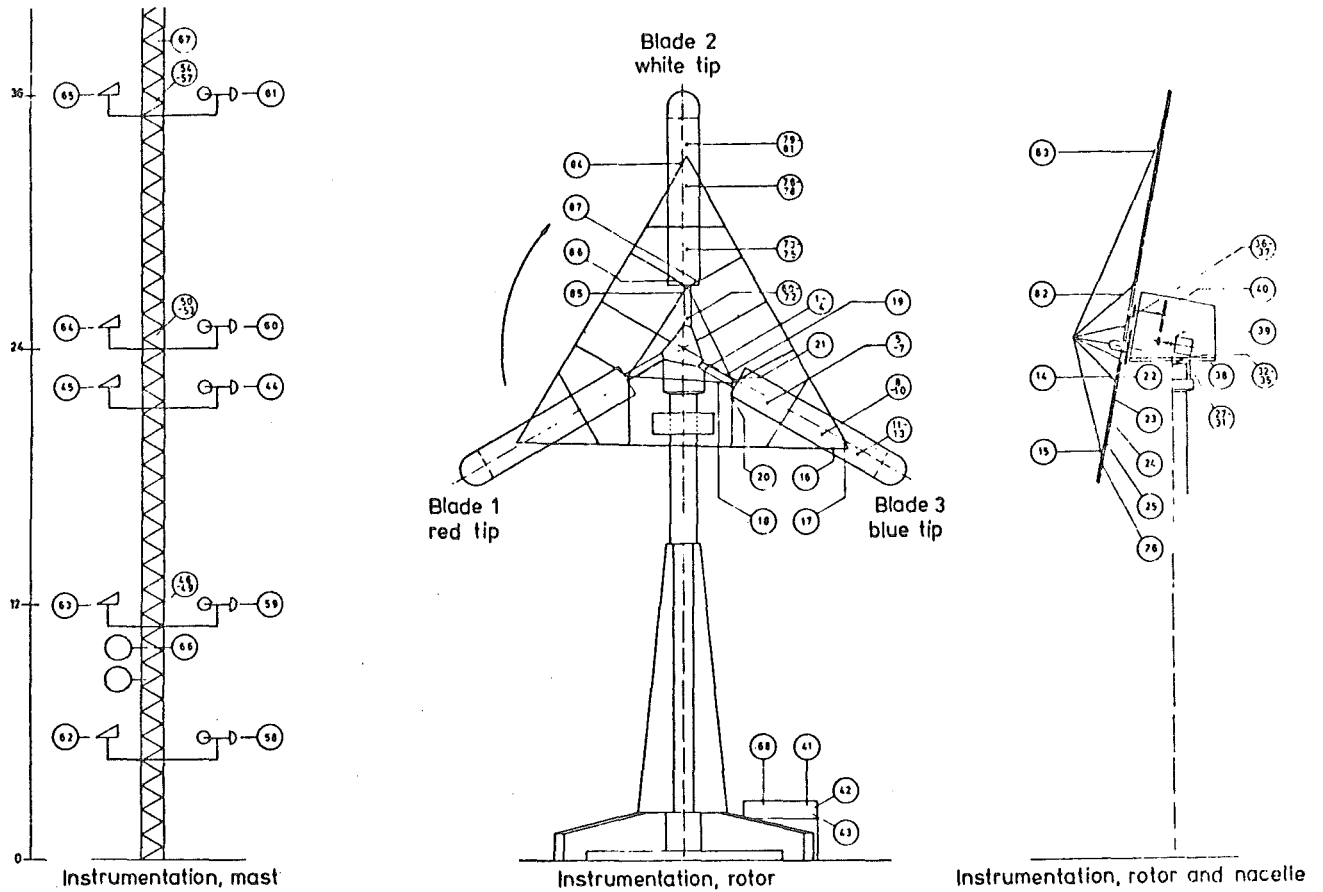
Fig. 10   Sensor locations for the entire instrumentation. Numbers refer to
          tables 6 and 7
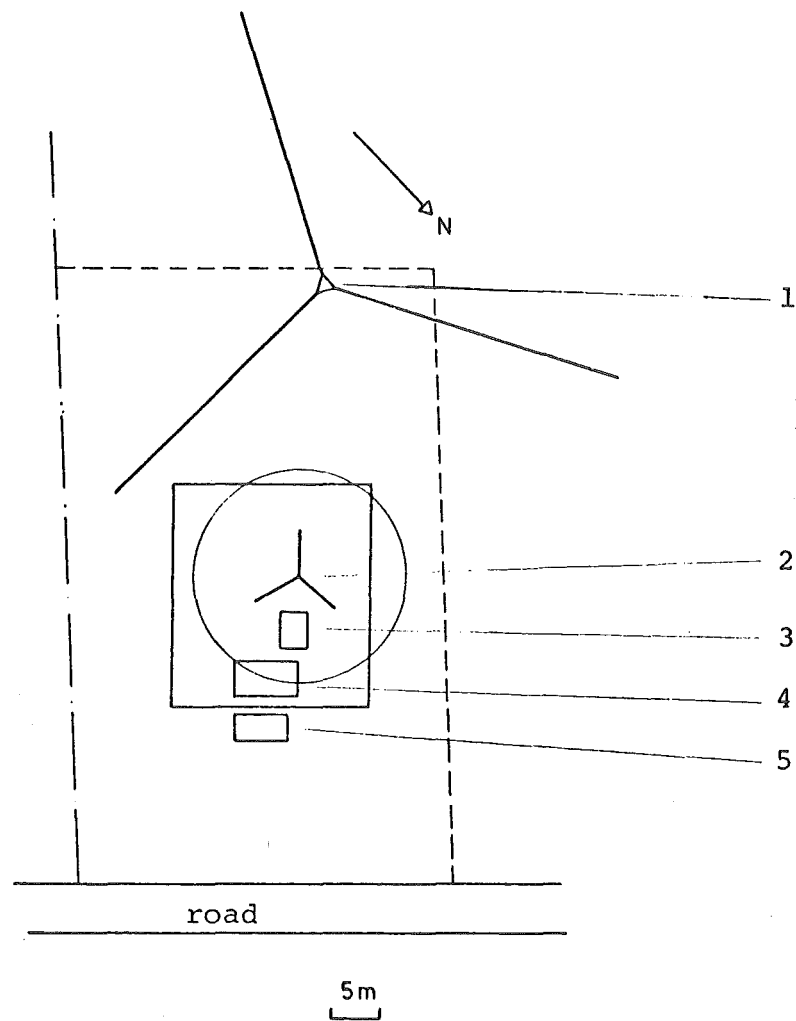
Fig. 11   Plan of the Gedser windmill site.

1   Meteorological tower
2   The mill
3   Transformer house
4   The instrument hut
5   The bus
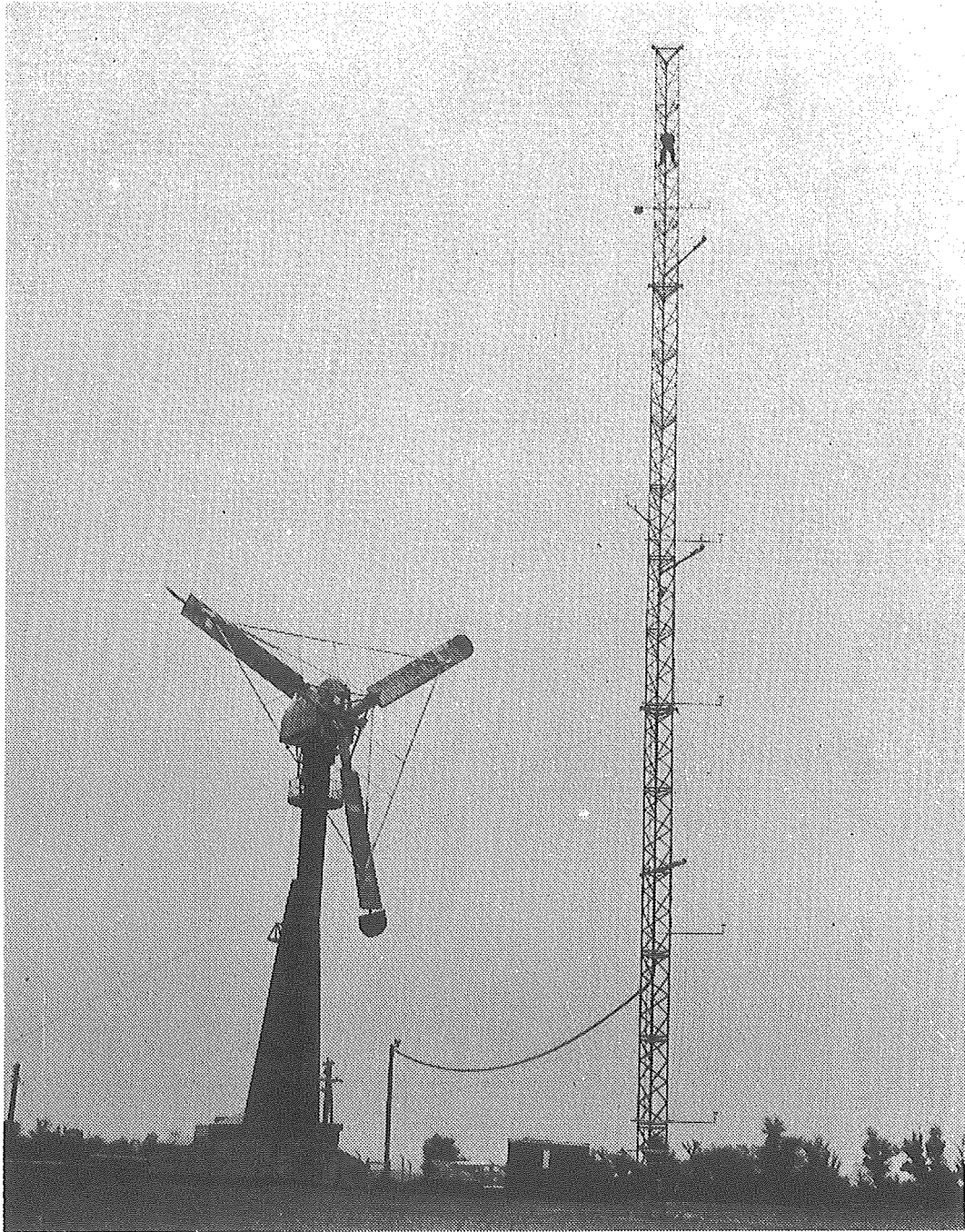
Fig. 12 The mill and the meteorological tower

RAWPLOT OF GEDSER2156/3/5

MEASURE CYLINDER P1 — P1 — 147KN — 0
MEASURE CYLINDER P2 — P2 — 45KN — 0
MEASURE CYLINDER M1 — M1 — 158 kNm — 0
MEASURE CYLINDER M2 — M2 — 166 kNm — 3
MEASURE CYLINDER M3 — M3 — 123 kNm — 0
KVAR — 96 KVAR — 0
POWER — POWER — 215 kW — 0
WINDSPEED, 25m — WIND SPEED — 17.4 m/s — S·7
WIND-DIRECTION — WIND DIR. SENSE — DUBIOUS

FIG 13

Figs.
13 - 17   Plots showing representative results from a short run including
           start and stop. The symbols refer to tables 6 and 7. Data are
           block-averaged over 10 scans. The range of each channel in physical
           units are listed, and zero is indicated. Arrows for syncronizing the
           plots together are shown on the time axes

Figs.
13 - 17 - Plots showing representative results from a short run including start and stop. The symbols refer to tables 6 and 7. Data are block-averaged over 10 scans. The range of each channel in physical units are listed, and zero is indicated. Arrows for syncronizing the plots together are shown on the time axes

GEDSER 2157. 28-4-78; NY FORST;

- 88 -
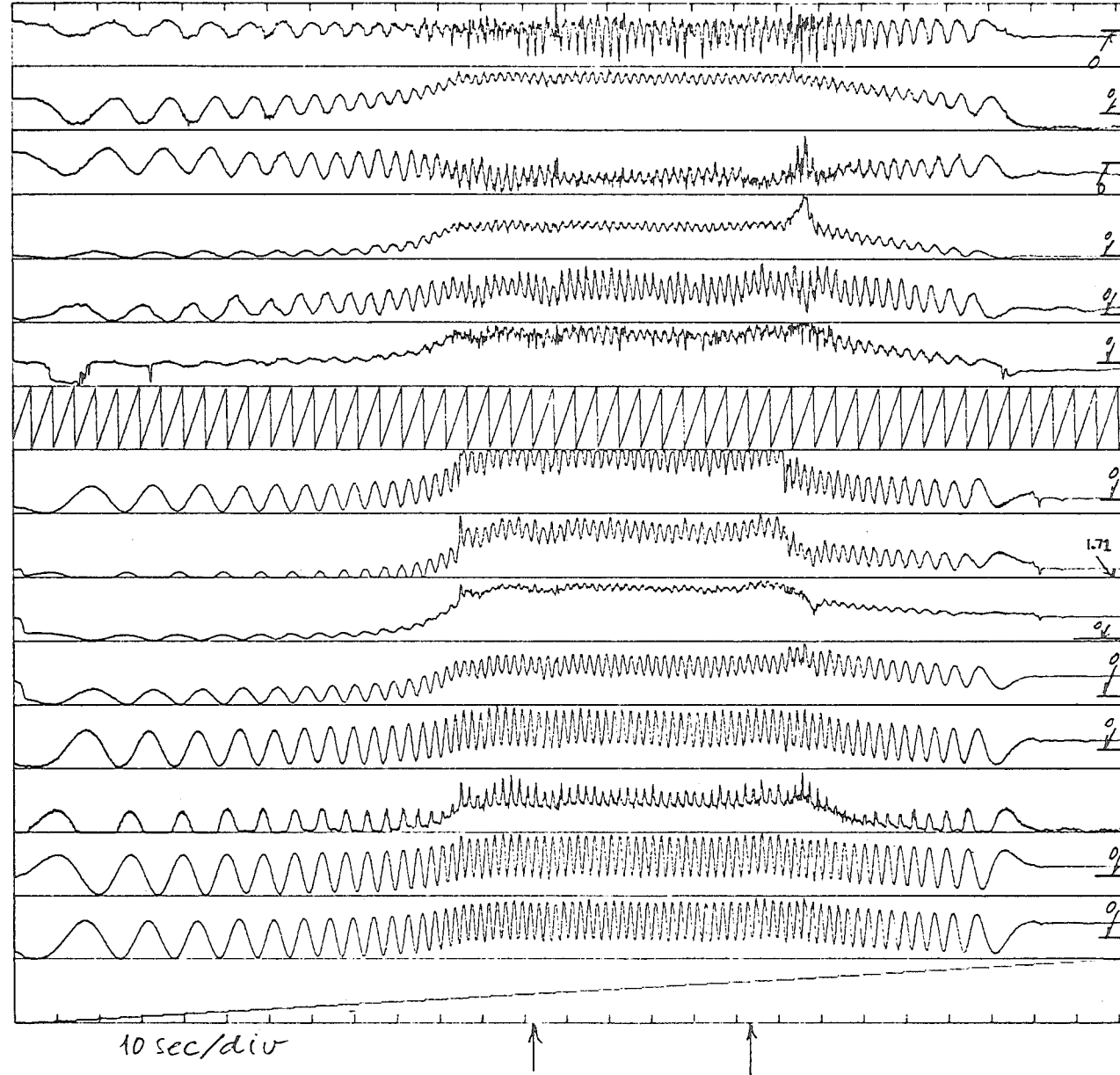
13.5 kNm	M31/3
4.1 kNm	M32/3
5.7 kNm	M33/3
5.8 kNm	M34/3
13.8 kN	NIS
39.5 kN	NYS
FASTTIMER	50 %/s
30 kNm	M21/3
12.3 kNm	M22/3
6.2 kNm	M23/3
7.3 kNm	M24/3
9.1 kN	NIB32
3.9 kN	NIB31
34.3 kN	NYB32
73.6 kN	NYB31
SLOW TIMER	50/256 c/s

10 sec/div

FIG 15

GEDSER2157, 28-4-78; NY FORST;
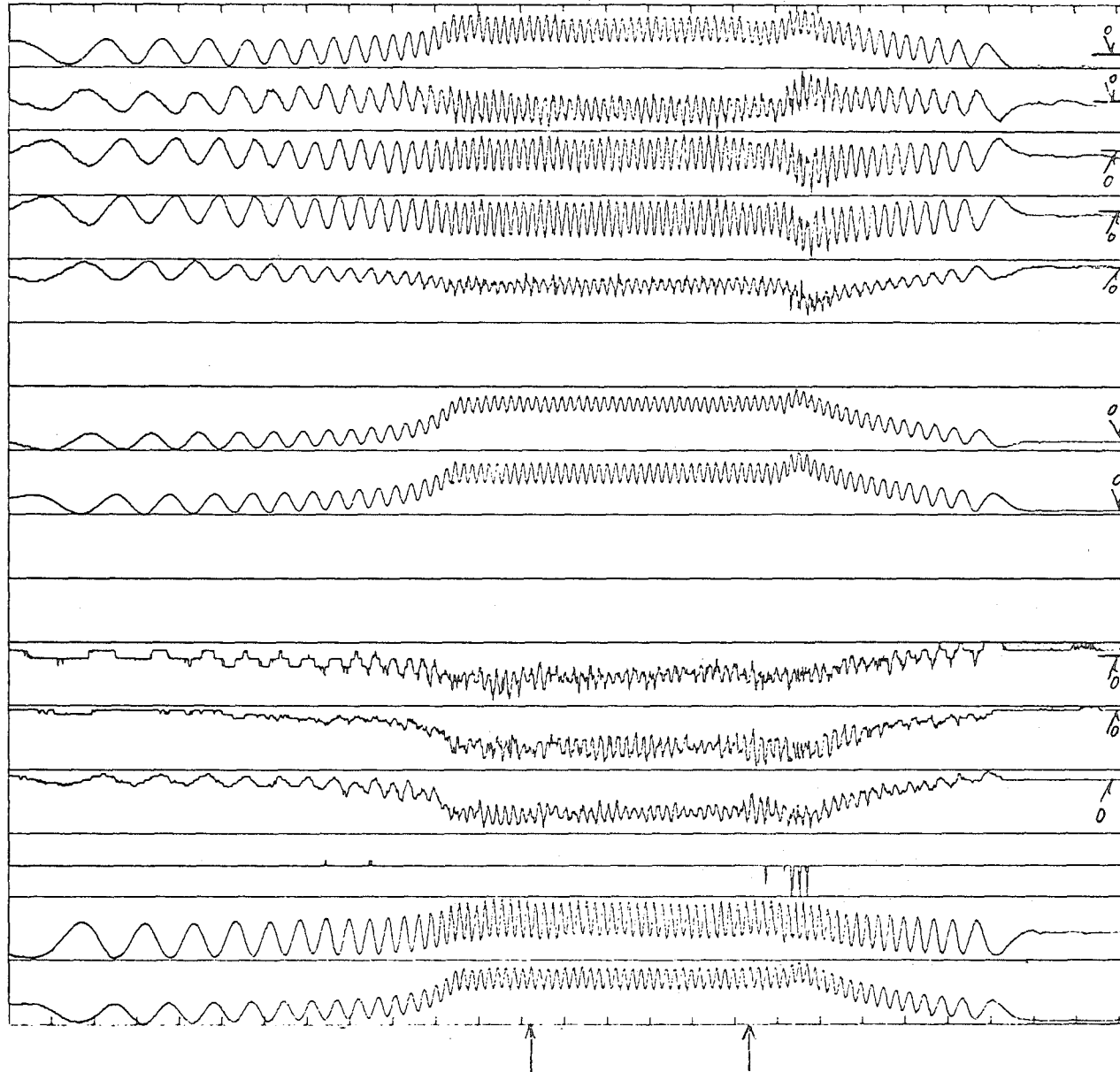
132 kN	N 11/3
3.1 kNm	M 11/3
3.5 kNm	M 12/3
3.4 kNm	M 13/3
2.5 kNm	M 14/3
2.1 kN	NBS31
2.3 kN	NBS32
(PA)	
250 N/m²	PB
960 N/m²	PC
990 N/m²	PD
(PE)	

FIG. 16

Figs. 13 - 17   Plots showing representative results from a short run including start and stop. The symbols refer to tables 6 and 7. Data are block-averaged over 10 scans. The range of each channel in physical units are listed, and zero is indicated. Arrows for syncronizing the plots together are shown on the time axes

RAWPLOT OF GEDSER2156/B/5

Figs.
13 - 17   Plots showing representative results from a short run including
           start and stop. The symbols refer to tables 6 and 7. Data are
           block-averaged over 10 scans. The range of each channel in physical
           units are listed, and zero is indicated. Arrows for syncronizing the
           plots together are shown on the time axes

Fig. 18 Full resolution plots of some channels

GEDSER TELE2157.28-4-78.1 SEC PR. DELING.2 SC/BL..

- 91 -
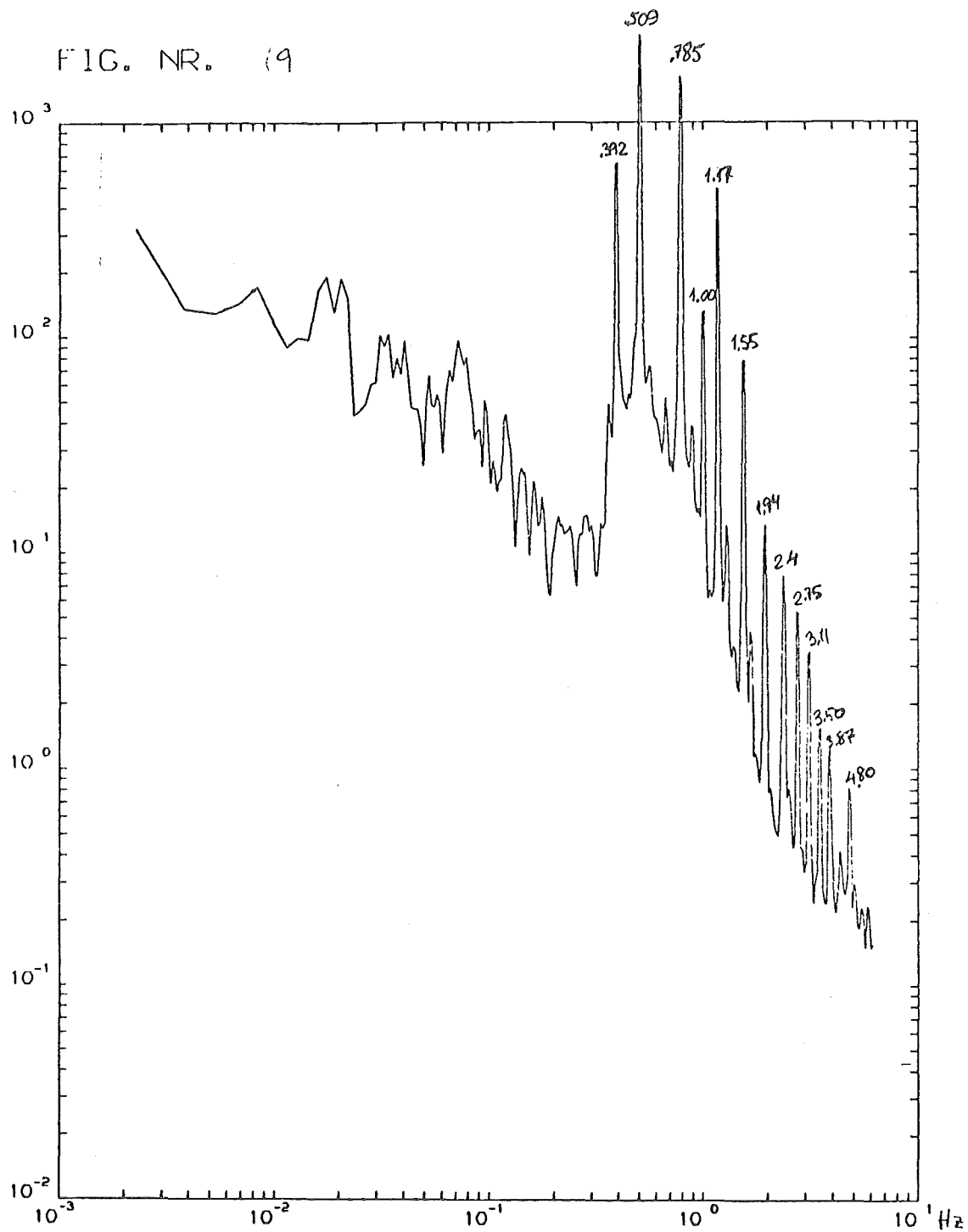
Fig. 19.   Electric power. Power spectrum multiplied by
frequency. Ordinate arbitrary units.

BLADE 3
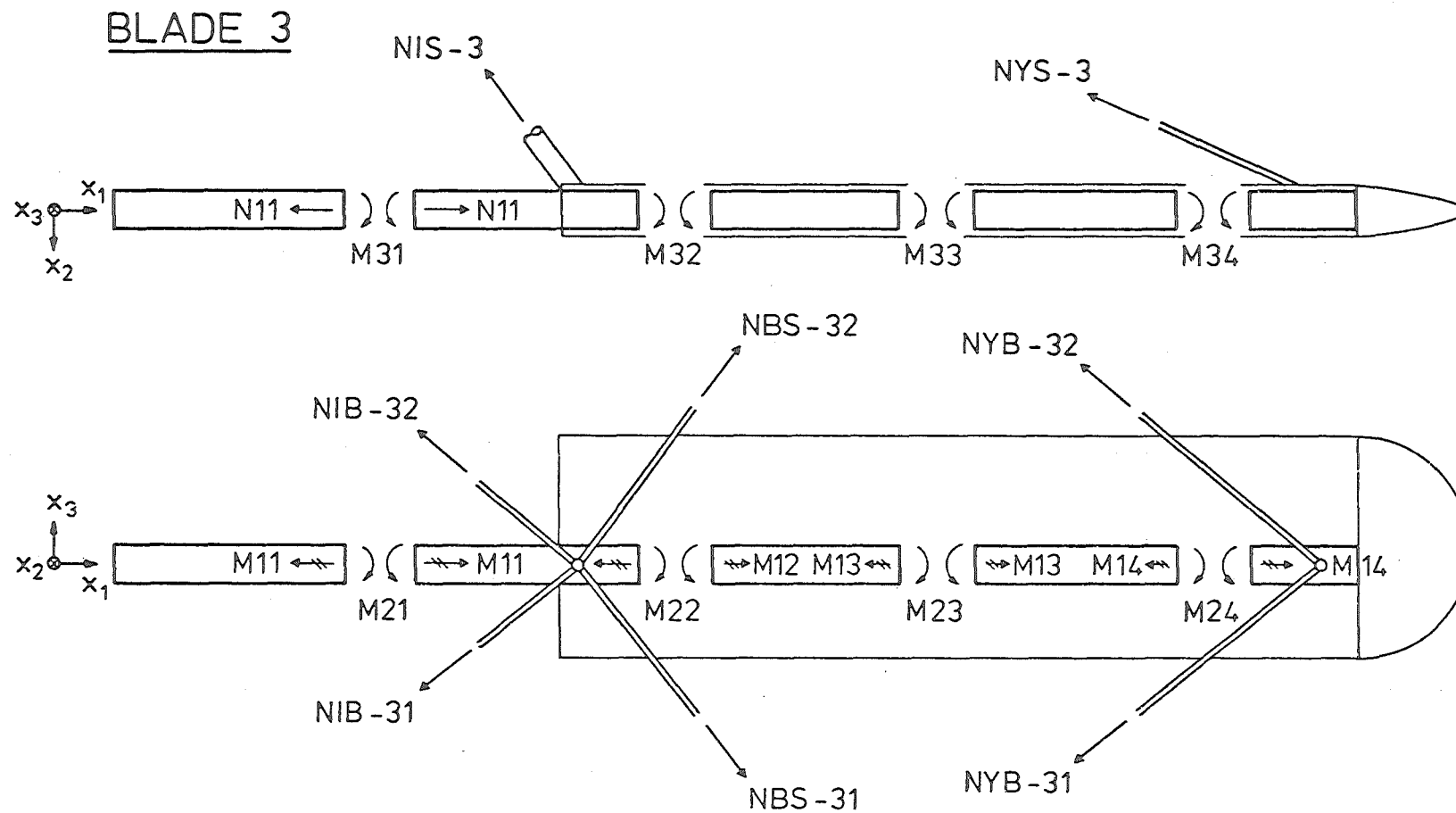
Fig. 20   Sketch showing the definition of cross
          sectional forces.
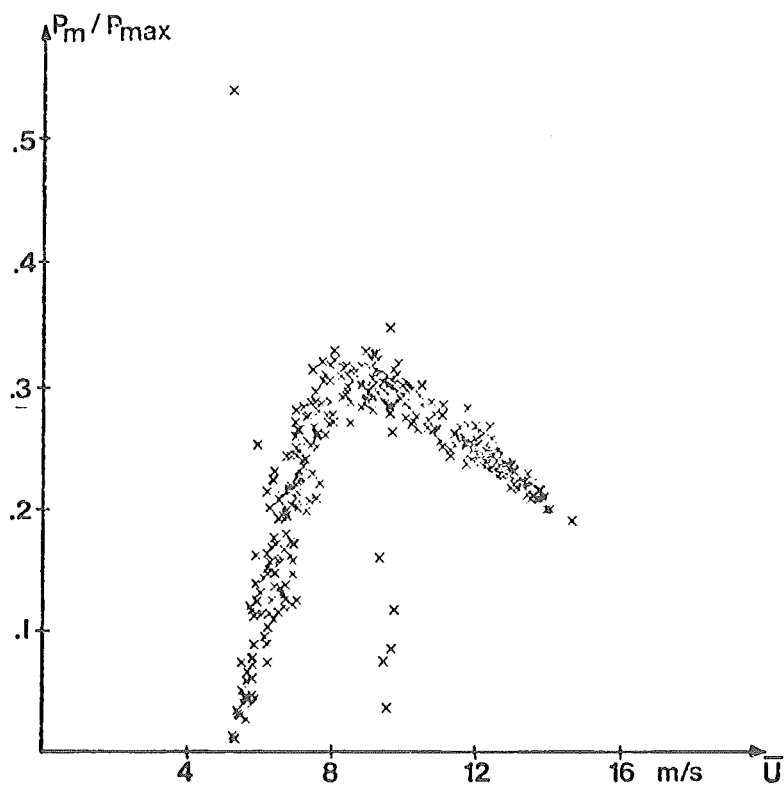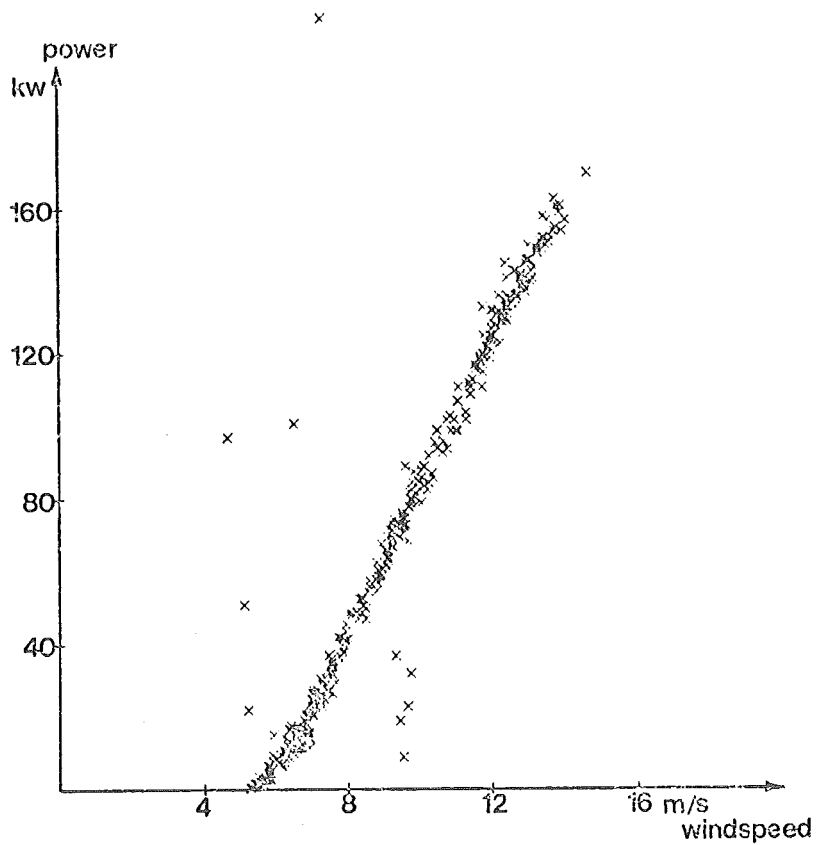
Fig. 21   Power curve and efficiency for windspeeds up to ~ 14 m/s based on
          block averaged data.

Afdeling For Fluid Mekanik DtH 2800 Lyngby
(02) 88 46 22

A STRATEGY FOR AEROELASTIC ANALYSIS OF WECS

by

Ole Fabian

(to be presented at the `1st meeting of experts
- structural dynamics - IEA-Implementing
Agreement for co-operation in the developement
of Large-Scale Wind Energy Conversion Systems
- Munich, October 12, 1978)

Summary:

Within the finite element method, the rotor blades
are usually modelled by beam elements belonging to a
co-ordinate system co-rotating with the rotor hub. In
the case of a flexible tower, however, this rotating
system is both pitched and yawed. The inclusion of
these additional motions in the vibration analysis
constitutes a severe problem.

The propositions presented concerns a purely iner-
tial formulation of the vibration problem avoiding
this difficulty.

A STRATEGY FOR AEROELASTIC ANALYSIS OF WECS

1. Introduction

This note is concerned with the aeroelastic analysis of the complete wind energy conversion system, that is, the structural coupling between the rotor blades, the drive-train, the tower etc. is accounted for in the analysis.

It should be emphasized, however, that the proposition put forward is in an early stage of developement, so therefore only the basic strategy will be given.

Within the finite element method, the aeroelastic behaviour of a single rotor blade is usually examined by employing beam elements in a space co-ordinate system co-rotating with the rotor hub. Thus the formulation of the dynamic equilibrium of the discretized blade must explicitly include the centrifugal forces and in the case of large coning angles, also the coriolis forces.

Because the flexibility of the blade mounting is neglected, this "fixed shaft" model is sufficient only for the determination of the flutter stability and the response to high-frequency changes of the wind velocity.

In the high-frequency range, we may assume that the vibration amplitude is small, so the dynamic equilibrium equations can be linearized around some static state and solved by means of a modal method, allowing for the aerodynamically induced damping.

The static deflection of the blade corresponding to some operating condition, however, may be large and may significantly change the coupling between bending and torsion of the blade. Therefore, a non-linear static analysis is needed for the determination of the incremental equilibrium equations required in the vibration analysis. In addition, this non-linear analysis include the static divergence problem.

For forced vibrations in the low-frequency range, as for example for vibrations caused by the wind shear across the rotor disc, the vibration amplitude becomes large, so that both the structural non-linearity and a non-linearity entering into

the aerodynamic damping must be taken into account. Of course, also the fixed shaft condition must be relaxed in this case.

The relaxation of the fixed shaft condition constitutes the main difficulty for proceeding with the concept of a rotating co-ordinate system, since the motion of the beam elements within this system now becomes relative with respect to the motion of the top of the tower, too , see Fig. 1

Fig. 1
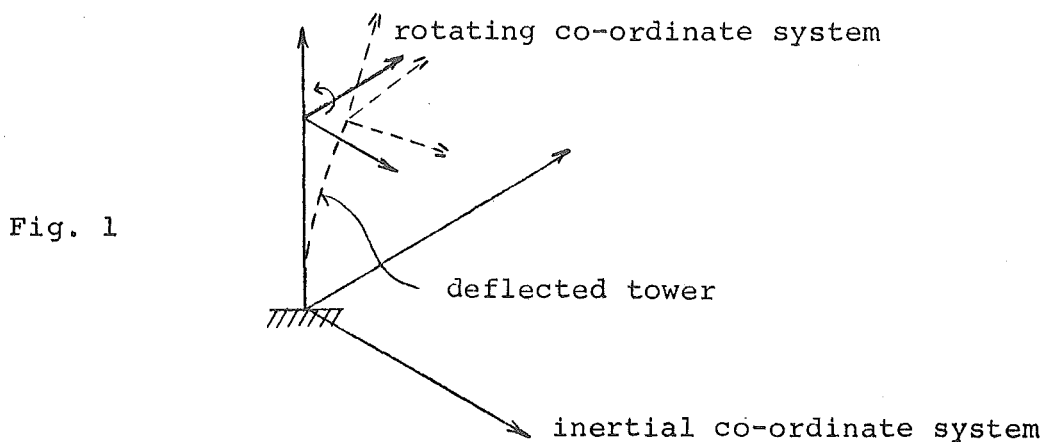
For this reason, it may be attractive to deal with both the beam elements representing the tower and the blade elements in a common co-ordinate system, the inertial one. Following this procedure, it is obvious that the blade elements become subjected to arbitrarily large rigid body rotations, thereby introducing additional non-linearity into the vibration problem.

The basic idea of the present proposition is now, that since the vibration problem is non-linear in any case and therefore a direct time integration technique must be employed, then this additional non-linearity and the previously mentioned ones can be treated simultaneously and by the same analytical effort as for a non-linear fixed shaft model of a complete rotor, approximately.

The advantages of this purely inertial formulation are expected to be

- usual non-linear beam element formulation

- all inertial effects automatically included

- blade pitch control, yawing dynamics etc. can be simulated

- simplified analytical effort

while the obvious disadvantages are

- deflections of the rotor blades are given implicitly

- large rigid body motion of the blade elements possibly giving numerical troubles.

The inertial formulation presented in what follows, applies to a beam element subjected to aerodynamic loads, i.e. a blade element. For other applications, f.i. for an element representing part of the rotor shaft, only the derivations concerning the element loads must be reformulated.

2. Non-linear beam element formulation

For the beam element in space, six degrees of freedom will be needed at each node. To allow for large displacements and rotations of the element, we choose provisionally these degrees of freedom as

$$\{q\}^T = \{x_1 y_1 z_1 \phi_1 \theta_1 \psi_1 x_2 y_2 z_2 \phi_2 \theta_2 \psi_2\}^T \quad , \tag{1}$$

where $(x,y,z)_\alpha$ and $(\phi,\theta,\psi)_\alpha$, $\alpha = 1,2$, are co-ordinates and Eulerian angles, respectively, referring to the inertial space co-ordinate system XYZ. $(x,y,z)_\alpha$ determine the positions of the nodes directly, while the orientations of the beam ends are given in terms of the angles $(\phi_1 + \phi_i, \theta_1 + \theta_i, \psi_1 + \psi_i)$ and $(\phi_2 + \phi_i, \theta_2 + \theta_i, \psi_2 + \psi_i)$, where $(\phi,\theta,\psi)_i$ are the Eulerian angles defining the initial orientation of the element.

As an example,

$$\{q\}^T = \{0\ 0\ 0,0\ 0\ 0,\ell\ 0\ 0,0\ 0\ 0\ \}^T\ ,\quad \phi_i = \theta_i = 0$$

means that the longitudinal axis of an element with the initial length ℓ co-incidents with the X-axis.

In order to establish the equilibrium equations for the element, we have to divide $\{q\}$ into two parts

$$\{q\} = \{q^{rig}\} + \{q^{def}\} \tag{2}$$

where $\{q^{rig}\}$ and $\{q^{def}\}$ represent the rigid body motion and the deformation of the element, respectively.§

It is obvious that the angles

$$(\bar{\phi}\ ,\bar{\theta}\ ,\bar{\psi}\ ) = \frac{1}{2}(\phi_1,\theta_1,\psi_1) + \frac{1}{2}(\phi_2,\theta_2,\psi_2) \tag{3}$$

determine most of the rigid body rotation, provided that the strains within the element are small. These averaged angles together with the initial angles $(\phi,\theta,\psi)_i$ define the orientation of a so-called "body co-ordinate system", $\hat{X}\hat{Y}\hat{Z}$, following the element through the space.

According to the application rules for the Eulerian angles, the orthogonal matrix

$$[t]\ =\ \begin{bmatrix} \cos\psi\ \cos\phi - \cos\theta\ \sin\phi\ \sin\psi & \cos\psi\ \sin\phi + \cos\theta\ \cos\phi\ \sin\psi & \sin\psi\ \sin\theta \\ -\sin\psi\ \cos\phi - \cos\theta\ \sin\phi\ \cos\psi & -\sin\psi\ \sin\phi + \cos\theta\ \cos\phi\ \cos\psi & \cos\psi\ \sin\theta \\ \sin\theta\ \sin\phi & -\sin\theta\ \cos\phi & \cos\theta \end{bmatrix}_0 \tag{4a}$$

$$(\phi_0,\theta_0,\psi_0) = (\phi_i,\theta_i,\psi_i) + (\bar{\phi},\bar{\theta},\bar{\psi}) \tag{4b}$$

determine the transformation of space co-ordinates of a vector to body co-ordinates by the relation

$$\begin{Bmatrix} \hat{x} \\ \hat{y} \\ \hat{z} \end{Bmatrix} = [t] \begin{Bmatrix} x \\ y \\ z \end{Bmatrix} \tag{5}$$

---

§ The components of $\{q^{def}\}$ corresponds to some extent to the so-called "natural modes" introduced by J.H. Argyris.

Thus $\{q^{rig}\}$ can be approached by

$$\{q^{rig}\} = \begin{Bmatrix} \begin{Bmatrix} x_0 \\ y_0 \\ z_0 \end{Bmatrix} + [t]^T \begin{Bmatrix} -\ell/2 \\ 0 \\ 0 \end{Bmatrix} \\ \bar{\phi} \\ \bar{\theta} \\ \bar{\psi} \\ \begin{Bmatrix} x_0 \\ y_0 \\ z_0 \end{Bmatrix} + [t]^T \begin{Bmatrix} +\ell/2 \\ 0 \\ 0 \end{Bmatrix} \\ \bar{\phi} \\ \bar{\theta} \\ \bar{\psi} \end{Bmatrix} \qquad (6a)$$

$$(x_0, y_0, z_0) = \frac{1}{2}(x_1, y_1, z_1) + \frac{1}{2}(x_2, y_2, z_2) \qquad (6b)$$

while $\{q^{def}\}$ then becomes

$$\{q^{def}\} = \{q\} - \{q^{rig}\} \qquad (7)$$

Due to the small strain assumption, the deformation angles $(\phi^{def}, \theta^{def}, \psi^{def})$ implicitly introduced into $\{q^{def}\}$ are small. These small angles and the time derivatives $(\dot{\phi}, \dot{\theta}, \dot{\psi})_\alpha$ and $(\ddot{\phi}, \ddot{\theta}, \ddot{\psi})_\alpha$ can be transformed to the body co-ordinate system and projected on the body set of axes by the common relation

$$\begin{Bmatrix} \omega_{\hat{x}} \\ \omega_{\hat{y}} \\ \omega_{\hat{z}} \end{Bmatrix} = [\tilde{t}] \begin{Bmatrix} \dot{\phi} \\ \dot{\theta} \\ \dot{\psi} \end{Bmatrix} \qquad (8a)$$

$$[\tilde{t}] = \begin{bmatrix} \sin\theta_0\sin\psi_0 & \cos\psi_0 & 0 \\ \sin\theta_0\cos\psi_0 & -\sin\psi_0 & 0 \\ \cos\theta_0 & & 1 \end{bmatrix} \qquad (8b)$$

which here is given for the angular velocities.

Denoting the stiffness matrix, the mass matrix and the load vector for the element by $[\hat{k}]$, $[\hat{m}]$ and $\{\hat{Q}\}$, respectively, the equilibrium equation referred to the body co-ordinate system takes the form

$$[\hat{k}][\tilde{T}]\{q^{def}\} + [\hat{m}][\tilde{T}]\{\ddot{q}\} = \{\hat{Q}\} \qquad (9a)$$

where

$$[\tilde{T}] = \begin{bmatrix} [t] & & & \\ & [\tilde{t}] & & \\ & & [t] & \\ & & & [\tilde{t}] \end{bmatrix} \qquad (9b)$$

Since the equilibrium equations for the individual elements must be referred to the common space co-ordinate system, eq.(9) is pre-multiplied by the transformation matrix

$$[T]^T = \begin{bmatrix} [t] & & & \\ & [t] & & \\ & & [t] & \\ & & & [t] \end{bmatrix}^T \qquad (10)$$

Thus the non-linear equilibrium equation becomes

$$[T]^T[\hat{k}][\tilde{T}]\{q^{def}\} + [T]^T[\hat{m}][\tilde{T}]\{\ddot{q}\} = [T]^T\{\hat{Q}\} \qquad (11a)$$

or abbreviated

$$[k]\{q^{def}\} + [m]\{\ddot{q}\} = \{Q\} \qquad (11b)$$

To solve the non-linear vibration problem, we need the linearized, incremental equilibrium equation, too.

Applying the linear incrementation operator Δ to

eq.(11), and rearranging we get

$$([k_\sigma] + [k])\{\Delta q\} + [m]\{\Delta \ddot{q}\} = [T]^T\{\Delta \hat{Q}\} \qquad (12a)$$

where $[k_\sigma]$ is the usual "initial stress matrix" given by

$$[k_\sigma]\{\Delta q\} = [\Delta T]^T\{\hat{P}\} \qquad (12b)$$

$$\{\hat{P}\} = [\hat{k}][\tilde{T}]\{q^{def}\} + [\hat{m}][\tilde{T}]\{\ddot{q}\} - \{\hat{Q}\} \qquad (12c)$$

The key point in this incrementation is the approach

$$[\hat{k}]\Delta([\tilde{T}]\{q^{def}\}) + [\hat{m}]\Delta([\tilde{T}]\{\ddot{q}\}) = [\hat{k}][\tilde{T}]\{\Delta q\} + [\hat{m}][\tilde{T}]\{\Delta \ddot{q}\}$$

which is valid since the fundamental beam theory permits of the small, incremental rotations.

To complete the incremental formulation, we must finally replace the incremental nodal point variables $(\Delta\phi, \Delta\theta, \Delta\psi)_\alpha$ and the corresponding time derivatives by quantities which are common to both the element considered and the neighbouring elements.

Defining the new incremental nodal point variables by

$$\{\Delta q^C\}^T = \{\Delta x_1 \, \Delta y_1 \, \Delta z_1 \, \Delta\theta_{x_1} \, \Delta\theta_{y_1} \, \Delta\theta_{z_1} \, \Delta x_2 \, \Delta y_2 \, \Delta z_2 \, \Delta\theta_{x_2} \, \Delta\theta_{y_2} \, \Delta\theta_{z_2}\}^T$$

where $(\Delta\theta_x, \Delta\theta_y, \Delta\theta_z)_\alpha$ refer to the usual rotations around the axes of the space co-ordinate system XYZ, then the final incremental equilibrium equation takes the form

$$([k_\sigma] + [k])[\tilde{T}]\{\Delta q^C\} + [m][\tilde{T}]\{\ddot{\Delta q}^C\} = [T]^T\{\Delta \hat{Q}\} \qquad (13a)$$

$$[\tilde{T}] = \begin{bmatrix} [I] & \tilde{} & & \\ & [\tilde{t}] & & \\ & & [I] & \tilde{} \\ & & & [\tilde{t}] \end{bmatrix} \qquad (13b)$$

$$[\tilde{t}] = \begin{bmatrix} 0 & \cos\phi_0 & \sin\theta_0\sin\phi_0 \\ 0 & \sin\phi_0 & -\sin\theta_0\cos\phi_0 \\ 1 & 0 & \cos\theta_0 \end{bmatrix}^{-1} \qquad (13c)$$

where $[I]$ denotes the identity matrix.

Employing a quasi-stationary, 2-dimensional aerodynamic theory, the load vector $\{\hat{Q}\}$ depends non-linearily on the relative velocity of the air flow. If unsteady lifting theory is required, also the relative acceleration enters.
In general

$$\{\hat{Q}\} = \left\{ \hat{Q}\left(\hat{\vec{V}}_{\infty}, \dot{\hat{\vec{V}}}_{\infty} \{\hat{q}^{def}\}, \{\dot{\hat{q}}\}, \{\ddot{\hat{q}}\} \right) \right\}$$

where $\vec{V}_{\infty} = \vec{V}_{\infty}(x,y,z)$ is the wind velocity. However, as for the stiffness matrix and the mass matrix, the details concerning $\{\hat{Q}\}$ will be omitted in this note.

For this reason the incrementation of $\{\hat{Q}\}$ would be rather symbolical, so it is preferred to end the incremental formulation of the equilibrium equation here.

Finally, it shall be remarked, that the linear incremental equilibrium equation (12-13) can be employed in two cases:

    (i)   "structurally" linear incremental advance in time

    (ii) iterative improvement of an approximate solution, i.e. $\{\Delta q^{c}\}$, $\{\Delta \dot{q}^{c}\}$ and $\{\Delta \ddot{q}^{c}\}$ are interpreted as corrections for the approximate solution.

3. Solution technique.

The direct time integration method imagined for this problem is the well-known Newmark algorithm. With regard to the structural non-linearity it is clear, that iteration within each time step is necessary, if just a few revolutions of the rotor shall be simulated. Therefore, and in order to minimize the computer costs, the version of Newmarks method using "point collocation" is preferred.

Requiring an unconditionally stable time marching scheme together with minimal artificial damping, the parameters entering into Newmarks method take the values

$$\gamma = \frac{\sqrt{3}}{2} \quad ; \quad \beta = \frac{1}{4} \quad ,$$

corresponding to a collocation point located at

$$\{q_{i-1}\} \qquad \{q_i\} \qquad \{q_{i+1}\}$$

```
  +----------------+----0--------+------> time
 t_{i-1}          t_i t_col    t_{i+1}
```
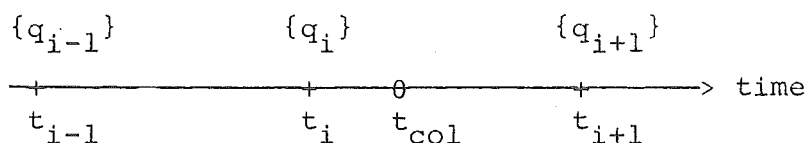
where t_{i-1} and t_i are the times for the known values of $\{q\}$.

It is well-known, however, that point collocation technique is hazardous. Therefore, the detailed time marching algorithm including "structural" iteration will not be given, as the success cannot be garanteed.

4. Concluding remarks.

It is the authors opinion, that most of the theories concerned with the coupled analysis of WECS, are based on models originally developed for a different purpose. It should be evident, however, that such models are not necessarily the optimal ones for the present problem. The purely inertial formulation given herein, is intended to stimulate a discussion on such optimal models.

DEUTSCHE FORSCHUNGS- UND VERSUCHSANSTALT FÜR LUFT- UND RAUMFAHRT E.V.

FORSCHUNGSZENTRUM BRAUNSCHWEIG
INSTITUT FÜR STRUKTURMECHANIK

Modes and Frequencies of GROWIAN - Rotor Blades

by

Dieter PETERSEN

Modes and Frequencies of GROWIAN - Rotor Blades

by Dieter PETERSEN

1. Aims and Investigation

Due to the known construction of GROWIAN rotor blades modes and frequencies were calculated. The computer program used takes into account centrifugal force effect, the offsets of shear center, center of bending stiffnesses, and center of gravity. Furthermore, the effects of pre-loading and pre-twist are induced within the current version [1].

Thus, modes and frequencies of a reference version could be calculated. But there are free regions were the mathematical modelling was uncertain due to a lack of information or difficulties of modelling.

First of all there are two regions were parts of the blades shall be connected by special constructions. The one region is at the length coordinates of 12 m to 15 m. Within this region the inner part, a steel construction, is connected with the middle part, a composite wing construction. The other region is situated at 30 m to 32 m, were the composite construction of the outer wing is connected to the middle part. A further region was the innermost one from 0 m to 6 m. Within this hub region there was a wider gap of stiffness information.

Therefore a suitable way of approach was chosen. At first a reference version of the wing was established. This version was treated as a rigidly clamped beam at 6 m. At the inner and outer connection regions stiffnesses were suggested as for a continous beam. Then the beam was described by 22 different parts. Each of them has constant properties in order to fasten the integration routines. The bending stiffnesses and the torsional stiffnesses are shown in the figures 1 to 3.

Within a second step of calculation parameter studies were made. This studies should show the influence on modes and frequencies of possible stiffness reduction within the above mentioned regions. The idea was that there will be reasonable drops in stiffnesses due to the constructions of connection. Thus, it was investigated the effect of stiffness within the regions 12 m to 15 m and 30 m to 32 m separately. The maximum amount of stiffness reduction was

was down to five percent of the undisturbed reference version as it is shown within the figures 1 to 3.

In the case of the hub region the rigid support was changed into an elastic one. The beam stiffnesses at 6.30 m were chosen for the missing part from 0 m to 6 m. Because the blades of GROWIAN will have a mechanism to change the angle of attack a drop in torsional stiffness had to be taken into account. Which was done down to five percent of the above said spring stiffness. This decrease in stiffness is shown within fig. 3.

2. Frequencies

Frequencies are shown within fig. 4. The lowest frequency is due to a flapwise mode. That means, the flapwise bending is the mean effect of this mode. Because there is coupling beween the deflections and the twist each mode presents flapwise and chordwise bending and twist too.

The lowest frequency of 1.42 Hz is high compared to a specification asking for a frequency higher than 0.5 Hz.

Within fig. 4 the frequencies of the above described stiffness reductions are given. As it can be seen there are no serious drops in frequencies due to the decreases in stiffnesses, although severe frequency reductions were suggested when starting the investigation.

Remarkable drops in frequencies are obtained for stiffness reductions down to five percent within the inner connection region for the first and second eigenfrequencies. Thus, the first modes in flapwise and chordwise bending are effected (see section 3.2 and figures 17 and 18)

Another remarkable frequency reduction is obtained for the stiffness decrease down to five percent in the outer region. These are the first modes in flapwise bending and in torsion (see section 3.3 and figures 20 and 23).

3. Modes

Nevertheless, there were no big drops in frequencies down to 0.5 Hz obtained the modes shall now be discussed. It will be shown how the shapes of the modes

will be changed by the stiffness reduction. There are a lot of effects.

3.1 Reference Version

First, the modes of the undisturbed continous blades are shown within the figures 5 to 14. There are given the first two modes in torsion with relatively high frequencies, the first three chordwise modes, and the first five flapwise modes. Thus, the first ten coupled modes of the GROWIAN wing are shown were the second torsional mode is the highest, the tenth frequency.

Although all modes show coupling between chordwise bending (v-deflection), flapwise bending (w-deflection), and twist (θ -deflection), the couplings are different. Generally speaking there are small coupling effects observed for the five, lowest frequencies (figs. 7 - 12), namely the first and second modes where chordwise bending is the oberwhelming part, and the first three modes where the flapwise bending dominates. But the higher frequencies show strong coupling effects (figs. 5, 6, 13, 14). Especially noticeable are the couplings within the first mode with dominant torsion (fig. 5) and the fourth mode with flapwise bending as the highest part (fig. 14).

3.2 Inner Stiffness Reduction

Here some modes are shown which have the strongest effects in the case of a stiffness reduction down to five percent within the region from 12 m to 15 m. The modes of the frequencies with the strongest drop, first flapwise and first chordwise bending, are given within the figures 17 and 18. There a hinge effect is observed very well. Beginning with the weak region the deflections increase stronger than before.

The same hinge effect is shown within the figures 15 and 16 for the torsional modes with a moderate "jump" within the twist curves. Furthermore, there are again strong coupling effects within the modes of the higher frequencies (figs. 15, 16, 19). Noticeable are the strong changes in curvatures compared with the reference version for the fifth bending mode (figs. 14 and 19).

3.3 Outer Stiffness Reduction

Some remarkable modes when the stiffness of the outer connection region is

reduced down to five percent are shown within the figures 20 to 21. Here the hinge effect again is observed for the first torsional, first chordwise, and the first flapwise modes (figs. 20, 21, 23). Within the figures 22 and 24 the twist is only due to coupling effects. Nevertheless, the twist curve shows strong discontinuities within the weak region. There are noticeable changes with respect to the reference version (figs. 8 and 12) within the modes of second chordwise and third flapwise bending.

Another effect for these two modes has to be regarded. As seen in Fig. 4 the frequency of the second chordwise bending has decreased more than the one of the third flapwise bending. The extraordinary high coupling of the second chordwise bending mode with a flapwise bending effect is due to the closed neighbourhood of the frequencies of the two modes.

3.4 Elastic Support

Replacing the rigidly clamped blade by an elastically supported one the modes as well as the frequencies do not change remarkably. Due to the elastic support the deflections and the twist are now not equal to zero at 6 m, the clamping point of the reference version. A visible example of this effects is given in fig. 25 for the third mode of flapwise bending.

A strong decrease of the torsional elastic support down to five percent did not influence the frequencies very strong. In this case the same is true for the modes shown in the figs. 26 to 28. Remarkable twist at 6 m is observed as expected. For the fifth mode of flapwise bending some stronger couplings with the chordwise bending and the twist is obtained compared to the reference version (figs. 14 and 18).

4. Conclusions

Reducing the stiffness of the anticipated GROWIAN blades within small regions does not result in a severe decrease of frequencies. Nevertheless, the modes show partially strong changes due to these effects. Very serious effects for the mode shapes were obtained in reducing the stiffness within the connection regions at 12 m to 15 m and 30 m to 32 m. The strongest effect was the hinge effect which will cause higher deflections also for static loadings. Even the

changes in the coupling effects will cause different response tending to stronger response of the "weaker" frequencies.

Not included are investigations of interactions of stiffness drops at more than one region. Furtheron, it is suggested that the effects of a static pre-loading by wind forces should be taken into account. That means that the constant part of the steady state wind forces with respect to one cycle of the rotor has to be taken as a static pre-loading in order to regard the stronger coupling effect between deflections and twist. Up to now the program includes only pre-twist. The effect of pre-deflections will also give stronger couplings.

5. References

[1] PETERSEN, D.   Berechnung der GROWIAN-Rotorblätter.
DFVLR IB 152-78/32, Braunschweig, Juni 1978.
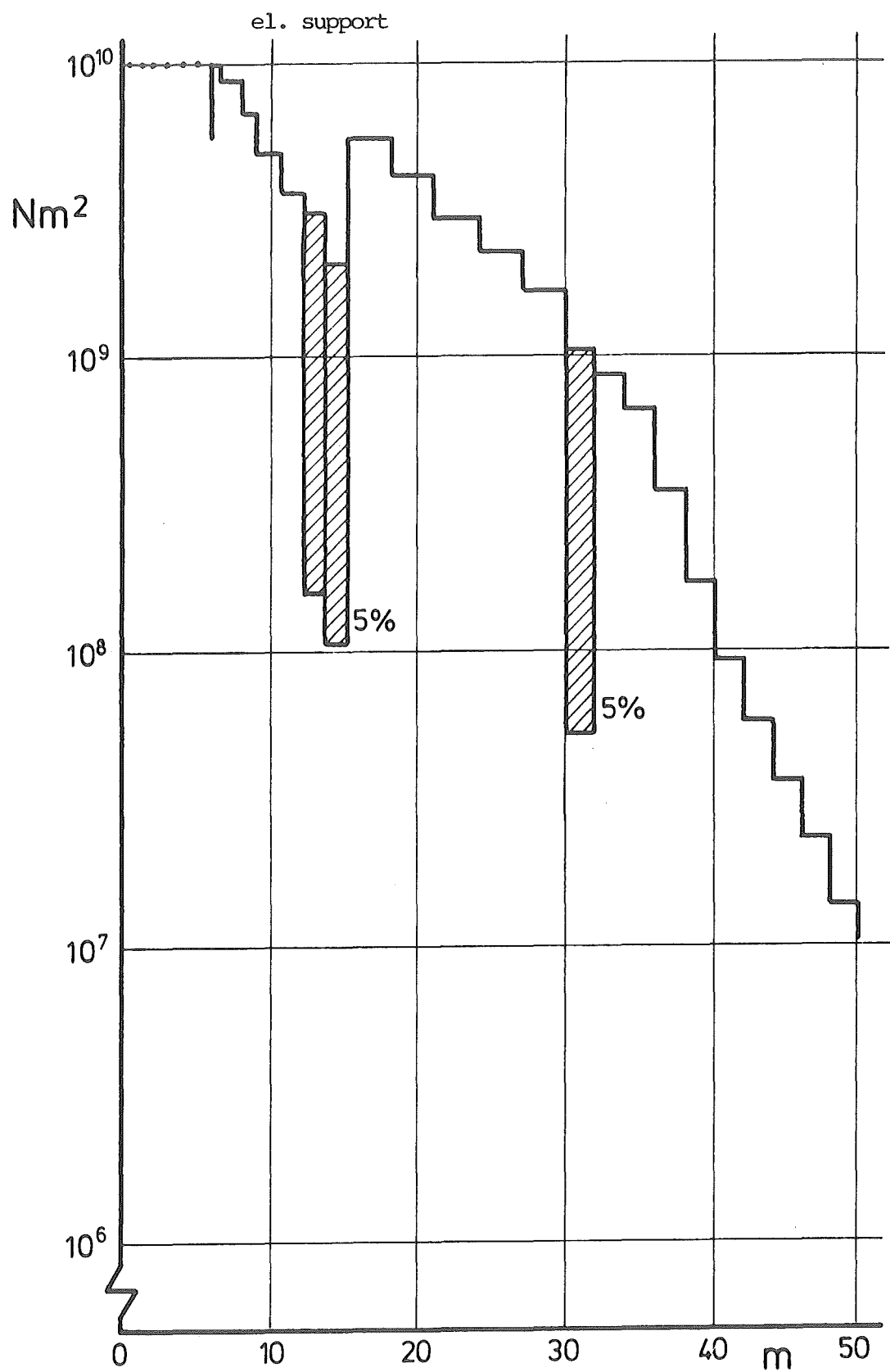
Fig. 1 Variation of bending stiffness EI_y and regions of decrease
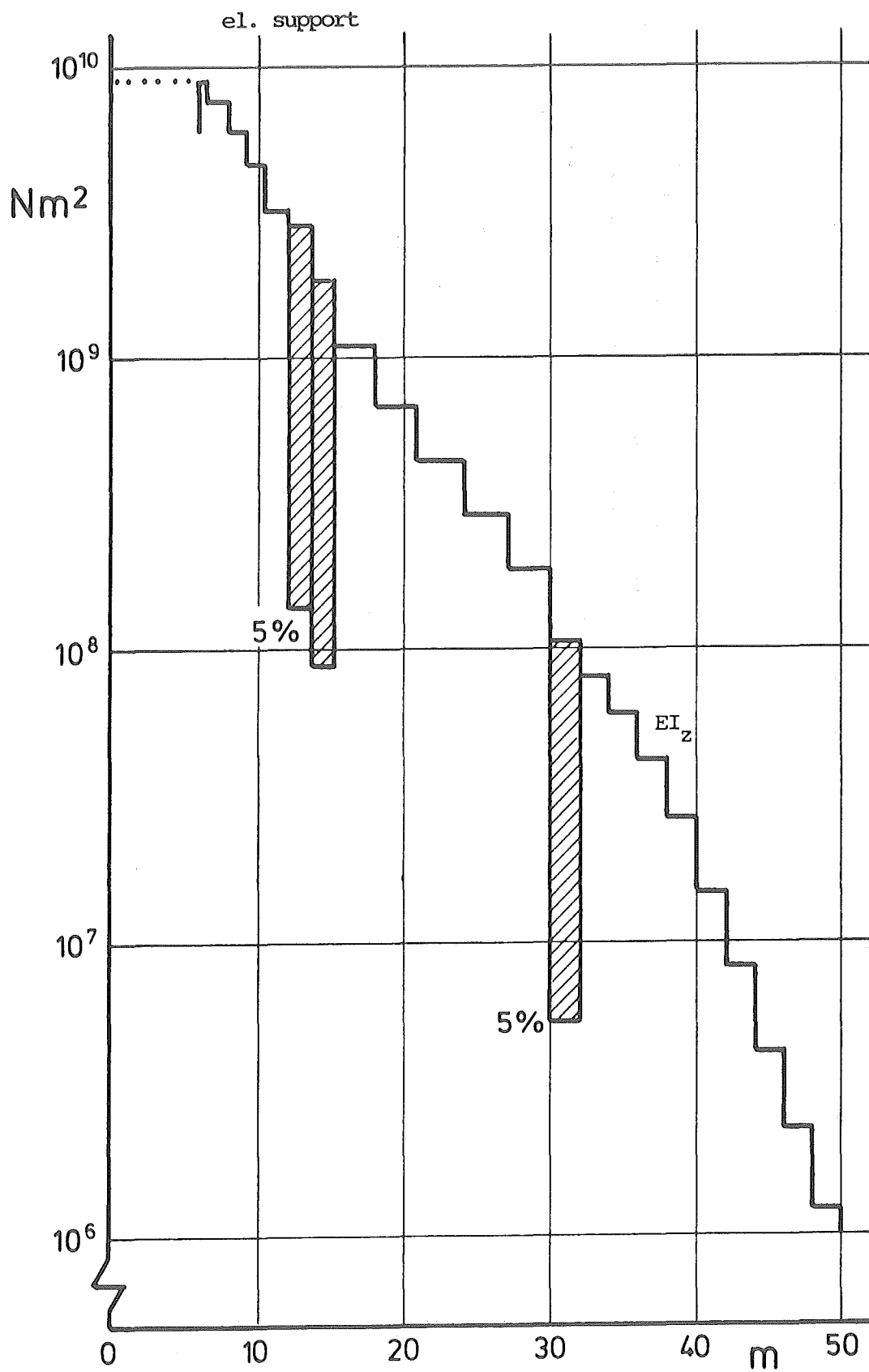
Fig. 2   Variation of bending stiffness EI_z
and regions of decrease
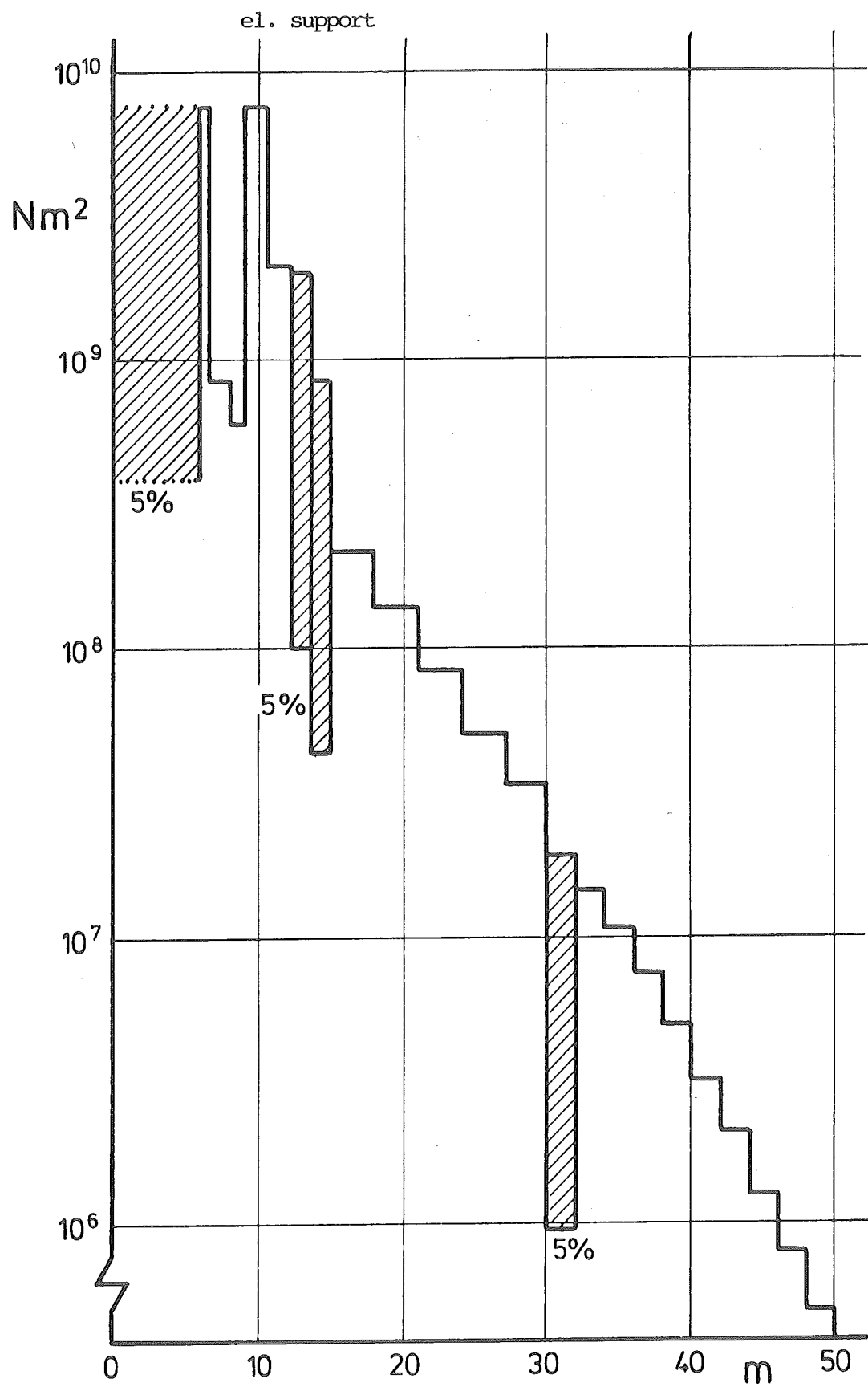
Fig. 3   Variation of torsional stiffness GI_t
and regions of decrease

	Ref. Vers	el. Sup.	$0.1\ GI_t$	$0.15\ GI_t$	12 m – 15 m		30 m – 32 m		Main Mode
					0.1	0.05	0.1	0.05	
1.	1.42	1.38	1.38	1.38	1.13	1.56	1.15	1.01	1st flapwise
2.	2.55	2.25	2.25	2.25	1.39	1.06	2.35	2.16	1st chordwise
3.	3.42	3.22	3.22	3.22	2.91	2.76	3.14	30.2	2nd flapwise
4.	6.69	6.13	6.12	6.12	6.15	6.02	5.84	5.55	3rd flapwise
5.	7.50	6.87	6.87	6.87	7.17	7.08	6.00	5.25	2nd chordwise
6.	11.26	11.25	11.05	10.72	10.72	10.00	7.71	6.13	1st torsion
7.	11.38	10.16	10.15	10.15	11.03	10.89	11.06	10.81	4th flapwise
8.	15.75	12.92	12.92	12.92	14.85	14.39	14.50	14.21	3rd chordwise
9.	17.21	15.34	15.34	15.34	16.41	15.22	15.17	14.77	5th flapwise
10.	18.16	18.06	17.08	15.38	17.18	16.80	18.09	18.00	2nd torsion

Fig. 4   Table of eigenfrequencies
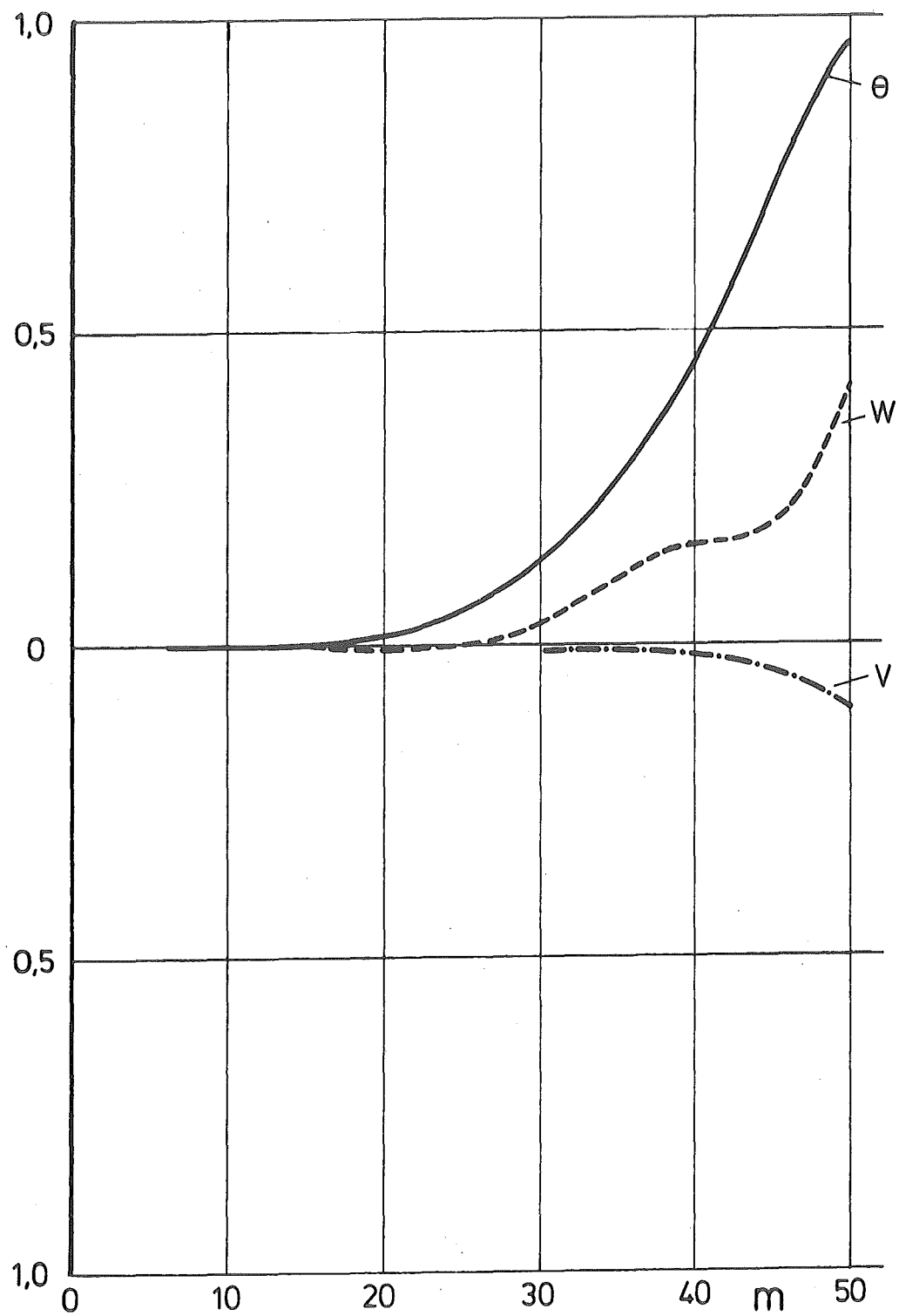
Fig. 5   Reference version,
           1st torsional mode   f = 11,26 Hz
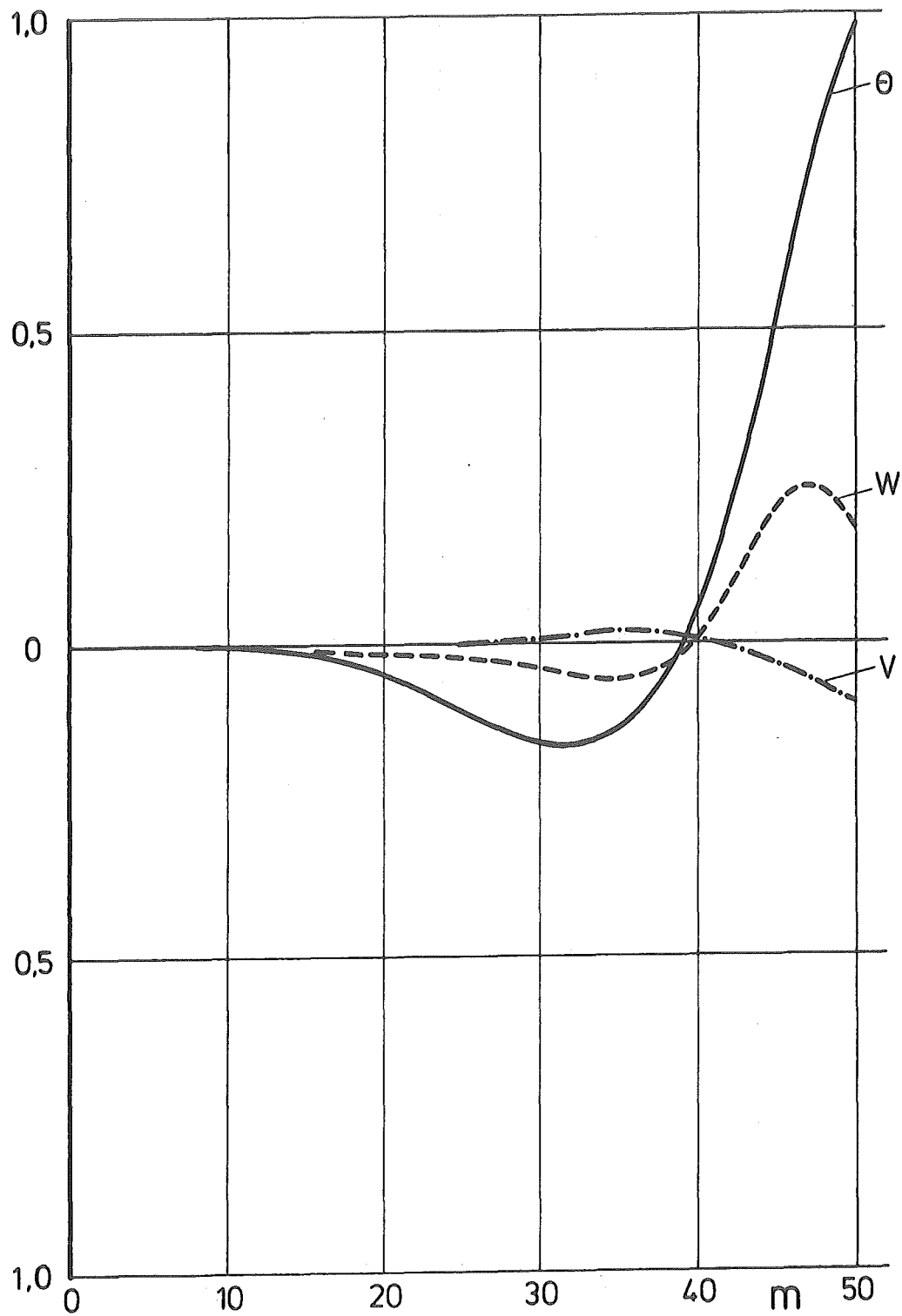
Fig. 6   Reference version,
          2nd torsional mode   f = 18.16 Hz
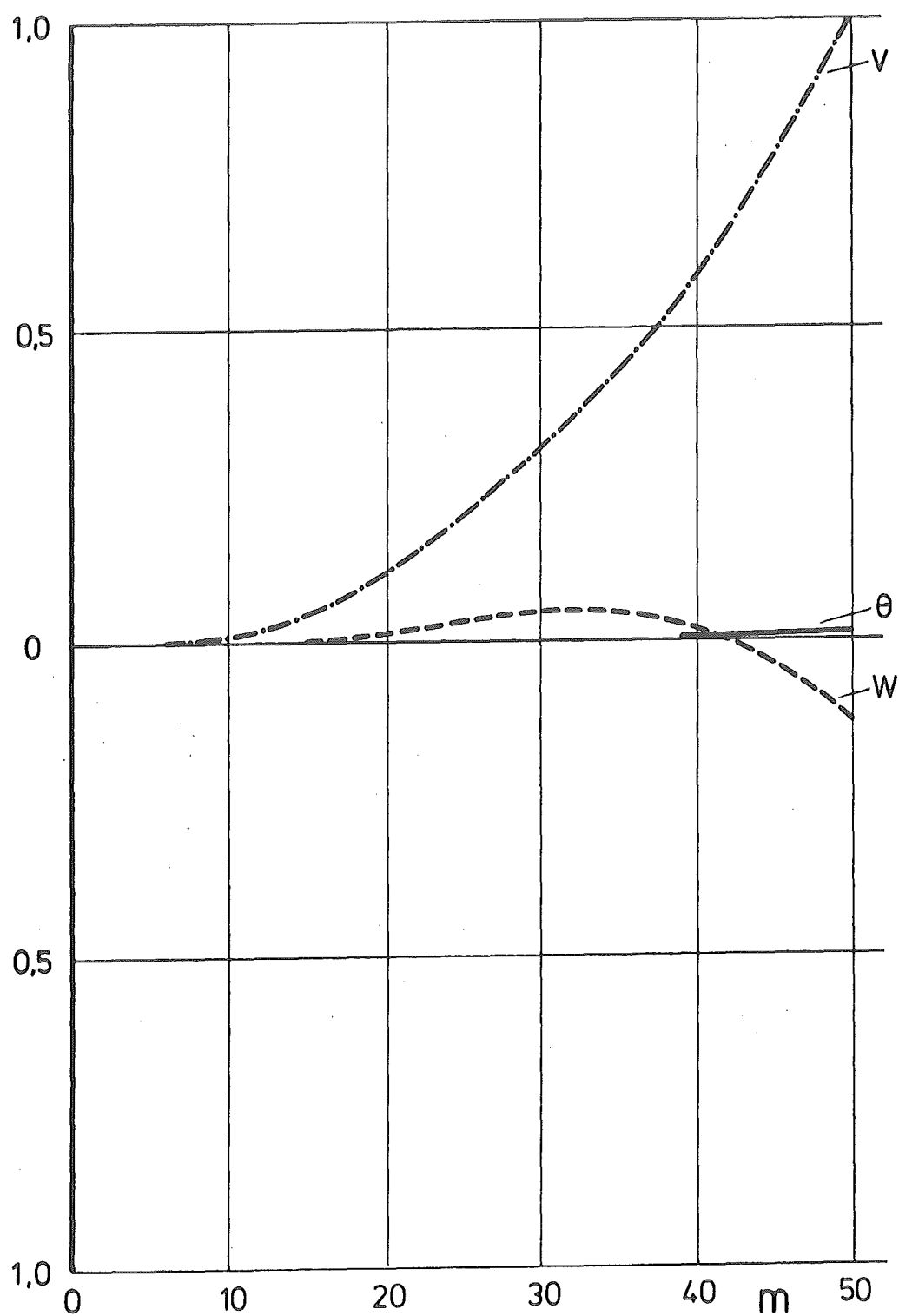
Fig. 7   Reference version,
1st chordwise bending mode   f = 2.55 Hz
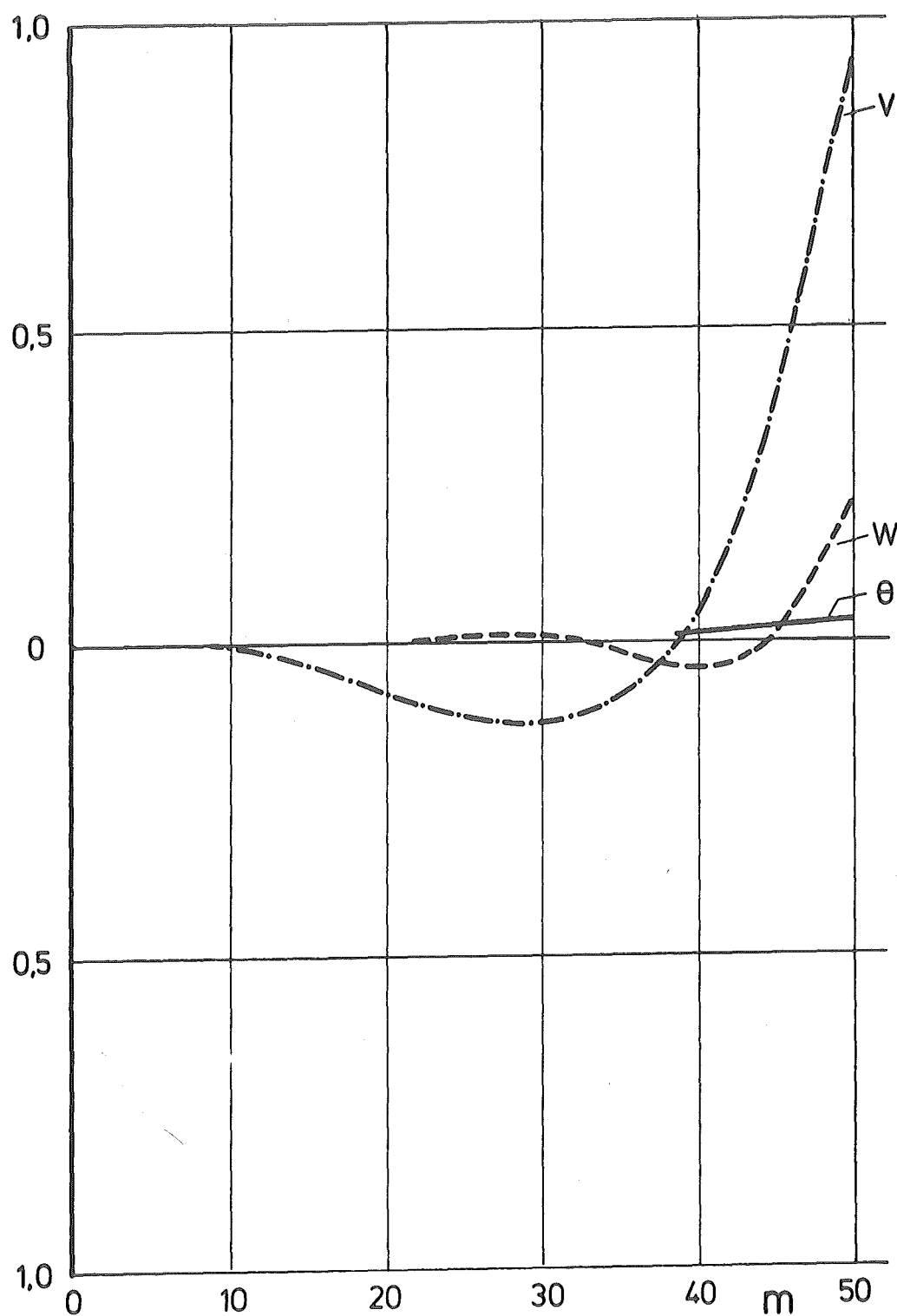
Fig. 8   Reference version,
          2nd chordwise bending mode   f = 2.50 Hz
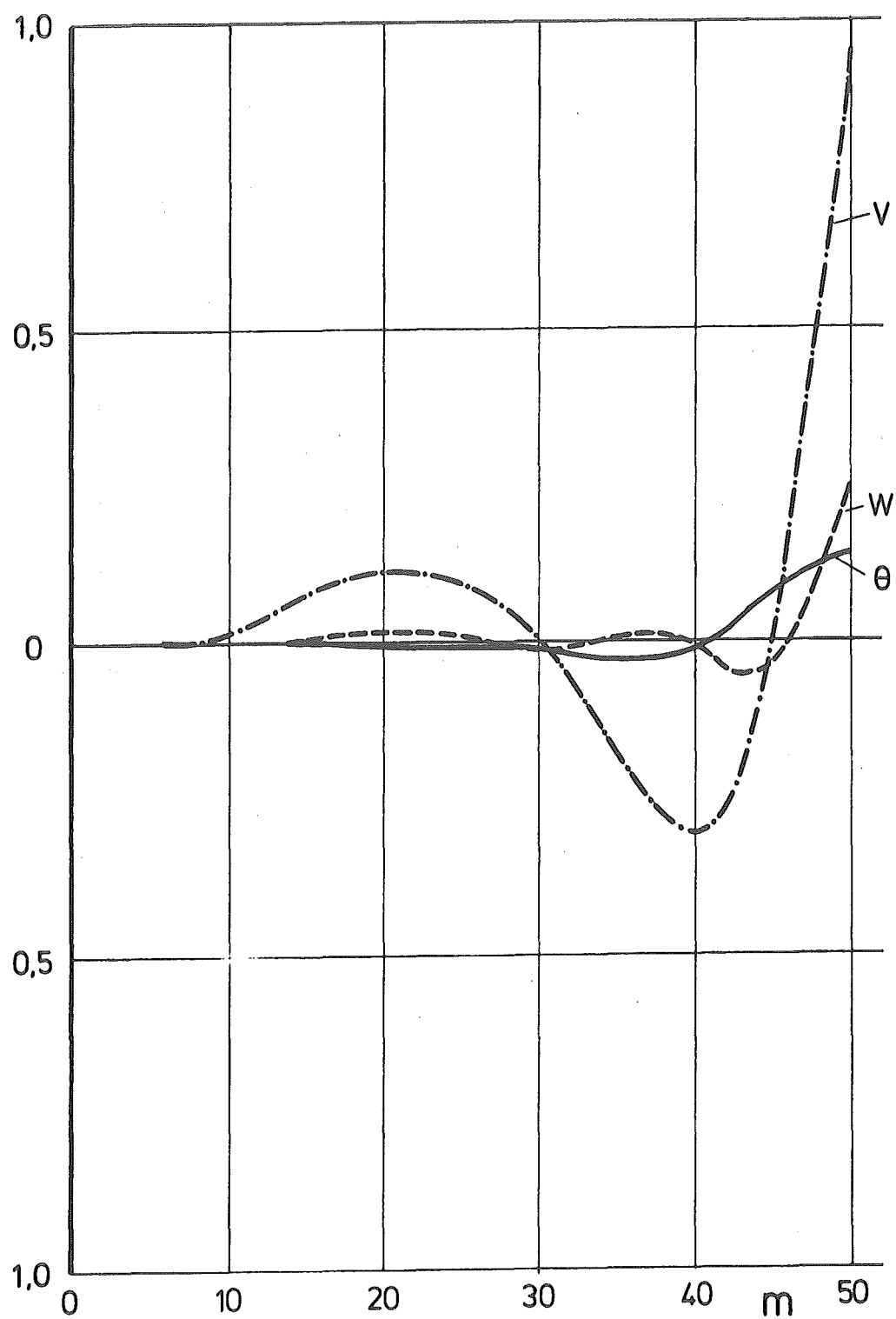
Fig. 9   Reference version,
3rd chordwise bending mode   f = 15.25 Hz
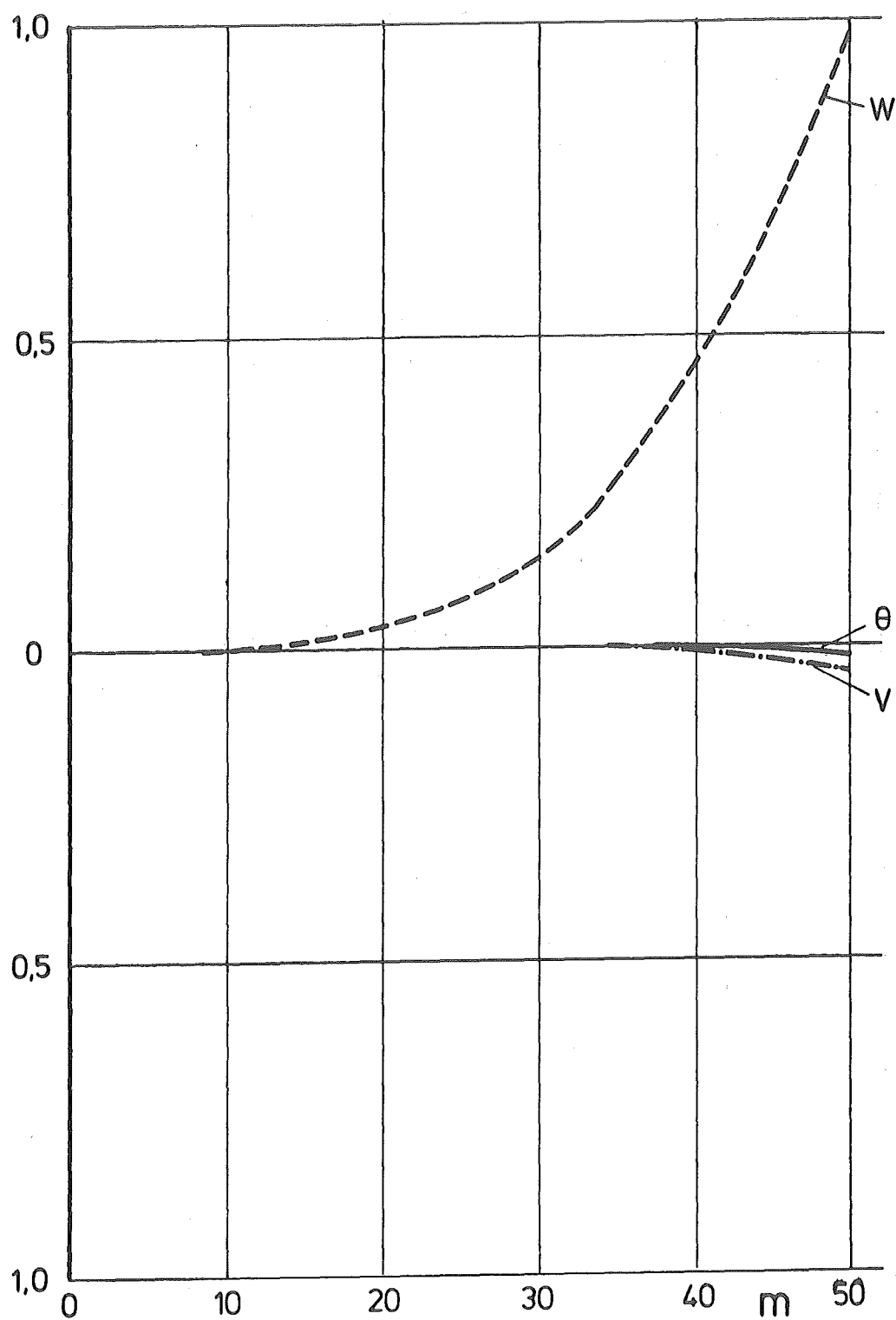
Fig. 10   Reference version,
1st flapwise bending mode   f = 1.42 Hz
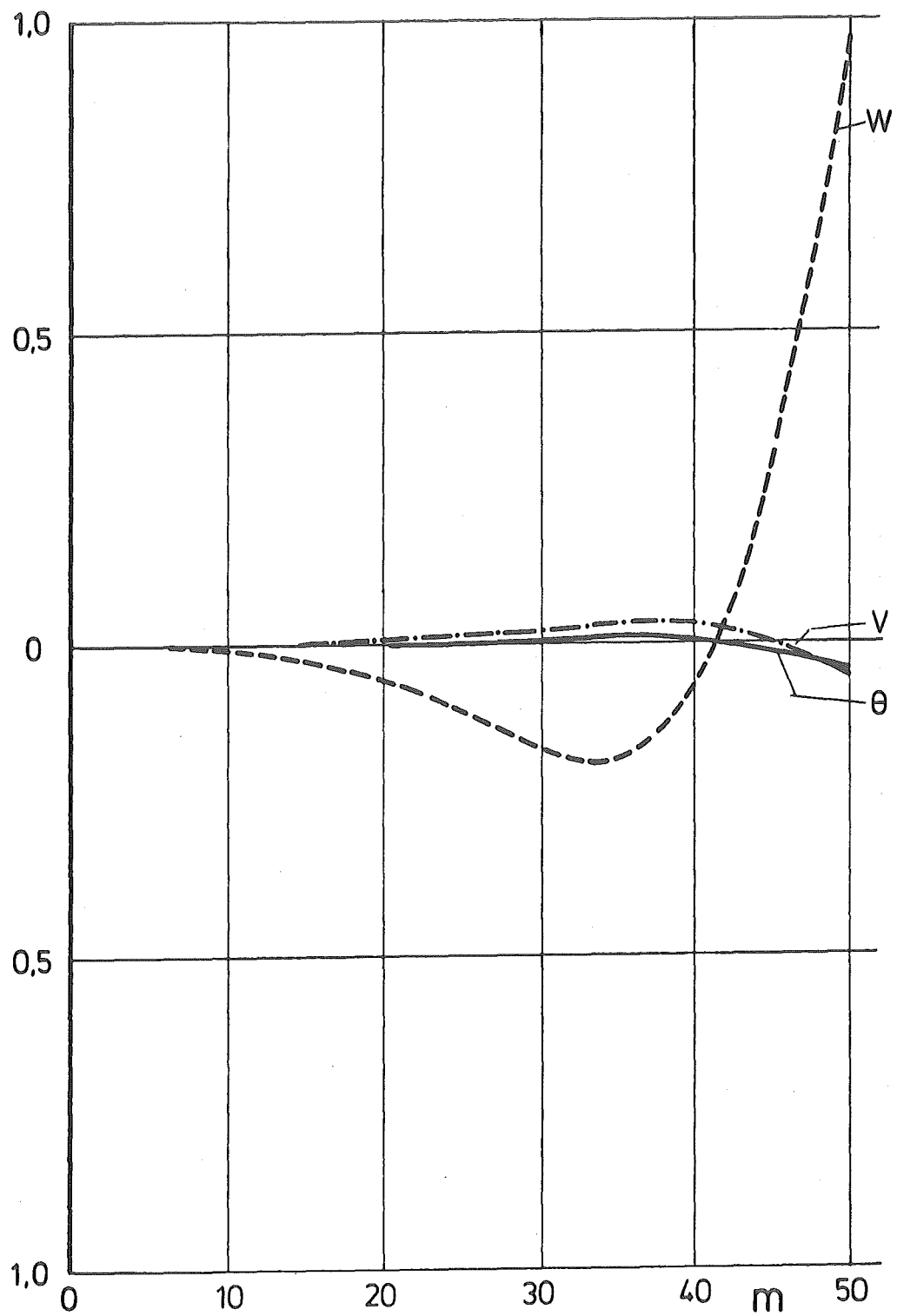
Fig. 11   Reference version,
2nd flapwise bending mode   f = 3.42 Hz
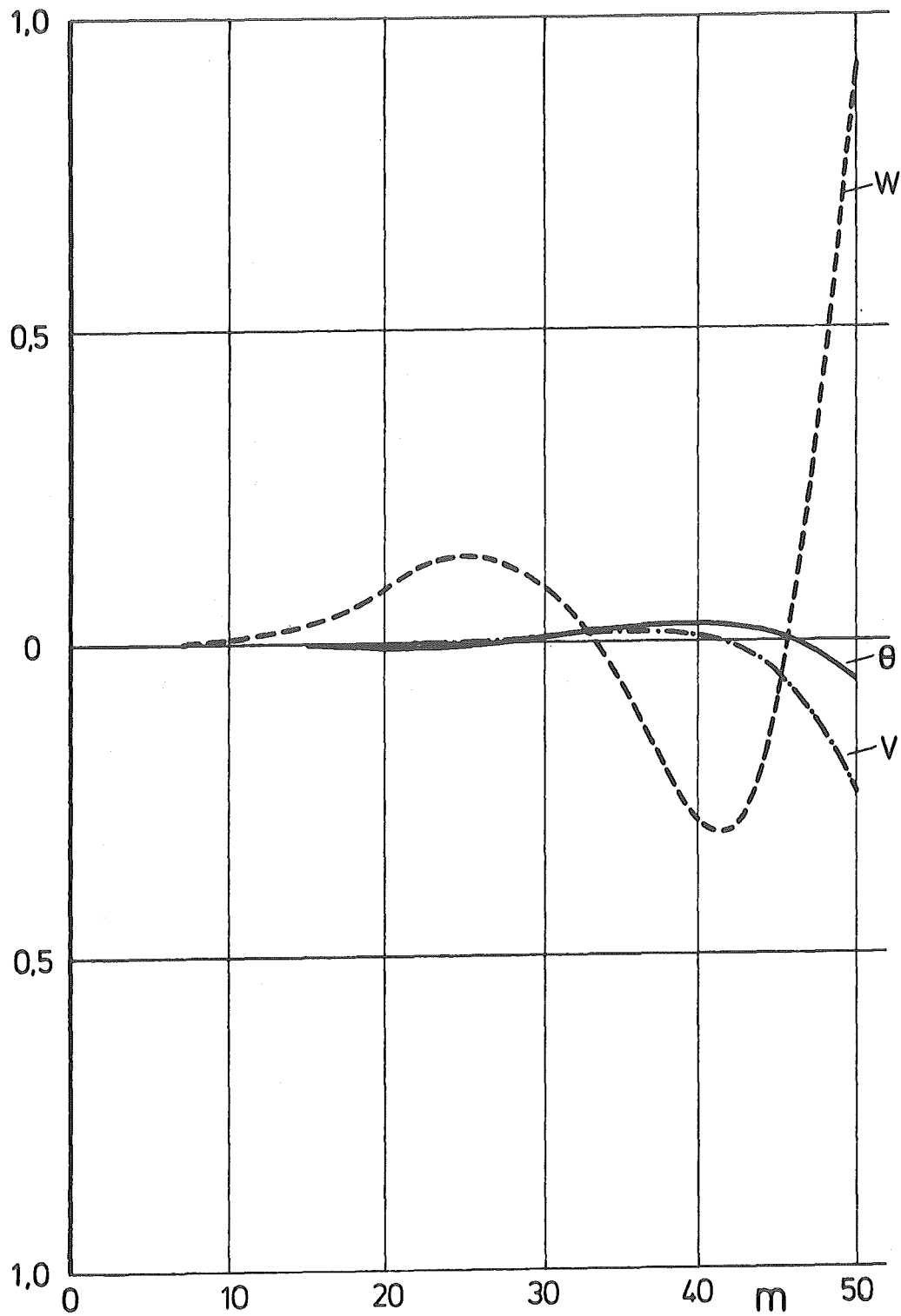
Fig. 12   Reference version,
3rd flapwise bending mode   f = 6.69 Hz
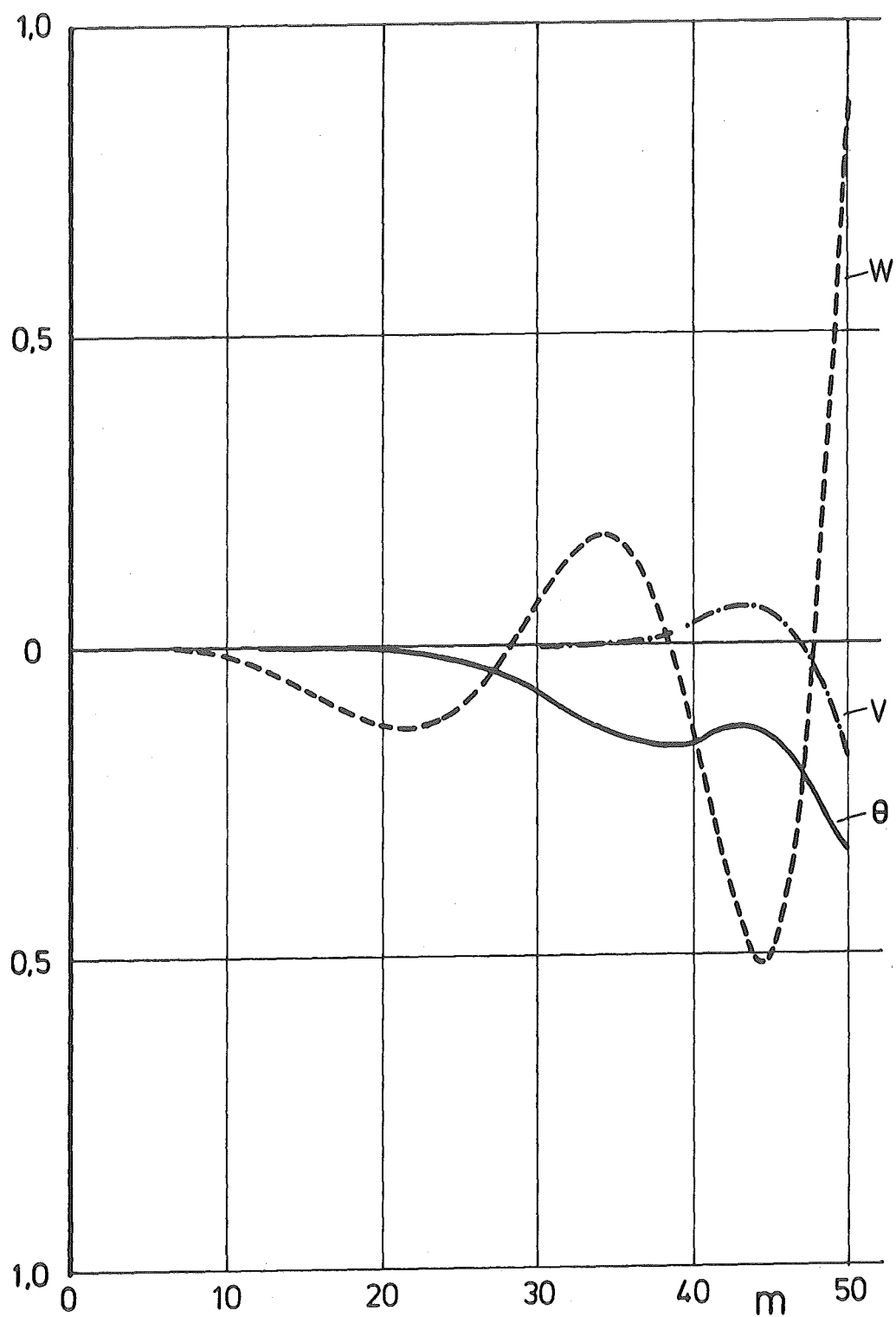
Fig. 13   Reference version,
4th flapwise bending mode   f = 11.38 Hz
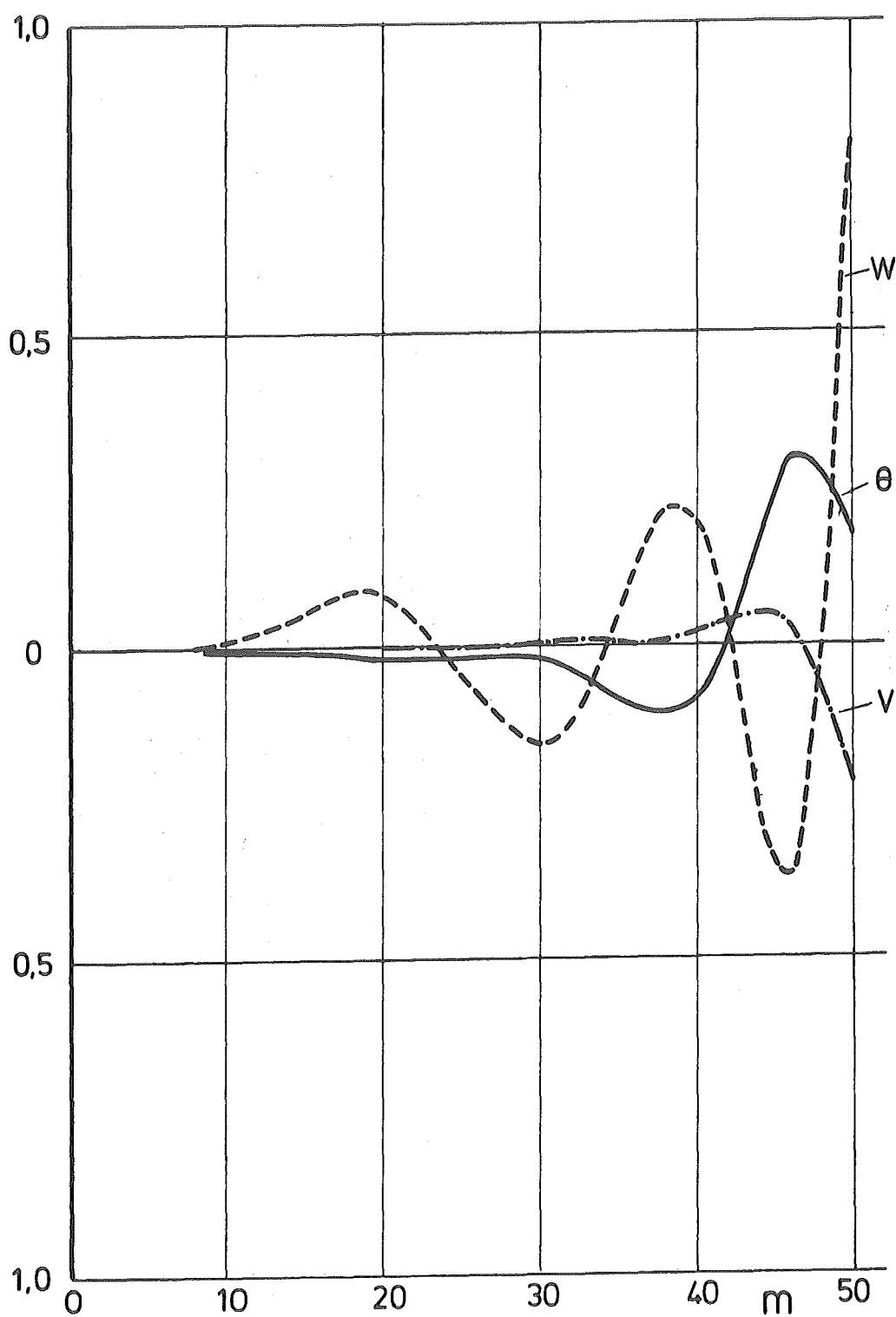
Fig. 14 Reference version,
5th chordwise bending mode   f = 12.21 Hz
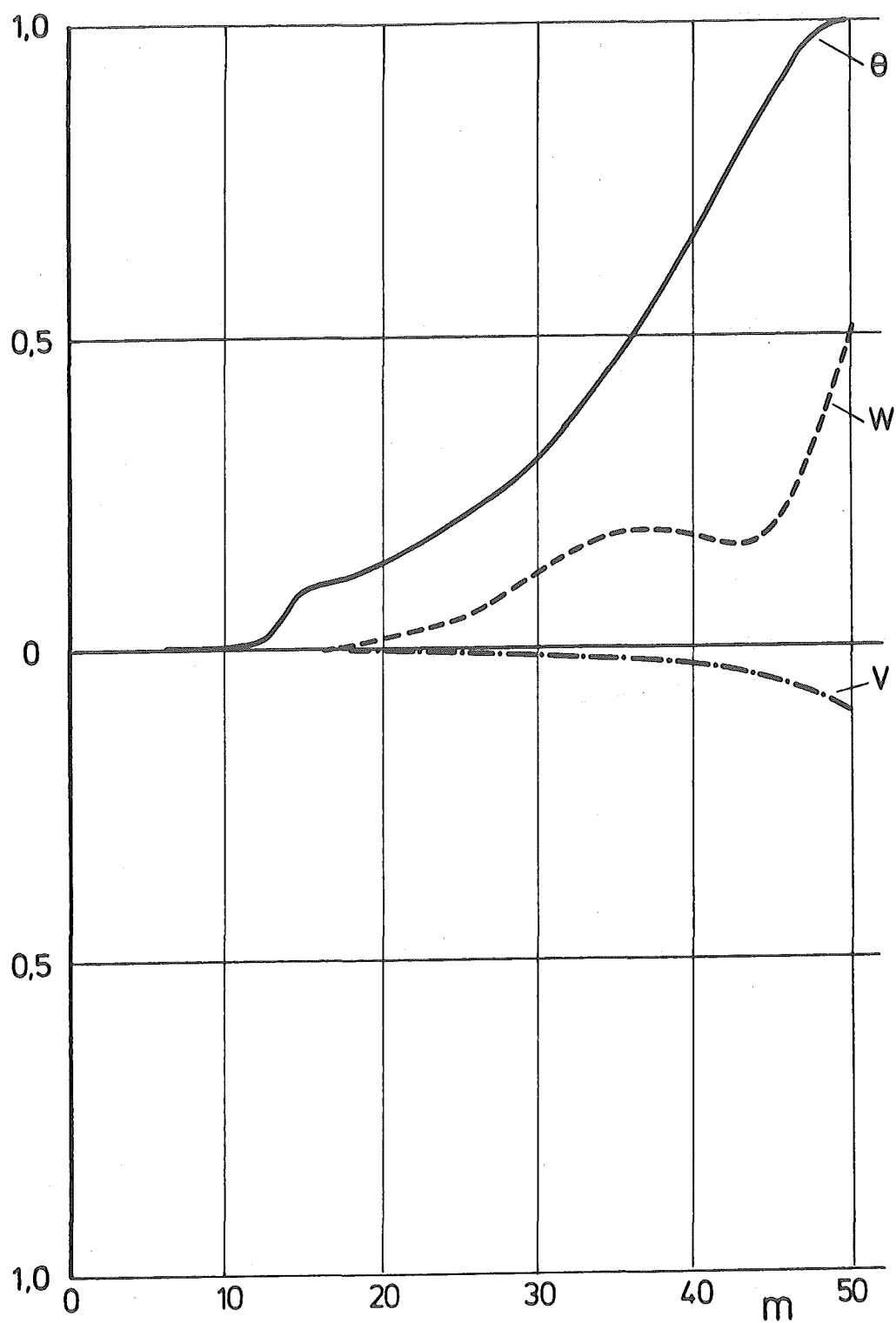
Fig. 15   5% stiffness at 12 m - 15 m,
           1st torsional mode   f = 10.00 Hz
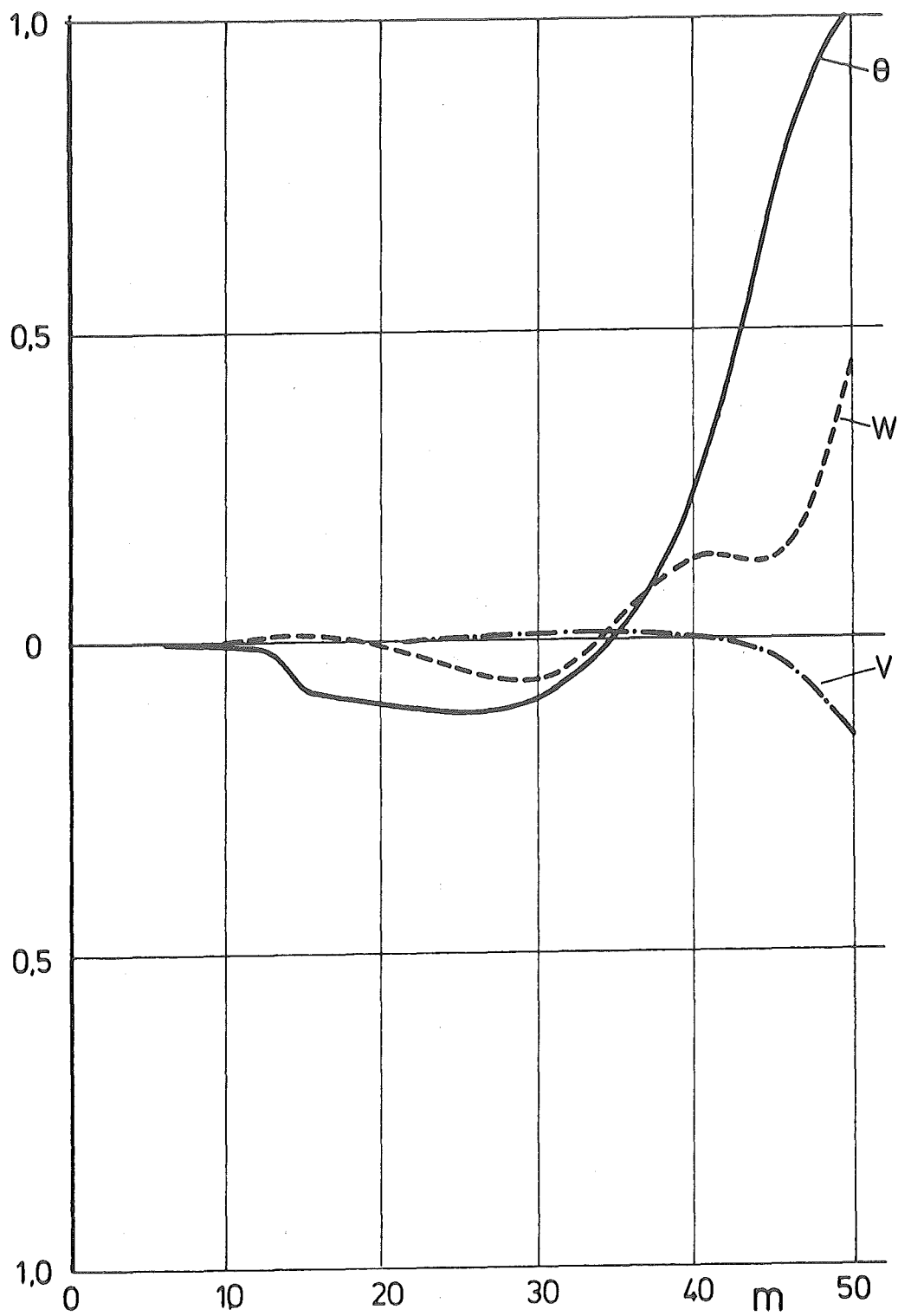
Fig. 16   5% stiffness at 12 m - 15 m,
2nd torsional mode   f = 15.22 Hz
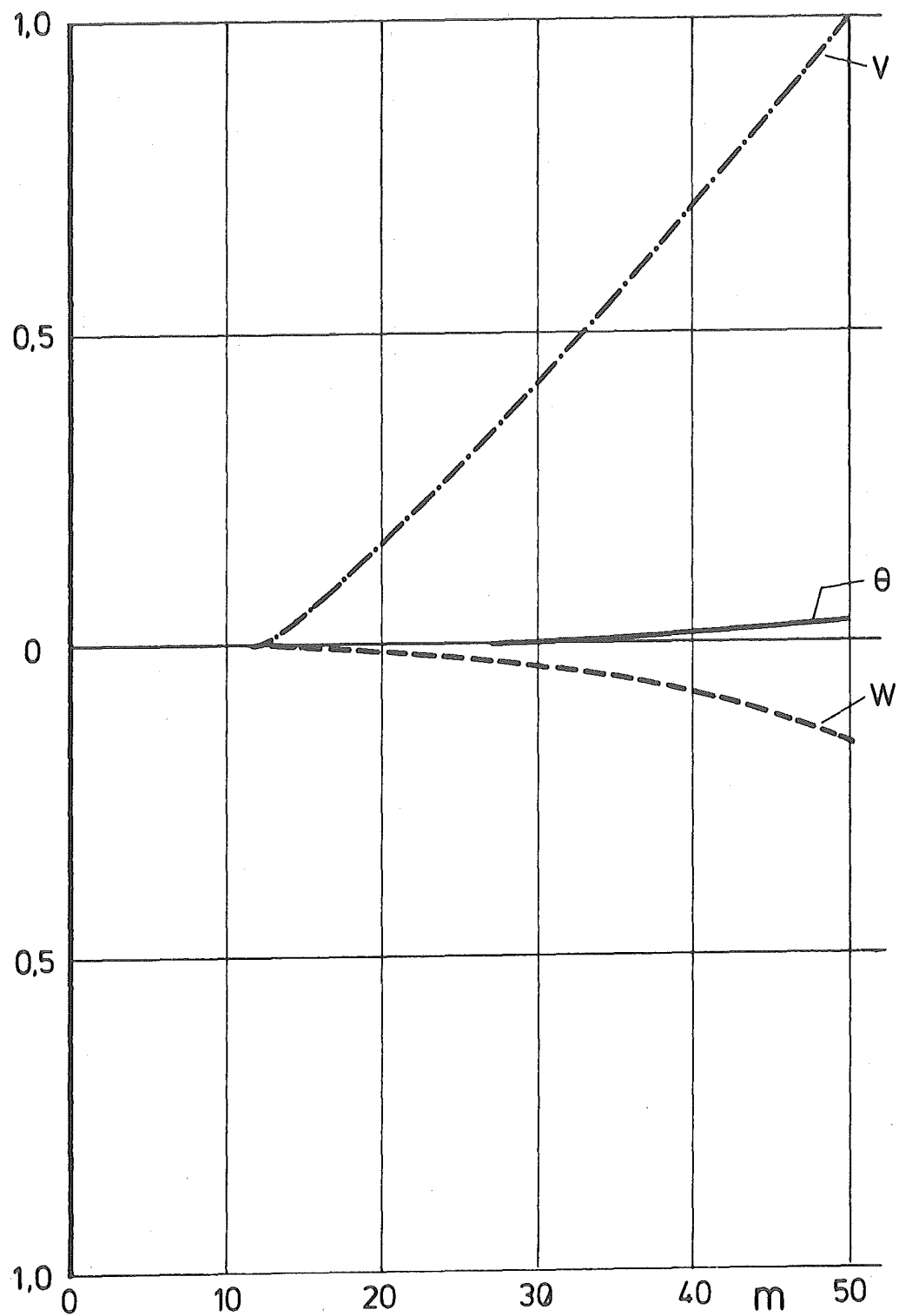
Fig. 17   5% stiffness at 12 m - 15 m,
           1st chordwise bending mode   f = 1.06 Hz
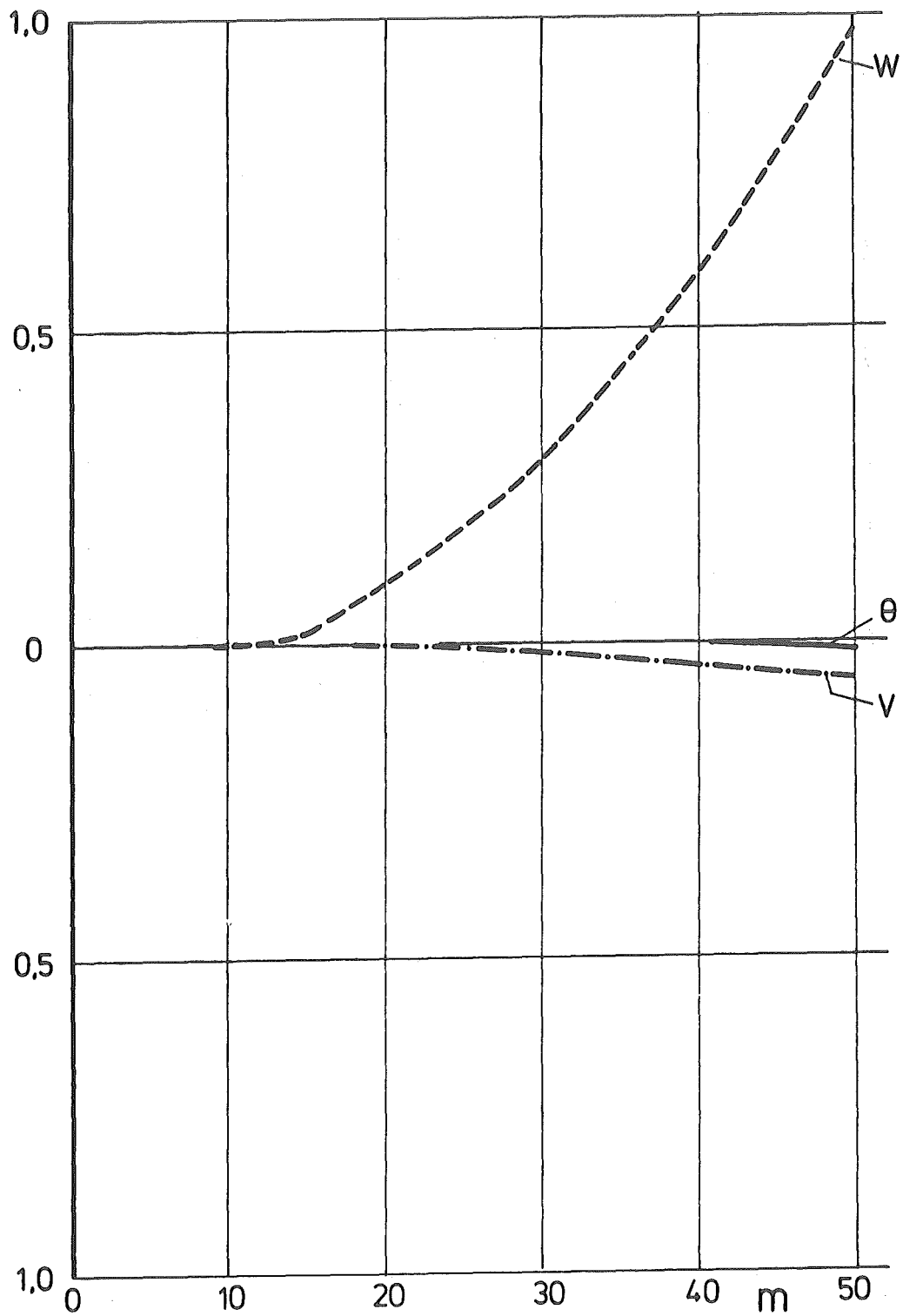
Fig. 18   5% stiffness at 12 m - 15 m,
1st flapwise bending mode   f = 0.96 Hz
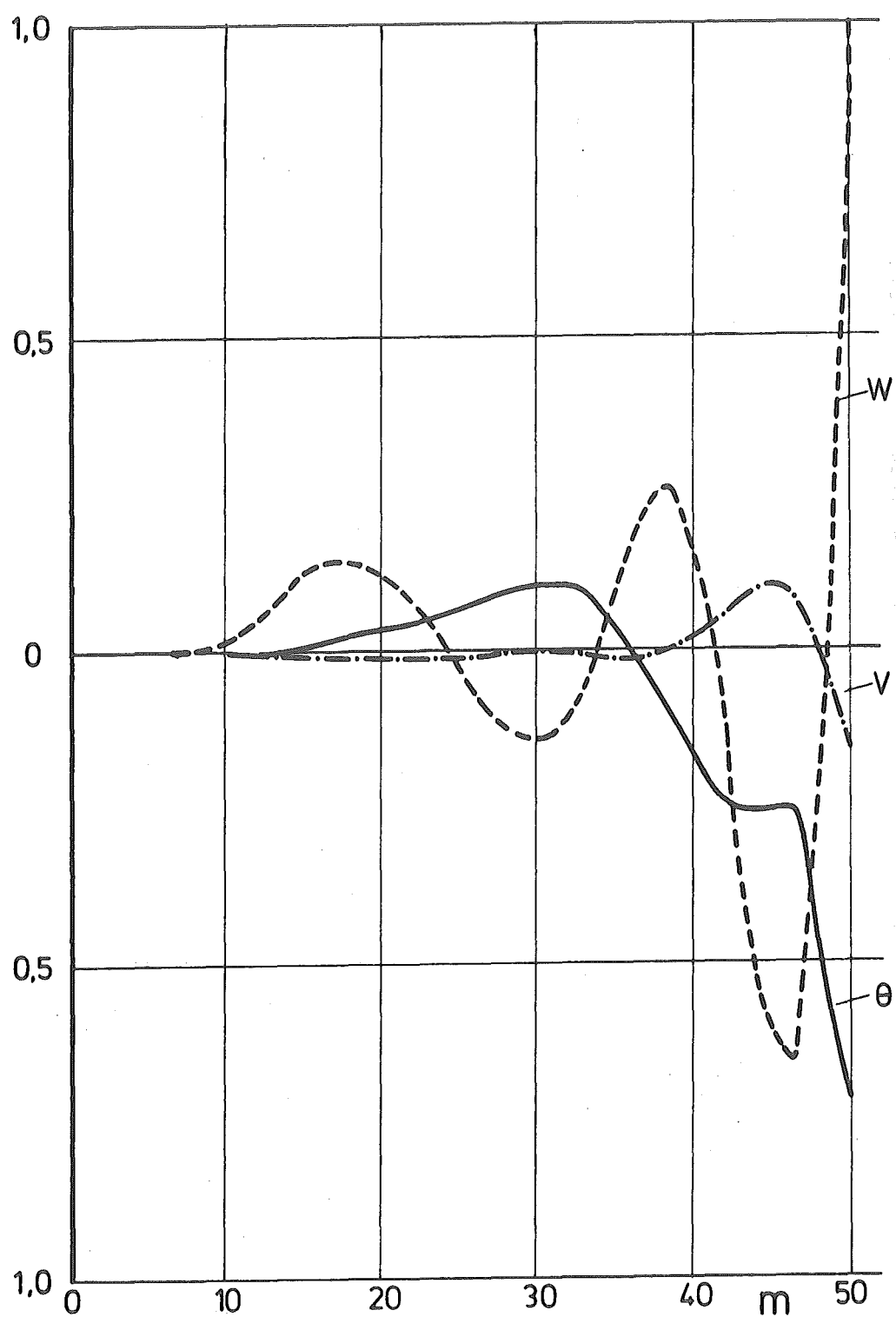
Fig. 19   5% stiffness at 12 m - 15 m,
          5th flapwise bending mode   f = 16.80 Hz
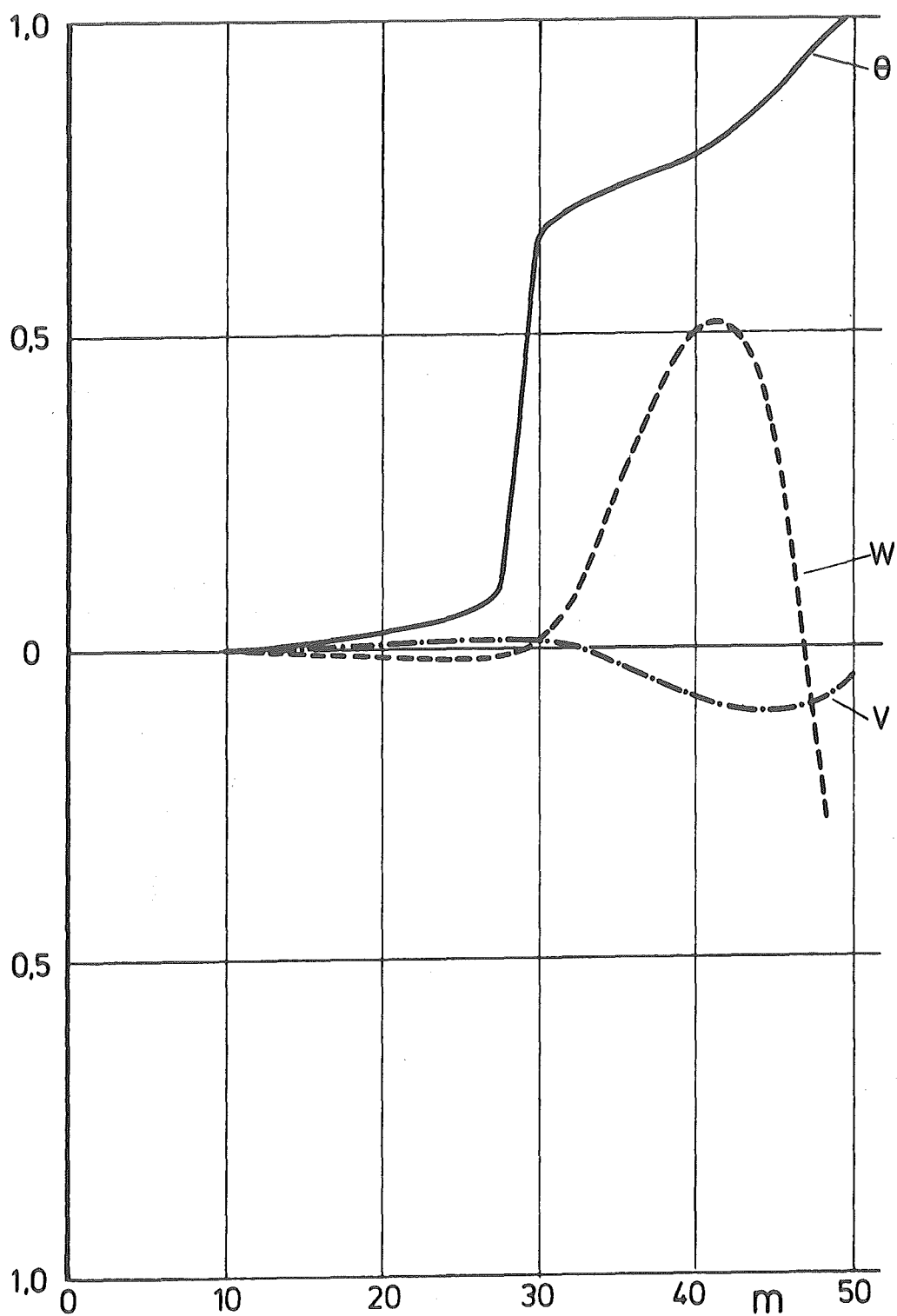
Fig. 20   5% stiffness at 30 m - 32 m,
           1st torsional mode   f = 6.14 Hz
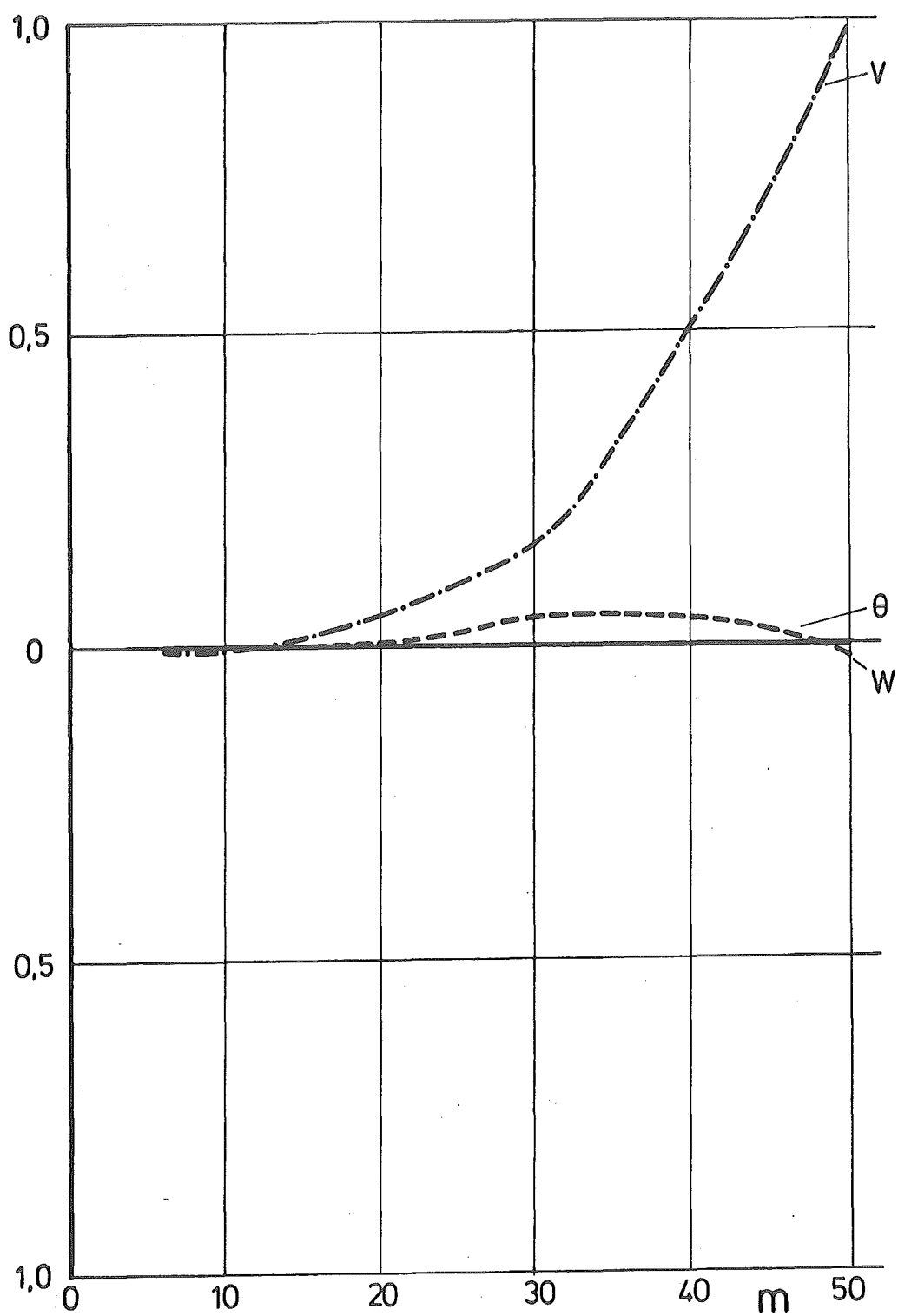
Fig. 21   5% stiffness at 30 m - 32 m,
1st chordwise bending mode   f = 2.16 Hz
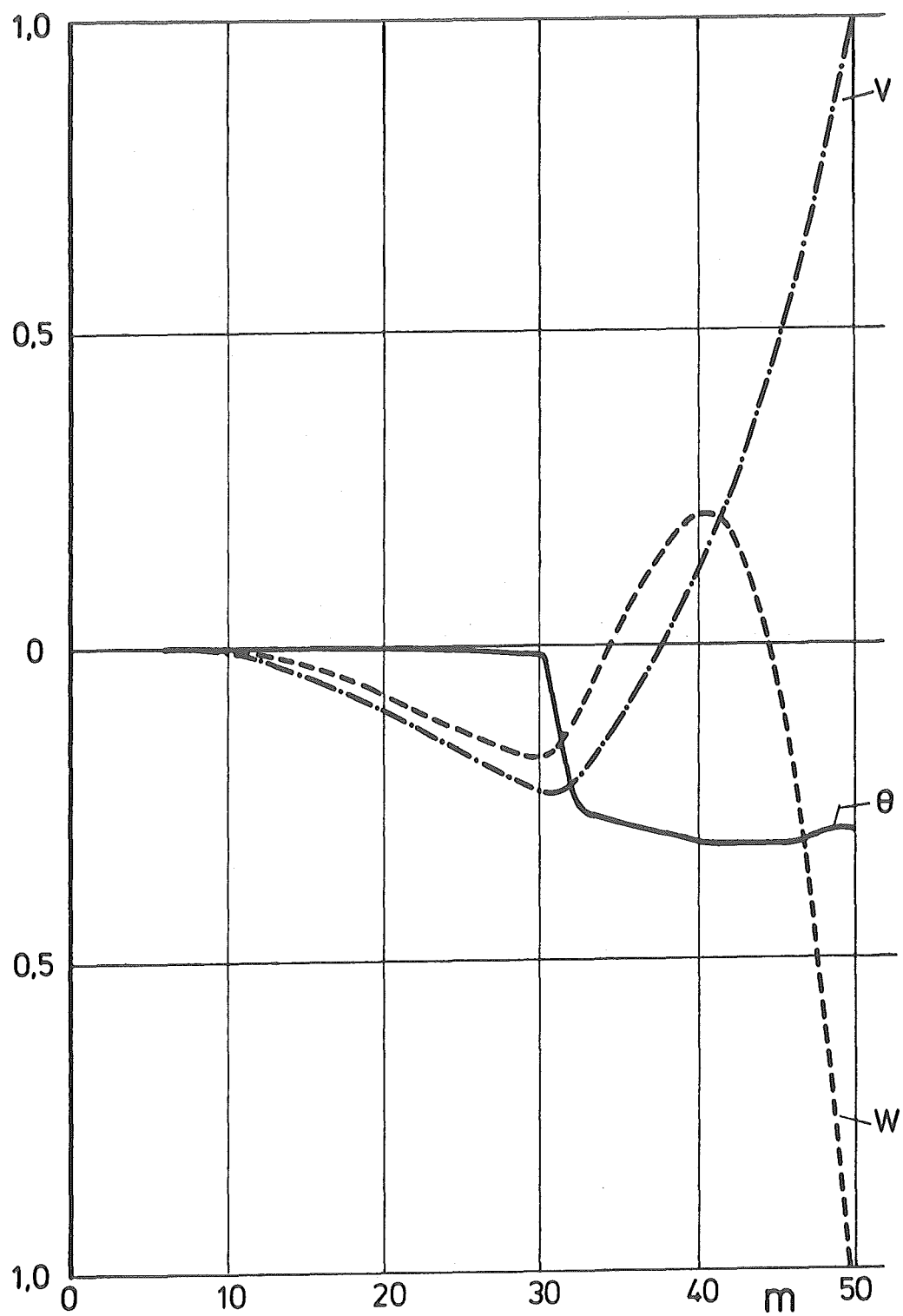
Fig. 22   5% stiffness at 30 m - 32 m,
2nd chordwise bending mode   f = 5.25 Hz
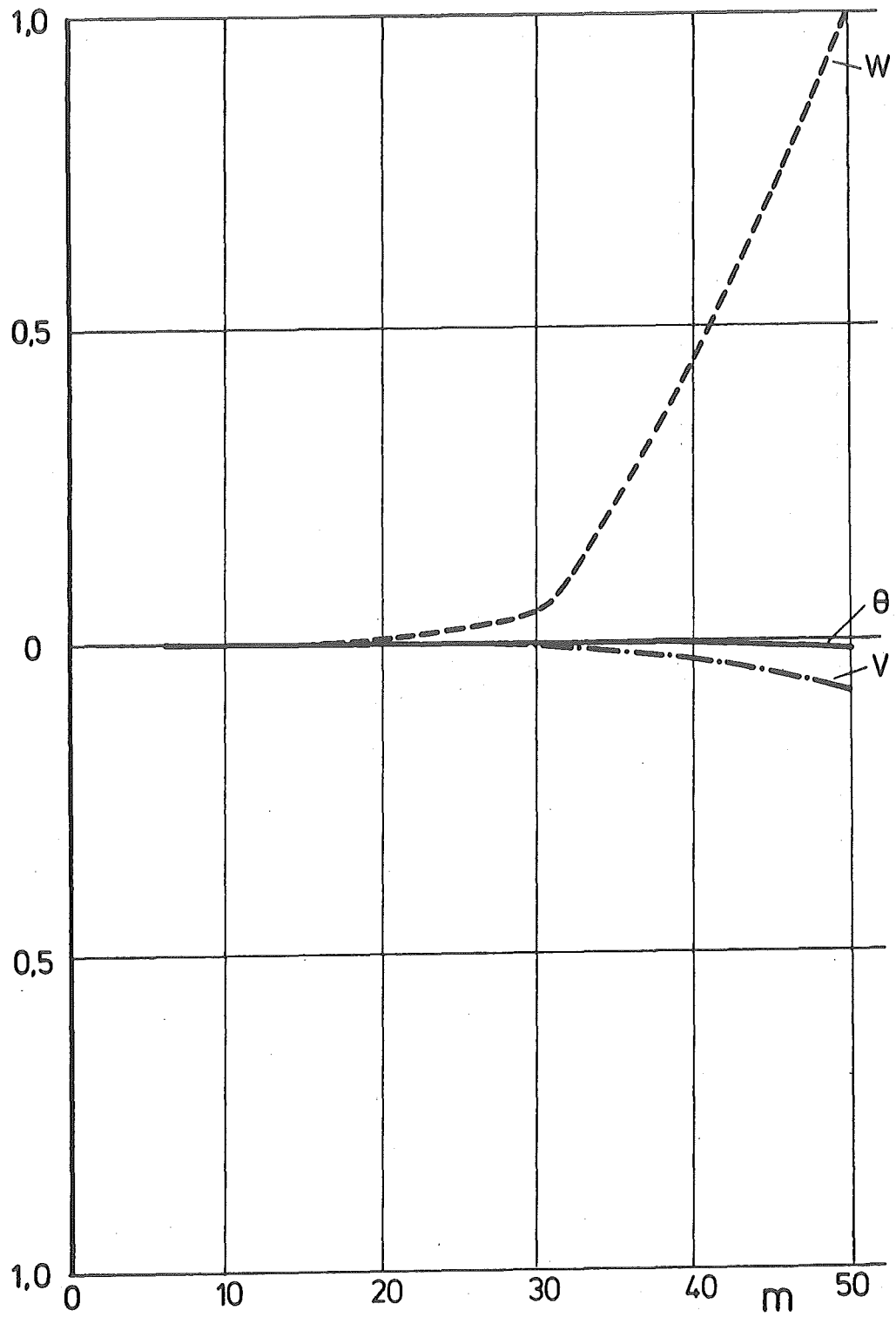
Fig. 23   5% stiffness at 30 m - 32 m,
           1st flapwise bending mode   f = 1.01 Hz
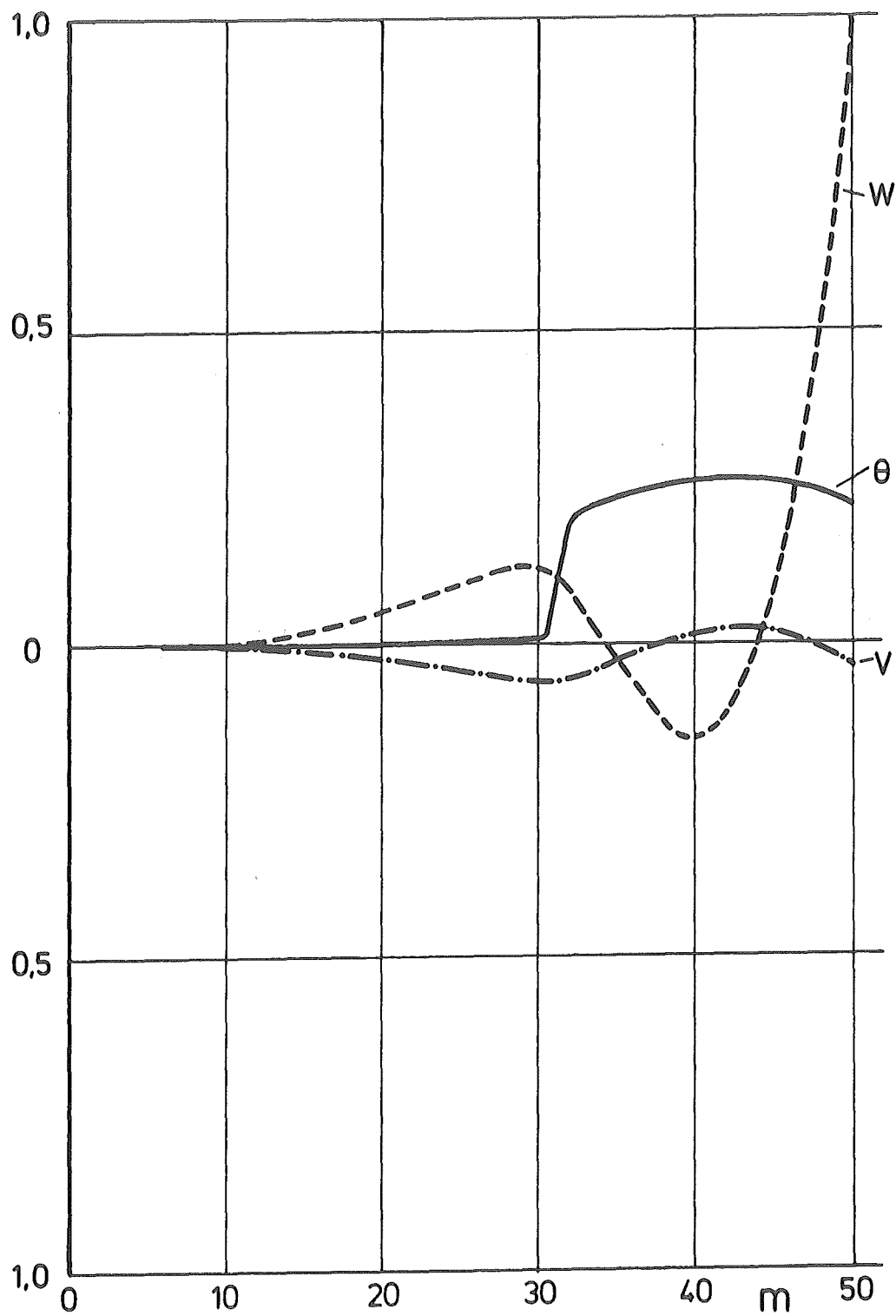
Fig. 24   5% stiffness at 30 m - 32 m,
           3rd flapwise bending mode   f = 5.55 Hz
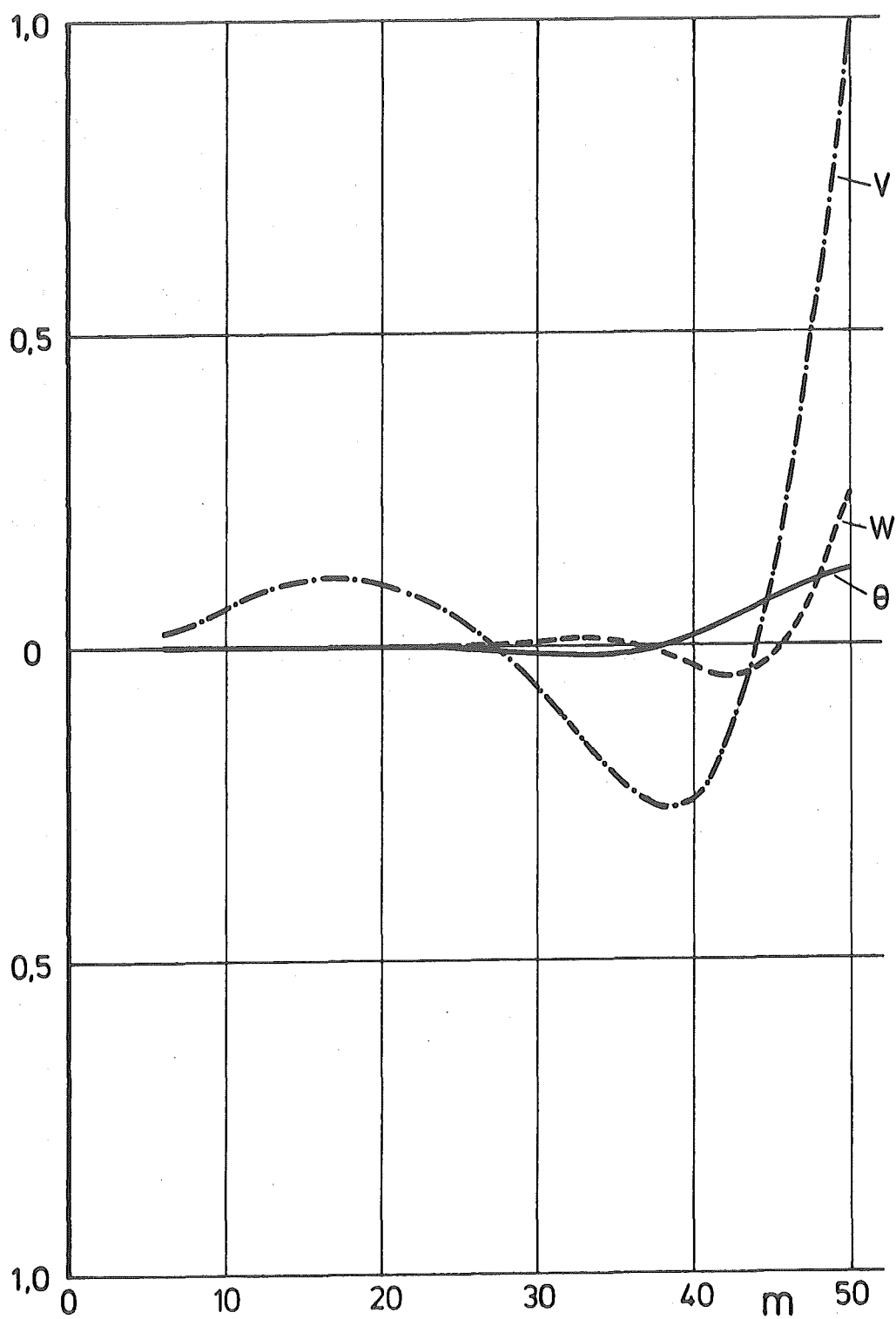
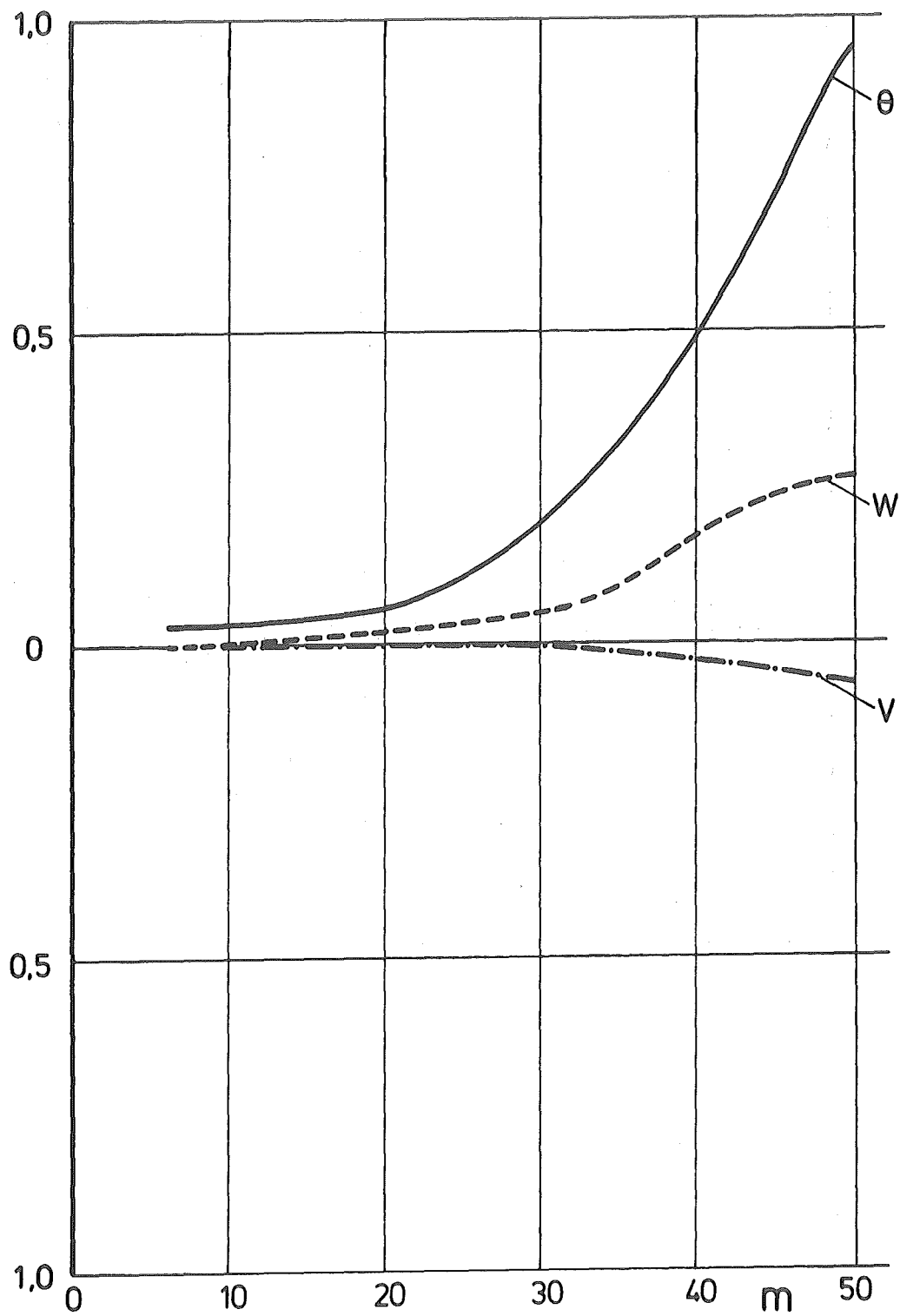Fig. 25   Elastic support,
3rd chordwise bending mode   f = 12.92 Hz

Fig. 26   5% torsional stiffness of elastic support,
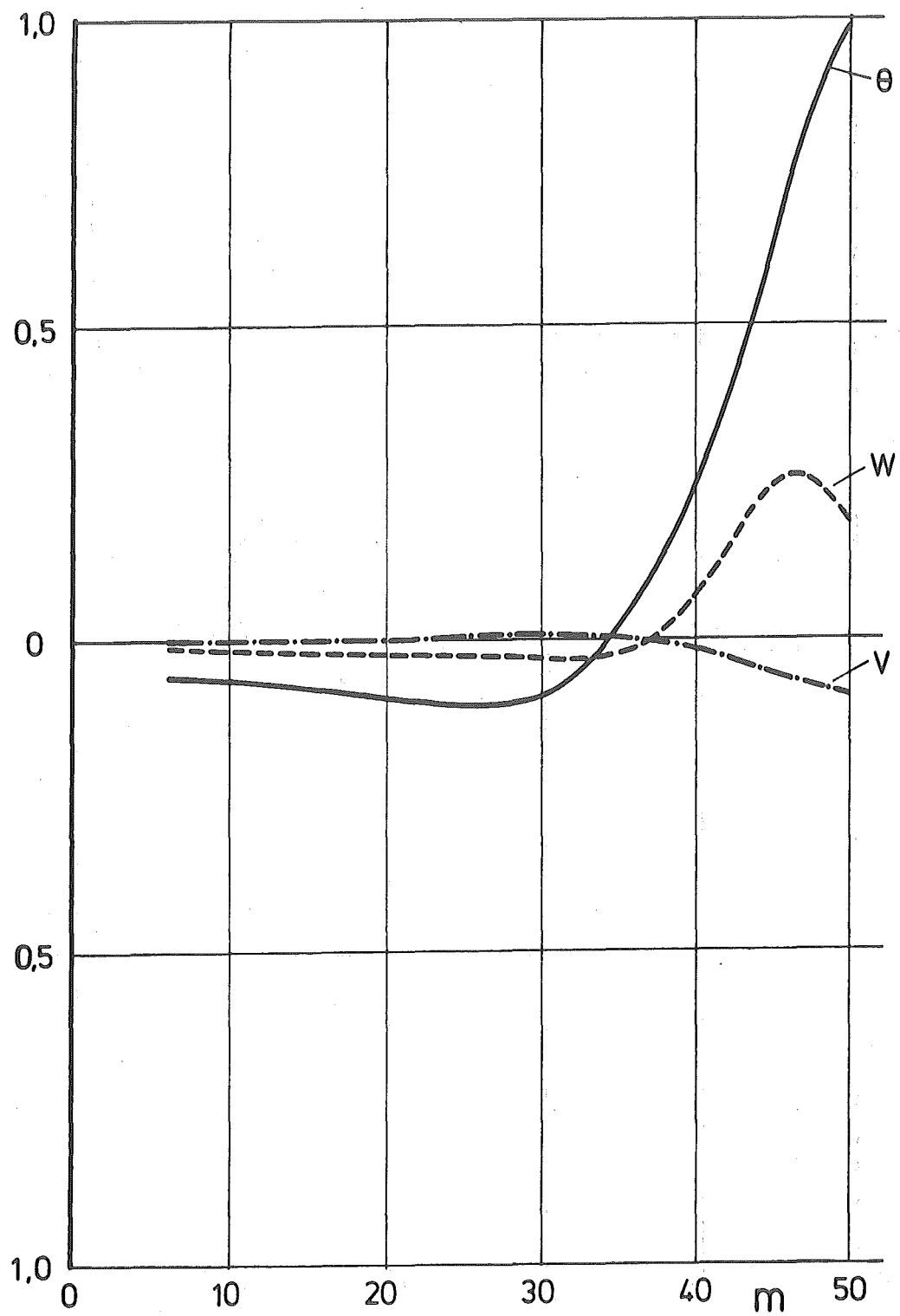1st torsional mode   f = 10.72 Hz

Fig. 27   5% torsional stiffness of elastic support,
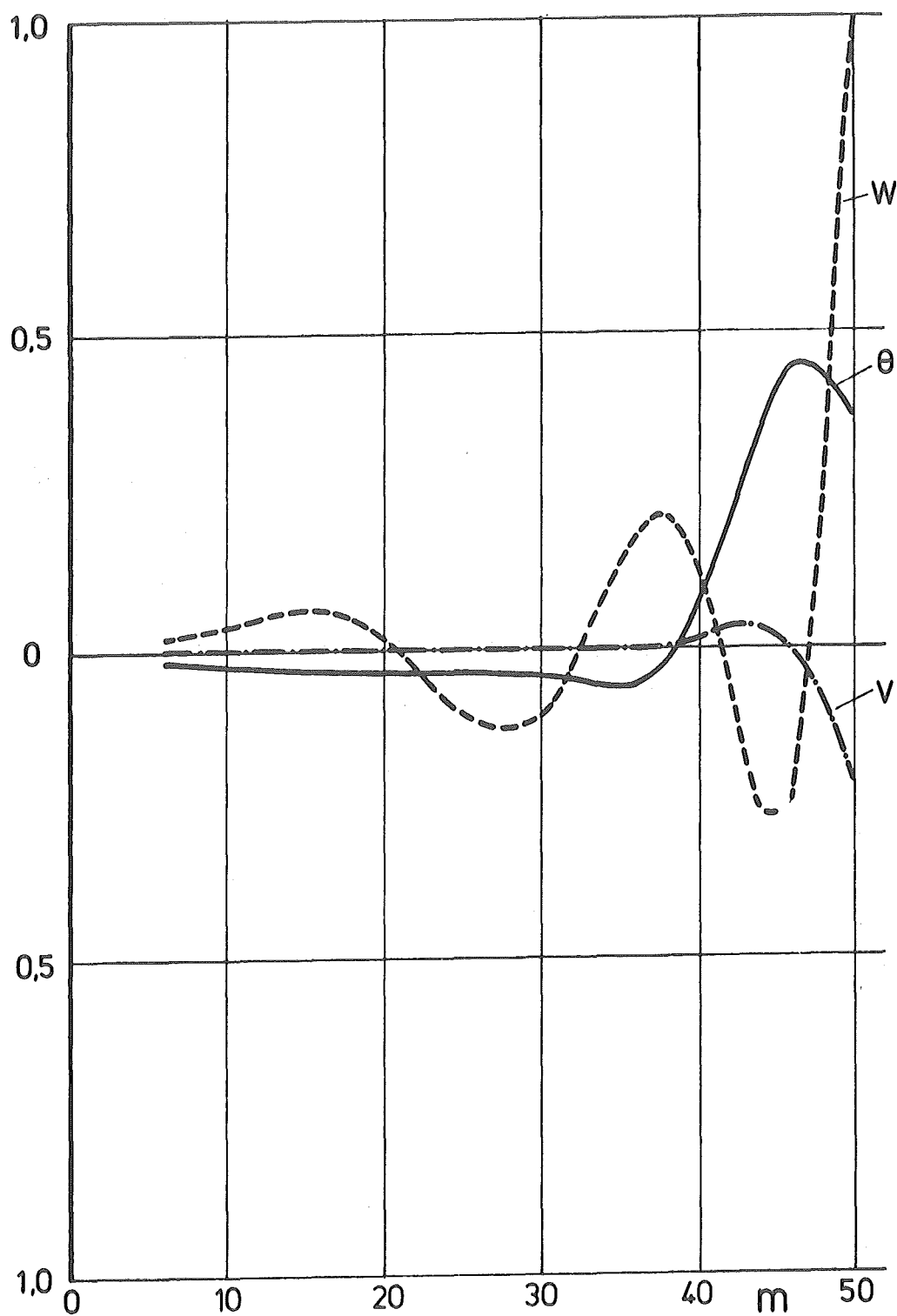2nd torsional mode   f = 15.38 Hz

Fig. 28   5% torsional stiffness of elastic support,
5th flapwise bending mode   f = 15.34 Hz

DYNAMICS OF WIND TURBINE ROTOR BLADES

Dipl.-Ing. D. Ludwig

Deutsche Forschungs- und Versuchsanstalt
für Luft- und Raumfahrt E. V.
- Aerodynamische Versuchsanstalt Göttingen -
Institut für Aeroelastik

Summary

Based on the eigenanalysis of wind turbine rotor blades stability and response charac-
teristics can be determined. The structure is modeled by finite beam elements, which
are specially developed for rotating blades. The p-k method was used to determine
the flutter stability. Finally, the problem of discrete gust loading is considered.

1. Introduction

The safety and reliability of such a flexible structure as a wind turbine must be insured by a number of stability and dynamic-response investigations. In the design stage the dynamic behaviour can be determined only theoretically. For this purpose a mathematical model is needed representing the essential physical properties of the real structure.

Before regarding the aeroelastic problems of the whole wind turbine composed of tower and rotor it is necessary to find out if there are any problems at the component level. Rotor blades of large wind energy converters are susceptible to the same aeroelastic problems occuring in principle with aircraft structures.

At the beginning of the aeroelastic analysis it is important to know the free vibration behaviour of the single rotor blade under various boundary conditions. Eigenfrequencies of the blade near to such of the tower and the rotor harmonics indicate coupling possibility and resonances, respectively. Besides, the aeroelastic equations can be formulated in terms of only a few modal coordinates. So in the following flutter stability and problems of discrete gusts based on the eigenanalysis of the single blade are discussed.

2. Free Vibration Analysis of Rotor Blades

The differential equations of motion for the bending and torsional deformations of twisted rotating beams are developed by J.C.HOUBOLT and G.W.BROOKS [1]. Contrary to previous theories they have made no restriction concerning the geometrical arrangement of the neutral, elastic and mass axes. Besides they have given special attention to the coupling terms resulting from the centrifugal forces.

Figure 1 shows a typical rotor beam element, the x-axis of which runs to the tip of the blade and coincides with the undeformed position of the elastic axis. The y-axis coincides with a reference chord line in the untwisted cross-section of the rotor blade. These two axes move with the blade around an axis of rotation with a given angular velocity Ω. The axis of rotation is parallel to the z-axis and may have a distance e_0. All deformations of the blade are referred to the x-y-z coordinate system.

The rotor beam element has 10 degrees of freedom, the two translational motions v and w and the three rotational motions Φ, γ and ϑ at each modal point. The characteristics of the beam element are described in Figure 2.

If we introduce the characteristics of the beam element in the final equation for both the total potential and kinetic energy it is possible to receive the mass matrix, the stiffness matrix and the column of displacements for one rotor beam element.

For free vibration analysis of the whole rotor blade we have to subdivide the blade into a sufficient number of beam elements along the blade radius. This is made for instance in Figure 3 for the 50 m blade of GROWIAN. Hereby, it has to be mentioned that there is a fictitious chord length between $x = 0$ m and $x = 15$ m .

The global matrices of stiffness and mass and the global column of displacements are to be calculated by superposing the matrices and columns of the elements. The modes of free vibration can be calculated for any desired boundary conditions if the desired degrees of freedom are constrained at the hub.

In Figure 4 to 6 the modes of free vibration are shown for GROWIAN rotor blade under the condition of rigid fixation at the hub. The first flapwise bending, lagwise bending and torsional modes are plotted versus rotor radius for the rotating blade at rated speed. The modes are normalized in this way that the generalized mass of each mode has the value 1 . It can be seen that there are lag components in the flap mode, flap components in the lag mode and flap and lag components in the torsional modes. This results from the coupling terms due to the noncoincident axes. If we compare these free vibration modes with the modes of the nonrotating blade we will find out that the influence of centrifugal forces is small.

The variation of the rotational velocity yields different eigenfrequencies for each mode. The three lowest free vibration modes are presented in the resonance diagram of Figure 7 where the eigenfrequency is plotted versus the rotational speed, both related to the rated speed. Whereas the eigenfrequency of the lag mode is nearly constant the eigenfrequencies of the flap modes are increasing if the rotational velocity is increasing, too. There is no possibility of resonance with the harmonics of the rotor blade at the rated speed. Only the 2nd flapwise bending mode is near to the 10th rotor harmonic.

3. Flutter Stability of Rotor Blades

The vibration behaviour of an elastomechanical structure can be described by means of the so-called modal degrees of freedom. The flutter equation can be written as follows in the well-known modal terms:

$$\underline{M}\,\ddot{q}(t) + \underline{D}\,\dot{q}(t) + \underline{K}\,q(t) = \underline{Q}(\ddot{q},\,\dot{q},\,q,\,t) \tag{1}$$

with

$\underline{\underline{M}}$ diagonal matrix of the generalized masses M_r,

$\underline{\underline{K}}$ diagonal matrix of the generalized stiffnesses K_r,

$\underline{\underline{D}}$ matrix of the generalized damping coefficients D_{rs},

$\underline{q}$ column of the generalized coordinates q_r,

$\underline{Q}$ column of the generalized unsteady aerodynamic forces Q_r.

The flutter equation written in this form is assuming structural linearity and viscose damping.

It is possible to solve this differential equation if we confine ourselves to determine the critical velocity. At this velocity the total damping added from structural and aerodynamical damping is zero and the structure is vibrating harmonically. For the special case of harmonic vibrations the generalized coordinate and force can be written as:

$$\underline{q} = \text{Re} \, [\underline{\hat{q}} \, e^{i\omega t}] \tag{2}$$

$$\underline{Q} = \text{Re} \, [\underline{\hat{Q}} \, e^{i\omega t}] \tag{3}$$

with the circular frequency ω and $i = \sqrt{-1}$.

The substitution of the equations (2) and (3) into equation (1) yields:

$$(-\omega^2 \underline{\underline{M}} + i\omega \underline{\underline{D}} + \underline{\underline{K}}) \, \underline{\hat{q}} - \underline{\hat{Q}} = \underline{0} . \tag{4}$$

The structural stiffness and damping terms of this equation can be combined and expressed by a complex stiffness:

$$\underline{\underline{K}} + i\omega \underline{\underline{D}} = \underline{\underline{\omega}}_e^2 \, \underline{\underline{M}}(1 + i \, g_r) \tag{5}$$

where $\underline{\underline{\omega}}_e$ is the diagonal matrix of the circular frequencies ω_r and g_r is the so called loss angle of the r-th mode.

Then, we obtain from equation (4):

$$[-\omega^2 \underline{\underline{M}} + \underline{\underline{\omega}}_e^2 \, \underline{\underline{M}}(1 + i \, g_r)] \, \underline{\hat{q}} - \underline{\hat{Q}} = \underline{0} . \tag{6}$$

The generalized aerodynamic forces are depending on the generalized coordinates, too, and can be written in the case of harmonic vibration as:

$$\underline{\hat{Q}} = -\rho \, \omega^2 \, \underline{\underline{F}} \, \underline{\hat{q}} \tag{7}$$

where $\underline{\underline{F}}$ is the complex matrix of the unsteady aerodynamic coefficients.

From equation (6) we obtain with equation (7):

$$[\omega_e^2 \underline{\underline{M}}(1 + i \underline{g}_r) - \omega^2(\underline{\underline{M}} - \rho\underline{\underline{F}})] \hat{\underline{q}} = \underline{0} \quad . \tag{8}$$

In the case of harmonic vibration the unsteady aerodynamic coefficients are functions of the reduced frequency.

For nontrioial solutions the determinant of equation (8) must be equal to zero. Therefore equation (7) can be written in such a way that we get a special complex eigenvalue problem:

$$\underline{\underline{A}} \, \hat{\underline{q}} = p \cdot \hat{\underline{q}} \tag{9}$$

with the complex eigenvalue $p = \gamma \, k \pm i \, k$.

$k = \omega c / U$ is the nondimensional reduced frequency.

$\gamma = (1/2\pi) \, \ln(a_{n+1}/a_n)$ is the rate-of-decay.

An approximate method of finding a rate-of-decay solution directly is the p-k method [2].

As mentioned in the case of harmonic vibration the aerodynamic forces are functions of the reduced frequency k . Therefore we can compute unsteady aerodynamic coefficients for an estimated value of k and can solve the eigenvalueproblem of equation (9). The solution of the eigenvalueproblem leads to a $p_1 = \gamma \, k_1 + i \, k_1$. Then we can compute the aerodynamic forces with k_1 and solve the eigenvalueproblem again which leads to a $p_2 = \gamma \, k_2 + i \, k_2$, etc. We have to do this until the imaginary part of the eigenvalue is equal to the reduced frequency used for the aerodynamics. This is, in principle, the p-k iteration for solving the flutter equation which leads to one solution at one specific speed.

It can easily be seen that much time is wasted in computer programs solving eigenvalueproblems in an iteration loop. Therefore it is usual to compute the roots within the p-k method by determinant iteration. If all the roots for one speed are found in this way, the process of determinant iteration can be applied to the next preselected speed.

A computer program was developed using the determinant iteration of p-k method and aerodynamic strip theory. Besides the aerodynamic coefficients the generalized masses, eigenfrequencies, loss angles and generalized coordinates of all modes are needed. The generalized masses, eigenfrequencies and eigenmodes can be determined by ground vibration test or by free vibration analysis, respectively. The loss angle is only to obtain by test. If the free vibration calculation is the input for the flutter program the loss angle may be set equal to zero to be conservative.

So all elastomechanical parameters are known and the aerodynamic coefficients can be computed for all modes and desired reduced frequencies using unsteady aerodynamic theory of oscillating wings.

In Figures 8 and 9 the rate-of-decay is plotted versus free-stream velocity for GROWIAN rotor blade rotating with rated speed and nonrotating. The results of free vibration analysis are the input data for the flutter program. The loss angle is equal to zero. The diagrams are plotted for the first 10 modes. There are 5 flap modes, 3 lag modes and 2 torsional modes within. Usually the lag modes are neglected in flutter calculation because there are no significant aerodynamic forces resulting from lag components. The free vibration analysis has shown that there are flap components in the lag modes. Therefore the flutter calculation was carried with for the lag modes, too.

It can be seen that there are several modes with small damping. These are the lag modes which have small aerodynamic damping. For the first 10 modes flutter is not occuring up to a free-stream velocity of 170 m/s. The limit of flutter stability is reached if the rate-of-decay is equal to zero.

4. Dynamic Response to a Discrete Gust

Fundamental to any method of predicting dynamic response to a discrete gust is a rotational representation of the gust configuration. Parameters such as gust intensity, gradient, profile and the spanwise distribution of gust velocity have important effects upon the rotor blade and the resulting stresses.

Referring to Figure 10, we assume that the rotor blade encounters a discrete gust of the distribution $w_G(s)$ normal to the direction of the free-stream velocity. U . The dimensionless time variable s is defined by

$$s = \frac{U t}{c_0} \quad , \tag{10}$$

where c_0 is the length of the half-chord in the reference cross-section. The rotor blade is permitted to move in rigid-body motions and any number of flapwise bending modes.

For the formulation of the dynamic response problem we can use the same differential equation as given in chapter 3. In this case the generalized forces consist of two parts, the generalized forces due to the gust and such due to the motion. If we assume that structural damping can be neglected we obtain in generalized terms with the dimensionless time variable s :

$$\frac{U^2}{c_0^2} \underline{\underline{M}} \, q''(s) + \underline{\underline{\omega}}_e^2 \, \underline{\underline{M}} \, \underline{q}(s) = \underline{Q}_G(s) + \underline{Q}_M(s) \ . \tag{11}$$

Assuming both an uniform spanwise chord distribution and application of the strip theory we are able to approximate the generalized forces due to the motion and due to the gust by means of the known exponential forms of WAGNER's function $\Phi(s)$ and KÜSSNER's function $\psi(s)$, respectively. Then we obtain:

$$\underline{\underline{\mu}} \, \underline{q}''(s) + \underline{\underline{\varkappa}} \, \underline{q}(s) + \underline{\underline{I}}_M \int_0^s \Phi(s-\sigma) \, \underline{q}''(\sigma) \, d\sigma = \underline{I}_G \int_0^s w_G(\sigma) \, \psi'(s-\sigma) \, d\sigma , \tag{12}$$

with

$$\Phi(s) \approx 1 + b_1 e^{\beta_1 s} + b_2 e^{\beta_2 s} \ ,$$

$$\psi(s) \approx 1 + a \, e^{\alpha_1 s} + a \, e^{\alpha_2 s} \ ,$$

$$a = -0.5, \quad \alpha_1 = -0.13, \quad \alpha_2 = -1.0 ,$$

$$b_1 = -0.165, \quad b_2 = -0.355,$$

$$\beta_1 = -0.0455, \quad \beta_2 = -0.3 \ .$$

$\underline{\underline{\mu}}$ diagonal matrix of the dimensionless generalized masses μ_r ,

$\underline{\underline{\varkappa}}$ diagonal matrix of the dimensionless generalized stiffnesses $\varkappa_r$,

$\underline{\underline{I}}_M$ symmetrical matrix with constant elements $I_{M,rs}$ which are to obtain by integration,

$\underline{\underline{I}}_G$ column with constant elements $I_{G,r}$ which are to obtain by integration, too.

It is possible to solve the differential equation (12) by the LAPLACE-transform method. Applying the LAPLACE transformation to equation (12) we obtain:

$$[p^2 \underline{\underline{\mu}} + p^2 \Phi(p) \, \underline{\underline{I}}_M + \underline{\underline{\varkappa}}] \, \underline{q}(p) = p \, w_G(p) \, \psi(p) \, \underline{I}_G \ . \tag{13}$$

The introduction of the approximated WAGNER function with its LAPLACE transformation into (13) yields to:

$$[p^2 \underline{\underline{\mu}} + p^2 (\frac{1}{p} + \frac{b_1}{p - \beta_1} + \frac{b_2}{p - \beta_2}) \, \underline{\underline{I}}_M + \underline{\underline{\varkappa}}] \, \underline{q}(p) =$$

$$= p \, w_G(p) \, \psi(p) \, \underline{I}_G \ . \tag{14}$$

If we multiply equation (14) with $(p - \beta_1)(p - \beta_2)$ we obtain this type of an algebraic matrix equation:

$$[p^4 \underline{\underline{A}}_4 + p^3 \underline{\underline{A}}_3 + p^2 \underline{\underline{A}}_2 + p \underline{\underline{A}}_1 + \underline{\underline{A}}_0] \underline{q}(p) =$$

$$= (p - \beta_1)(p - \beta_2) p \ w_G(p) \psi(p) \underline{l}_G \quad . \tag{15}$$

For inverse transformation we have to determine $\underline{q}(p)$ expanded into a sum:

$$q(p) = \sum_{i=1}^{m} \frac{\underline{F}_i}{p - p_i} (p - \beta_1)(p - \beta_2) p \ w_G(p) \psi(p) \underline{l}_G \quad . \tag{16}$$

We obtain $m = 4 * n$ roots if we solve the eigenvalue problem of order four:

$$[p^4 \underline{\underline{A}}_4 + p^3 \underline{\underline{A}}_3 + p^2 \underline{\underline{A}}_2 + p \underline{\underline{A}}_1 + \underline{\underline{A}}_0] \underline{q}(p) = \underline{0} \quad , \tag{17}$$

by reducing it to a linear eigenvalue problem:

$$\underline{\underline{A}} \ \underline{x} = p \underline{x} \quad . \tag{18}$$

$\underline{F}_i$ are square matrices of order $m = 4 * n$ and rank one which are to determine by

$$\underline{\underline{F}}_i = \underline{x}_i^r \ \underline{x}_i^{lT}, \quad (i = 1, 2, \ldots, m) \tag{19}$$

where $\underline{x}_i^r$ are the right hand eigenvectors and $\underline{x}_i^l$ the left hand eigenvectors of the i-th root.

Before the inverse transformation of equation (16) can be done, we have to introduce the gust distribution. It is often usual to assume a sharp-edged gust, however a more realistic assumption would be a sine-wave or a cosine-wave gust distribution.

In Figure 11 the generalized coordinates are plotted versus time for an (1-cos)-gust distribution inside the gust period. The rotor blade is rotating with rated speed and the generalized masses, eigenfrequencies and eigenmodes of the first 5 flapwise bending modes calculated by free vibration analysis are the input data. The maximal gust velocity has the value of 12 m/s and the gust period is 1.5 s . It can be seen that the maximal value for the generalized coordinate of the first mode appears at the time $t = 1.0$ s.

The graph of the total physical deformation at the time $t = 1.0$ s is plotted versus rotor radius in Figure 12. At this time the deformation at the top of the blade has the maximum value of 4.3 m . With the known deformation distribution it is possible to determine the stresses due to this discrete gust, which can be compared with the allowable stresses.

Beside the maximum gust velocity which can occur the gust period is an essential parameter. In [3] the dynamic response of an airplane to a (1 - cos)-gust distribution is calculated. Two degrees of freedom, one rigid body mode and the first symmetrical bending mode,

are considered. The maximal stresses occur if the gust period is equal to the period of the first bending mode. However, this does not prove to be a general result especially in cases of more than one flapwise bending modes. In this case we have to vary the gust period to determine the maximal stress value.

5. References

[1] HOUBOLT, J.C., BROOKS, G.W.

Differential equations of motion for combined flapwise bending, chordwise bending, and torsion of twisted non uniform rotor blades.

NACA Rep. 1346 (1958)

[2] HASSIG, H.J.

An approximate true damping solution of the flutter equation by determinant iteration.

J. Aircraft, Vol.8, No.11 (Nov. 1971)

[3] BISPLINGHOFF, R.L., ASHLEY, H.

Principles of aeroelasticity.

Dover Publications, Inc., New York

elastic axis
tension axis
mass axis
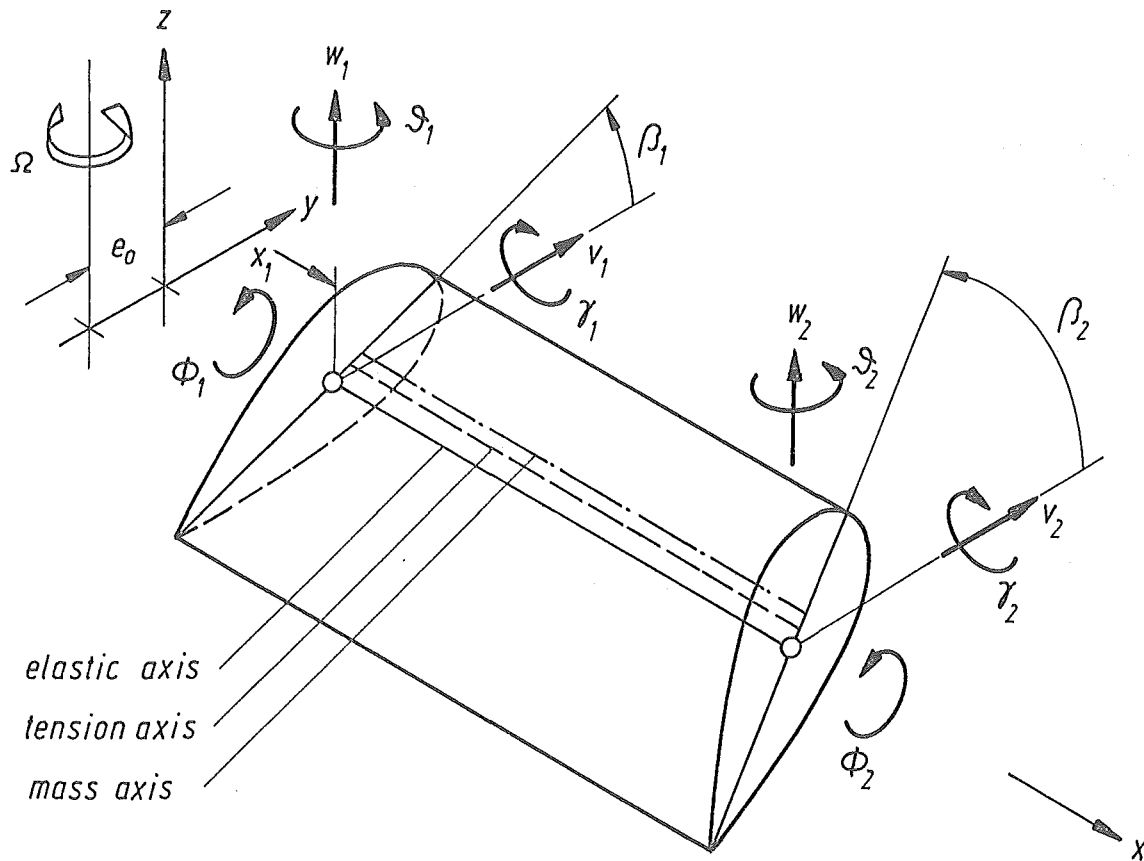
symmetrical cross-section
10 degrees of freedom
deformations: flapwise bending
                lagwise bending
                torsion

Figure 1: Rotor beam element

	Aerodynamische Versuchsanstalt Göttingen		Blatt-Nr. 11
			Figure 2

1. Displacement functions:

   - linear distribution for torsion ϕ

   - cubic distribution for flapwise and lagwise bending w, v

2. Parameters of masses:

   - constant mass distribution m/l

   - constant distance between mass and elastic axis e

   - constant mass radii of gyration km_1, km_2

3. Parameters of tension and bending

   - constant bending stiffness EI_1, EI_2

   - constant distance between area centroid in carrying tensile stresses and elastic axis e_A

   - constant polar radii of gyration of area centroid in carrying tensile stresses k_A

   - constant tension stiffness EF

4. Parameters of torsions

   - constant torsional stiffness GJ

   - constant parameters of section constants defined by HOUBOLT/BROOKS EB_1, EB_2

5. Geometrical parameters

   - linear distribution of built-in twist ß

   - constant distance between elastic axis and axis about which the blade is rotating e_0

Figure 2: Characteristics of the rotor beam element
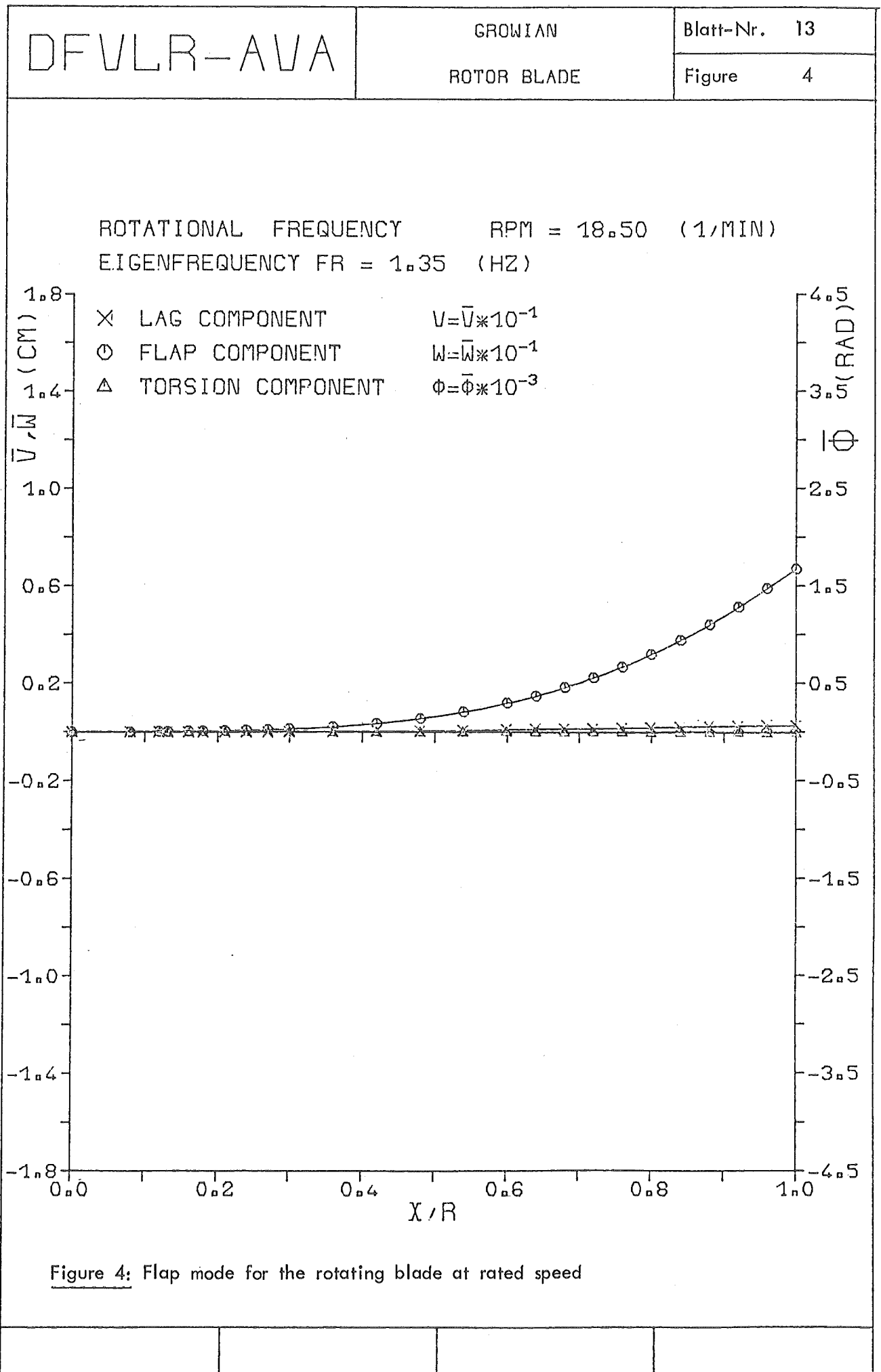
Datum:	Abteilung:	Gesehen:	Bericht:
Bearbeitet:			

Schleicher + Schull GmbH, Eroach
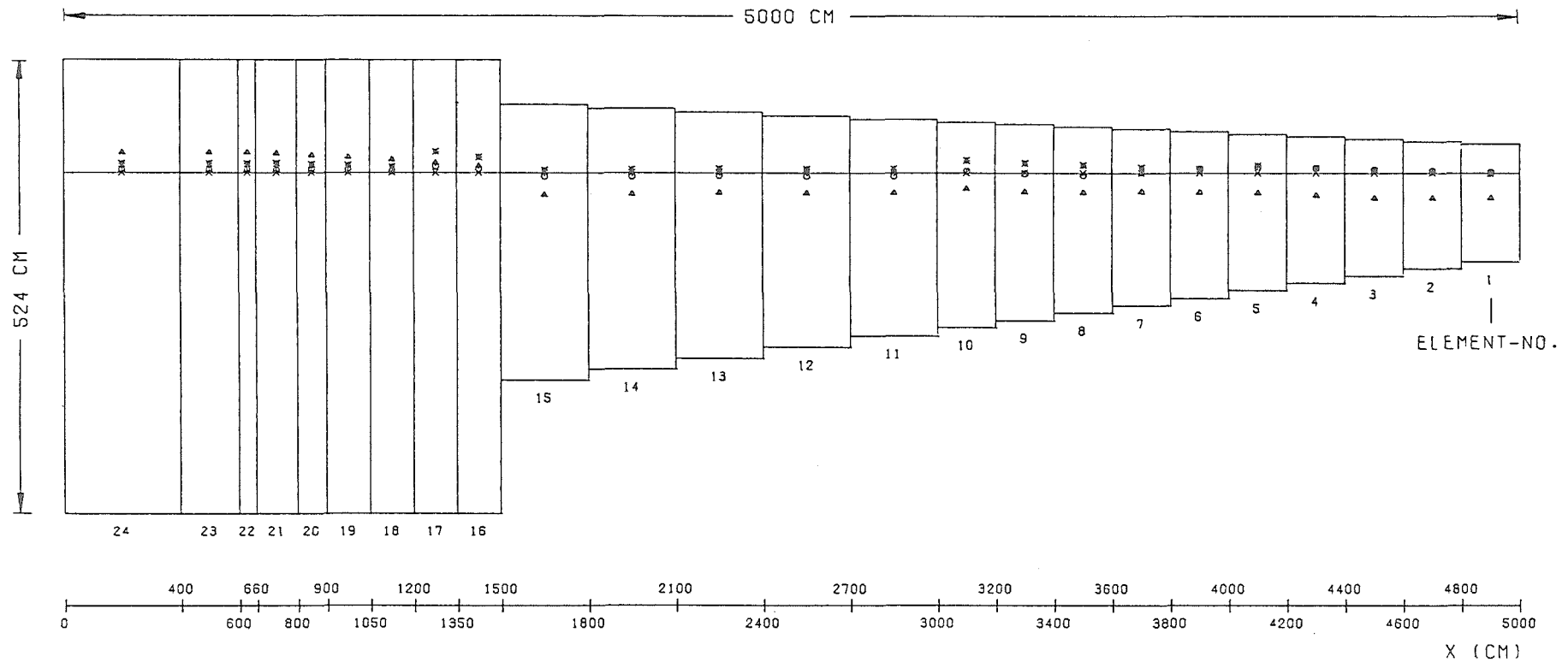
Figure 3: Idealized rotor blade

5000 CM

524 CM

ELEMENT-NO.

X (CM)

ⓞ CENTROID OF CROSS-SECTIONAL AREA EFFECTIVE
IN CARRYING TENSILE STRESSES

△ MASS AXIS

✳ ELASTIC AXIS

✕ AXIS OF ROTATION

Figure 4: Flap mode for the rotating blade at rated speed
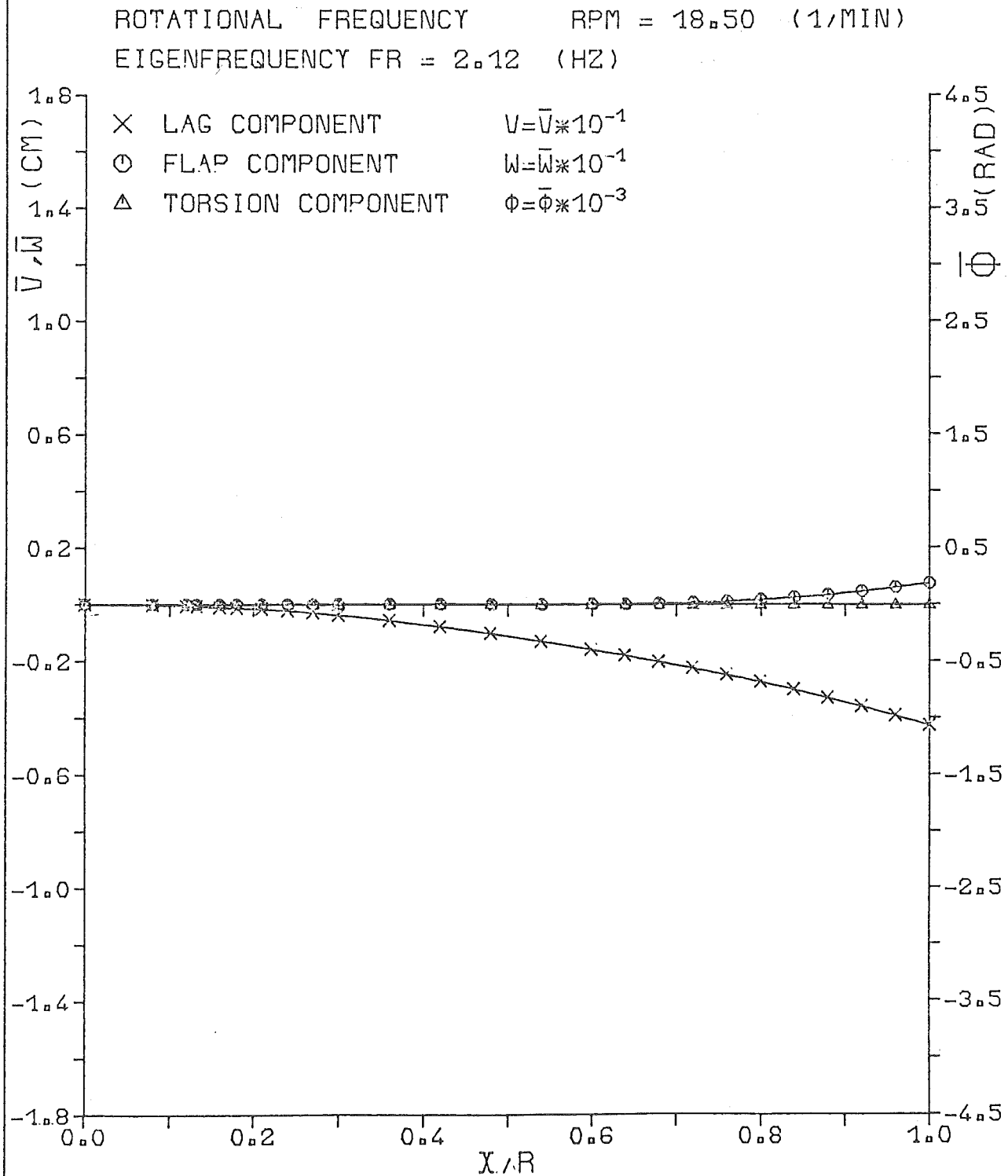
Figure 5: Lag mode for the rotating blade at rated speed

| DFVLR–AVA | GROWIAN | Blatt–Nr. 15 |
| | ROTOR BLADE | Figure 6 |

ROTATIONAL FREQUENCY   RPM = 18.50 (1/MIN)
EIGENFREQUENCY FR = 11.13 (HZ)

X LAG COMPONENT $V=\bar{V}*10^{-1}$
O FLAP COMPONENT $W=\bar{W}*10^{-1}$
△ TORSION COMPONENT $\Phi=\bar{\Phi}*10^{-3}$

Figure 6: Torsional mode for the rotating blade at rated speed

Figure 7: Resonance diagram

Figure 8: Rate-of-decay versus free-stream velocity of the nonrotating blad

DFVLR-AVA
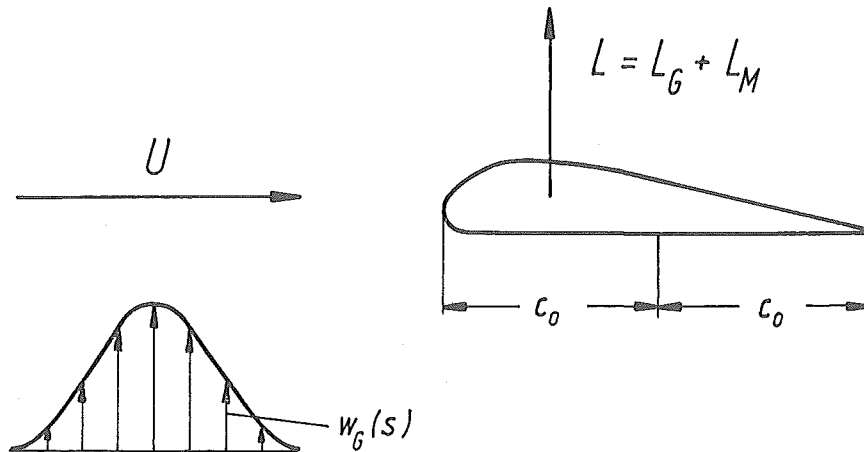
- 156 -

GROWIAN

ROTOR BLADE

Blatt-Nr. 18

Figure 9
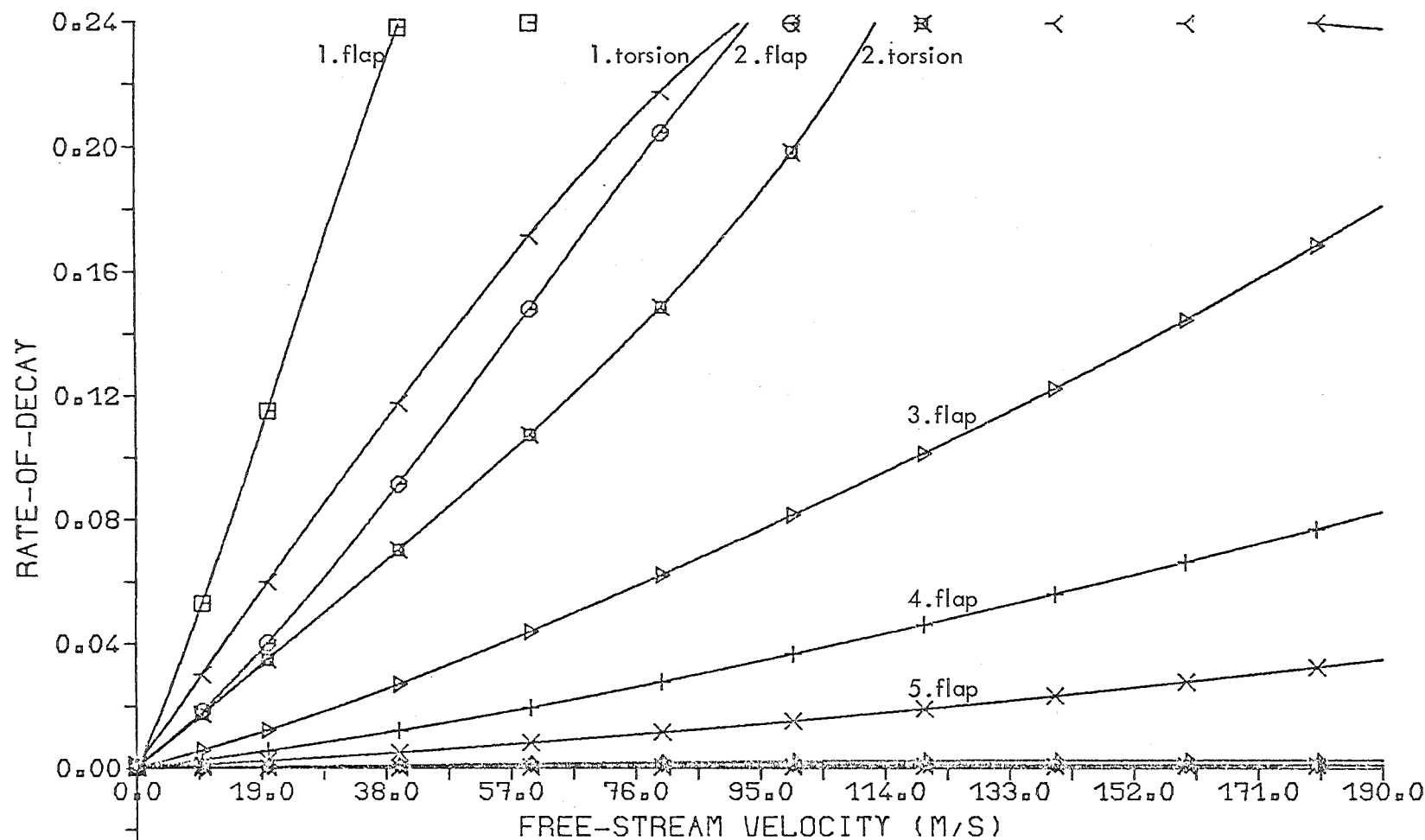
Figure 9: Rate-of-decay versus free-stream velocity of the rotating blade at rated speed

			Blatt-Nr.	19
DFVLR	Aerodynamische Versuchsanstalt Göttingen		Figure	10

$$L = L_G + L_M$$

$$U \longrightarrow$$

$$c_0 \qquad c_0$$

$$w_G(s)$$

$$S = \frac{Ut}{c_0} \qquad dimensionless \ time \ variable$$

$$L_G \qquad unsteady \ lift \ due \ to \ the \ gust$$

$$L_M \qquad unsteady \ lift \ due \ to \ the \ motion$$

Figure 10: Rotor blade encountering a gust

Datum:	Abteilung:	Gesehen:	Bericht:
Bearbeitet:			

| DFVLR-AVA | GROWIAN | Blatt-Nr. 20 |
| | ROTOR BLADE | Figure 11 |

RESPONSE TO A (1-COS) GUST
TG = 1.50 (S)
WG = 12.00 (M/S)
$Q=\bar{Q}*10^{3}$

Figure 11: Generalized coordinates versus time inside the gust period

RESPONSE TO A (1-COS) GUST

TG = 1.50 (S)

WG = 12.00 (M/S)

T = 1.02 (S)

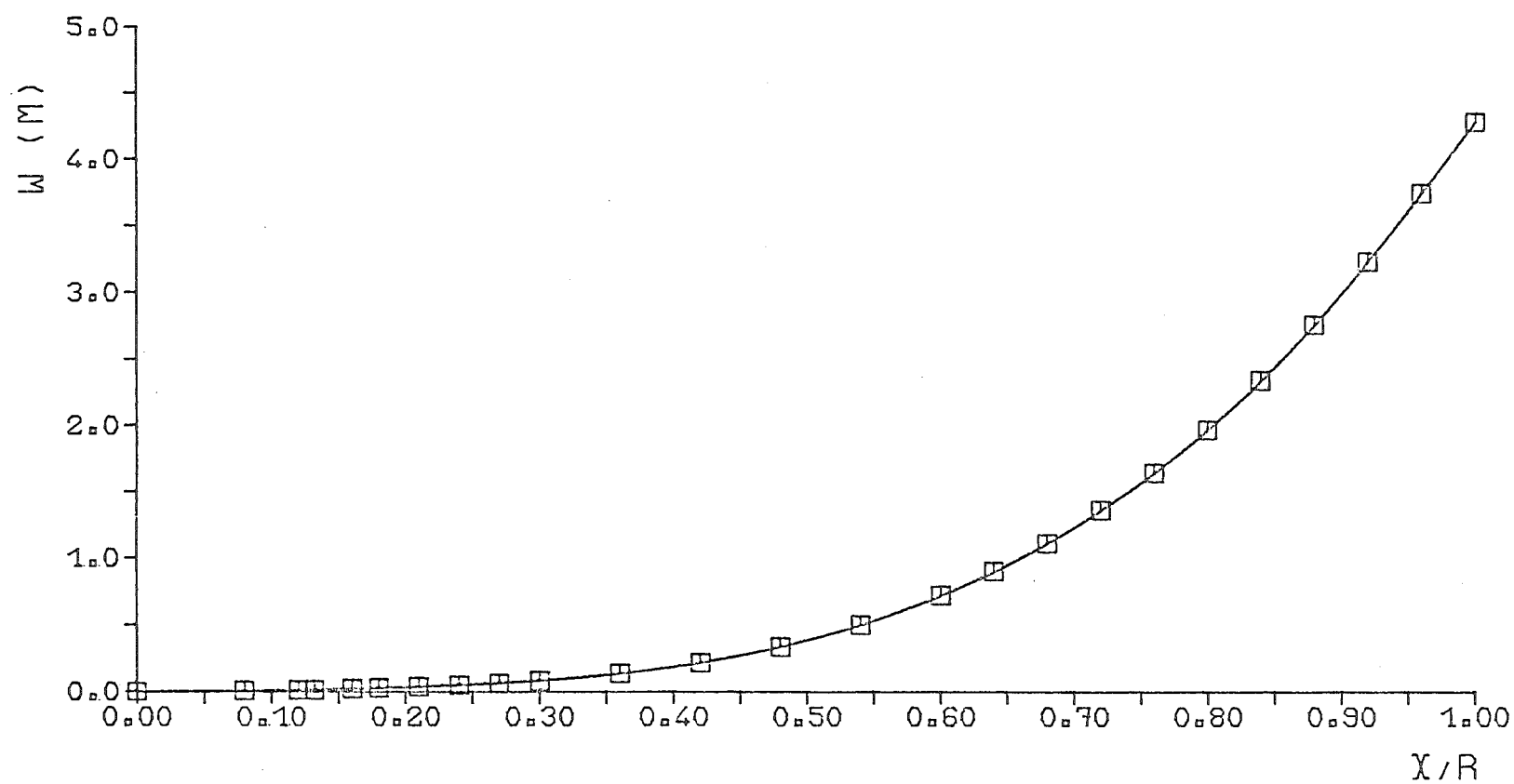Figure 12: Total physical deformation versus rotor radius at the time t = 1.02 s

DFVLR-AVA

GROWIAN

ROTOR BLADE

Figure

Blatt-Nr. 21

12

AEROELASTIC MODELING OF THE COUPLED WIND TURBINE ROTOR/TOWER SYSTEM

Dipl.-Ing. Fritz Kießling

DEUTSCHE FORSCHUNGS- UND VERSUCHSANSTALT
FÜR LUFT- UND RAUMFAHRT E. V.
- Aerodynamische Versuchsanstalt Göttingen -
Institut für Aeroelastik

Summary:

Vibration and aeroelastic stability analyses of wind turbines generally cannot neglected the interaction between rotor and tower. So at least finally an aeroelastic model of the complete system must be considered. The derivation of the corresponding equations of motion is described together with the more important parameters of the wind turbine system.

1. Introduction

The economic use of wind energy on a large scale requires conversion systems with enormous dimensions because of the low energy density of the working medium. At least for minimizing the costs of large wind turbines, the structure cannot be designed excessive stiff. In this case the vibratory loads and stresses would be easy to determine statically if the time-dependent forces acting on the system are known and no stability problems would be encountered. But unfortunately, wind turbines must be considered quiet flexible concerning both the supporting tower and the rotor. Elastic deformations give rise to additional dynamic and aerodynamic forces and the task to determine the stresses is much more difficult. On the one side inertial forces can relief the "static" loads, but on the other there exist the possibility of resonances and aeroelastic instabilities.

In the following the complete rotor/tower system is considered. Although many aeroelastic problems can be solved in a satisfactory manner by looking at the rotor and the tower separately, there are certain phenomena, which need the treatment of the system as a whole. There is much to be learnt from VTOL aircraft experience, especially from the dynamics of prop-rotors interacting with flexible wings. But it must be remarked, that quite large differences exist in the design compared with today's wind turbine rotors.

2. Forces and Deformations

In Figure 1 the forces with their origins are summarized, which are to be considered in an aeroelastic analysis of a horizontal axis wind turbine. Principally, there are purely time-dependent forces and forces, which are created by the motion of the structure itself.

Time dependent fluctuating aerodynamic forces are caused by the ground boundary layer, gusts, and oblique flow due to a skewed rotor axis and operating conditions, under which the system is not aligned with the mean wind direction. The tower wake contributes mainly to higher harmonic loads on a rotor located downstream. Possibly thereby a mutual interference exists between rotor blades and tower. Because of the time-varying character of the flow relative to the structure, unsteady aerodynamic forces are generated, which cannot always regarded as quasisteady.

Gravity produces a cyclic loading for the rotating blades and influences the eigenvibrations of the system. The rotation of the rotor introduce complex inertial forces, from which only the gyroscopic moment due to yaw velocity of the nacelle and the centrifugal forces on the blades are illustrated as typical contributors.

Figure 2 shows the deformations occuring on a wind turbine. Only the fundamental modes are are indicated. The tower can bend in two directions and twist around its axis. Due to un-symmetric mass distributions these motions can be coupled. Resulting from the tower defor-mations the nacelle excutes pitching, yawing and rolling motions. In some designs the ro-tor is allowed to move in a rigid motion (teetering rotor) about an axis perpendicular to the axis of rotation and to the blade span. The rigid pitching motion of the blades can be coupled kinematically with the rotation around the teetering hinge (pitch-flap-coupling) to reduce the transient response. The rotor blades themselves can bend out-of-plane (flapping) and in-plane (lagging). Finally the blades can twist elastically (torsion).

Usually aeroelastic analyses of aircraft are performed under the assumption, that the de-formations are infinitesimal small, so that equilibrium equations can be formulated appro-ximately looking at the undeformed structure.

In the case of rotors and guyed masts this is not correct, because the structure is preloaded to a large extent, which influences the vibration behaviour via geometric stiffness ef-fects. So the theory to apply must be at least of second order (moderately large rotations).

3. Mathematical Modeling

In view of the forces and possible deformations described it is easy to imagine, that the derivation of a mathematical model for the whole system, in which all these featuresare re-presented, is very complex. Many questions cannot be answered by theory alone. For example the tower wake/blade interaction can only be incorporated empirically on the basis of wind tunnel measurements. For cylindrical towers measurements of the flow field at sufficient high REYNOLDS-numbers are presently not available. A rough estimate can be made with the results of [1], where the depth and width of the wake of a cylinder is given, Figure 3. Ad-justing the drag coefficient according to the REYNOLDS-number, the mean velocity profile is given for the distance, where the blade is passing. From this input a gust response calcu-lation can be performed for the rotor blade. But it is clear, that for reliable answers to the tower wake question fundamental experimental work must be done in the future.

In the following some remarks on the derivation of the equations of motion are given. For aeroelastic problems it is very desirable to have linearized perturbation equations about a steady state as an endproduct, because the stability can be investigated by an eigenanalysis. Thereby, the influence of parameters of the system on its behaviour and the stability bounda-ries can be studied more easily and economically, than by a direct integration of nonlinear

equations of motion with various initial conditions. In principle, the rotor and tower can be described by partial differential equations with the proper boundary conditions. For solving these equations GALERKIN's method can be applied to eliminate the space dependence and to arrive at ordinary differential equations for the generalized coordinates.

Another way to produce approximate equations of motion is the use of a finite number of displacement modes and corresponding generalized coordinates from the very beginning. This can be accomplished by the LAGRANGian approach. The equations read

$$\frac{d}{dt}\left(\frac{\partial \mathcal{T}}{\partial \underline{\dot{q}}^T}\right) - \frac{\partial \mathcal{T}}{\partial \underline{q}^T} + \frac{\partial \mathcal{U}}{\partial \underline{q}^T} = \underline{Q} \quad , \tag{1}$$

for a column of generalized coordinates $\underline{q}$, which can be discrete or distributed. Thereby are $\mathcal{T}$ the kinetic energy, $\mathcal{U} = \mathcal{U}_e + \mathcal{U}_g$ the potential energy (elastic and gravity), and $\underline{Q}$ the remaining generalized (nonconservative) forces. The integrations occuring in the energy expressions are conveniently subdivided into a sum of integrals over the subsystems tower, nacelle, teetering frame, and rotor blades. The use of eigenmodes of the various elastic subsystems (with suitable boundary conditions) results in a much simplified form for their elastic potential energy with diagonal generalized stiffness

$$\mathcal{U}_e = \frac{1}{2} \underline{q}^T \underline{\mathcal{K}} \underline{q} \quad . \tag{2}$$

There is no need to make any theoretical assumption about the deformation behaviour of the structure if its eigenvibration behaviour is known. Usually the lowest modes are sufficient, which can be obtained either from analysis or from test. In the presence of rotor rotation some assumptions must be made about the kinematics of blade deformation, when nonrotating modes from first order theory or test are used. Generally, all effects of rotor rotation can enter the equations of motion via the kinetic energy contributions. The expression

$$\mathcal{T} = \frac{1}{2} \int\limits_V \vec{\dot{R}} \cdot \vec{\dot{R}} \, dm \tag{3}$$

requires first the inertial coordinates of a material point of a subsystem and abviously one on a rotorblade is most difficult to describe. In principle

$$\vec{R}_B = \vec{R}_B(\underline{q}, t) \tag{4}$$

is a nonlinear function of the column of generalized coordinates and the explicit time dependence is given for the yawing of the nacelle, the rotor rotation, and the blade feathering. All other motions can be linearized about a steady state.

The inertial coordinates of a blade point read in matrix notation

$$\underline{R}_B^i = \underline{h} + \underline{\psi}_D(t)\,\underline{\underline{\Theta}}_G\,\{\underline{1} + \underline{r}_N +$$

$$+ \underline{\psi}_N\,\underline{\underline{\Theta}}_N\,\underline{\underline{\Phi}}_N\,\underline{\underline{\Phi}}_K(t)\,\underline{\underline{B}}_K\,[\underline{a} +$$

$$+ \underline{\underline{B}}_A\,\underline{\underline{\Theta}}_k(t)\,\underline{\underline{\Phi}}_B\,\underline{\underline{B}}_B(\underline{r}_B + \underline{r}_{ek} +$$

$$+ \underline{\underline{V}}'_{ek}\,\underline{\underline{W}}'_{ek}\,\underline{\underline{\Gamma}}_{ek}\,\underline{\underline{\Phi}}_{ek}\,\underline{r}_Q)]\}$$

(5)

where the following column and transformation matrices are used

$\underline{h}$	=	tower height
$\underline{\psi}_D(t)$	=	nacelle azimuth
$\underline{\underline{\Theta}}_G$	=	inclination of rotation axis
$\underline{1}$	=	overhung of the teetering hinge point
$\underline{r}_N$	=	elastic translations of the nonrotating teetering hinge point
$\underline{\psi}_N,\ \underline{\underline{\Theta}}_N,\ \underline{\underline{\Phi}}_N$	=	elastic rotations of the nonrotating teetering hinge point
$\underline{\underline{\Phi}}_k$	=	azimuth angle of the kth blade
$\underline{\underline{B}}_k$	=	flapping angle of the kth blade about the teetering hinge
$\underline{a}$	=	offsets of the blade pitch bearing
$\underline{\underline{B}}_A$	=	coning angle of the blade pitch bearing
$\underline{\underline{\Theta}}_k(t)$	=	pitch angle of the kth blade
$\underline{\underline{\Phi}}_B$	=	sweep angle of the blade span axis
$\underline{\underline{B}}_B$	=	droop angle of the blade span axis
$\underline{r}_B$	=	position of the elastic axis in the undeformed section in question
$\underline{r}_{e_k}$	=	elastic translations of the elastic axis (k^{th} blade)
$\underline{\underline{V}}'_{ek},\ \underline{\underline{W}}'_{ek}$	=	elastic rotations of the elastic axis of the kth blade
$\underline{\underline{\Gamma}}_{ek}$	=	elastic bending/torsion rotation about the elastic axis (k^{th} blade)
$\underline{\underline{\Phi}}_{ek}$	=	elastic torsion about the elastic axis (k^{th} blade)
$\underline{r}_Q$	=	section coordinates of the point in question

All terms up to second order must be retained for elastic displacements and flapping. The radial elastic translation of the elastic axis is of second order and can be written, neglecting the offset of the tensile axis, as

$$u_e = -\frac{1}{2} \int_0^R (w_e'^2 + v_e'^2)\, dr \ .$$

(6)

This is the well-known foreshortening effect.

Also the bending/torsion rotation [2] is of second order with an angle of

$$\gamma_{ek} = -\int_0^r v_{e_k}'' \ w_{e_k}' \ dr \ .$$

(7)

For the description of elastic deformation of the blades the eigenmodes of the nonrotating blade fixed at the pitch bearing will be used. For the derivation of consistent linear equations substitutions for the deformations of the elastic axis have to be made of the general form

$$u_{B_k}^L = \underline{U}_B^{L\,T} \ \underline{q}_{B_k}$$

(8)

$$u_{B_k}^Q = \underline{q}_{B_k}^T \ \underline{\underline{U}}_B^Q \ \underline{q}_{B_k}$$

(9)

for the terms of linear and quadratic order, respectively. Thereby, $\underline{U}_B^L$ and $\underline{\underline{U}}_B^Q$ are functions of the nonrotating blade mode shapes. The displacements of the teetering hinge point are described by the corresponding displacements of the tower eigenmodes. By this way the generalized coordinates of the tower enter the equations of motion. The expression (5) must be differentiated with respect to time, the dot product must be evaluated, and introduced it into the kinetic energy. Then the LAGRANGE procedure can be applied to complete the first two parts of the equations.

The generalized gravity forces can be obtained by

$$\mathcal{U}_g = -\int \vec{g} \cdot \vec{R}\, dm \ .$$

(10)

Due to second order terms in R_B^i, the gravity forces will also be present in stiffness terms on the left side of the equations.

The generalized aerodynamic forces are derived from virtual work

$$\underline{Q} = \int \frac{\partial \vec{R}}{\partial \underline{q}^T} \cdot d\vec{F} \qquad (11)$$

where $d\vec{F}$ is the aerodynamic force and $\vec{R}$ describes the point of action. The aerodynamic forces can be integrated chordwise to obtain a resultant force at the aerodynamic center and a resultant moment around this point. The translations and rotations of this point are functions of $\underline{q}$ and time using a similar expression like (5). For the evaluation of $d\vec{F}$ in the blade section system strip theory shall be used. Then the velocity of the air relative to the blade must be known. This is accomplished by

$$\vec{U} = \vec{V} - \vec{V}_{kin} \qquad (12)$$

where $\vec{V}$ is the undisturbed free-stream velocity, depending on height and $\vec{V}_{kin}$ is the kinematic velocity of the aerodynamic center depending on $\underline{q}$ and its time derivative and time explicitly. Because $\vec{U}$ will be given in the inertial frame, there must be a transformation to the section frame. Only the components lying in the section plane are to consider. Finally, the forces (moments) must be back-transformed to the inertial frame for the dot-multiplication with $\partial\vec{R}/\partial\underline{q}$ given in that frame. The generalized aerodynamic forces consist of a steady part, which is in equilibrium with the other steady forces including the torque transmitted from the gear-box and a perturbation part, which becomes the form of real-valued aerodynamic damping and stiffness matrices in the case of quasisteady linearized theory. Its application is justified for the low frequency stability investigations of the coupled rotor/tower system.

It is obvious, that writting down the procedure outlined above by hand is much to laborious and error-prone. So presently use is made of the symbolic computer code REDUCE, to derive the equations in nonnumerical form with various ordering schemes. Thereby, it is possible to arrive at the formulas for each matrix element leading to insight in coupling mechanisms and efficient numerical investigations.

4. Solution Methods

The linearized perturbation equations of the mathematical model are in general time-dependent and of the form

$$\underline{\underline{M}}(t)\,\underline{\ddot{q}} + \left(\underline{\underline{D}}(t) + \underline{\underline{D}}_A(t)\right)\underline{\dot{q}} + \left(\underline{\underline{K}}(t) + \underline{\underline{K}}_A(t)\right)\underline{q} = \underline{Q}(t)\,. \tag{13}$$

Only in the special case, when at least one of the two subsystems, the rotor and/or the supporting structure, possess inertial, damping, elastic and aerodynamic axial symmetry the equations can be easily transformed by a timevariant matrix to a system with constant coefficients. Unfortunately, the preferred use of two-bladed rotors, which possess no axial symmetry leads to the situation, that the timevariant coefficients cannot be eliminated by a transformation to the so-called multiblade coordinates for the rotor degrees of freedom. A time-averaging of the coefficients is perhaps allowed as an approximation, but thereby the possibility of parameter resonances, which can occur due to periodic coefficients, will be suppressed. Instead of solving a simple eigenvalue problem, now the FLOQUET-method must be applied [3], which requires in addition the numerical integration of the equations of motion for one rotor revolution, because this is the fundamental period T of the coefficients. In first order form the 2n equations read

$$\underline{\dot{x}} = \underline{\underline{A}}\,\underline{x} + \underline{b} \tag{14}$$

where the state variable

$$\underline{x} = \begin{bmatrix} \underline{q} \\ \underline{\dot{q}} \end{bmatrix} \tag{15}$$

the system matrix

$$\underline{\underline{A}} = \begin{bmatrix} \underline{\underline{0}} & \vdots & \underline{\underline{1}} \\ \text{-----} & + & \text{-----} \\ -\underline{\underline{M}}^{-1}\underline{\underline{K}} & \vdots & -\underline{\underline{M}}^{-1}\underline{\underline{D}} \end{bmatrix}\,, \tag{16}$$

and the extended right hand side

$$\underline{b} = \begin{bmatrix} \underline{0} \\ \underline{Q} \end{bmatrix}\,. \tag{17}$$

Only the stability of the system will be considered now. For the fundamental matrix $\underline{\underline{\Phi}}(t,t_0)$ of the system, we have the property

$$\underline{\underline{\Phi}}(t + T, t_0) = \underline{\underline{\Phi}}(t,t_0) \cdot \underline{\underline{C}} \tag{18}$$

The matrix $\underline{\underline{C}}$ can be obtained by 2n integrations over one rotor revolution with unit initial conditions. The state variables at $t_0 + T$ will form the columns of $\underline{\underline{C}}$

$$\underline{\underline{C}} = \underline{\underline{\Phi}}(t_0 + T,\, t_0) \tag{19}$$

The fundamental matrix can be written as

$$\underline{\underline{\Phi}}(t,t_0) = \underline{\underline{Z}}(t) \cdot e^{\underline{\underline{R}}(t-t_0)}$$

(20)

where $\underline{\underline{Z}}(t)$ is periodic with T and $\underline{\underline{Z}}(t_0) = \underline{\underline{1}}$ and

$$\underline{\underline{R}} = \frac{1}{T} \ln \underline{\underline{C}} \quad .$$

(21)

For distinct eigenvalues λ_i of $\underline{\underline{C}}$ the system is stable if $|\lambda_i| \leq 1$ for all $i = 1, 2, \ldots, 2n$. For numerical efficiency a method has been applied, which integrates from the 2n initial conditions simultaneously, [4].

5. Results

In Figure 4 a typical model for simplified rotor/tower stability investigations is shown. The equations of motion of the system have constant coefficients. The degrees of freedom are tower roll, pitch and yaw and the tilting of the rotor disk seen from a stationary observer (flapping rigid blades). The coning of the rotor is locked out. Figure 5 shows a small wind tunnel model for exploratory tests with a coupled rotor/tower system. The system has very low eigenfrequencies in the tower degrees of freedom to produce instability at low speeds. Figure 6 shows an unstable mode predicted by the mathematical model. Because of the sensibility of the unstable motion to small structural damping variations, the stability boundary could not be precisely verified. The frequency and the mode agree reasonable well between experiment and theory.

The same mathematical model was also applied to preliminary GROWIAN data. The results are shown in Figure 7. The mode containing mainly tower roll exhibits the lowest damping but no instability is occuring, because of the relative high stiffness. For the pitch and yaw mode the aerodynamic damping of the rotor is quite effective.

As an preliminary investigation with periodic coefficients a FLOQUET-stability analysis was carried out for a simplified plane system with a two-bladed rotor in which the nacelle can move vertically and horizontally (Figure 8). The blades can lag and gravity loads are acting on the structure. Aerodynamic forces are neglected. The system was at least asymptotically stable with GROWIAN-data, but with much lower blade lag frequencies, parametric instability can possibly occur.

6. Conclusions

The design of large wind turbines requires aeroelastic modeling for prediction of vibratory stresses and possible instabilities. With regard to the complete rotor/tower system it has been shown that the formulation can be very complex due to the large number of design parameters. The work to refine the mathematical model and to eliminate crude simplifications is not yet completed. Confidence into predictions with these models can be placed when further correlation studies are made with tests on aeroelastic wind tunnel models. For this purpose their physical properties and environment must be accurately defined.

7. References

[1] SCHLICHTING, H.   Über das ebene Windschattenproblem.

Diss., Göttingen, 1930
Ing.Arch.1, (1930), p.533-571

[2] HODGES, D.H.,   Nonlinear Equations of Motion for the Elastic Bending
    DOWELL, E.H.   and Torsion of Twisted Nonuniform Rotor Blades.

NASA TN D-7818 (1974)

[3] MÜLLER, P.C.,   Lineare Schwingungen.
    SCHIEHLEN, W.O.
Akademische Verlagsgesellschaft, Wiesbaden, 1976

[4] KAZA, K.R.V.,   An Investigation of Flap-Lag Stability of Wind Turbine
    HAMMOND, C.E.   Rotors in the Presence of Velocity Gradients and Heli-
                          copter Rotors in Forward Flight

Proc.AIAA/ASME/SAE 17th Structures, Structural Dynamics, and Materials Conference, King-of-Prussia, Pa., 1976, pp.421-431
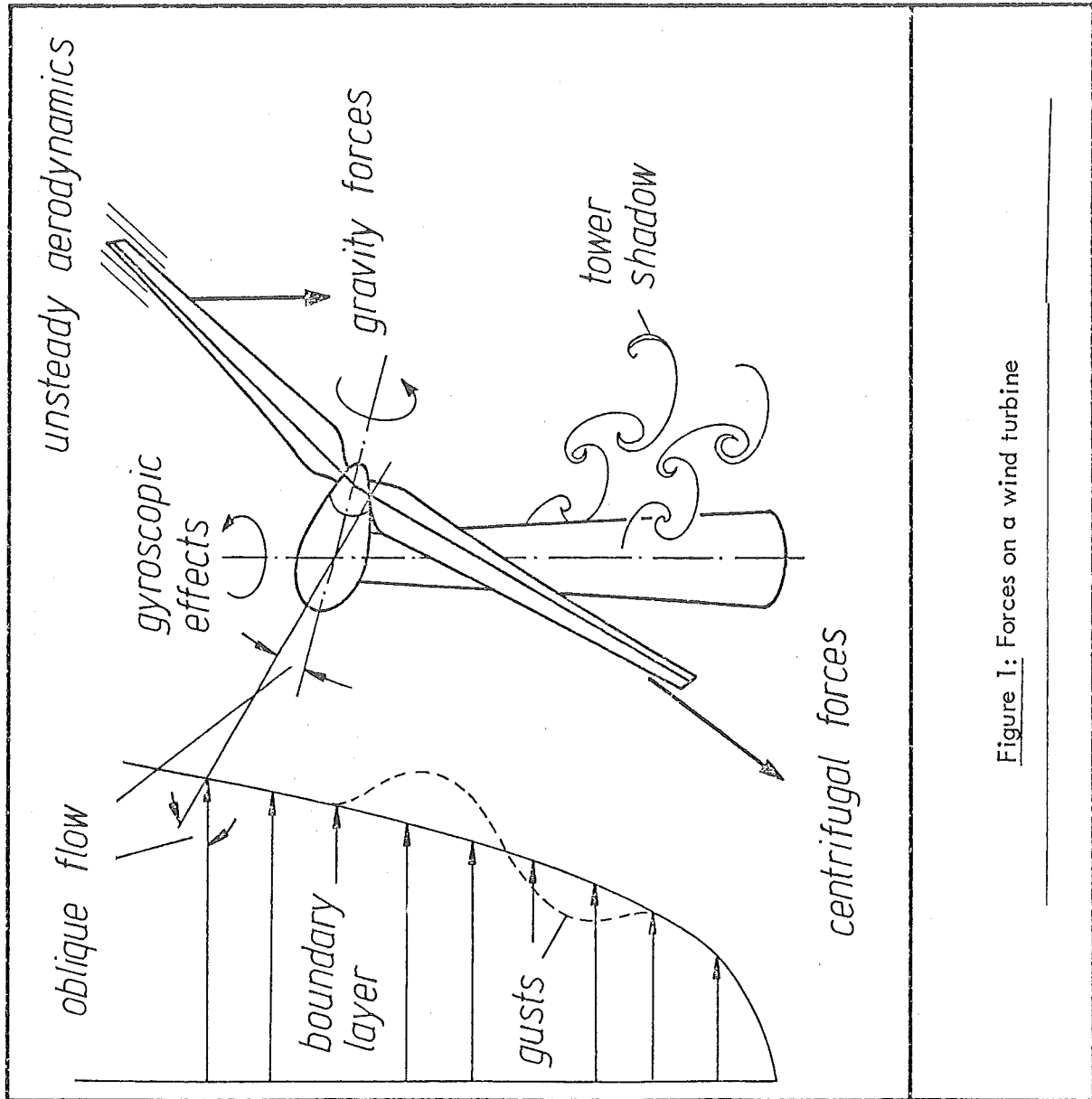
Figure 1: Forces on a wind turbine

Figure 2: Deformations of a wind turbine
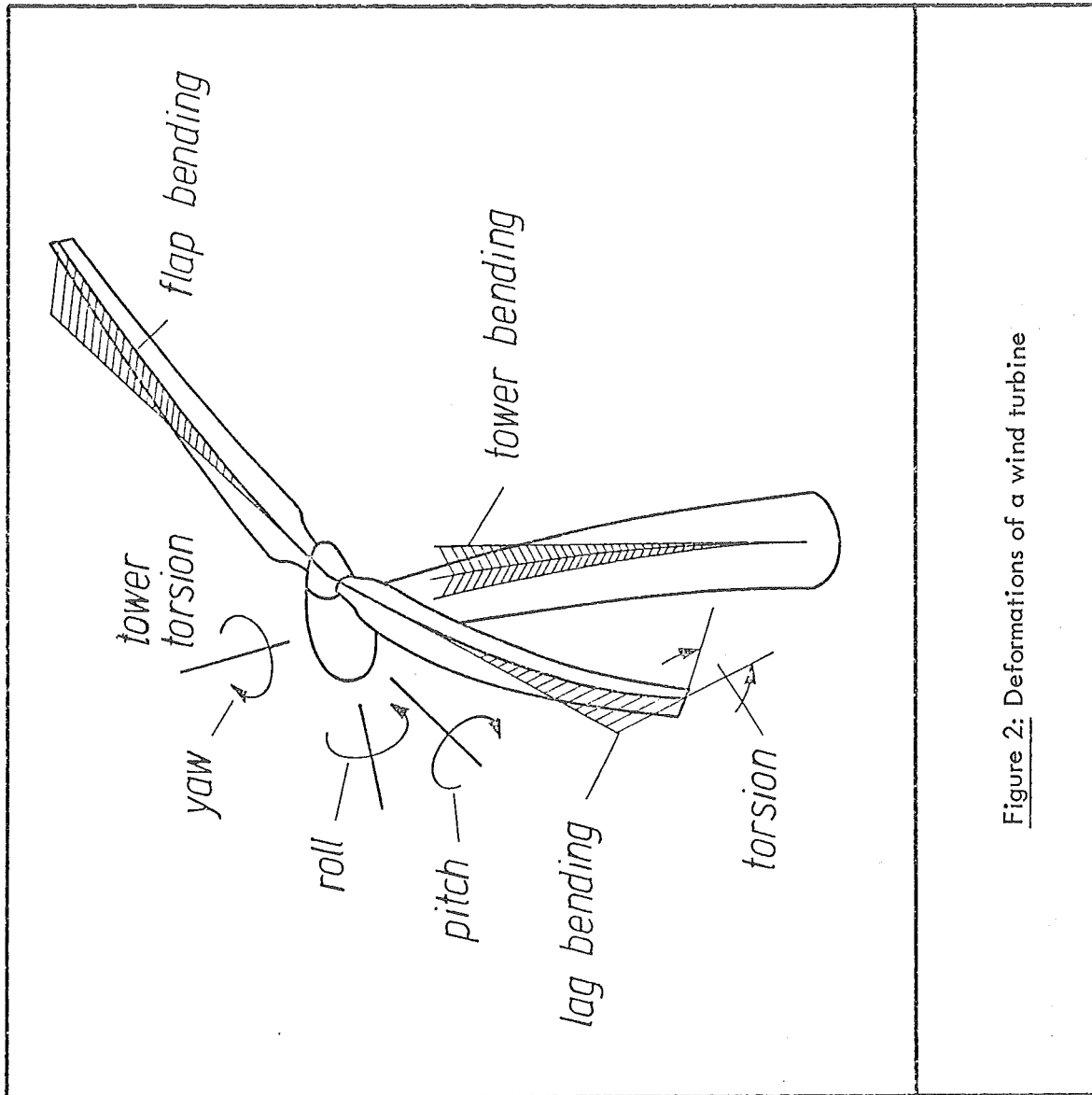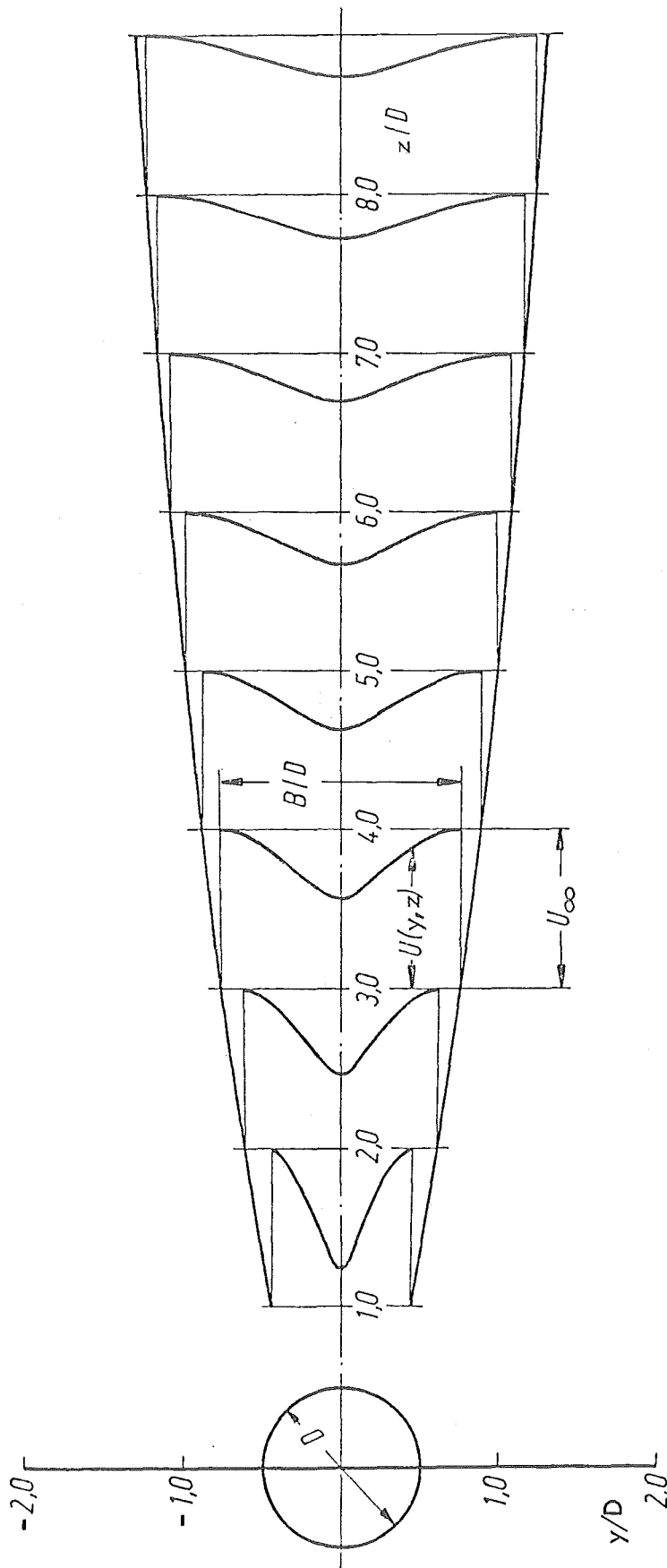
Figure 3: Tower wake $(c_D = 0.6)$

Figure 4: Simplified rotor/tower model
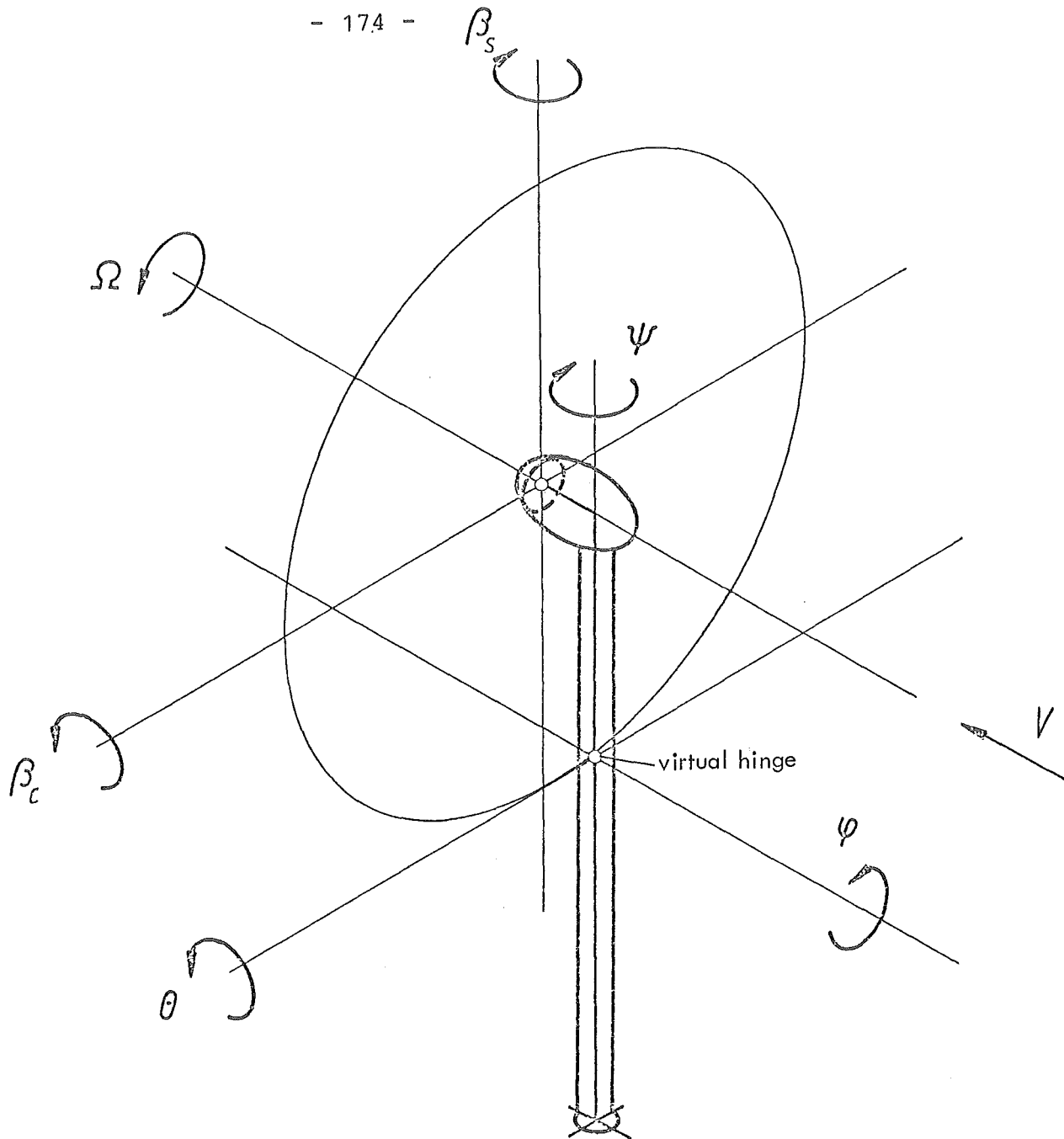
V	free-stream velocity	Ω	rotor circular frequency
φ	elastic tower roll	Θ	elastic tower pitch
ψ	elastic tower yaw	β_c	tip-path plane pitch
β_s	tip-path plane yaw		
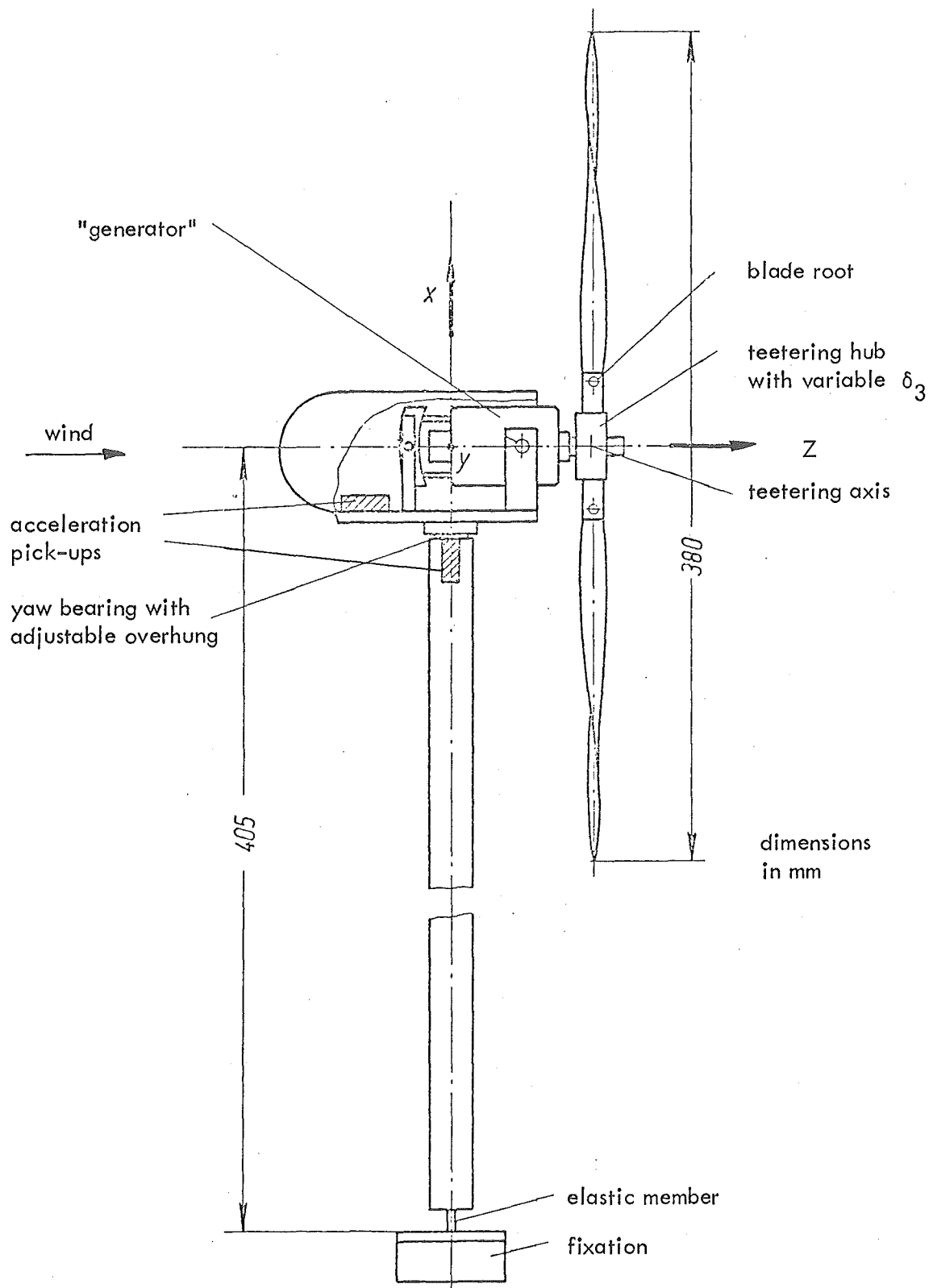
Figure 5: Exploratory wind tunnel model
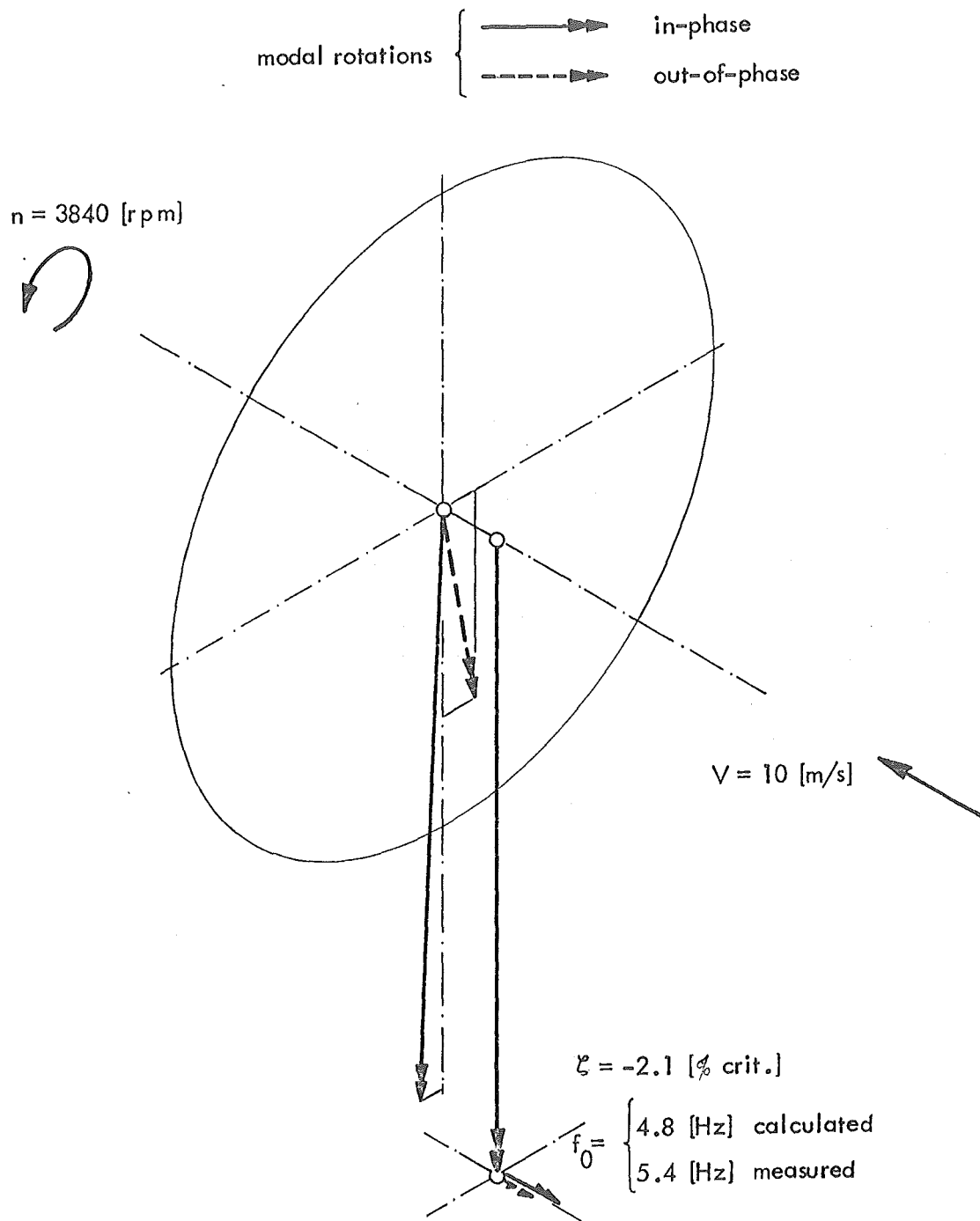
Figure 6: Unstable mode of the windtunnel model

$\bar{f}_0 = 1.66$

$\zeta = 71.0 \ [\%]$

$\bar{f}_0 = 3.15$

$\zeta = 35.9 \ [\%]$
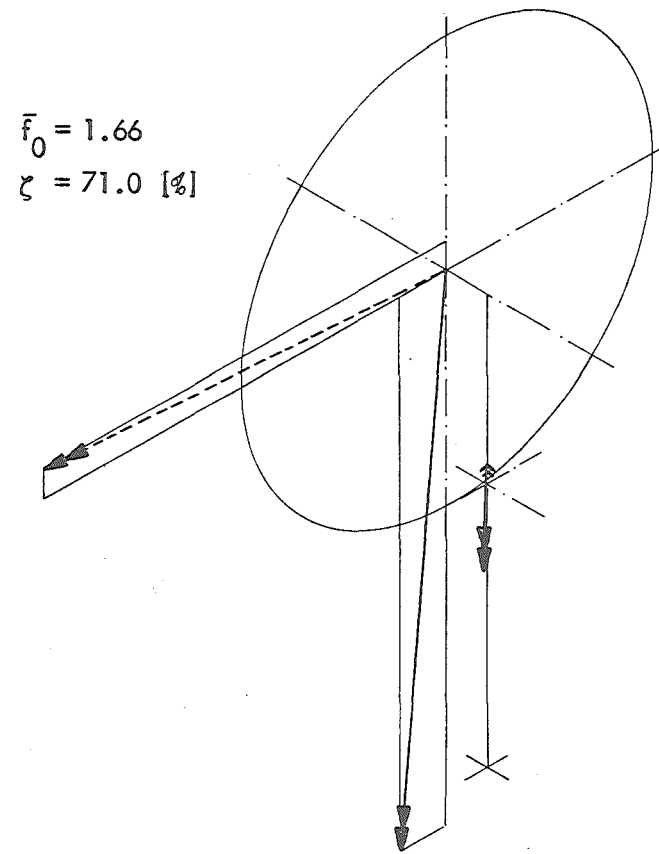
rotor backward precession
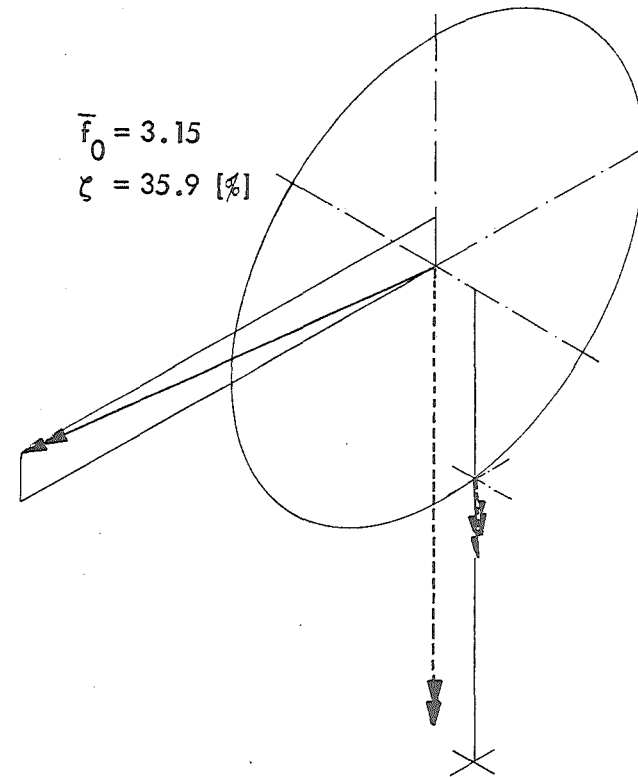
rotor foreward precession

Figure 7a: Typical aeroelastic modes of GROWIAN (rotor modes)

$\bar{f}_0 = 3.60$
$\zeta = 3.6 [\%]$

tower yaw

$\bar{f}_0 = 1.42$
$\zeta = 3.2 [\%]$

tower pitch

$\bar{f}_0 = 1.40$
$\zeta = 0.7 [\%]$

tower roll
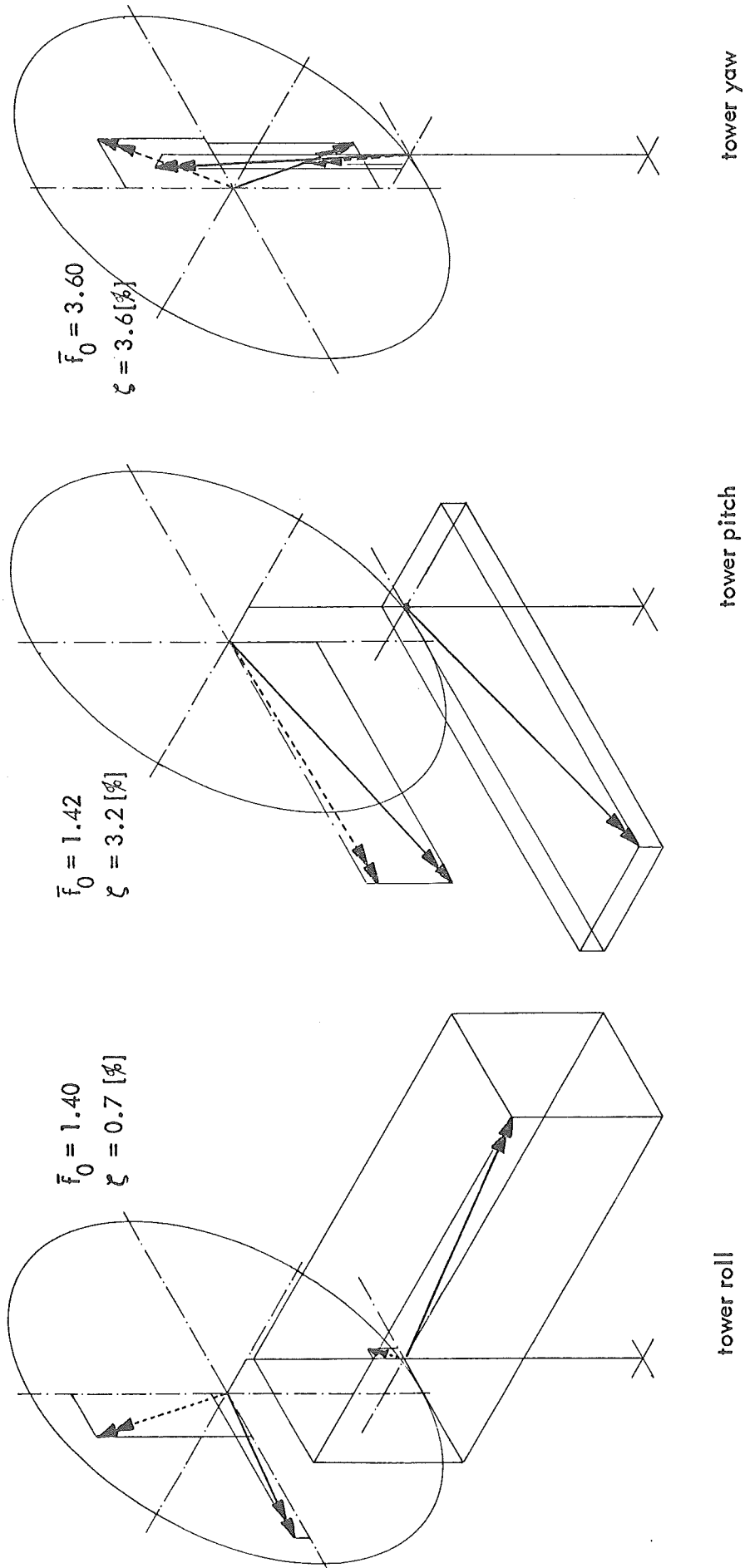
Figure 7b: Typical aeroelastic modes of GROWIAN (tower modes)
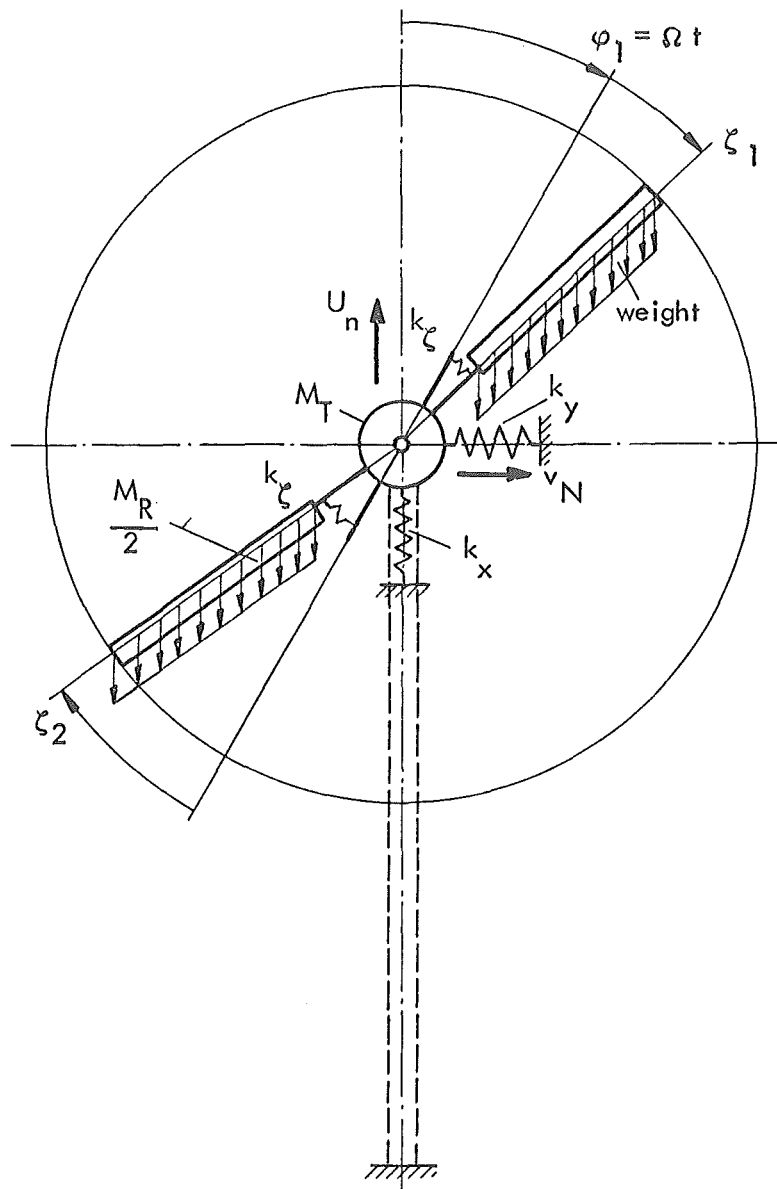
Figure 8: Simplified plane system with gravity effects

DYNAMIC DESIGN OF A MEDIUM STIFF WIND ENERGY TOWER

I. Kovacs, Dr.-Ing.
Leonhardt und Andrä, Consulting Engineers, Stuttgart

SUMMARY

As a rule, wind energy towers are designed for high
eigenfrequencies, which can be obtained only through
high stiffnesses.

Against this, a design concept with only medium stiff-
nesses is presented here: The first eigenfrequencies
of the tower are designed to lie between the lower
rotor frequency and the higher blade-passage frequency.
Thereby all sensitive system resonances can be isolated.

The frequency bands in which the eigenfrequencies of
the tower cannot be excited are extremely narrow.
Therefore the towers must be prepared for a supple-
mentary tuning for cases if their actual eigenfrequencies
deviate from the predetermined values.

The cable-stayed masts as proposed here have different
advantages for wind energy towers. Amongst others,
theyare most suitable for the medium stiffness concept
and their actual eigenfrequencies can be easily tuned
afterwards.

1   INTRODUCTION

While dimensioning a wind energy tower with
conventional high stiffness (i.e. conventional
high first eigenfrequencies, higher than the
blade passage frequency) the engineer can come
to unsatisfactory and contradictory results.
The required load-carrying capacity is reached
very soon by having a lower eigenfrequency at
the same time. However, one must increase the
stiffnesses to counteract critical frequencies
by getting more and more load-carrying capacity
automatically without being able to utilize it.
On the contrary: effective loading will be even
smaller and smaller, and by coming to the in-
tended high eigenfrequencies, resonances will
be completely eliminated.

The very high stiffness and its non-utilized
load-carrying capacity is very expensive, and
more so for higher towers. This fact can also
be shown by the GROWIAN example.

Fig. 1 presents an example of stiff tower alter-
natives, together with the medium stiff GROWIAN
tower, being described later.

Fig. 2 shows a simplified hight-versus-cost
diagram, derived from the GROWIAN optimizing
procedure. The moderately rising line demon-
strates the costs of the tower, as based upon
periodic loads acting under resonant conditions
without laying dynamic restrictions on eigen-
frequencies. The large cost increment of stiff
towers is caused by the increased stiffness only.

Due to these very large cost differencies, bound-
ary conditions about eigenfrequencies had to be
examined critically. High eigenfrequencies are
recognized as advantageous because they avoid
resonances during operation. But we found and will

show later that this assumption is only
partly correct and that resonancies can
also be avoided more economically. It is
also true that high stiffness guarantees
generally small motion amplitudes, but we
found, too, that motion amplitudes of me-
dium stiff alternative are also sufficiently
small.

Due to lack of space here, the following
short explanations can deal only with the
most favourable tower concepts, which are
mainly several cable-stayed tower alterna-
tives and this not only due to dynamic and
economic reasons. Beyond that, cable-stayed
towers have extremely good aerodynamic prop-
erties by combining relatively high stiffness
with relatively low wind resistance. Despite
of the fact that the stiffening cables have
a small diameter, their own eigenfrequency
will still be high, because of their geometri-
cal stiffness.

2   COMPARISON OF DYNAMIC CONCEPTS

In the case of the excited complex system
GROWIAN, as against machine foundations, we
cannot simply speak about a high or low
frequency ratio. As a result of the strong
non-sinusoidal time function of disturbing
periodic forces, a series of harmonic exciting
frequencies will originate, which are nearly
equally dangerous because of their inherent
relatively high forces. On the other side, in
case of elastic systems as tower constructions,
there is a parallel series of sensitive eigen-
frequencies, being approximately equally ex-
citable. We had to ensure that the sensitive
eigenfrequencies shall be satisfactorily far
away from the exciting frequencies. The fore-
going is a simplified description of the dyna-
mic condition of the GROWIAN tower, being simul-
taneously imposed with many other boundary condi-
tions.

Fig. 3 shows the frequency spectrum of ex-
citation for GROWIAN during operation. Large
periodic forces are found for frequencies
N, 2N, 4N, 6N etc. (shaded areas). The widths
of the exciting bands depend on cycle tolerances,
they range for GROWIAN between $\pm$ 15 % and extend
in few cases for short overspeeding to + 30 %.
The distances between the increasing exciting
frequencies will be progressively smaller. For
frequencies above 6N, the exciting bands overlap
each other leaving no non-excited gaps in-between.
On the other hand, the very large area below N,
practically, remains non-excited.

Fig. 3 also presents the most important periodic
force systems. They determine the sensitivity of
the several modes and their eigenfrequencies.
But sensitivity can be defined only in connection
with the respective forces. As most of the forces
occur only at a part of the presented exciting
bands, corresponding eigenfrequencies are also
sensitive only in the same domains.

The values of the higher harmonic forces mainly
depend on the wind resistance properties of the
tower. Forces generally diminish by increasing
harmonics. Fig. 3 specifies the relative values
for the medium stiff GROWIAN tower which demon-
strate that there is large excitation at higher
frequencies,too.

The excitation spectrum also shows the desirable
position of the sensitive eigenfrequencies. First
these should be brought within the white excitation
gaps   as far as possible. Eventually, they can be
allowed in the light shaded frequency bands as they
have only short resonance time, or at very high
frequencies because they have lower corresponding
exciting forces. In the shaded areas, at lower
frequencies, they must be avoided.

Even this cannot be obtained in the case of a stiff
tower. Fig. 4 illustrates the position of the eigen-
frequencies for two stiff alternatives. The lowest
eigenfrequency is about 3N. This causes disadvan-
tages in the dynamic behaviour: as can be seen from
fig. 4, certain resonances at higher sensitive
eigenfrequencies cannot be avoided. (But it must
be said that these resonances are, by not too high
towers, less problematical. E.g. for a 100 m
GROWIAN tower they produced a yet allowable motion
amplitude.)

Fig. 5 represents the dynamic concept of a medium
stiff GROWIAN tower. The first eigenfrequencies
lie between the rotor frequency (N) and the blade-
passage one (2N). Consequently, we have two free
intervals for eigenfrequencies, adequately spaced
from one another, at our disposal and all sensitive
eigenfrequencies can be arranged in these non-excited
gaps. The presented concept produces an advantageous
relation among the several eigenfrequencies as they
can be well realized in the practice and corrected
in case of deviations. As one extra advantage it
can be established that the low first eigenfrequency
moderates also some sensitivities in higher frequency
ranges (e.g. cable vibrations at 4N frequency).

Similar to the medium stiff tower, a flexible
tower can also be designed. The first group of
eigenfrequencies then lies under the rotor
frequency. The designer has more freedom for
the arrangement of sensitive eigenfrequencies,
but also more difficulties in out-of-operation
states. In regard to its mere dynamic proper-
ties, flexible concept was also a possible
solution and was calculated during the GROWIAN
optimizing procedure.

As a totally other solution, the possibility
for using one or more vibration absorbers was
investigated. In this case the tower would be
designed for its load-carrying capacity only,
by damping high resonant amplitudes at the same
time. But we found that there are also damped
motion amplitudes yet too large for the operation
state. Damping construction has also other dis-
advantages as large place requirement etc.

For an optimum design, besides dynamic behaviour,
an economic comparison has a decisive importance.
Fig. 6 shows the diagram height-versus-cost of
the foregoingly explained most favourable concept
alternatives for cable-stayed GROWIAN towers.
The starting point was, for all previous examples,
a statically optimum tower, which has the required
load-carrying capacity also for resonance states,
represented by diagram line 1. The tower was then
tuned, by varying parameters, until dynamic concept
also was satisfied. A continued critical checking
of structural dimensions and stiffness relations
was for the procedure indispensible, mainly in
cases where eigenfrequencies were diminished as
by lines 3 and 5 in fig. 6. Our results proved
clearly that, in regard to the dimensions of the
construction, the required statcally-dynamically
optimum solution lies close to the mere statical
optimum.

As shown in fig. 6, cable-stayed mast system
presents a possible solution for all practicable
heights. The diagram also shows that, in dif-
ferent height ranges, there are different dyna-
mic concepts favourable. In conform to that,
the 100 m tower, as projected for GROWIAN, will
be based upon medium stiffness dynamic concept.

3 TECHNICAL QUESTIONS

The stiffness properties of the whole construc-
tion were to be correctly calculable. Therefore,
as far as possible, all construction parts were
designed as clear, simple and without any compli-
cations.

For the realization of medium stiffness concept,
we had to use also non-structural, mere tuning
elements. This was necessary because all six
desired eigenfrequencies could be exactly aimed
only if there was a sufficient number of free
parameters at our disposal and the cable-stayed
mast construction had less of them. Simplified
it can be said that a part of sensitive eigen-
frequencies was "corrected" by these extra tuning
elements as shown in fig. 5. This procedure was
designated as the "first eigenfrequency-correction".
Together with the structural parameters, also the
free parameters of the tuning elements were cal-
culated during the designing phase already.

Extra vibration parameters are also necessary
for another purpose. The dynamic design, together
with the "first correction", can guarantee only
the analytical accuracy of the desired eigen-
frequencies. Actual elastic properties and speci-
fic density of the building materials, method of
design etc. have in any case not ignorable toler-
ances which make differences between calculation
and reality unavoidable. These differences are,
as expected, too large for the narrow boundaries,
permitted for sensitive eigenfrequencies.
Consequently, a supplementary so-called "final
eigenfrequency-correction" may be necessary after-
wards and the construction must be prepared for it.

Reasonable for this final correction is, similarly
as for the first one, the use of extra tuning ele-
ments. For GROWIAN we applied partly the same
correction method for both procedures. There were

a lot of possibilities to select as supplemen-
tary masses or inertias in several points,
geometrical modification of cables, employing
extra springs or dynamic dampers. Chosen solu-
tions are not detailed here. Each of them was
designed for tuning mainly one of the sensitive
eigenfrequencies without influencing much of
the rest, otherwise frequency correction would
become a complex problem and will have to be
calculated and planned more exactly.

4   SUITABILITY OF CABLE-STAYED CONSTRUCTION
     AND MEDIUM STIFFNESS CONCEPT

After profound comparison of various alter-
natives, we selected the cable-stayed tower
as the most efficient structural system. For
the height ranges of approximately 100 m,
the design was to be based on the dynamic
concept of medium stiffness. The advantages
of this solution are manifold and will be
enumerated only in parts.

The structural system of a cable-stayed tower
has first of all improved aerodynamic proper-
ties and permits a simplified solution for the
machine house erection.

The medium stiffness concept results in very
large savings. It eliminates resonances, also
in the case of the higher sensitive eigen-
frequencies. The aerodynamic damping due to
rotor blades is increased considerably. The
whole tower becomes slender, producing sub-
stantial reduction of wind resistance and
providing an aesthetically pleasant appearance.
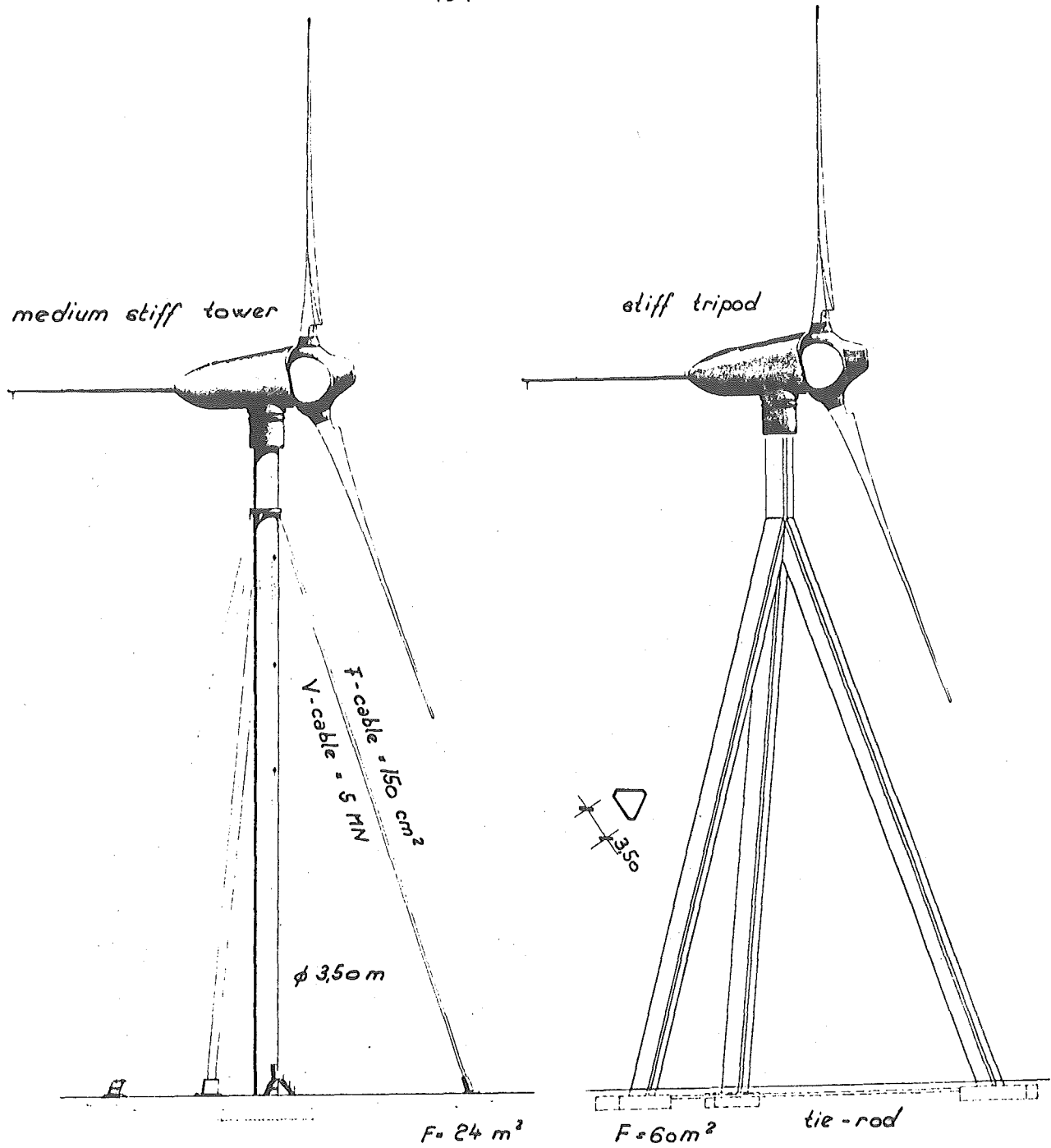
Fig.1 Examples for medium stiff and stiff GROWIAN towers
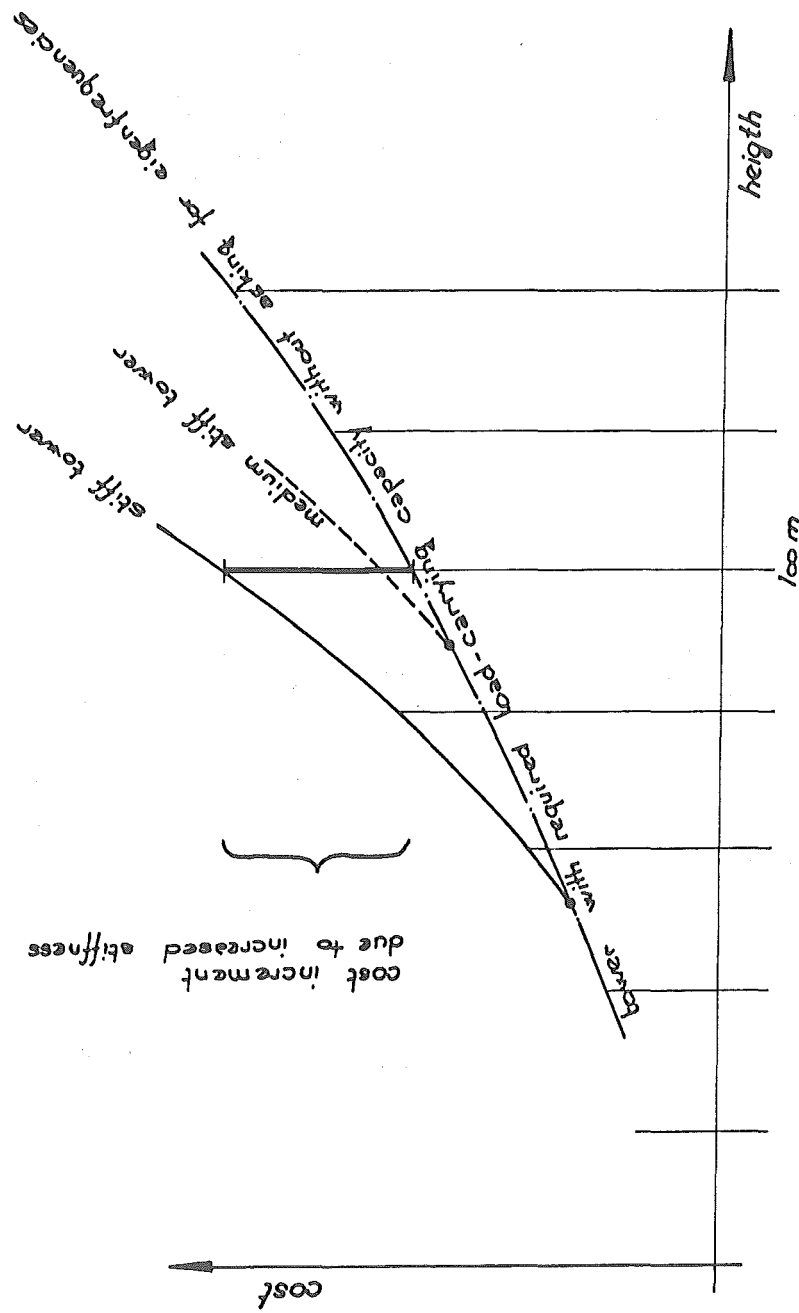
Fig. 2   Detail of GROWIAN optimizing diagram

Fig. 3 Exciting forces and frequencies of GROWIAN
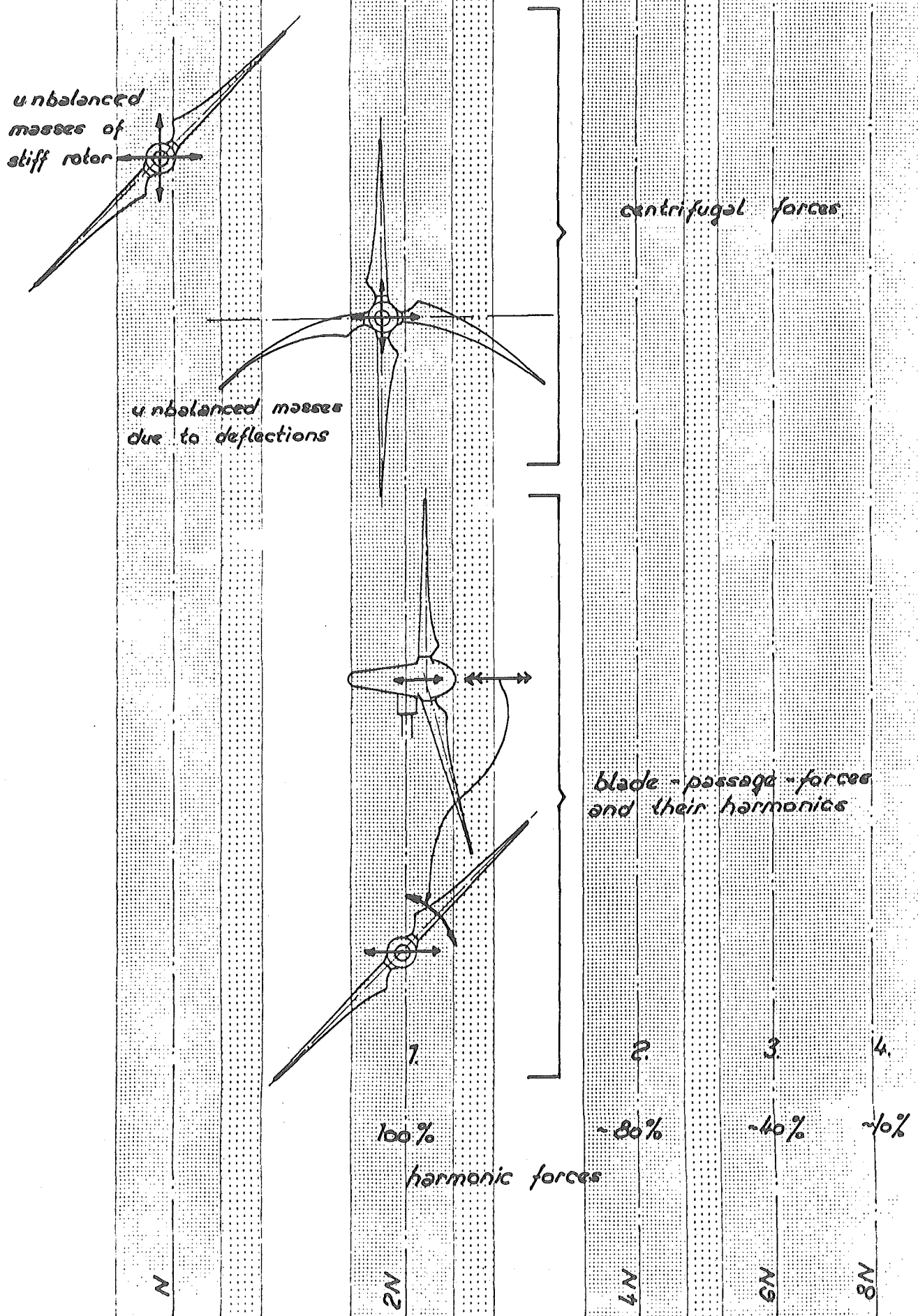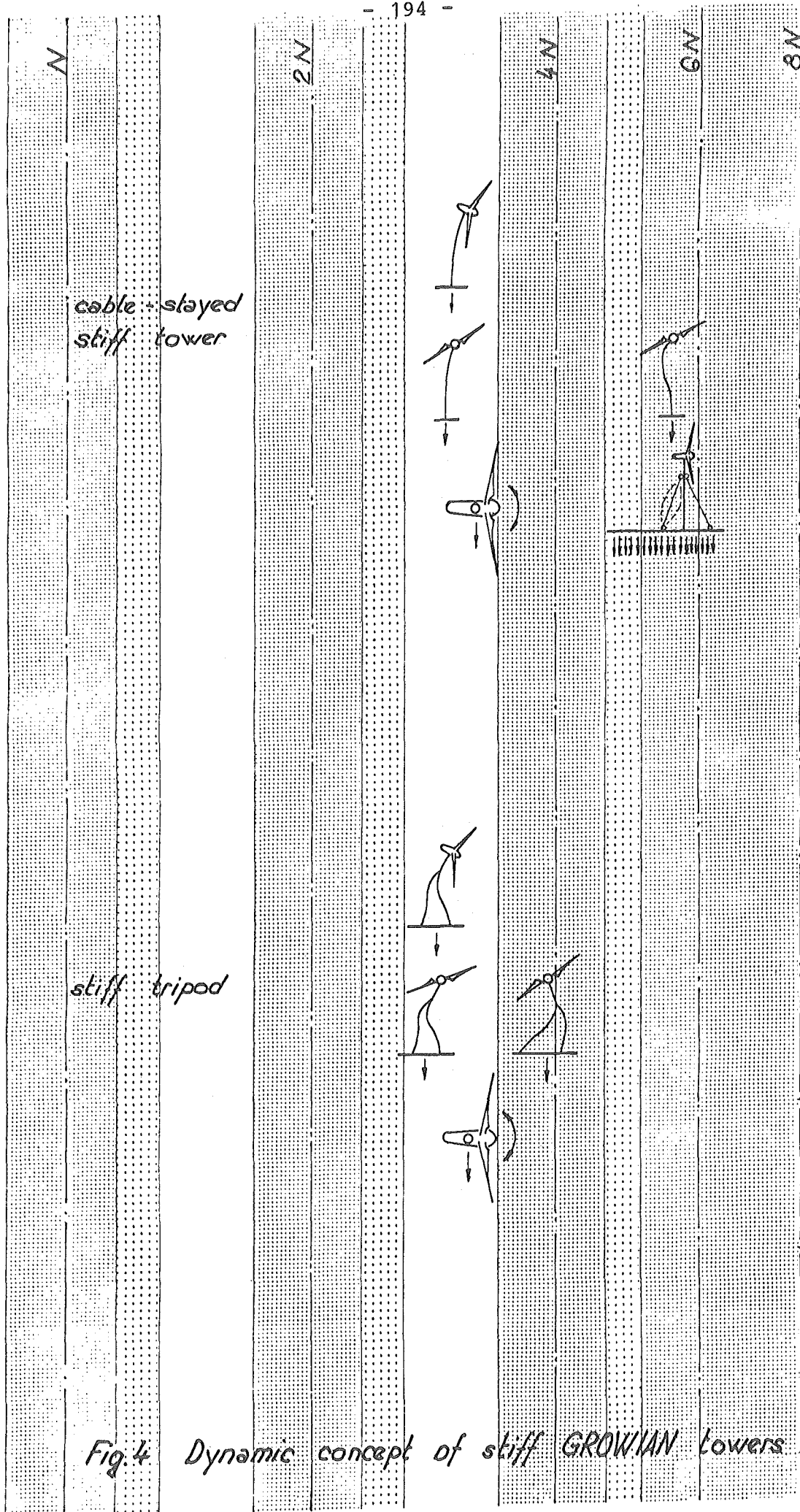
Fig.4 Dynamic concept of stiff GROWIAN towers

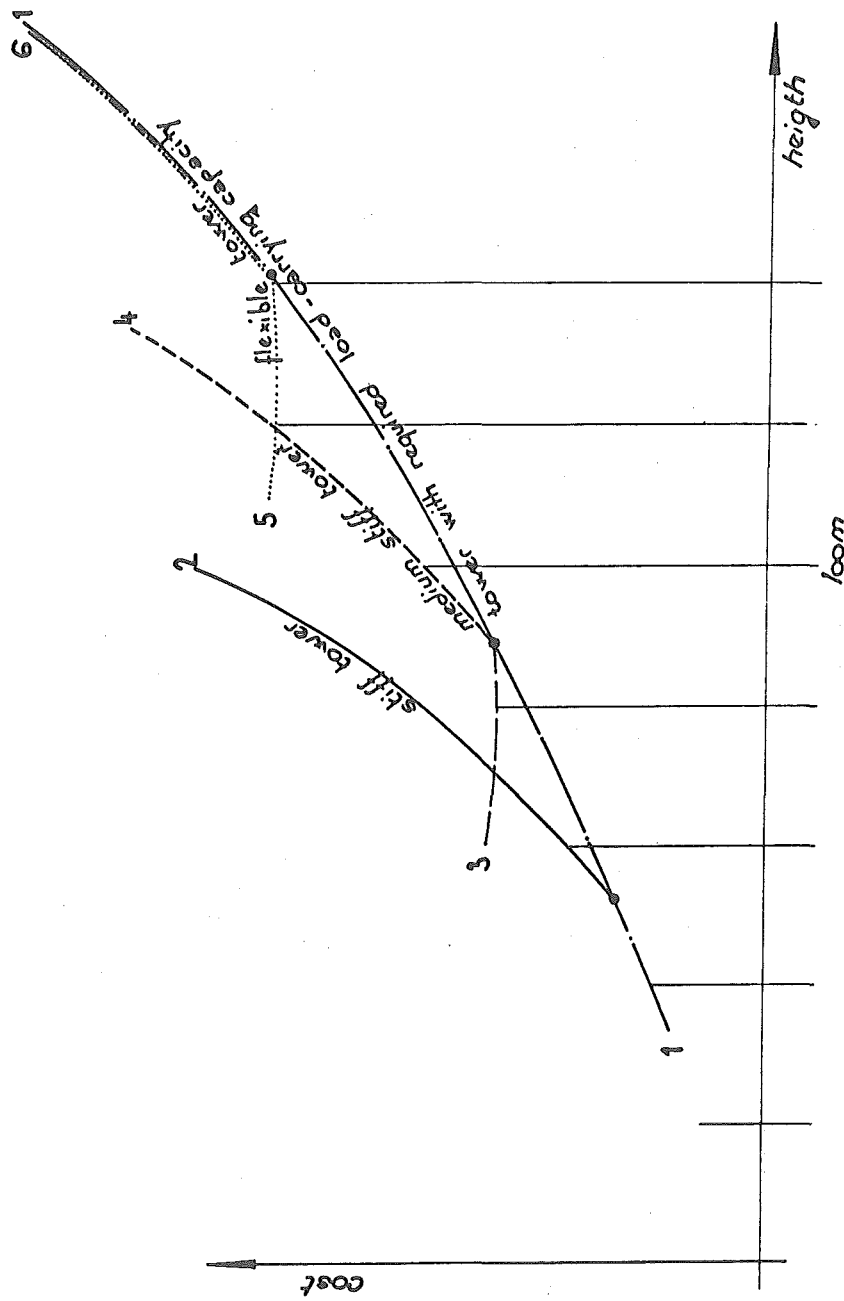Fig. 5 Dynamic concept of medium stiff GROWIAN tower
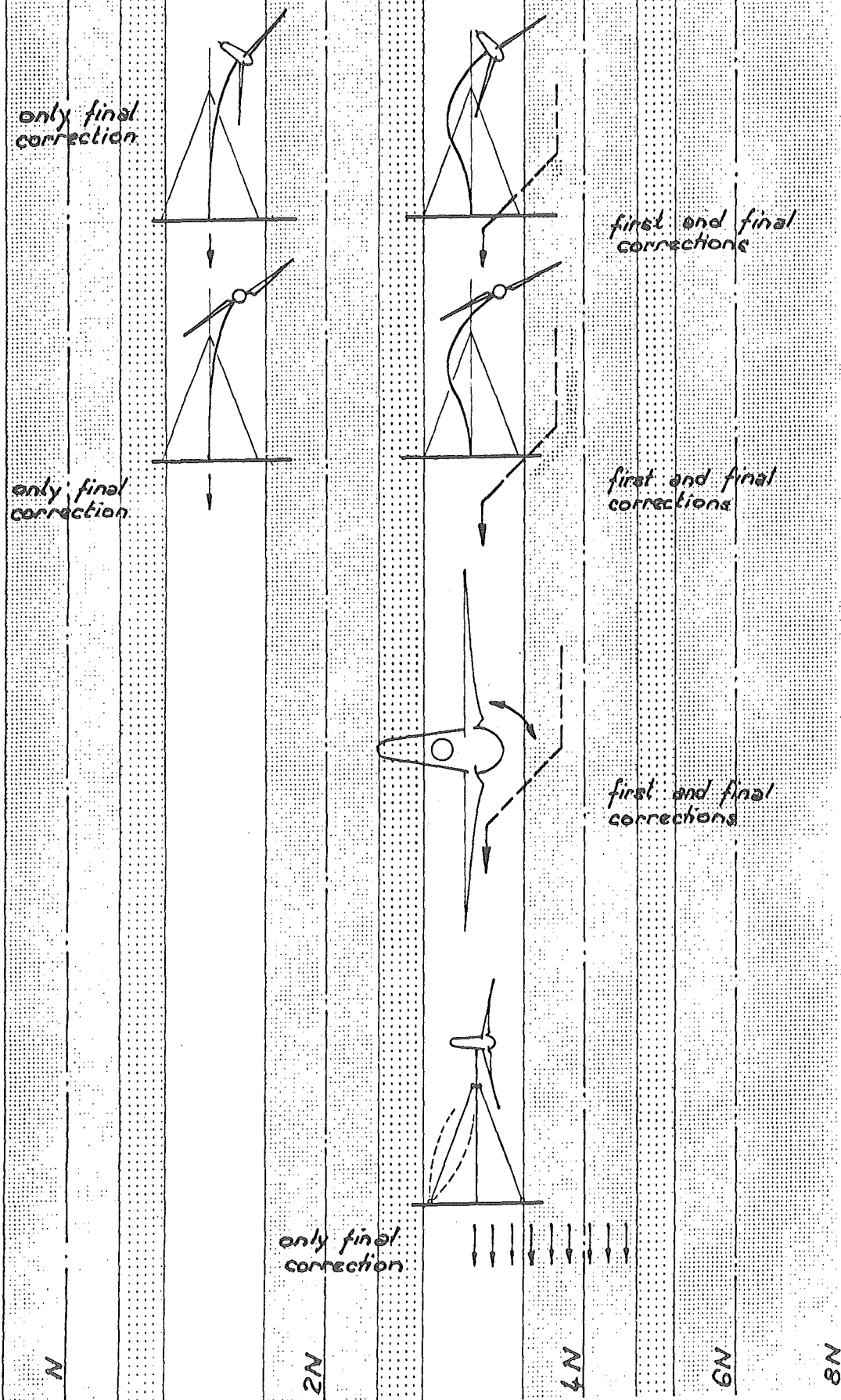
Fig. 6 GROWIAN optimizing diagram for cable-stayed towers

Calculation of the natural frequencies of the braced GROWIAN tower with dead head mass

by Dr.-Ing. habil. Ralf Cuntze and Dipl.-Ing. Josef Zaun

To be presented at the 1st Meeting of Experts on Structural Dynamics of Large Scale WECS (Wind Energy Conversion Systems) on the 12th Oct. 1978 at M.A.N. - Munich.

Summary

The natural frequencies of the braced GROWIAN (see following figure) steel and concrete tower were determined. In the calculation the main assumption to treat the machine house and the rotor as a dead mass was made. The FEM model consisted of the tower-bar element-structure and the rope-cable structures. All substructures were elastically bound to the soil. The prestressing of tower and cables was taken into account. The calculation procedure and the mechanical and numerical difficulties were discussed. Parametric investigations were undertaken to get an idea of the sensitivities of some main parameters. A comparison of the steel and the concrete tower natural frequency results are given at the end of the lecture.

The authors are with
M.A.N. - Neue Technologie
Dachauer Str. 667
8000 München 50

1. Introduction

One of the most important parts in the GROWIAN design are the
structural dynamic investigations. These works belong to special
work packages of the subcontractors DFVLR-Göttingen (system
dynamics) and Leonhardt & Andrä (structural dynamics lay out of
the tower).
Leonhardt & Andrä found out a medium stiffness wind energy tower
would be best. To get sure as soon as possible that this design
was acceptable M.A.N. assisted this subcontractor. By means of a
finite element programme M.A.N. computed the natural frequencies
of the braced steel and concrete tower systems.

Fig. 1 shows us the main dimensions and notations of GROWIAN.
It also gives us the quantities of the cone angle and the hub
axle angle. Furthermore we find a view downward.

In the calculation one main assumption was made by treating
the engine house and the rotor including the generator as a
dead mass with excentricity. The FEM Model consisted of bar-
elements for the tower and rope-elements for the cables. All
substructures were elastically bound to the soil. The prestressing
of tower and cables was taken into account.

2. Finite element model of the tower construction

First thing to derive is the calculation model of the tower
construction.
On fig. 2 we find the idealization of the whole structure. We
see the tower subdivided into ten finite bar elements. An eleventh
bar element has to carry the excentrical head mass. We further see
the sixteen rope elements of one pair of cables and the three bar
elements simulating the fixation of the cables to the tower. The
tower beam and the cables are elastically fixed to the foundation
by springs.

The engine house with its interiors and the rotor with the blades
and the hub are roughly simulated by a dead mass with three and a
half meter excentricity and by inertia moments. The inertia moments
of the rotor itself need nottobe considered because of the elastic
hinge bearing in the hub.

3. Loads on the model

Because of the nonlinear dynamic behaviour we now have to speak
about preloads or generally to the loads on the model.

Fig. 3 shows the external loads of the normal operational load
case and the internal forces of the cables caused by the external
loads and the pretension.
In the static load case - as the input for the dynamic load case -
the wind direction was assumed to be as shown in fig. 3. Any other
position or attack angle will practically lead to the same overall
stiffness of the tower system.

The weight of the structure is taken into account by bringing the
earth acceleration of 1 g into the computation.
The head of the tower is loaded by horizontal wind force of
$5,0 \cdot 10^5$ Newton and a mass of $2,54 \cdot 10^5$ kg. As an additional mass
for the cable fixation we estimated 10^4 kg.

For those who are not so familiar with WECS:
GROWIAN has to withstand wind, rotor and seismic excitations.
Apart from the rotor loads we have of course other loadings which
are affecting the dynamic behaviour of the tower. On fig. 4 you
see the wind profile over the height, then the wind turbulences,
the vertical wandering of the center of gravity of the rotor because
of the deformed rotor blades, the tower shadow excitations and the
turning of the wind.

4. Input data for the natural frequency computation

The next point attends the input data for the computation of both
the steel and the steel reinforced concrete tower system.

On table 1 you will find all specific quantities of the geometric
and elastic properties of tower and cable, the spring constants

of the foundation and the masses and inertia moments. Meanwhile
the above quantities have altered a little bit.

5. Calculation procedure within the used programme

For the calculation of the natural frequencies the finite element
programme ANSYS was taken.

In the slender structure of GROWIAN we noticed an influence of
the stresses caused by the static loads on the stiffness and on
the frequencies. To get this influence a special calculation run
has to be done before the dynamic run that finally finds out the
natural frequencies and modes of vibration. This effect of the static
deformations on the natural frequencies of the structure caused
by the prestressing of tower and cables is called stress stiffening
effect. It is taken into consideration as is shown now:

Usually a static finite element calculation is formulated by this
equation of equilibrium

$$[K_o] \{u\} = \{F\} \tag{1}$$

with

$$[K_o] = \text{small displacement stiffness matrix}$$

and

$$\{u\} = \text{node displacement vector}$$

$$\{F\} = \text{applied nodal load vector.}$$

This means the use of linear theory of elasticity.

Now we are going one step into the direction of nonlinear theory.
We are still sticking to the small deformation theory but we are taking
into account the effect of the stressing. So we have to add the
initial stress stiffness matrix

$$[[K_o] + [K_\sigma]] \{u\} = \{F\} \tag{2}$$

Both stiffness matrices $[K_o]$ and $[K_\sigma]$ are computed and stored for

the dynamic run. Now one is prepared for the dynamic calculation.

For the free vibration the load vector $\{F\}$ is replaced by the d'Alembert inertia force vector $-[M]\{\ddot{u}\}$ with $[M]$ is the mass matrix and $\{\ddot{u}\}$ are the mass accelerations. This relation put in equation (2) leads after rearrangement to the following eigenvalue problem

$$+ [M]\{\ddot{u}\} + \left[[K_o] + [K_\sigma] \right]\{u\} = \{0\} . \quad (3)$$

For harmonic vibrations

$$\{u\} = \{u_n\} \cdot e^{i\omega_n t} \quad (4)$$

represents a solution of equation (3), where-in the $\{u_n\}$ are the n modes and ω_n are the natural frequencies. The introduction of $\{u\}$ and of the derivation $\{\ddot{u}\}$ into equation (3) finally gives the homogeneous equation

$$\left[-\omega^2_n [M] + [K_o] + [K_\sigma] \right]\{u_n\} = \{0\}. \quad (5)$$

As you know for this equation nontrivial solutions for $\{u_n\}$ do exist if the determinant of (5) gets zero. This delivers us the eigenvalues or natural frequencies ω_n.

By means of the "Reduced Mode Frequency Analysis" the user is able to specify a set of n "master" degrees of freedom, which he feels will characterize the natural frequencies of interest in the system. Additionally the computercosts can be reduced by this procedure, called "Guyan Reduction".

Coming to this point we should reflect that the computed natural frequencies belong to a special state of static loads as a reference basis.

6. Two small problems within the calculation process

During the calculation we have had two small problems:

The first problem was a numerical one caused by the difference
in stiffness between the tower and the cable elements. The computer
pointed out that a typical stiffness ratio between the most stiff
bar and the cable element was bigger than an allowed limit of ten
power eight. But as we found out we didn't reach the critical area,
because an increase from eight elements to the chosen sixteen cable
elements (that increase lowered that typical ratio by a factor of
two) didn't practically alter the numerical eigenvalue results. So
we could be pretty content with our idealization from numerical
point of view.

The second problem depended on the input possibilities of the
programme. For the dynamic run we needed the right deformation
state defined by boundary displacements. Therefore we first had
to compute the displacement of the connection point cable to spring.
Then we had to add the deformations of each cablespring under its
special cableload. This gave us the real boundary condition at the
cable spring end.

As you can see here, to get the dynamic calculation run, one had
to do much pre-work.

7. Results of the towers with nominal geometry and loads

In the figures 5.1 to 5.5 you will see the lowest modes of the steel
tower system.
The lowest mode is the first transversal mode. It belongs to a
natural frequency of 0.438 Hz. Further modes are shown on the
following pictures.

Conclusively we should have a look at table 2. This table contains
the lowest natural frequencies of both tower systems. You recognize
some differences in the results. The main reason for this is that
both towers are not opimised equal well.

As you could have deduced from the dense location of the natural frequencies there are not always sharp separated modes too.

Both the first and the second cable modes belong to the less tensioned cable.

All the cable bending frequencies are dependant on the wind direction. A tuning can only be made by the pretension.

8. Main excitation frequencies and natural frequencies

Just now we have heard what natural frequencies we have reached with the towersystem. That enables us to see how far we have fulfilled the design wishes of Leonhardt & Andrä.

Fig. 6 shows the natural frequencies on the ordinate and the excitation frequencies on the abscissa. The dimension is Hertz. We further see the upspeeding lines of the rotor, ^{of} the blade and of the three superharmonics. Of interest for excitation are only the superharmonics.

On this figure you recognize some forbidden frequency areas (obliquely shadowed) caused by the most important excitation frequencies of the one - the two-and the four - fold rotor frequency. These areas are defined by the crossings of the vertical exciting frequency lines with the upspeeding lines. They are limited on the bottom side by the nominal operation frequency f_1 minus 15 per cent tolerance caused by the control-system. On the upper side the limit is the nominal value plus 15 per cent (caused by the control system) and plus 35 per cent in emergency switch off case (dashed plotted line).

What we learn:

Only with the rotor harmonic we are not coming through the deepest natural frequency.

The lowest natural frequencies of both tower types fit into the free areas.

We still have the possibility of tuning the system down in case of essential tolerances of geometry mass and load.

9. Parameter variation influences

Because of the big effort getting natural frequency results
of a prestressed construction we only altered two parameters
the head mass and the Youngs modulus of the cables. Furthermore
we only took the concrete tower into account.

On the top half of fig. 7 we have the curve of the 1st lateral
and the 1st pitching frequency as a function of the head mass.
On the bottom half you find the above frequencies versus Youngs
modulus of the cables.
The upper curve shows a relative   big influence of an ascending
headmass. For the taken cable configuration we are not allowed
to increase mass.
The bottom curve shows the effect if we would not have chosen the
higher modulus parallel wire cables.

Concluding remarks

In this lecture we recorded the finite element work we have done
for determining the natural frequencies of the GROWIAN steel and
concrete towers. The main assumption for the calculations was the
treatment of the engine house and the rotor system as a dead mass.
All substructures were elastically bound to the soil. Prestressing
of tower and cables was taken into account.

As we have seen, the lowest natural frequencies fit to the design
criteria of the GROWIAN system. A tuning is possible.

Restricted to the topic "DYNAMICS" there is still further work to
be done by us to prove the tower having a safe life under its
excitations.

Underestimation of applied research may lead to serious
disappointments. Of course, in the long run, a good "product"
will find its way, but without systematic applicational research
much time and also much money will get lost.

And at the very end we say to all colleagues on the GROWIAN
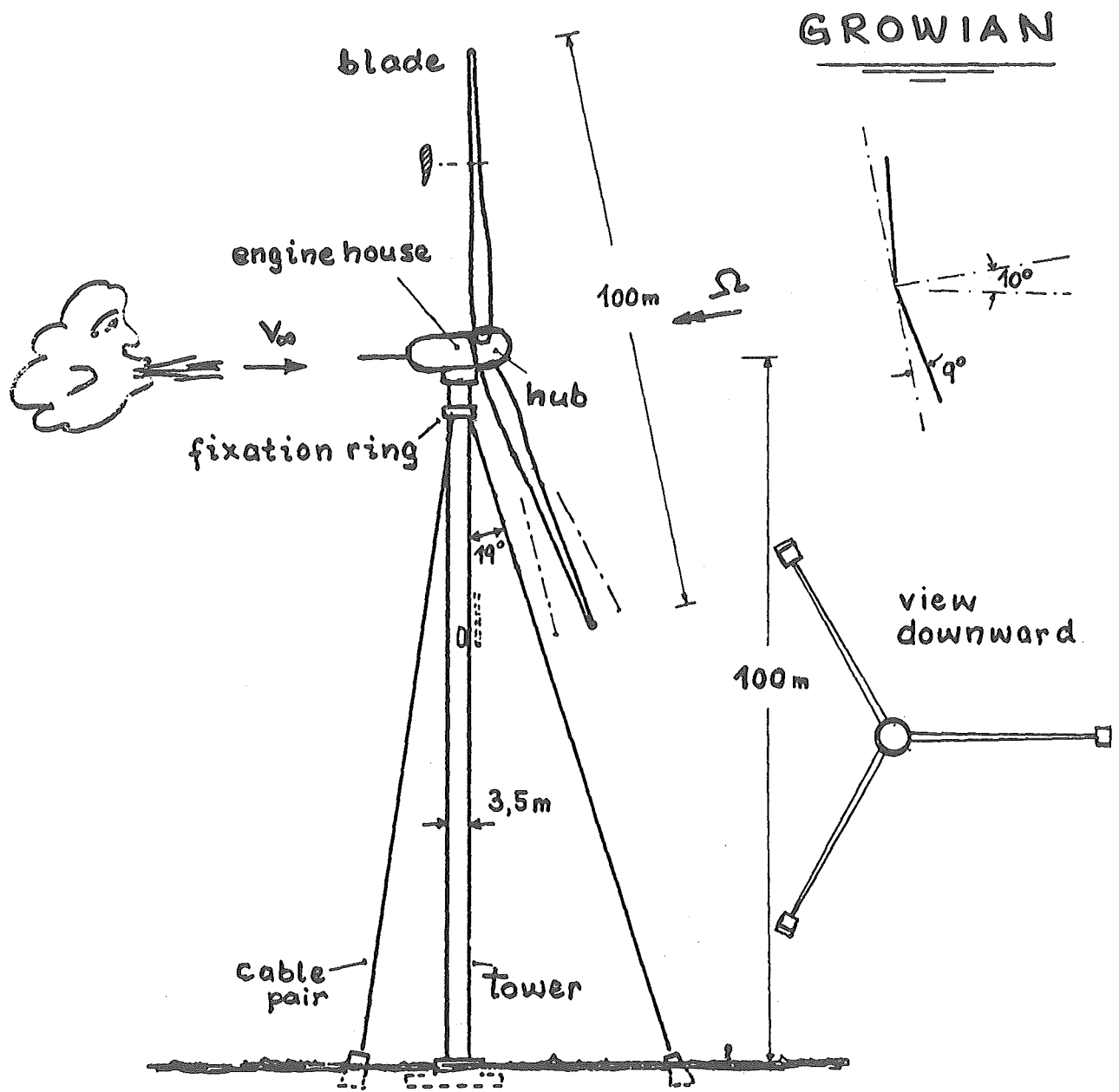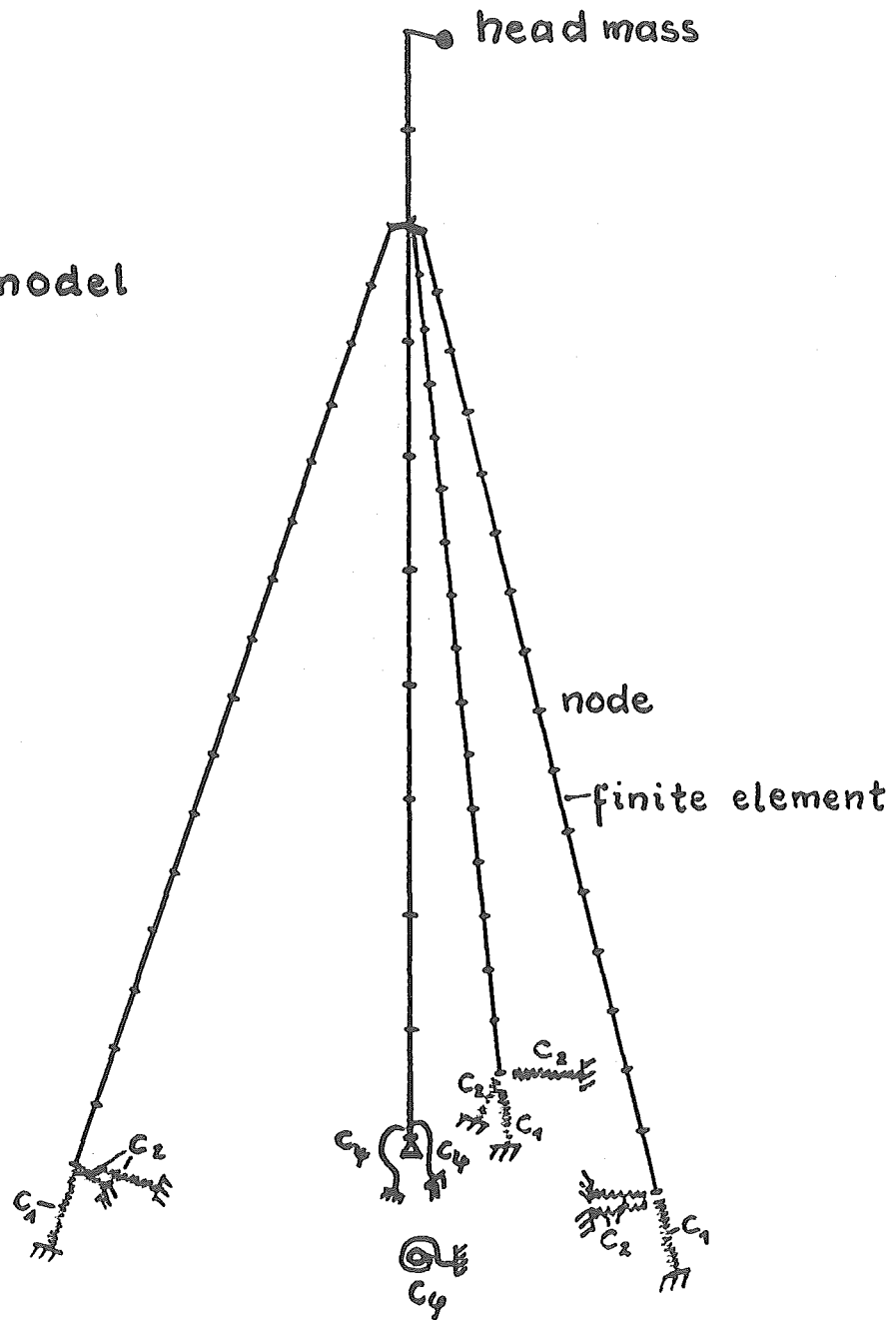project: Let's get the large work done as soon as possible.

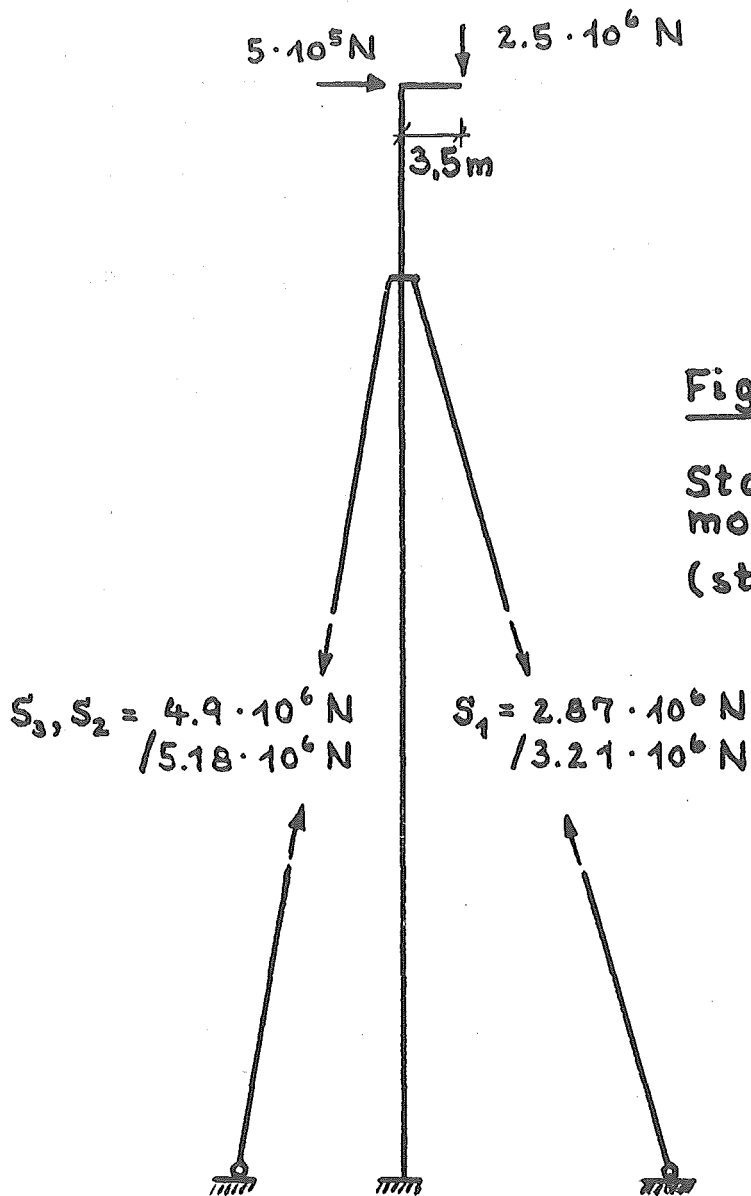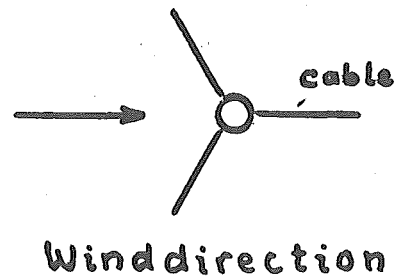Fig. 1   Main Dimensions and Notations

Fig.2 FEM - model

$5 \cdot 10^5 N$ $\downarrow$ $2.5 \cdot 10^6 N$

3,5m

Fig. 3

Static loads on the model
(steel tower / concrete tow.)

$S_3, S_2 = 4.9 \cdot 10^6 N$
$/ 5.18 \cdot 10^6 N$

$S_1 = 2.87 \cdot 10^6 N$
$/ 3.21 \cdot 10^6 N$

cable

Winddirection

		dimensions	steel tower	steel reinforced concrete tower
Tower	cross sectional area	mm²	$1.97 \cdot 10^5$	$2.55 \cdot 10^6$
	2nd moment of area	mm⁴	$2.99 \cdot 10^{11}$	$3.38 \cdot 10^{12}$
	polar moment of inertia	mm⁴	$6.64 \cdot 10^{11}$	$6.11 \cdot 10^{12}$
	shear correction factor	-	0.50	0.50
	density	N mm⁻⁴s²	$1.05 \cdot 10^{-8}$	$2.62 \cdot 10^{-9}$
	Youngs modulus	N mm⁻²	$2.10 \cdot 10^5$	$3.40 \cdot 10^4$
	Poissons ratio	-	0.30	0.167
Cable	cross sectional area of one pair of cables	mm²	$1.19 \cdot 10^4$	$1.50 \cdot 10^4$
	density	N mm⁻⁴s²	$8.50 \cdot 10^{-9}$	$8.80 \cdot 10^{-9}$
	Youngs modulus	N mm⁻²	$2.10 \cdot 10^5$	$2.10 \cdot 10^5$
Elastic Foundation	TOWER			
	torsional spring constant	N mm	$1.37 \cdot 10^{13}$	$8.00 \cdot 10^{12}$
	bending spring constant	N mm	$4.61 \cdot 10^{13}$	$3.70 \cdot 10^{13}$
	CABLE			
	axial spring constant	N mm⁻¹	$3.30 \cdot 10^5$	$3.60 \cdot 10^5$
	transverse spring const.	N mm⁻¹	$1.00 \cdot 10^{10}$	$1.00 \cdot 10^{10}$
Masses & Inertias	headmass (engine house, generator, gearing, rotor)	N mm⁻¹s²	$2.54 \cdot 10^2$	
	cable fixation ring	N mm⁻¹s²	$1.00 \cdot 10^1$	
	excentricity of the headm.	mm	$3.50 \cdot 10^3$	
	mass moments of inertia of the head about tower axis	N mm s²	$1.34 \cdot 10^{10}$	
	lateral axis	"	$1.34 \cdot 10^{10}$	
	engine house main axis	"	$5.50 \cdot 10^8$	

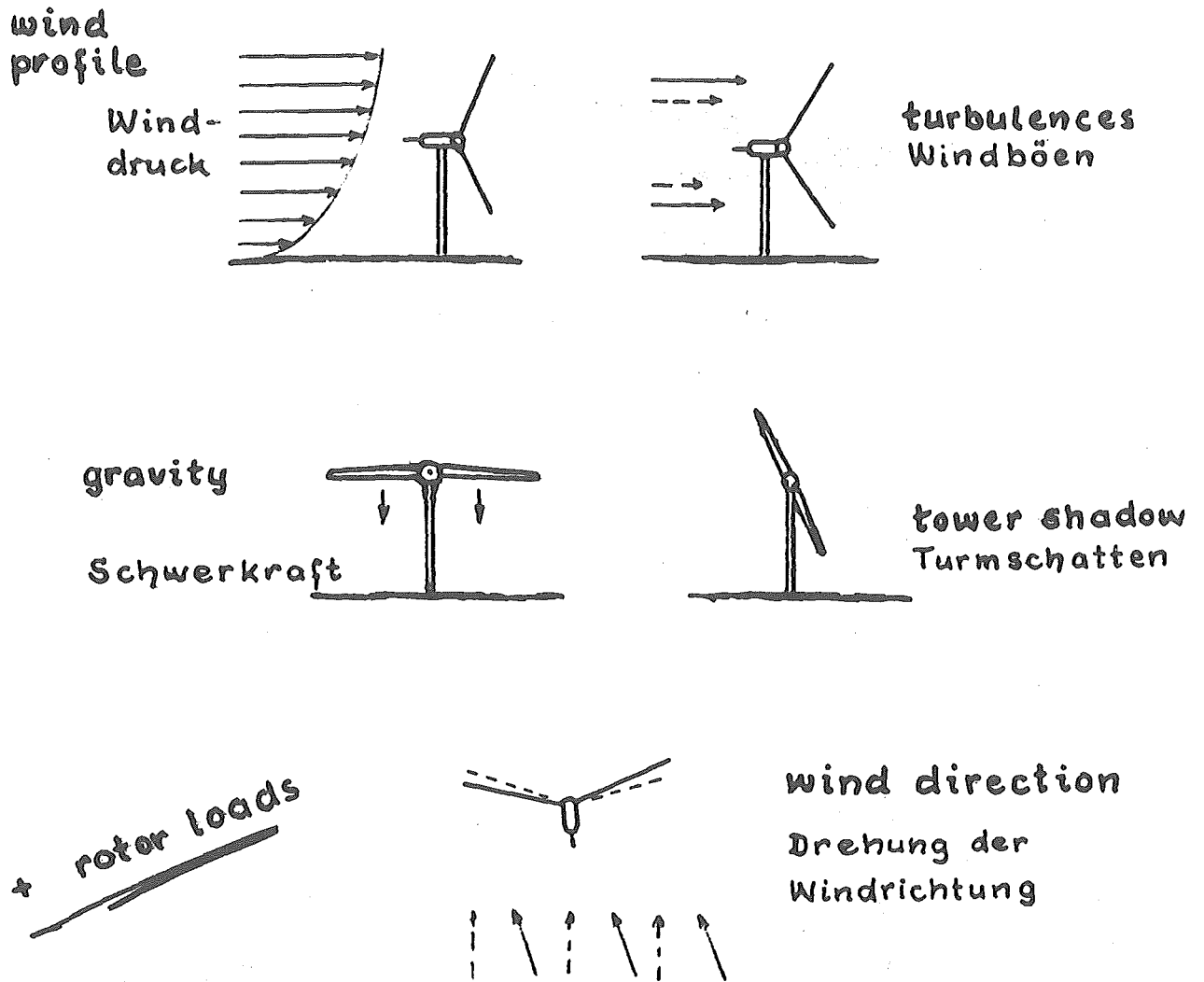Table 1   Input data for the frequency computation
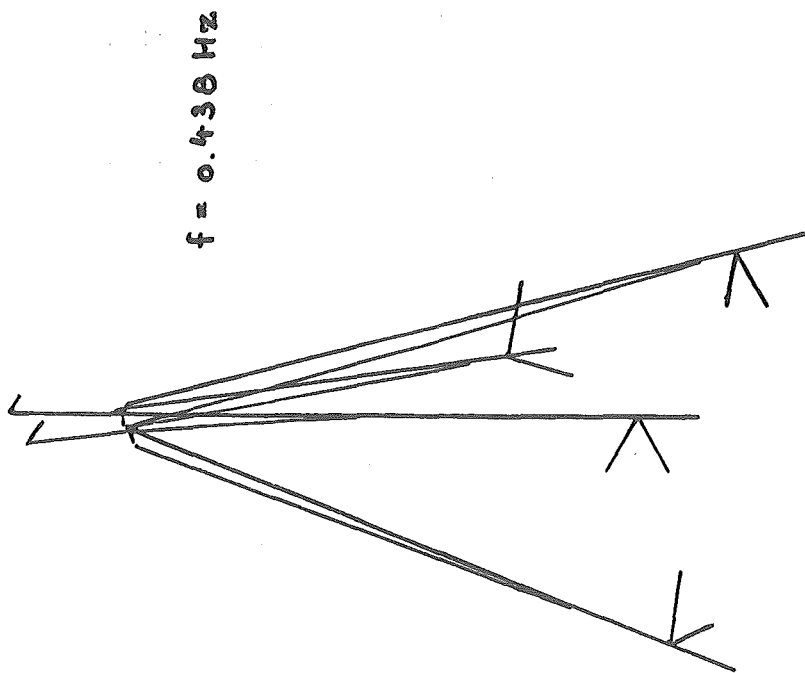
Fig. 4   Loads on the model

f = 0.441 Hz

Fig.5/2   1st pitching mode

f = 0.438 Hz

Fig.5/1   1st transversal mode
(steel tower)

f = 0.98 Hz
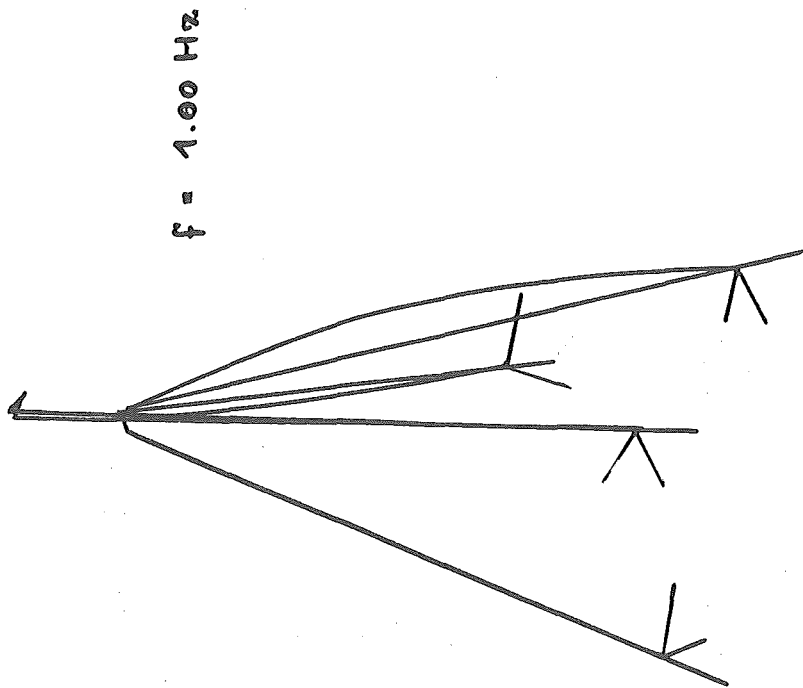
Fig. 5/3   1st mode of the cable

f = 1.00 Hz

Fig. 5/4   1st torsional mode
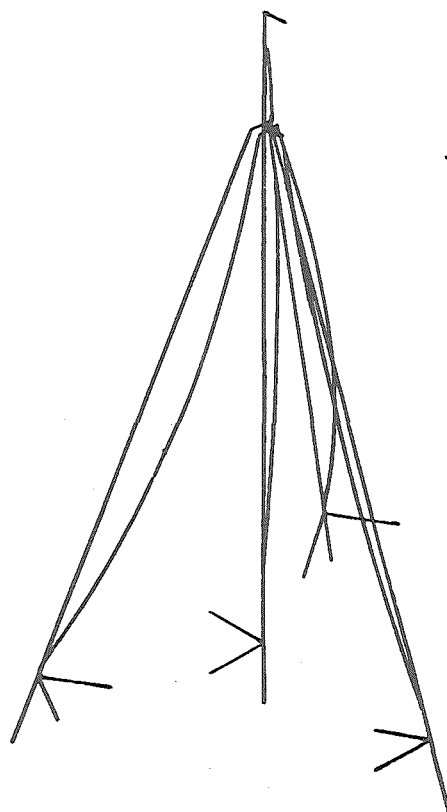
$$f = 1.19 \text{ Hz}$$

Fig. 5/5   2nd pitching mode

name of the mode	steel tower	steel re-inforced concrete tower
1. lateral	.438	.454
1. pitching	.441	.456
1. cable	.981 (1.3)	.898 (1.4)
1. torsion	1.00	> 1.00
2. pitching	1.19	.971
2. lateral	1.42	.985
2. cable	> 2.0 (>2.0)	1.83 (>2.0)

Table 2   Natural frequencies of steel tower and concrete tower

with   parentheses maximal prestressed
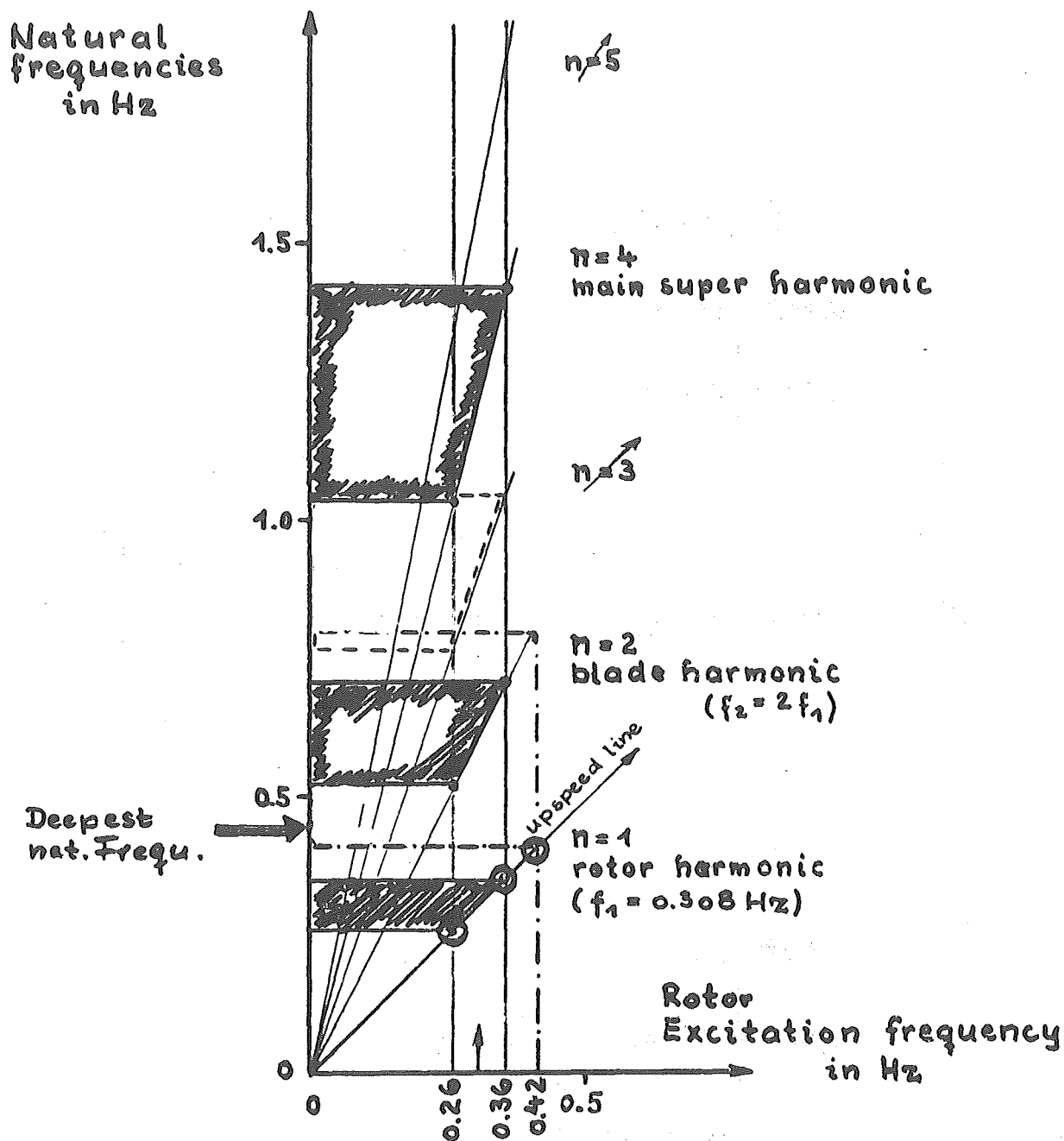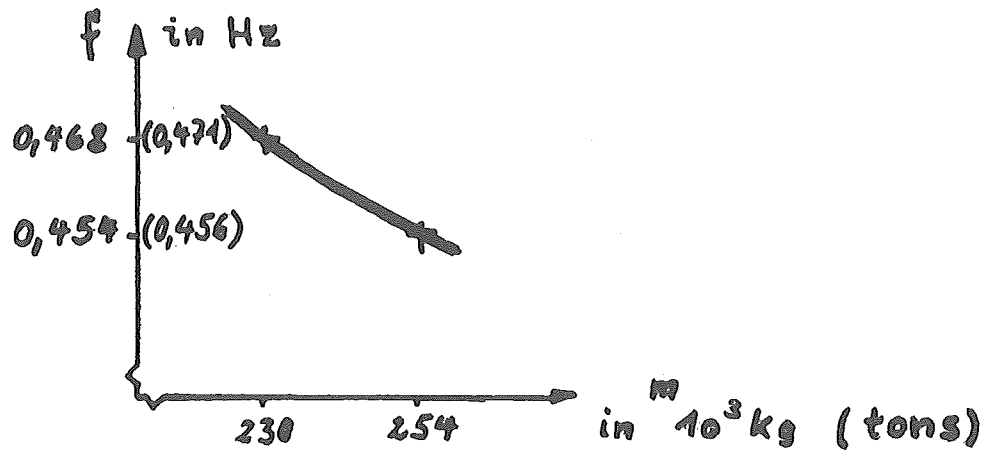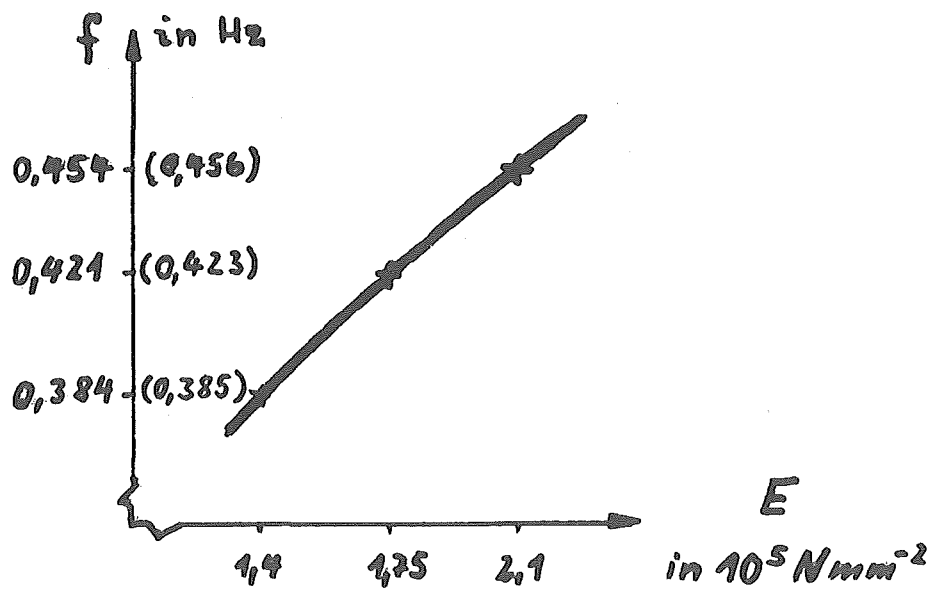without   "   minimal   "

Fig.6 Excitation and natural frequencies

1st lateral (pitching) nat. frequency vs head mass

1st lateral (pitching) nat. frequency vs Young's Modulus of cables

Fig. 7   Parameter investigation (concrete tower)

FFA

FLYGTEKNISKA FÖRSÖKSANSTALTEN

THE AERONAUTICAL RESEARCH INSTITUTE OF SWEDEN

COMPUTER METHODS FOR STRUCTURAL WEIGHT
OPTIMIZATION OF FIBER REINFORCED PLASTICS

by

Sven-Erik Thor

COMPUTER METHODS FOR STRUCTURAL WEIGHT OPTIMIZATION OF FIBER REINFORCED PLASTICS

by Sven-Erik Thor

1. Introduction

Some of FFA:s computerprograms for analysis and optimum design of fiber reinforced plastics will be discussed.

A general flow chart for analysis of fiber reinforced structures is shown in fig 1. The septs B and C can either be manual or computerized. However, by manual analysis it is only exeptionally possible to find the theoretically optimum design when the structure is loaded with many loadcases.

Different types of aids have been developed in order to help the designer e. g. strength diagrams fig 2, 3. The disadvantage with this type of tool is that they are difficult to use when the structure is loaded with many loadcases at the same time.

Another alternative is to use computerprograms which are specially designed to handle weight minimization of fiber reinforced plastics.

At FFA we use the following programs for optimum design of flat fiberreinforced plastic structures fig 4.

LOPT   Minimum weight design of laminates   Ref [1], [2]

SOPT   Minimum weight design of orthotropic sandwich panels
       Ref [3], [4]

WBOPT   Minimum weight design of multicell composite wing-box
        beams. Ref [5]

2.   LOPT

This program optimizes fiber layup   angles $(0, 90, \pm \beta)$ and relative layerthicknesses for applied loads   fig 5.

The space in which the optimization is done is shown in fig 6, where ν_1 and ν_k represents the relative thicknesses in the 0° and 90°- direction, β represents the third and fourth angle in the laminate. The laminate properties and thicknesses are calculated for a number of points in the ν_1, ν_k and β space.

As result of the calculation the optimum fiber angle and relative thicknesses is obtained for the laminate subjected to the specified loadcases.

During optimization minimum required stiffness also is checked. The optimization is carried out for both continum and netting analysis. Fig 7, 8 shows typical printout from a run with two different loadcases, with four levels of optimization.

3.   SOPT

This program calculates optimum face and core materal thicknesses for sandwichpanels subjected to in plane loads and with the sides of the panel simply supported, fig 9.

During optimization the following strength and stability constraints are analyzed.

1. Maximum admissible stress
2. Maximum admissible stiffness
3. Face wrinkling
4. Dimpling
5. Core shear instability
6. General buckling

Fig 10 shows failure modes for points 3-6.

Points 1 through 4 gives limit for face material thickness
and point 5 gives minimum admissible core height to avoid
core shear instability.

Now the limiting lines for t and H (face-core thicknesses)
are established, fig 11. Areas to the left and below these
lines are prohibited areas. In fig 11 there are also curves
for global buckling and constant weight. The intersecton
between these two last curves represents the point(s) where
global buckling occurs.

In order to find the optimum configuration the curve for
constant weight is translated towards the global buckling curve
fig 12. Now one can distinguish three different things that
can happen when minimum weight is fullfilled.

1. General buckling
2. Minimum admissible core material thickness
3. Minimum admissible face material thickness.

4.   WBOPT

A true structural optimization of a box beam implies that the
disigner optimizes shape, determines optimal geometrical con-
figuration, chooses the optimum member thicknesses and selects
the most suitable structural materials. In the design process
each of these variables must be assigned a certain level in a
preference list defining the order in which various properties
are to be optimized. The most commonly used hierarchy is the
following one: 1) Shape and spatial configuration of the
structure, 2) Material properties, 3) Member thickness and
cross-sectional areas.

The optimization of shape and spatial configuration is beyond
the scope of this program. Any such optimization would
require the consideration of other than structural criteria,
e.g. questions of aerodynamics, which cannot be defined on
general premises. In the following spatial configuration
is, therefore, considered a parameter and kept constant
throughout the optimization process. In particular, it is
assumed that the cross-sectional shape of the box beam is
known and that the location of ribs and shear webs has already
been chosen. By these assumptions, the lengths and widths
of all panels are given. Hence, as far as geometry is concerned,
the optimization procedure only has to deal with the determina-
tion of member thicknesses and cross-sectional areas, fig 13.

5. Example

As an example the 19 m GPP blade that was designed for
Karlskronavarvet will be used.

The principle layout of the blade is shown in fig 14.

The blade is manufactured with a polyurethan foam core as a
positive mould, and the core is divided in two parts by the
shear web. The forward part of the section is the loadcarring
part, this layout enables us to put the shearcenter and the
masscenter at their proper places.

First of all the face material in the load carrieng part was
optimized with LOPT, WBOPT at six radial stations. This gives
the radial and cordvise distribution of material, fig 15.
During the precess the location of shear- and masscenter was
checked, fig 16.

Finally a general static and dynamic FEM analysis was carried
out for the whole structure, with the BASIS computerprogram,
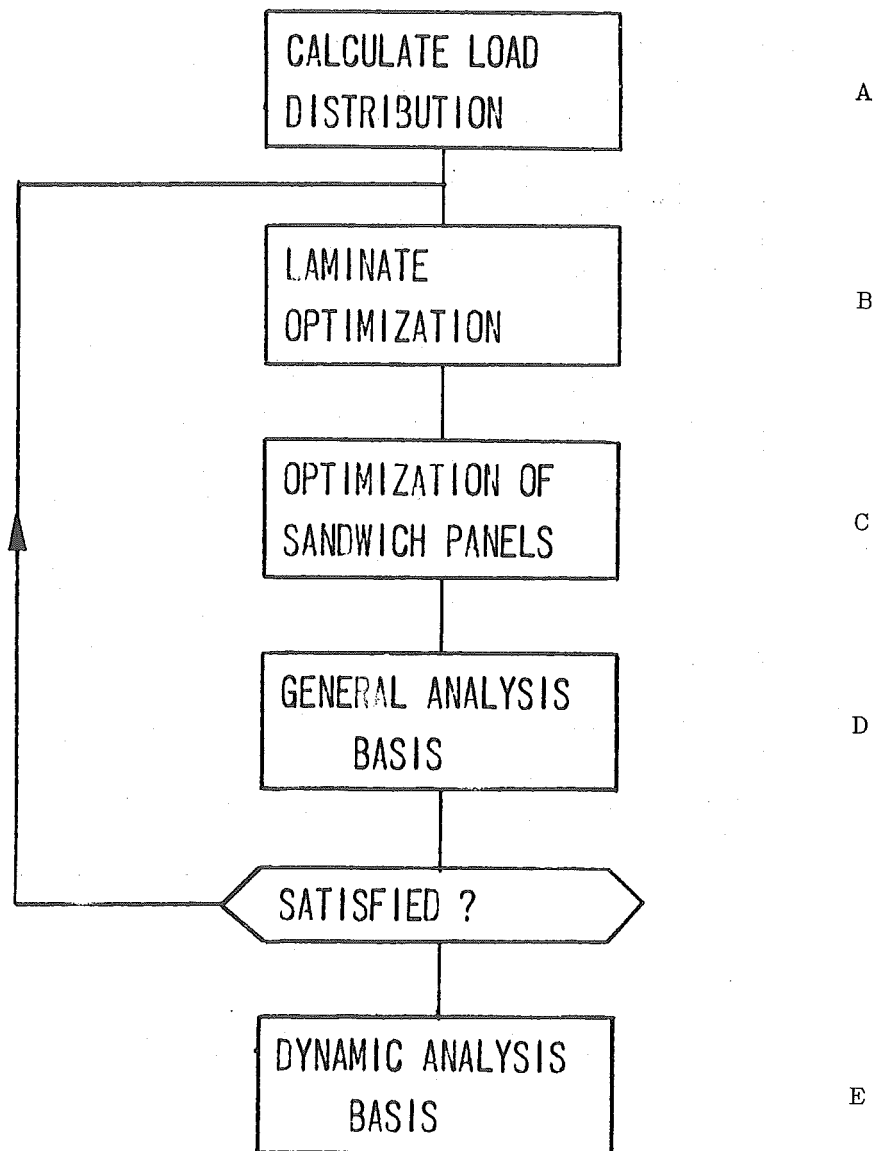fig 17.

REFERENCES

[1]   P Stehlin
      Dimensionierung von Laminaten aus Faserverstärkten
      Kunststoffen
      FFA Rapport HF-1278:1   Maj 1968
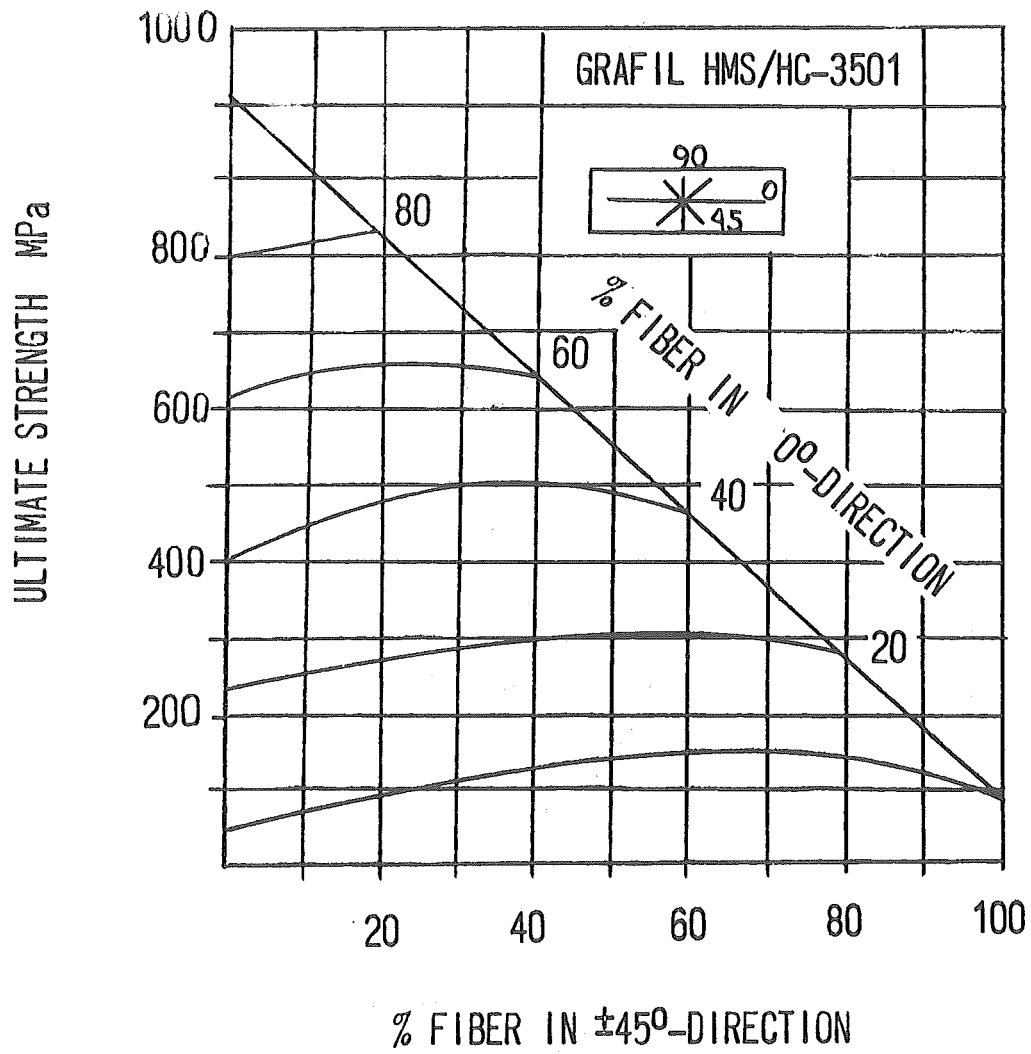

[2]   U Borkén
      Konvertering av datorprogram PS 003C för användning på
      timesharingterminal
      FFA Rapport HU- 1756   1975

[3]   P Stehlin   L Holsteinsson
      Minimum weight design of orthotropic sandwich panels
   loaded in compression and shear
      FFA Report 122   1971

[4]   L Knutsson
      Användaranvisning till beräkningsprogrammet PS03TS (SOPT)
      FFA Rapport HU-2076   1977

[5]   P Stehlin
      Minimum weight design of multicell composite wing-box beams
      FFA Report HF-1330:3 Part 1   1971

```
                    ┌─────────────────┐
                    │ CALCULATE LOAD  │          A
                    │ DISTRIBUTION    │
                    └─────────────────┘
          ┌─────────────────┐
          │         ┌─────────────────┐
          │         │ LAMINATE        │          B
          │         │ OPTIMIZATION    │
          │         └─────────────────┘
          │                  │
          │         ┌─────────────────┐
          │         │ OPTIMIZATION OF │          C
          │         │ SANDWICH PANELS │
          │         └─────────────────┘
          │                  │
          │         ┌─────────────────┐
          ▲         │ GENERAL ANALYSIS│          D
          │         │     BASIS       │
          │         └─────────────────┘
          │                  │
          │      ╱───────────────────╲
          └─────<   SATISFIED ?        >
                 ╲───────────────────╱
                           │
                  ┌─────────────────┐
                  │ DYNAMIC ANALYSIS │          E
                  │     BASIS       │
                  └─────────────────┘
```

LAMINATE STRENGTH
COMBINED LOADING
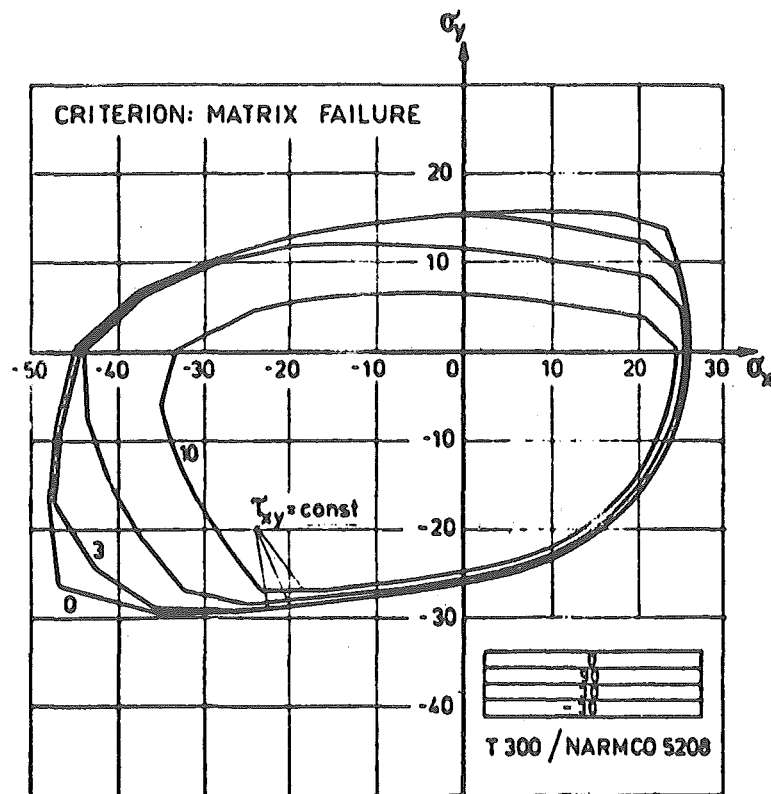
COMPUTER PROGRAMS FOR ANALYSIS OF COMPOSITE

# STRUCTURES DEVELOPED AT FFA

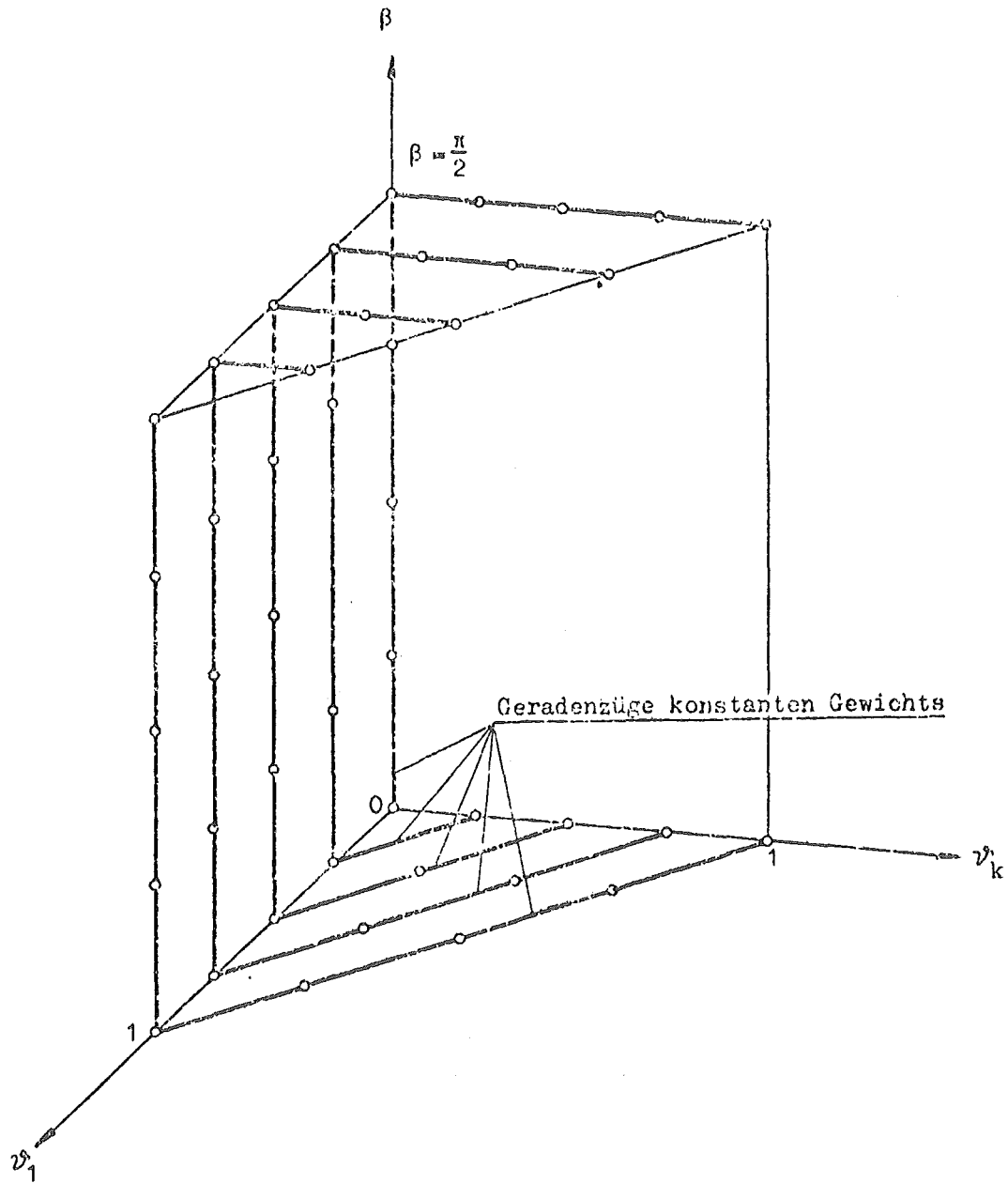## OPTIMUM DESIGN

LOPT   Minimum weight design of laminates

SOPT   Minimum weight design of orthotropic

            sandwich panels

WBOPT   Minimum weight design of multicell
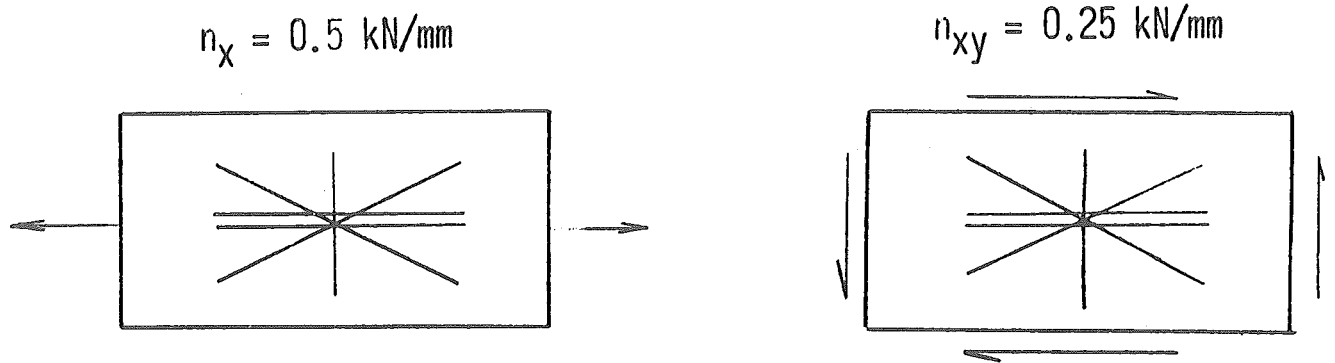
            composite wing-box beams

ANALYSIS

BASIS   General purpose program for structural

            analysis (finite elements)

LST   Nonlinear strength analysis of laminates.

WST   Strength and geometrical analysis of

            composite wing-box beams

Geradenzüge konstanten Gewichts

E X A M P L E

$n_x = 0.5$ kN/mm $n_{xy} = 0.25$ kN/mm
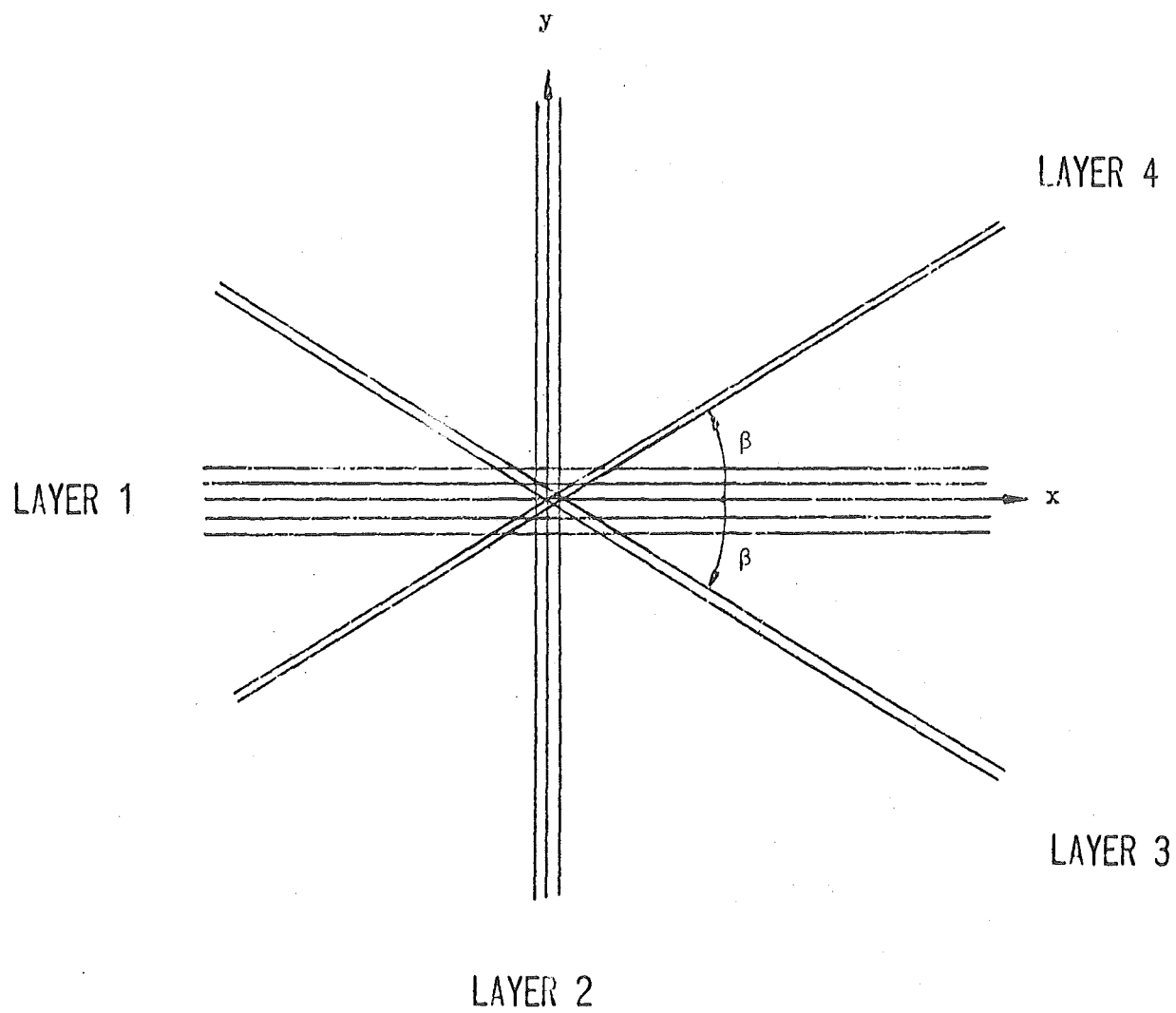
DESIGN CONDITION: ULTIMATE STRENGTH ONLY (J=2.0)

MATERIAL   :   T300/5208 -   =1150 N/mm^2 (tension)
                                          850 N/mm^2 (compression)

OPTIMUM CONFIG. :   25% OF FIBERS IN DIRECTION   0^0
                     15%   90^0
                     60%   ±25^0

COST   : $ 4:-

LAMINATE OPTIMIZED FOR CRAZING AND FAILURE

4 SOLUTIONS FOUND

NUMBER OF PLIES

I	0	90	-B	+B	BETA	TLAM	EX	EY	GXY
1	4	2	10	10	25.00	3.302	86.3	21.1	19.1
2	5	2	10	10	25.00	3.429	88.3	20.8	18.5
3	4	3	10	10	25.00	3.429	85.5	25.5	18.5
4	3	4	10	10	25.00	3.429	82.1	30.1	18.5

I	FMAX (CONT)	FMAX (NETG)	REX	REY	RGXY	LC	PLY CONTINUUM	JP	LC	PLY NETTING	JP
1	.96	.74	0.00	0.00	0.00	1	2	1	1	2	1
2	.90	.69	0.00	0.00	0.00	1	2	1	1	2	1
3	.93	.62	0.00	0.00	0.00	1	2	1	2	3	1
4	.98	.62	0.00	0.00	0.00	1	2	1	2	3	1

ELAPSED TIME   4.258 CP SECONDS

NUMBER OF CONFIGURATIONS INVESTIGATED =   151

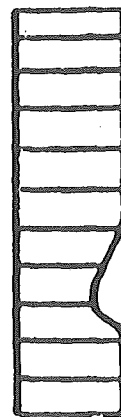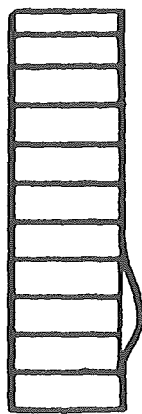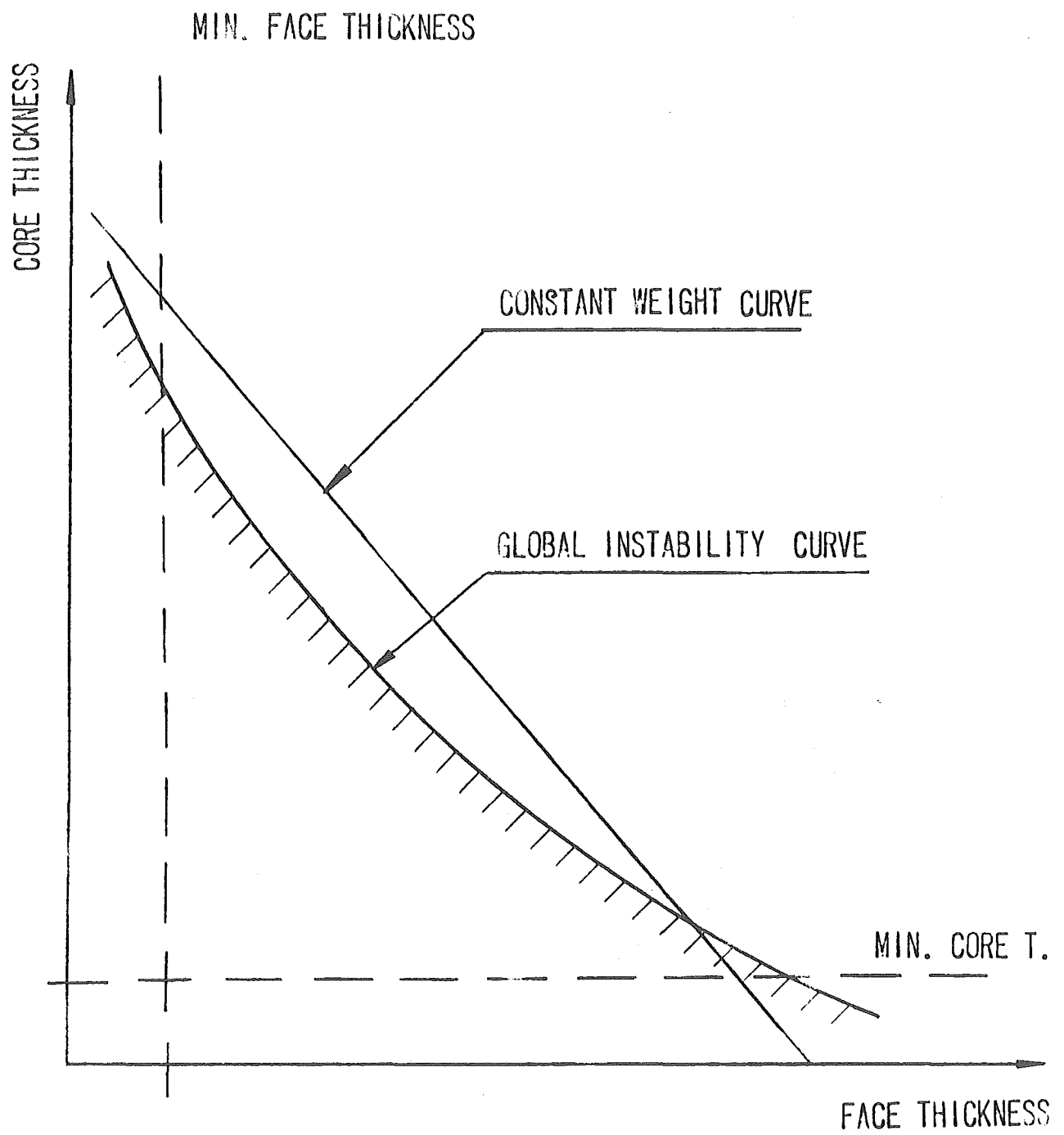# MINIMUM WEIGHT DESIGN OF SANDWICH PANELS
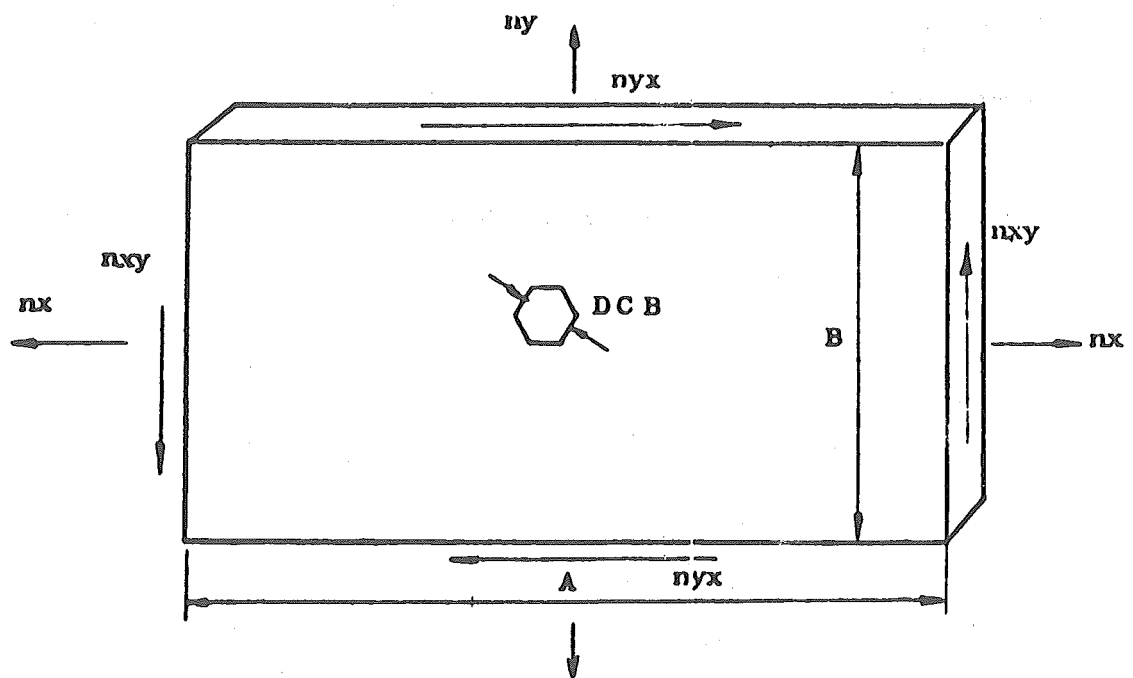
FAILURE MODES
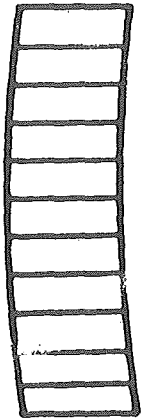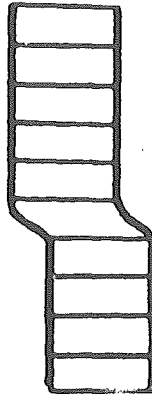
General buckling   Shear crimpling   Face dimpling
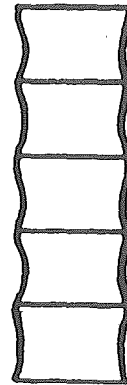
Face wrinkling

$$\frac{G}{A \cdot B} = \text{konst}$$

SIDE STEP PLUS

STEEPEST ASCENT

STEEPEST DESCENT

A startpunkt

SIDE STEP TEST

MULTICELL BOX-BEAM

SHEAR WEB

MAIN SPAR

POLYURETHAN CORE
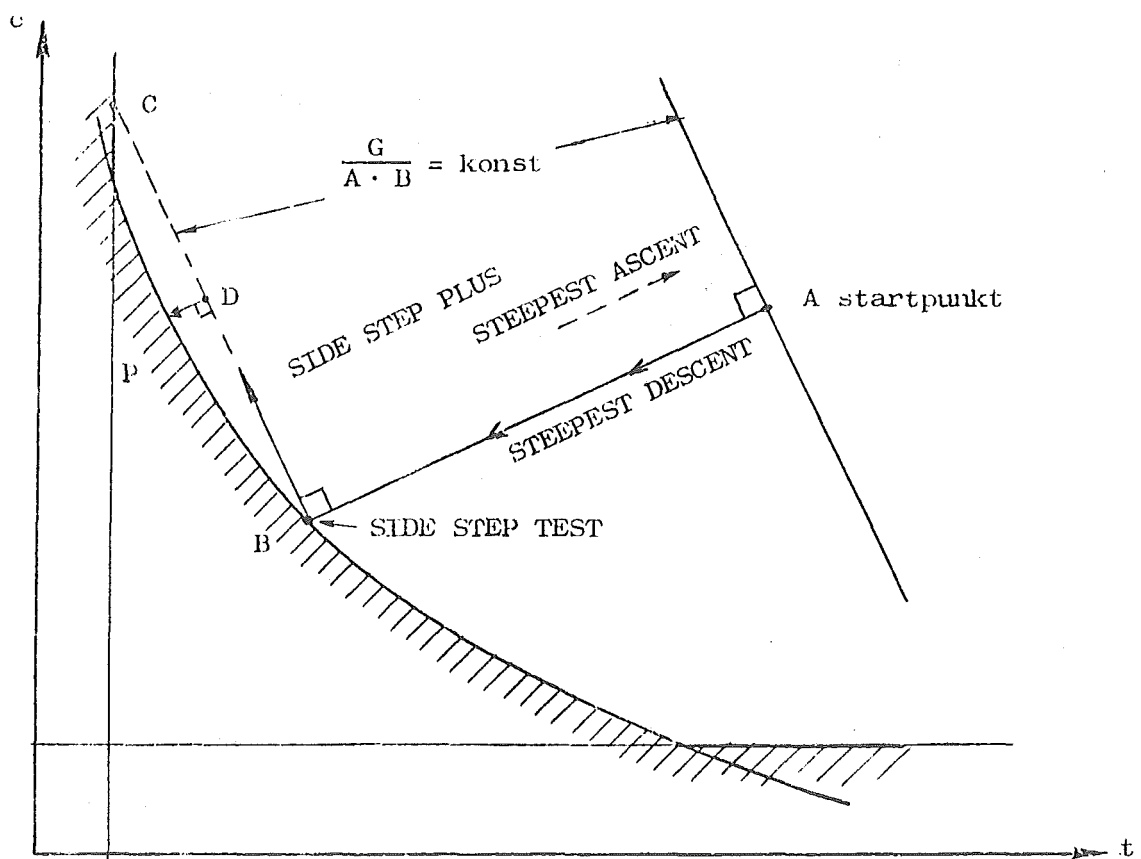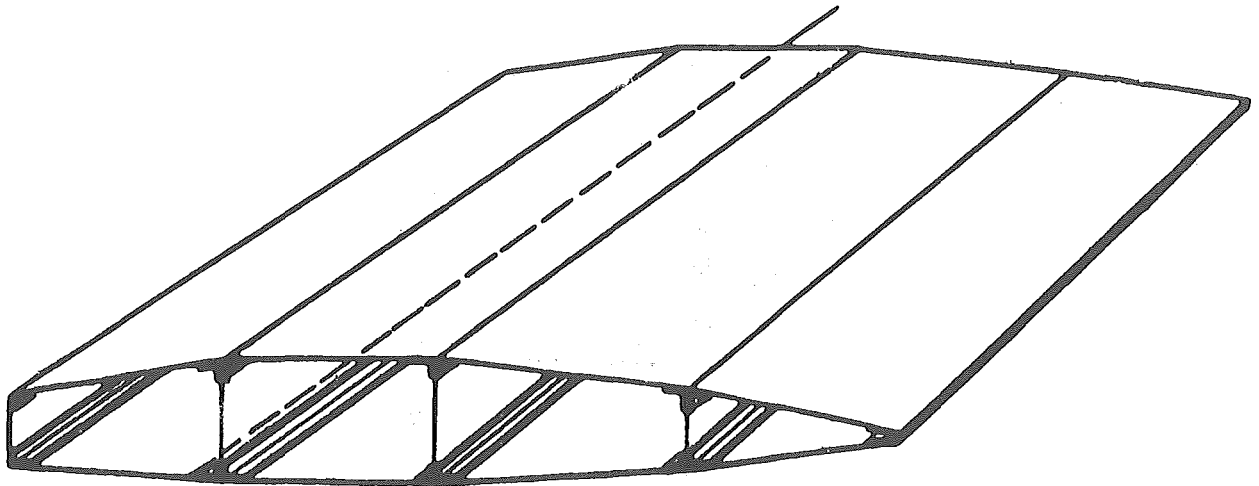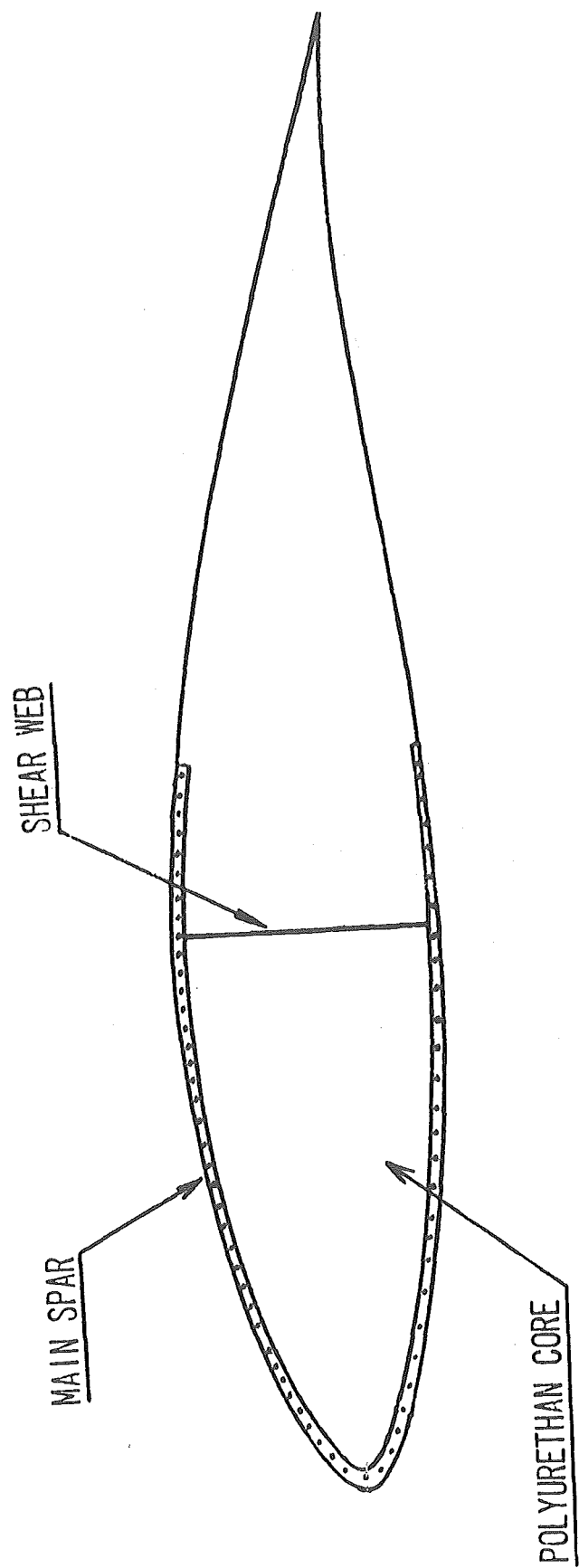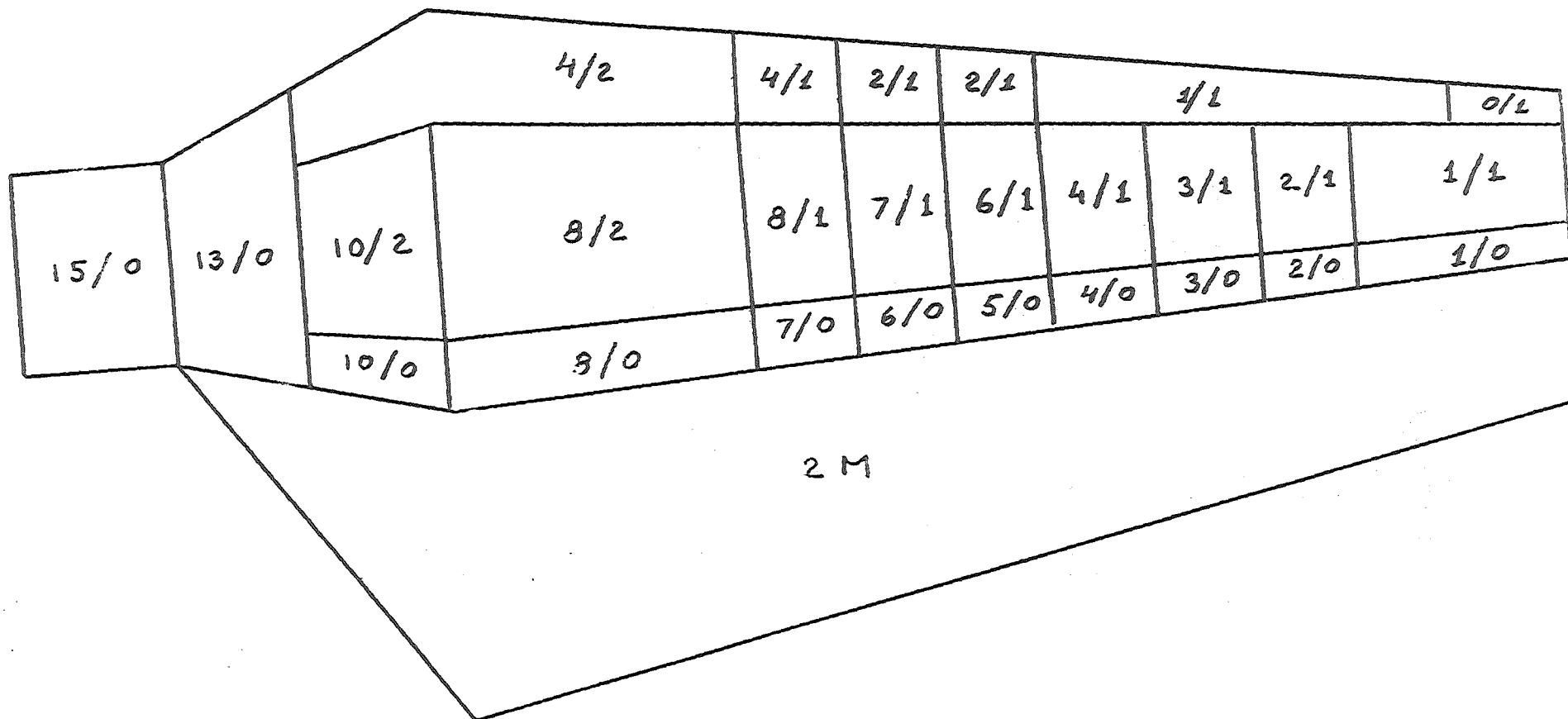
LAMINATE LAYUP

8/1 = 8 layers in 0°-direction

1 layer in ± 45°-direction

2M = 2 layers mat

```
┌─────────────────────────┐
│ DISTRIBUTION            │
│ OF LOADS               │
└─────────────────────────┘
             │
┌─────────────────────────┐
│ OPTIMIZE LAMINATE AND BOX │
│ AT SIX RADIAL STATIONS   │
└─────────────────────────┘
             │
┌─────────────────────────┐
│ CHECK SHEAR CENTER      │
└─────────────────────────┘
             │
┌─────────────────────────┐
│ CHECK MASS CENTER       │
└─────────────────────────┘
             │
      ⟨ SATISFIED ? ⟩
             │
┌─────────────────────────┐
│ GENERAL STATIC FEM ANALYSIS │
│ WITH BASIS              │
└─────────────────────────┘
             │
┌─────────────────────────┐
│ DYNAMIC ANALISIS        │
└─────────────────────────┘
```
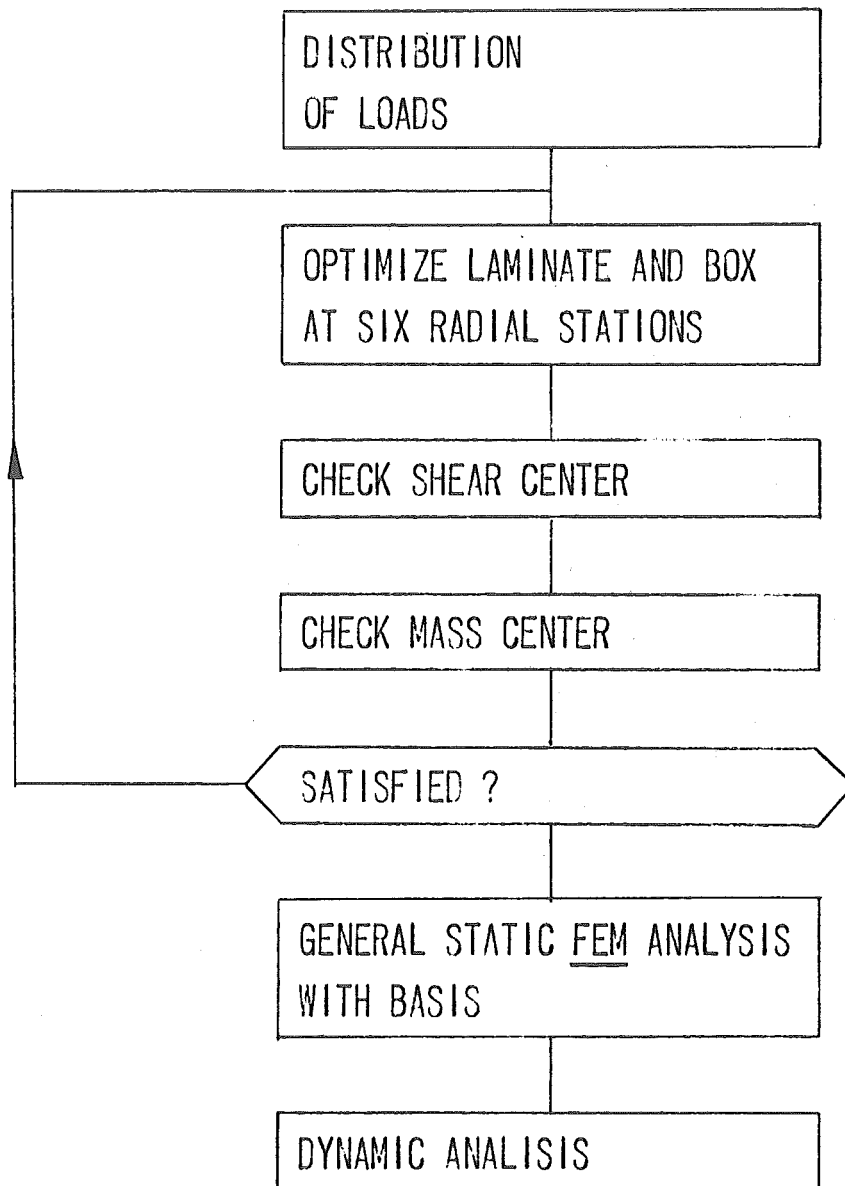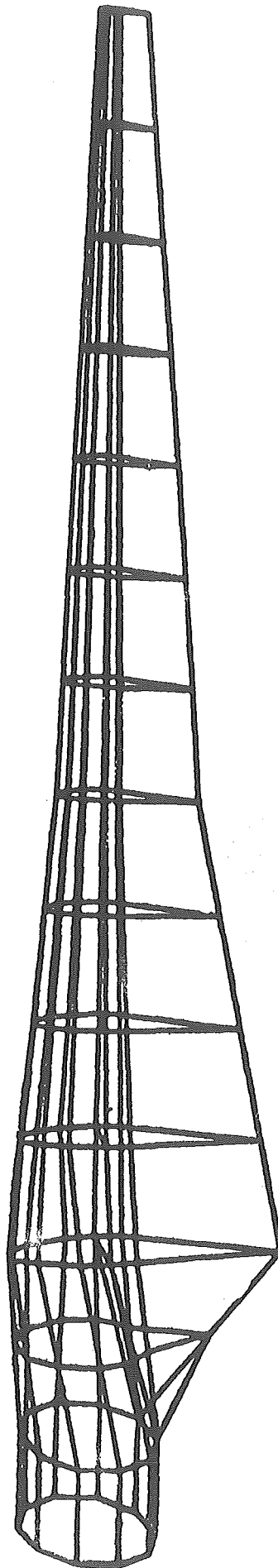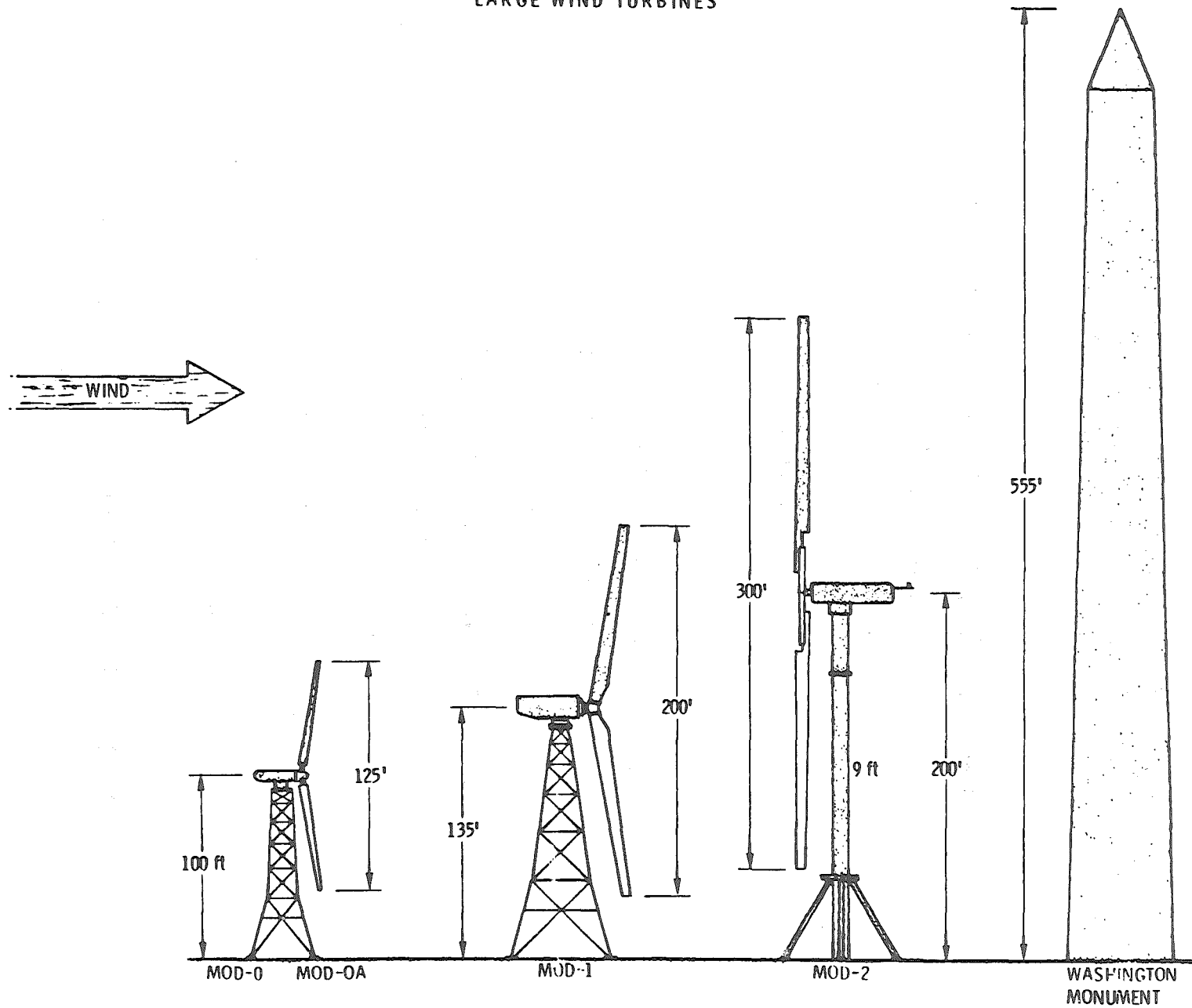
STRUCTURAL DYNAMICS ANALYSIS

OF

LARGE WIND TURBINES IN THE USA

DAVID A. SPERA

NATIONAL AERONAUTICS AND SPACE ADMINISTRATION

LEWIS RESEARCH CENTER

CLEVELAND, OHIO   44135

CONTENTS

PRESENTED AT THE IEA EXPERT MEETING, MUNICH, WEST GERMANY

OCTOBER 12, 1978

LARGE WIND TURBINES

WIND

555'

300'

200'

125'

135'

100 ft

9 ft

200'

MOD-0   MOD-OA

MOD-1

MOD-2

WASHINGTON
MONUMENT

WTG COMPUTER CODE DEVELOPMENT

1. WIND STATISTICS
   --HANDBOOK, UNIVERSITY OF TENN. (TULLAHOMA)
   --BATTELLE NORTHWEST LABS (RICHLAND)

2. STRUCTURAL DYNAMICS AND PERFORMANCE
   --LOCKHEED (CALAC, LOS ANGELES)
   --GE (VALLEY FORGE)
   --HAMILTON STANDARD (HARTFORD)
   --BOEING (BEC, SEATTLE)
   --PARAGON PACIFIC, INC (LOS ANGELES)
   --MECHANICS RESEARCH, INC (LOS ANGELES)
   --LERC (IN-HOUSE AND DATA VAN)
   --WEST HYBRID SIMULATOR (PPI)

3. POWER TRAIN AND CONTROL DYNAMICS
   --GE (VALLEY FORGE)
   --LERC
   --LOCKHEED

4. ELECTRICAL DISTRIBUTION SYSTEM DYNAMICS
   --GE (SCHNECTADY AND VALLEY FORGE)
   --POWER TECHNOLOGY, INC. (SCHNECTADY)

16

Table 1. - Computer codes presently used for aero-elastic analysis of dynamic
loads and deformations in horizontal axis wind turbines.

| Code	Type (domain)	Source for Information
MOSTAB-WT	Single blade; 1 DOF [a] (time)	Mr. Barry Holchin Mechanics Research Incorporated 9841 Airport Boulevard Los Angeles, CA 90045
MOSTAB-WTE	Same, plus empirical constants	Dr. David A. Spera NASA-Lewis 49-6 21000 Brookpark Road Cleveland, Ohio 44135
MOSTAB-HFW	Rotor; 4 DOF plus gimballing (time)	Mr. John A. Hoffman Paragon Pacific Incorporated 1601 E. El Segundo Boulevard El Segundo, CA 90245
REXOR-WT	System; multi-DOF (time)	Mr. Robert E. Donham Dept 75-21, Bldg. 360, Plant B-6 Lockheed-California Company Burbank, CA 91520
GETSS	System; multi-DOF (freq.)	Mr. Clyde Stahle General Electric Space Division Box 8661 Philadelphia, PA 19101
F-762	System; multi-DOF, (time)	Dr. Richard Bielawa United Technologies Research Center East Hartford, CT 06108
MOSTAS	System; multi-DOF, (time/freq.)	Mr. John A. Hoffman Paragon Pacific Incorporated 1601 E. El Segundo Boulevard El Segundo, CA 90245

[a] Degrees of freedom

MOD-O WTG REFERENCE DATA CASES

| CASE NO.	DATE	CONFIGURATION	WIND SPEED, MPH
I	18 DEC 75	DOWNWIND ROTOR STAIRS IN TOWER SINGLE YAW DRIVE	28
IV	11 SEP 76	DOWNWIND ROTOR NO STAIRS LOCKED YAW DRIVE	25
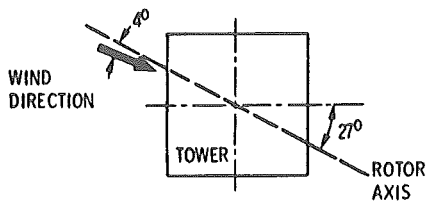
(a) DATA CASE I: TOWER WITH STAIRS, SINGLE YAW DRIVE, AND 28 mph WIND SPEED.
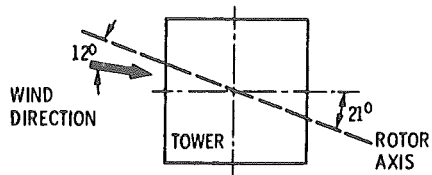
(b) DATA CASE IV: TOWER WITHOUT STAIRS, LOCKED YAW DRIVE, AND 25 mph WIND SPEED.

Figure 2. - Schematic plan views showing Mod-0 orientation during data cases I and IV (98 to 100 kW power, 40 rpm rotor speed).

$$\bar{M}_{y,b} = \frac{1}{2}(M_{y,max} + M_{y,min})$$

$$\delta M_{y,b} = \pm \frac{1}{2}(M_{y,max} - M_{y,min})$$
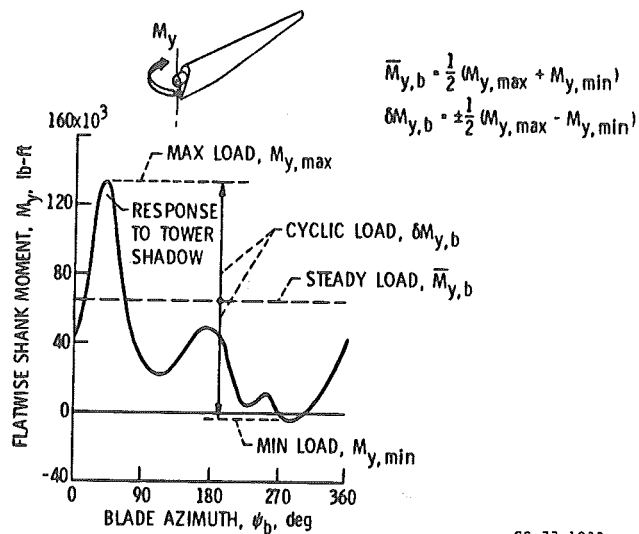
Figure 3. - Typical cycle of blade flatwise moment measured on the ERDA-NASA 100 kW Mod-0 wind turbine.
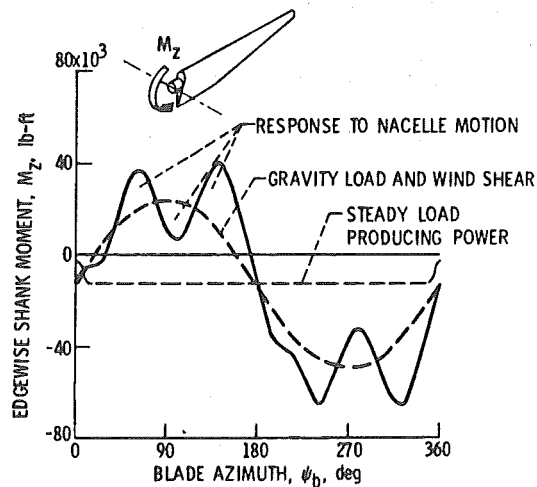
CS-77-1033

CS-77-1031

Figure 4. - Typical cycle of blade edgewise moment measured on the Mod-0 wind turbine.

(a) STATION 40 (5% SPAN), FLATWISE BENDING.

(b) STATION 40 (5% SPAN), EDGEWISE BENDING.

(c) STATION 370 (49% SPAN), FLATWISE BENDING.

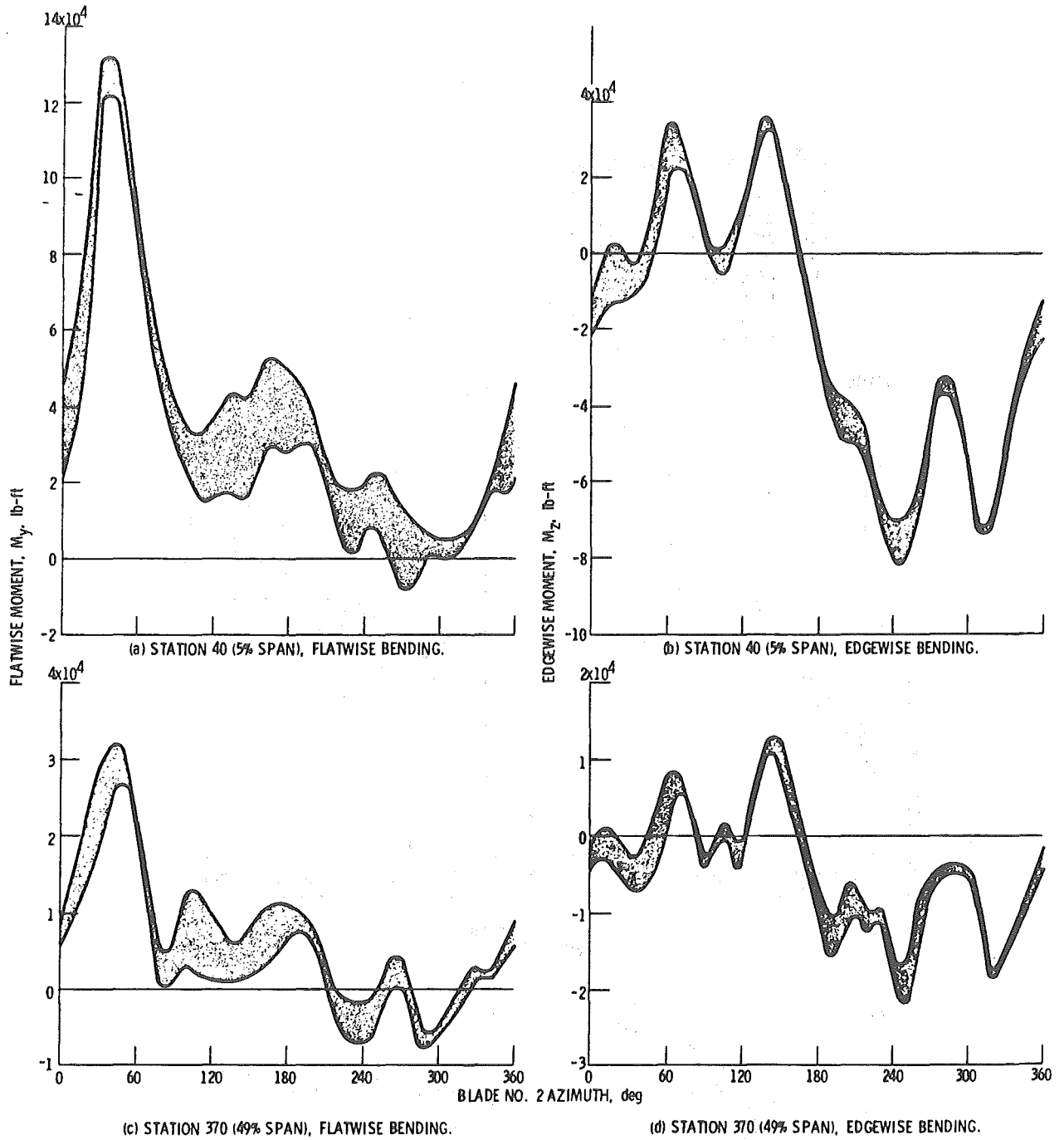(d) STATION 370 (49% SPAN), EDGEWISE BENDING.

Figure 5. - Time histories of Mod-0 data case 1 bending loads in blade no. 2 (envelopes of three consecutive revolutions).
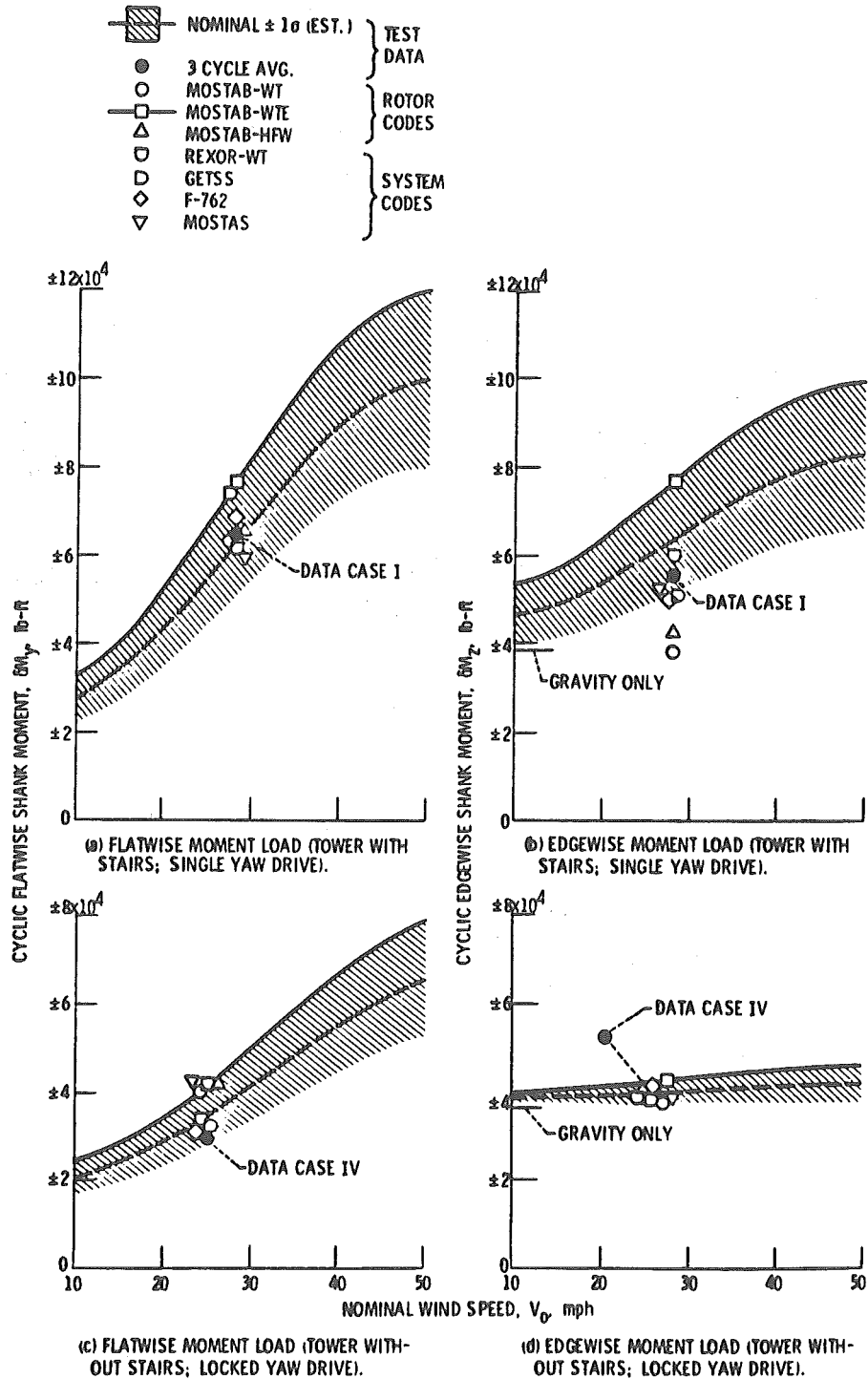
Figure 8. - Comparison of measured and calculated shank moment loads at various wind speeds (Station 40, 5% span).
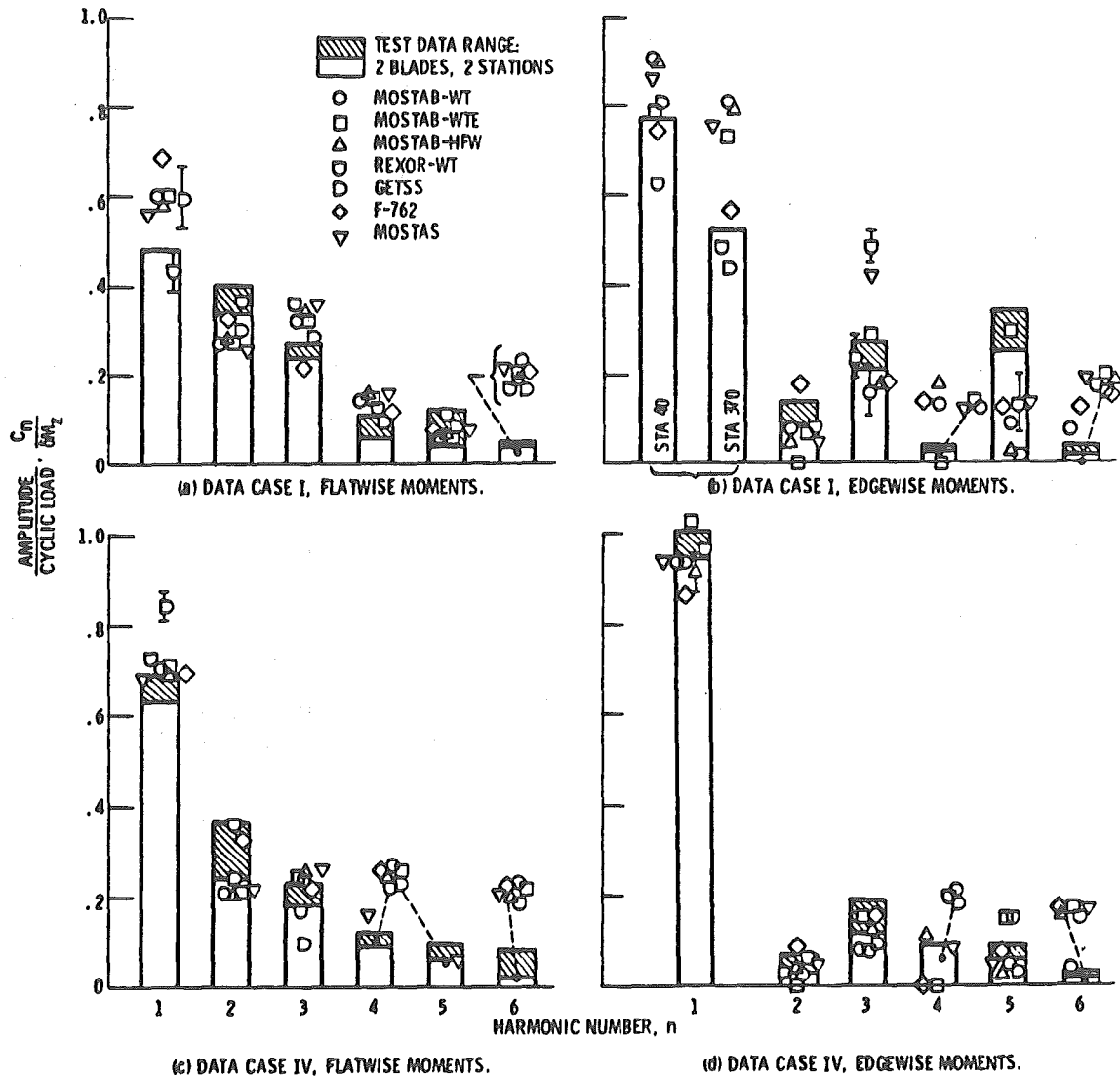
Figure 9. - Comparison of measured and calculated harmonic contents of moment load cycles. Each harmonic amplitude is normalized with respect to its total cyclic load (stations 40 and 370).

27

Table 11. - Summary of load ratios obtained using various computer codes and
Mod-O wind turbine test data.

Code Type and Name		Goal of Calc. Load	Blade Load Ratio [a]	
			Average	RMS Dev. [b]
Rotor Codes	MOSTAB-WTE	Nom. + 1σ	1.15	± 0.10
	MOSTAB-HFW	Nom.	1.00	± 0.20
	MOSTAB-WT	"	0.95	± 0.24
System Codes	F-762	"	0.99	± 0.14
	MOSTAS	"	0.98	± 0.12
	REXOR-WT	"	0.95	± 0.05
	GETSS	"	0.94	± 0.16

[a] Calculated-to-nominal measured; based on 16 ratios combining 2 data cases, 2 blade stations, flatwise and edgewise directions, and cyclic and peak bending moments.

[b] Root-mean-square deviation; includes approximately 11 of 16 ratios.
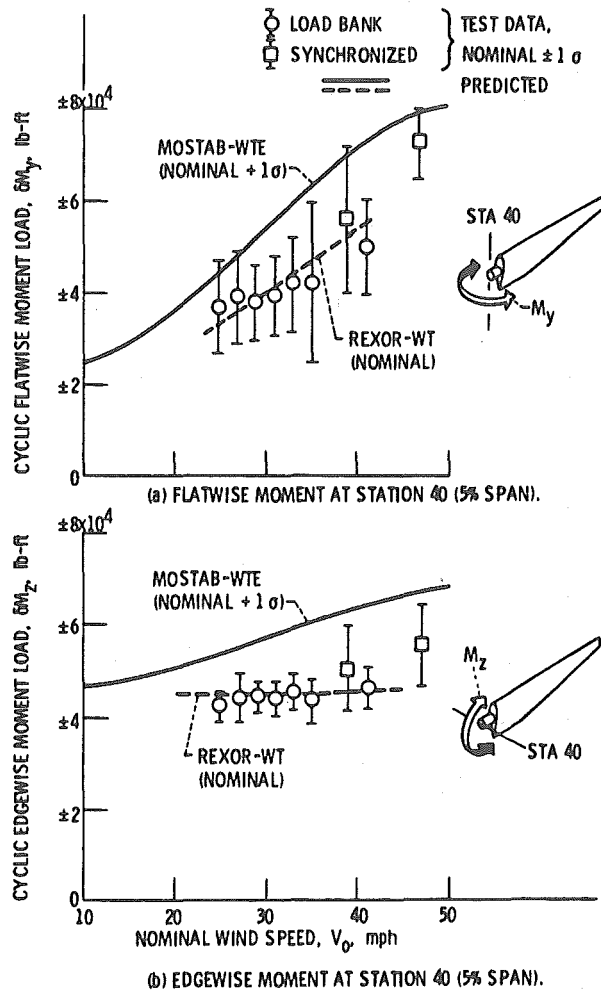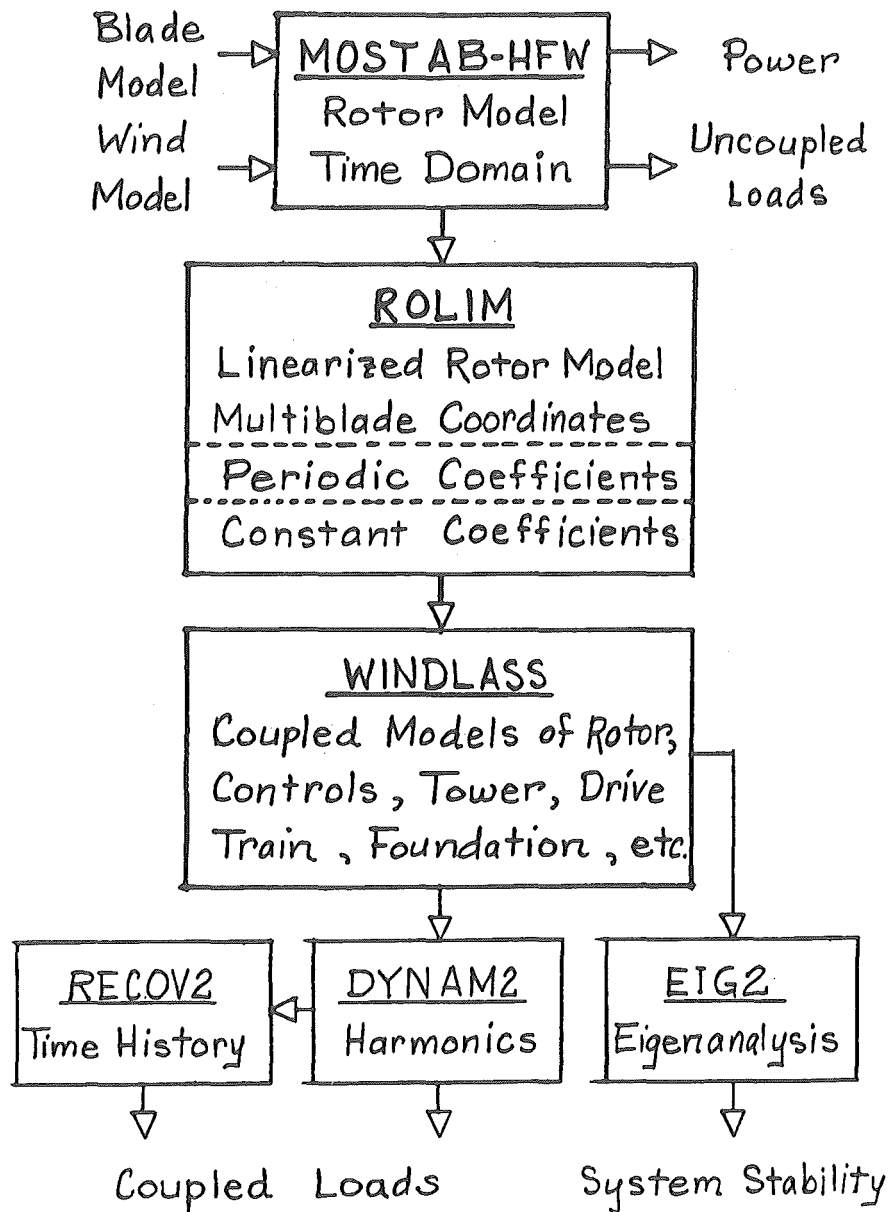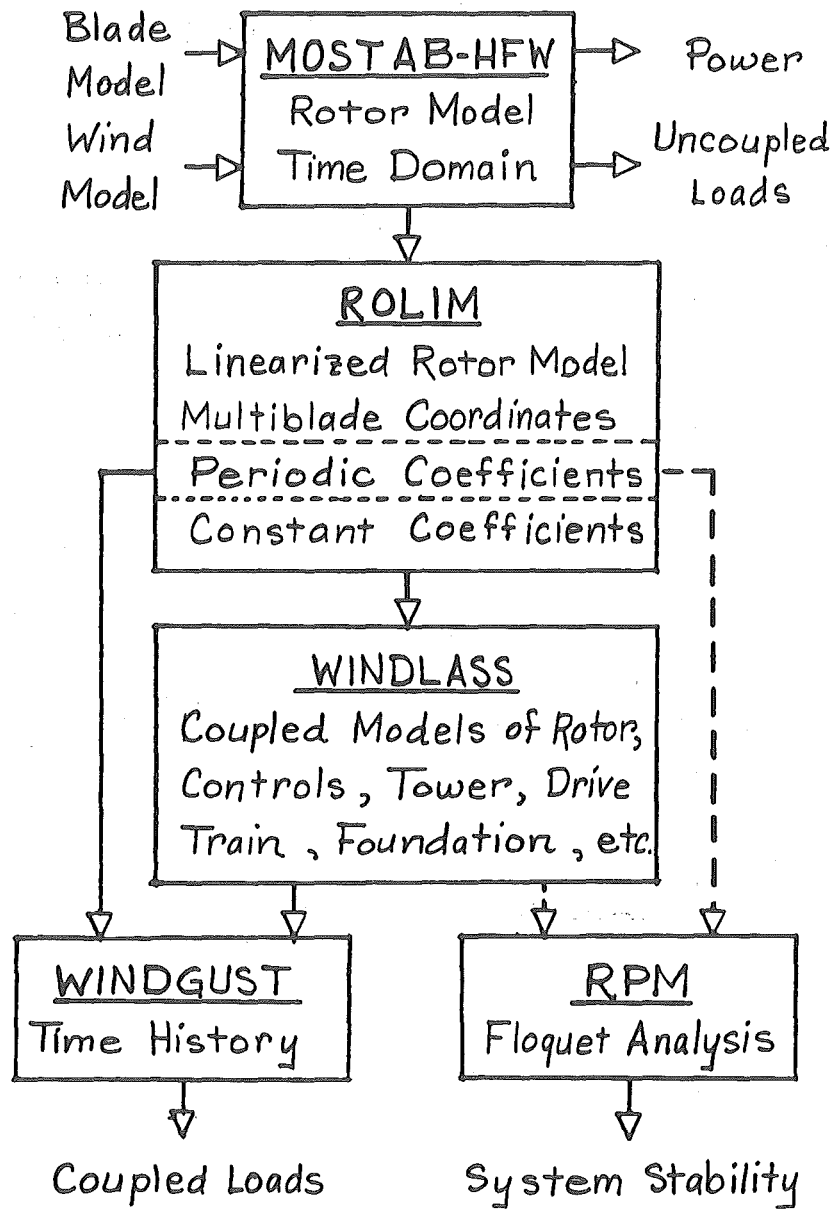
(a) FLATWISE MOMENT AT STATION 40 (5% SPAN).

(b) EDGEWISE MOMENT AT STATION 40 (5% SPAN).

Figure 10. - Comparison of measured and predicted cyclic blade loads for the Mod-0 wind turbine with dual yaw drive installed and stairs removed.

SCHEMATIC DIAGRAM OF MOSTAS-A

Blade Model → **MOSTAB-HFW** → Power
Rotor Model
Wind Model → Time Domain → Uncoupled Loads

ROLIM
Linearized Rotor Model
Multiblade Coordinates
Periodic Coefficients
Constant Coefficients

WINDLASS
Coupled Models of Rotor, Controls, Tower, Drive Train, Foundation, etc.

RECOV2
Time History

DYNAM2
Harmonics

EIG2
Eigenanalysis

Coupled Loads   System Stability

9-17-78
Das

SCHEMATIC DIAGRAM OF MOSTAS-B

Blade Model
Wind Model

MOSTAB-HFW
Rotor Model
Time Domain

Power

Uncoupled Loads

ROLIM
Linearized Rotor Model
Multiblade Coordinates
Periodic Coefficients
Constant Coefficients

WINDLASS
Coupled Models of Rotor,
Controls, Tower, Drive
Train, Foundation, etc.

WINDGUST
Time History

RPM
Floquet Analysis

Coupled Loads

System Stability

9-17-78
Das

MOD-O WTG
BLADE LOADS VS. YAW STIFFNESS
25 MPH WIND

Edgewise cyclic shank moment, δM_z, lb·ft

Single drive

Calculated (MOSTAS-B)

Dual drive

No drive

Braked

Measured: Mean ± 1σ

Percent of braked yaw stiffness
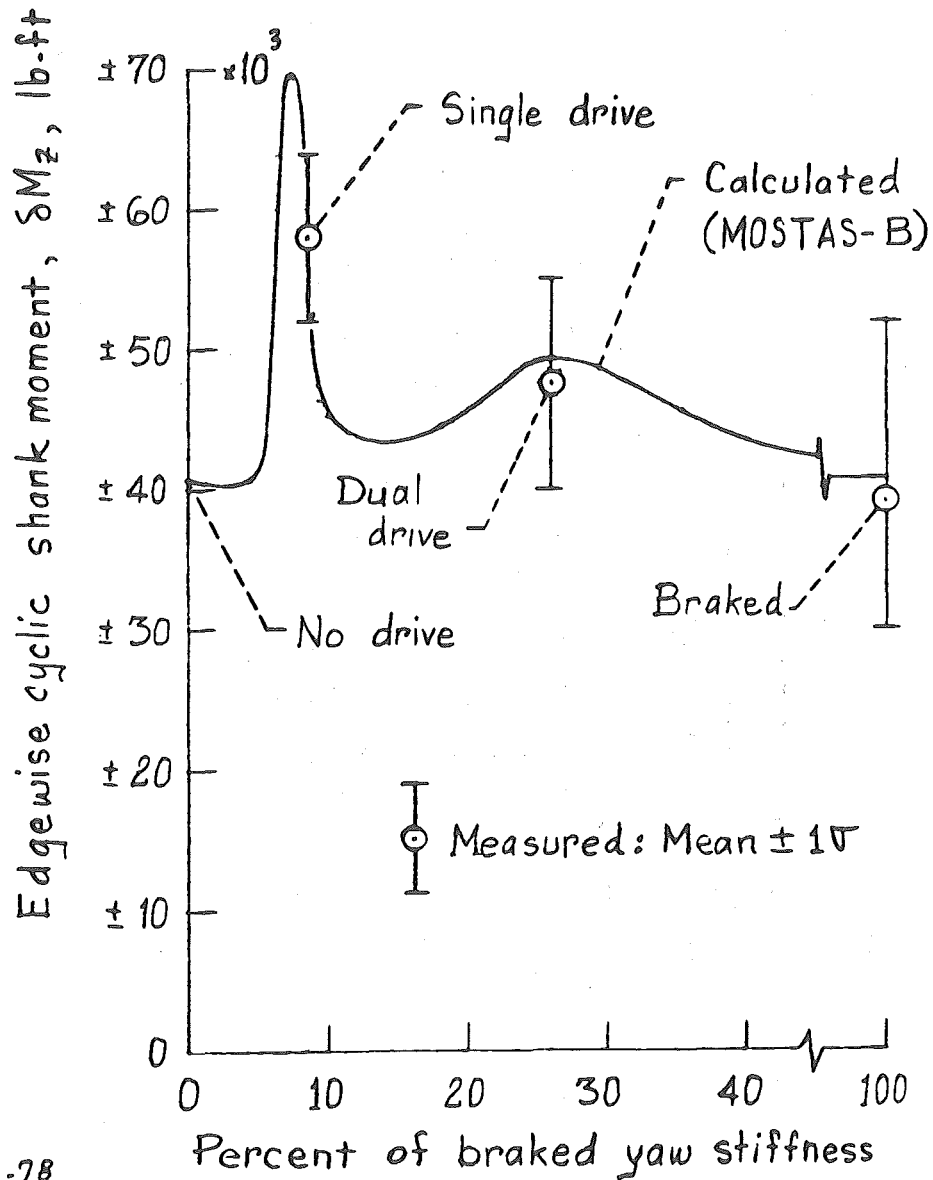
3-13-78
Das

CONCLUSIONS

- WTG LOAD PREDICTION CODES ARE IN AN ADVANCED STATE OF DEVELOPMENT.

- LOAD MARGIN MUST BE EXPLICITLY INTRODUCED INTO INPUT OR OUTPUT DATA; SYSTEM CODES TEND TO PREDICT NOMINAL LOADS.

- AVAILABLE SYSTEM CODES (MOSTAS, REXOR-WT, GETSS, AND F-762) ARE

        .....VALIDATED FOR "RIGID" WTG SYSTEMS
        .....PARTIALLY VALIDATED FOR "SEMI-RIGID" WTG SYSTEMS
        .....NOT YET VALIDATED FOR "FLEXIBLE" WTG SYSTEMS

- ROTOR-ONLY CODES ARE OFTEN SUFFICIENT FOR LOADS ANALYSIS OF RIGID AND SEMI-RIGID WTG SYSTEMS.
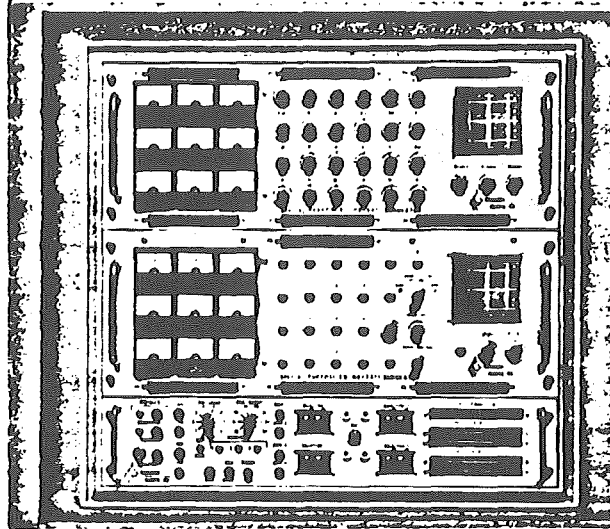
"WEST"

WIND ENERGY SYSTEM TIME DOMAIN SIMULATOR

- HARD-WIRED HYBRID COMPUTER

- COMPLETE HORIZONTAL AXIS WTG MODEL

- COUPLED DYNAMIC BEHAVIOR SIMULATION

- OPERATIONAL MODES

    "STAND ALONE"
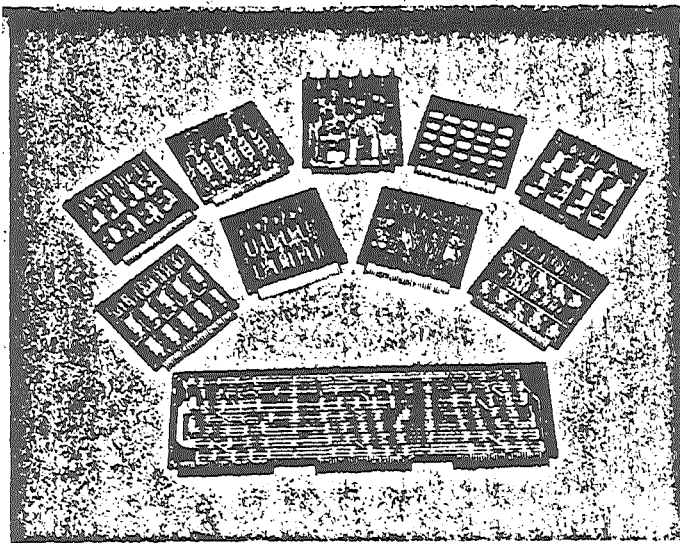
    INTEGRATED

PARAGON PACIFIC
INTRODUCES

THE

SPECIAL
PURPOSE
ROTORCRAFT
SIMULATOR

FEATURING
REAL TIME
### HYBRID COMPUTER SIMULATION OF
AEROELASTIC ROTOR SYSTEMS

PARAGON
PACIFIC INC.

1601 E. El Segundo Boulevard
El Segundo, California 90245

THE SPURS PRINTED CIRCUIT HARDWARE —
ARRANGED BY COMPONENTS, NOT FUNCTION.

THE "ROTOR" TRAY REMOVED FROM SPURS. THIS
TRAY CONTAINS ALL THE COMPONENTS (EXCEPT POWER)
REQUIRED TO FULLY SIMULATE AN AEROELASTIC
ROTOR SYSTEM IN REAL TIME.
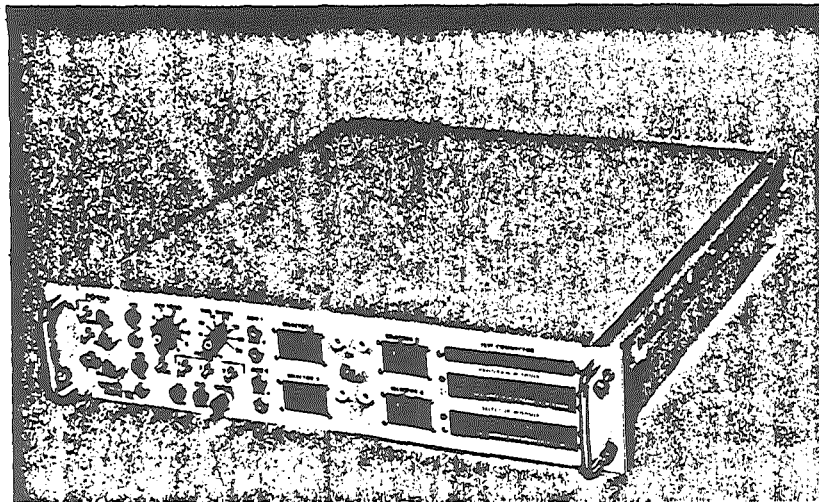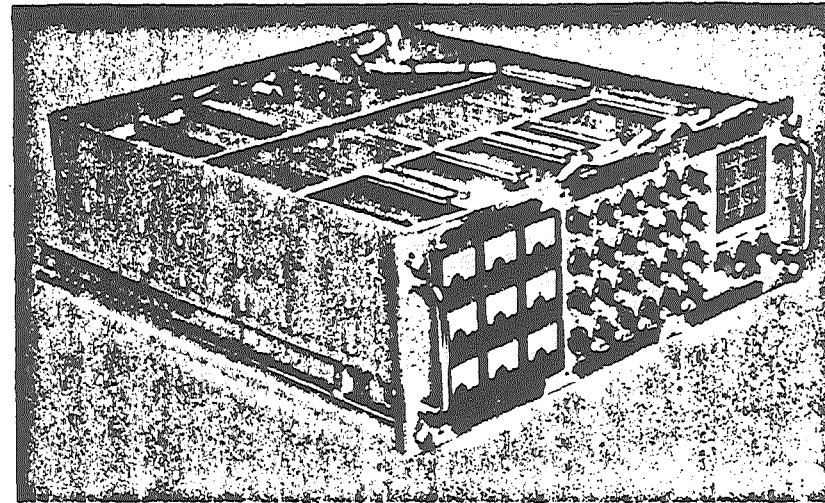
THE VERIFICATION AND CALIBRATION EQUIPMENT (VACE).
VACE PROVIDES THE SPURS USER WITH ALL THE TESTING
CIRCUITRY NEEDED TO MAINTAIN THE COMPUTER ON SITE.

PHOTOGRAPH OF A CRT DISPLAY GENERATED
BY SPURS. PICTURED IS THE DISTRIBUTED
ANGLE OF ATTACK ON THE BLADES OF A
2-BLADED ROTOR IN FORWARD FLIGHT. ZERO
AZIMUTH ANGLE IS AT THE BOTTOM OF THE
PAGE, WE ARE LOOKING DOWN FROM ABOVE
THE COUNTER-CLOCKWISE TURNING ROTOR.
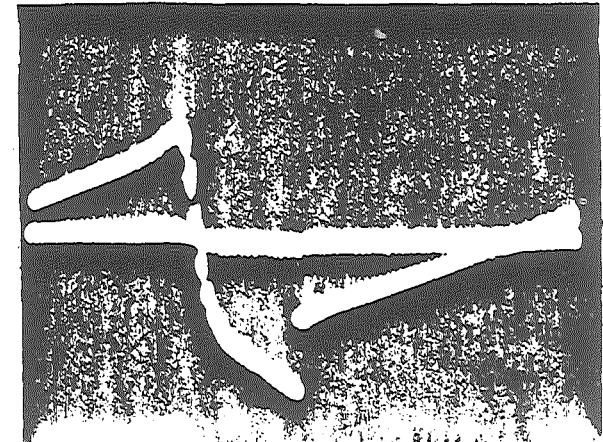
MATHEMATICAL MODELS IN "WEST" (TO INCLUDE)

- ROTOR BLADES -- COMPLETE AEROELASTIC MODEL

- FOUNDATION

- CONTROL ELEMENTS

- POWER TRAIN -- ADJUSTABLE INCLINATION ANGLE

- TOWER AND NACELLE BEDPLATE

- ELECTRICAL MACHINERY

- ELECTRICAL NETWORK

- YAWING MECHANISM

- ARTICULATED HUB

INPUTS TO "TEST"

SIGNALS (TO INCLUDE)

- BASIC INPUT DATA FROM NOSTAB-NFY

- WIND FUNCTIONS -- DETERMINISTIC AND STOCHASTIC

- ELECTRICAL LOAD DEMANDS AND TRANSIENTS

- COMPONENT MODELING PARAMETERS

- PRESCRIBED TRANSIENT INPUTS

- TRANSFER FUNCTION PARAMETERS

FORM

- POTENTIOMETERS FOR PROGRAMMABLE INPUTS
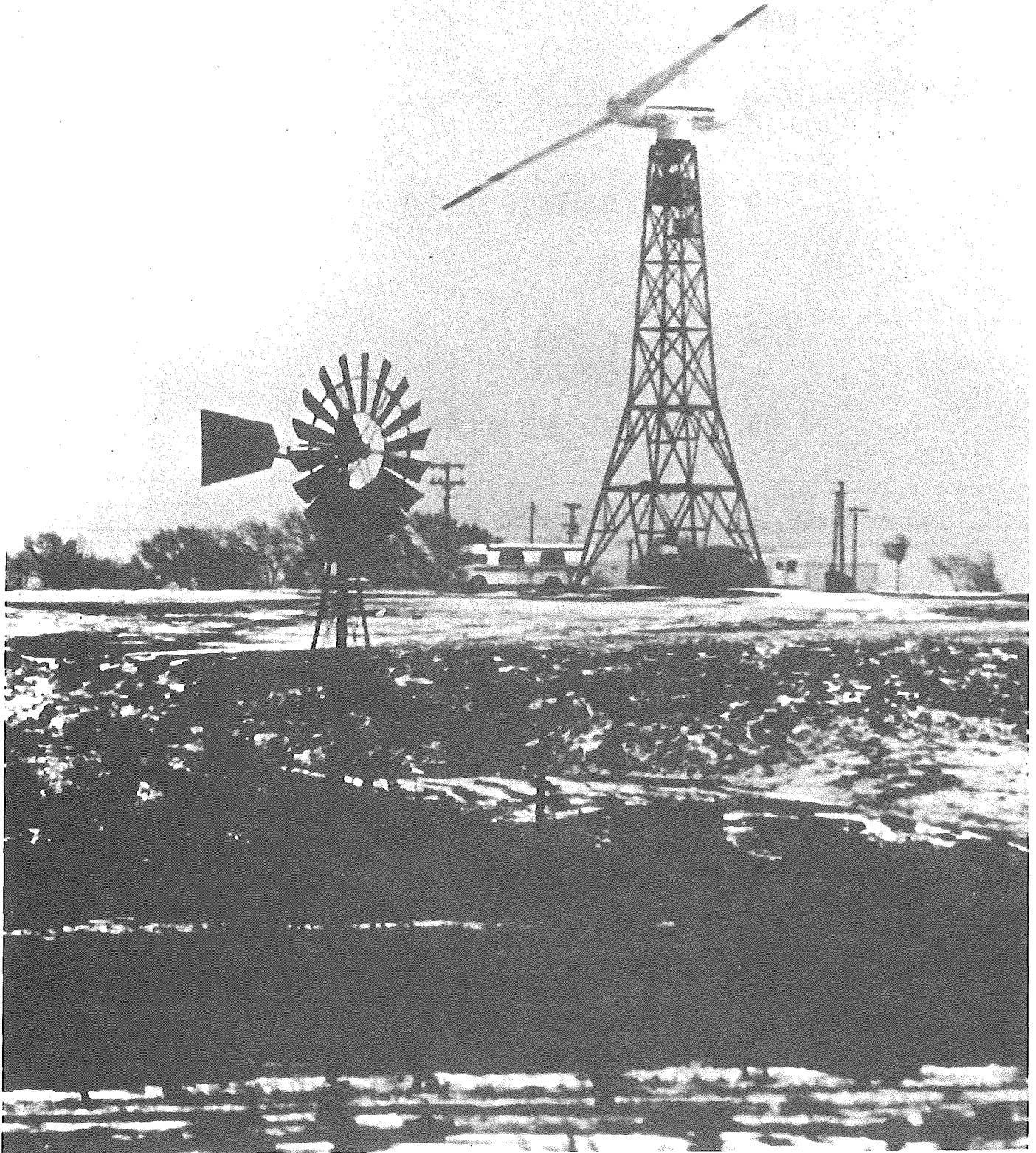
- TERMINALS FOR SIGNAL INPUTS

OUTPUTS OF "WEST"

FORM

- STRIPCHART

- CRT STROBOSCOPIC DISPLAY

SIGNALS (TO INCLUDE)

- BLADE LOADS AND MOTIONS

- POWER TRAIN LOADS AND MOTIONS

- TOWER/NACELLE LOADS AND MOTIONS

- ELECTRICAL MACHINERY PERFORMANCE

- CONTROL SYSTEM RESPONSES

- STATISTICAL RESULTS

DOE/NASA 200kW EXPERIMENTAL WIND TURBINE
Clayton, New Mexico

200 KILOWATT WIND TURBINE SPECIFICATIONS

Rotor

Number of blades. 2
Diameter, ft. 125
Speed, rpm 40
Direction of rotation . . . . . Counterclockwise (looking upwind)
Location relative to tower. . . . . Downwind
Type of hub . . . . Rigid
Method of power regulation. . . . . Variable Pitch
Cone angle, deg 7
Tilt angle, deg 0

Blade

Length, ft. 59.9
Material. . . . . Aluminum
Weight, lb/blade. 2300
Airfoil . . . . NACA 23000
Twist, deg. 26.5
Solidity, percent 3
Tip chord, ft 1.5
Root chord, ft. 4
Chord taper . . . . .Linear

Tower

Type. . . . . .Pipe truss
Height, ft. 93
Ground clearance, ft. 37
Hub height, ft. 100
Access. . . . . Hoist

Transmission

Type. . . . . Three-stage conventional
Ratio 45:1
Rating, hp. 460

Generator

Type. . . . . Synchronous ac
Rating, kVA 250
Power factor. 0.8
Voltage, V. . . . . 480 (three phase)
Speed, rpm. 1800
Frequency, Hz 60

Orientation drive

Type. . . . . Ring gear
Yaw rate, rpm 1/6
Yaw drive . . . . Electric motors

Control system

Supervisory . . . . .Microprocessor
Pitch actuator. . . . . Hydraulic

Performance

Rated power, kW 200
Wind speed at 30 ft, mph (at hub):
    Cut-in 6.9 (9.5)
    Rated 18.3 (22.4)
    Cut-out. 34.2 (40)
    Maximum design 125 (150)

Weight (klb)

Rotor (including blades). 12.2
Above tower 44.9
Tower 44.0
Total 88.9
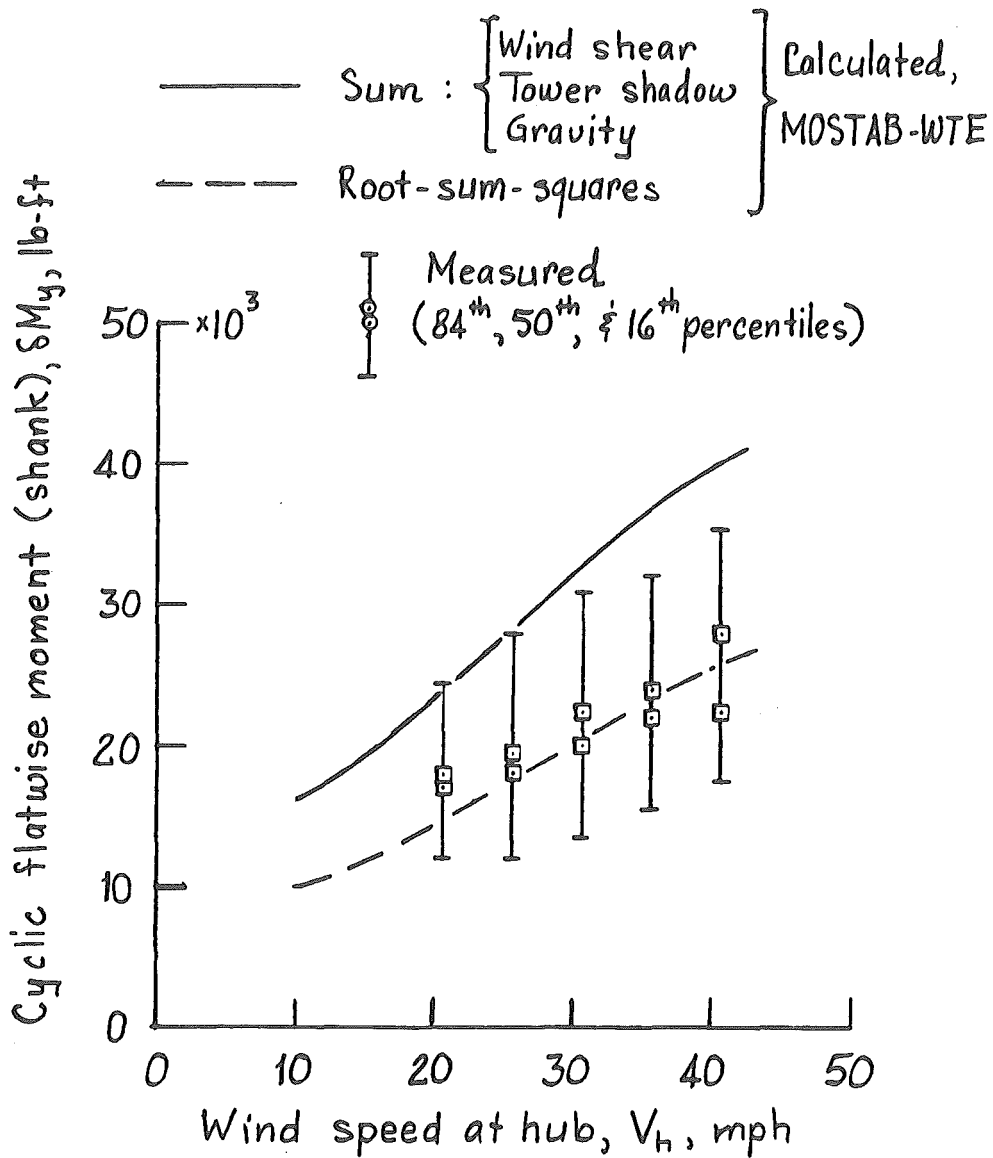
System life

All components, yr. 30

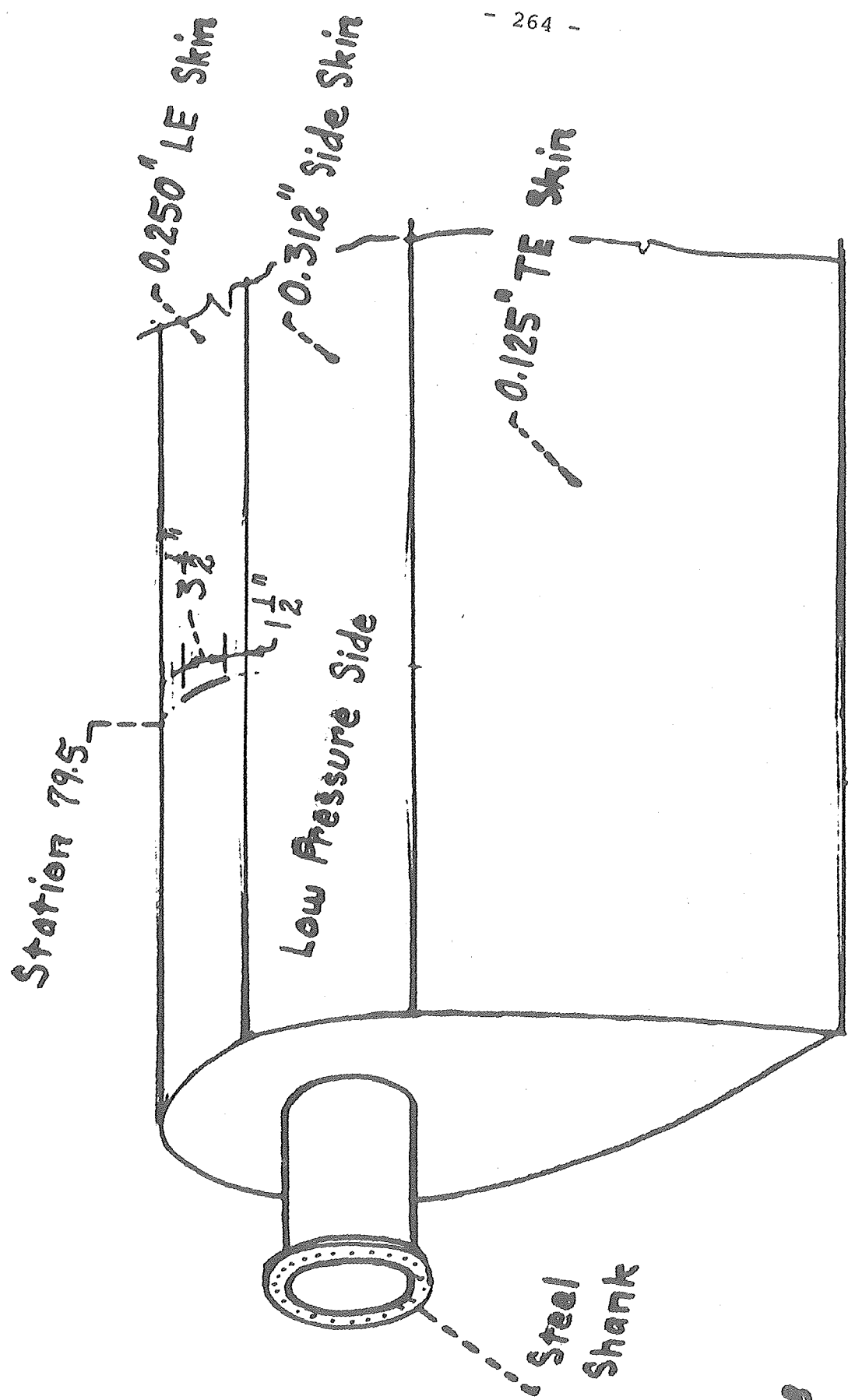# COMPARISON OF MOD-0 AND MOD-0A LOADS
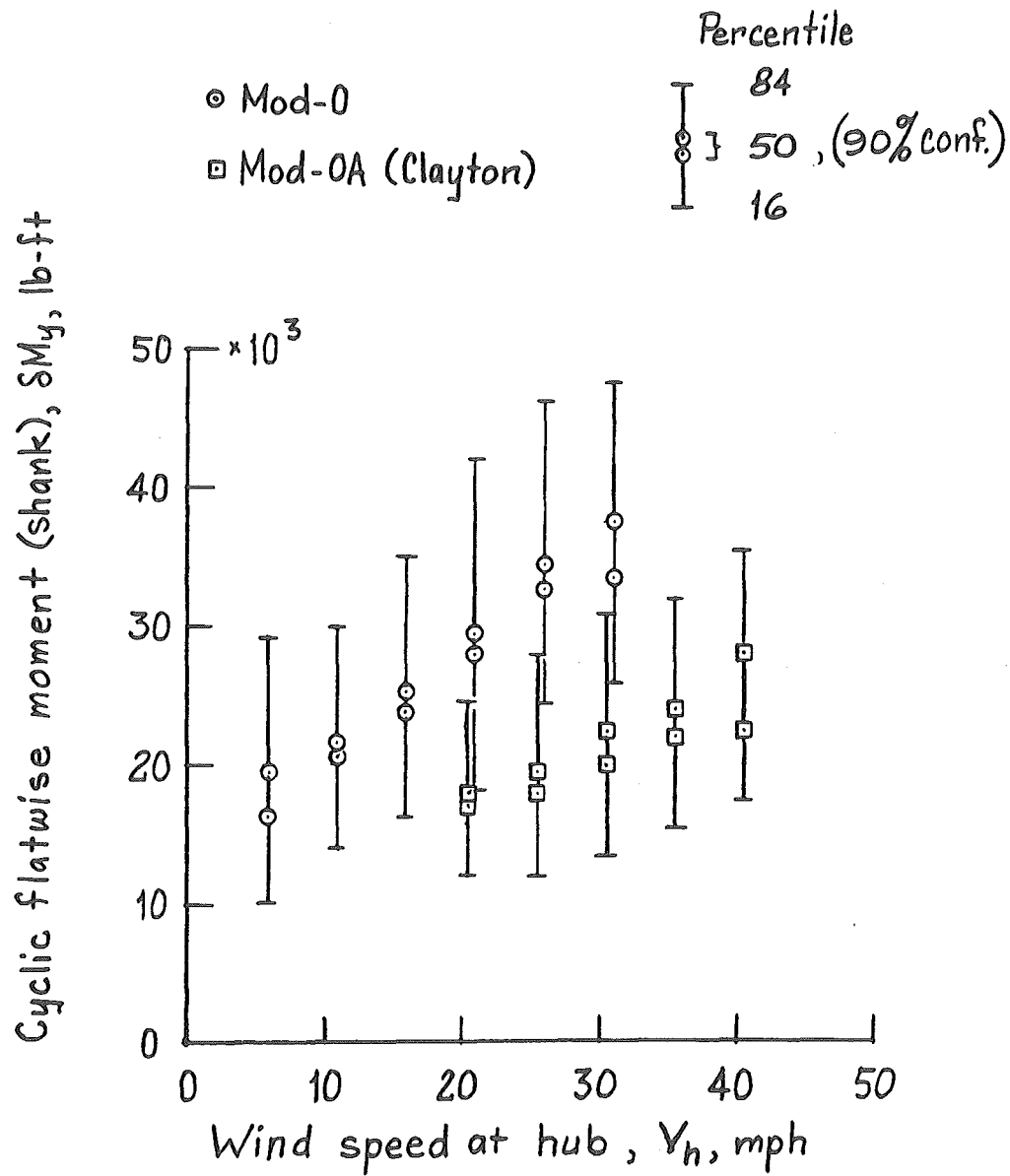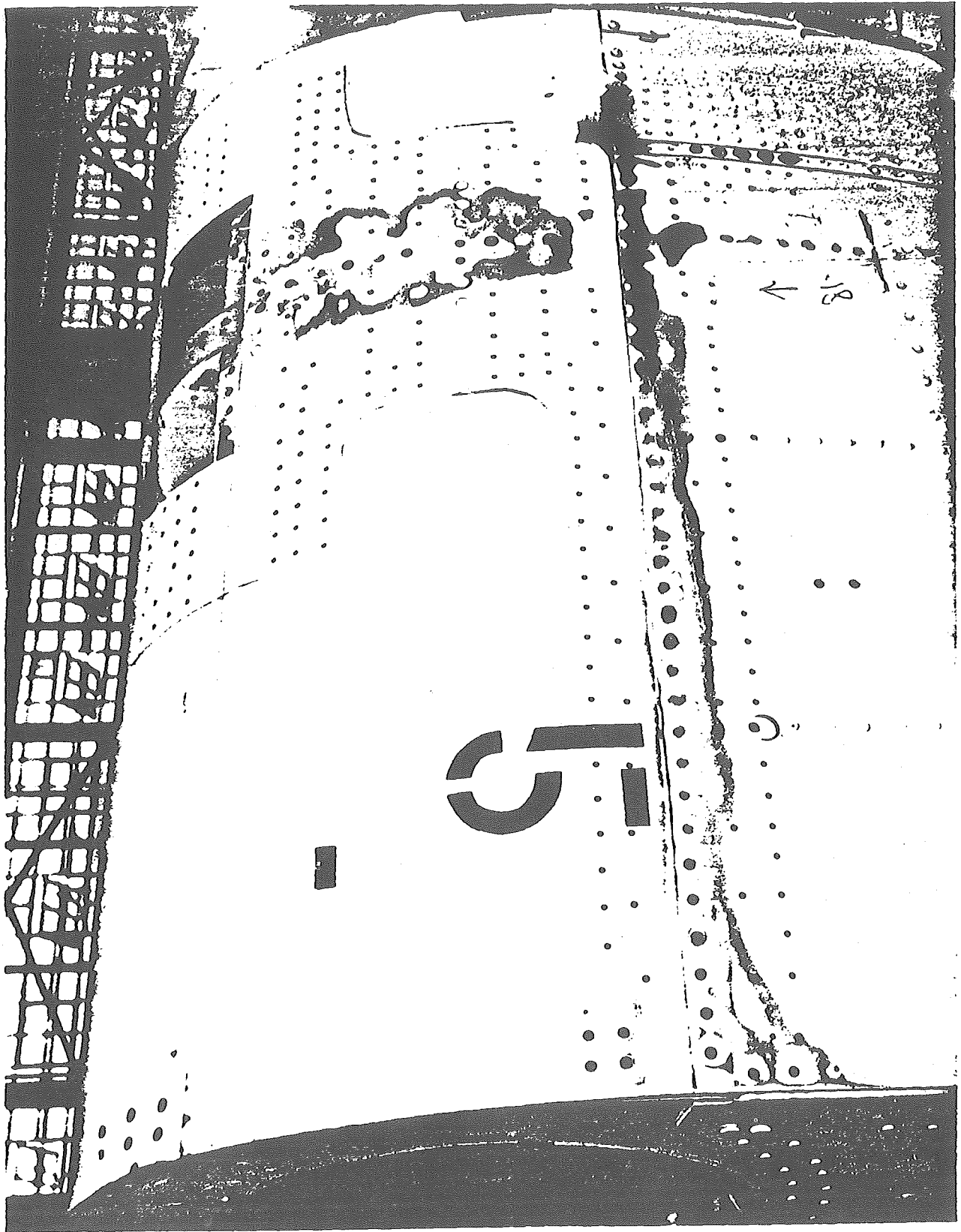

9-17-78
Das

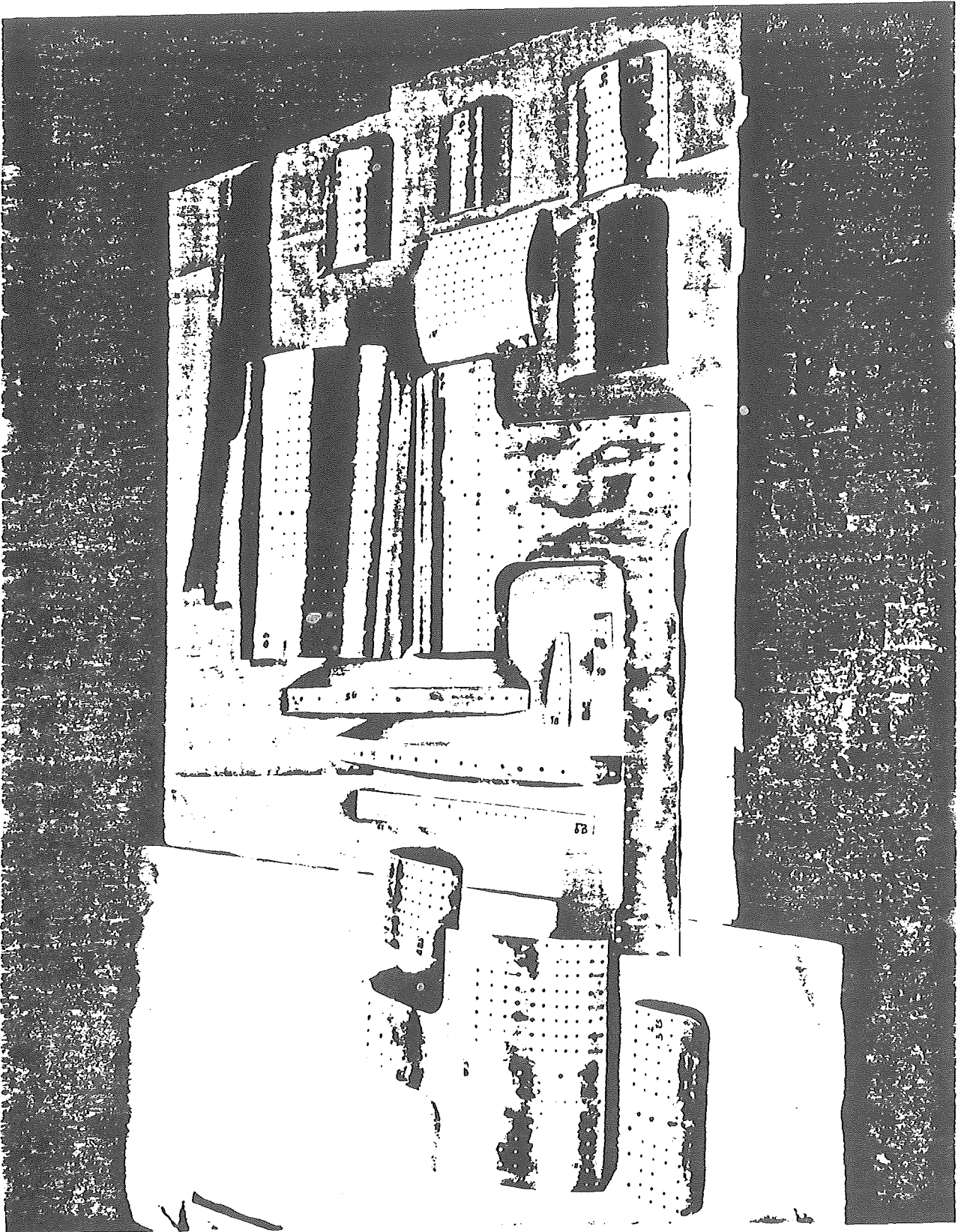# COMPARISON OF MEASURED AND CALCULATED MOD-OA BLADE LOADS

9-17-78
Das

LOCATION OF LEADING EDGE CRACK
BLADE No. 5

Station 79.5
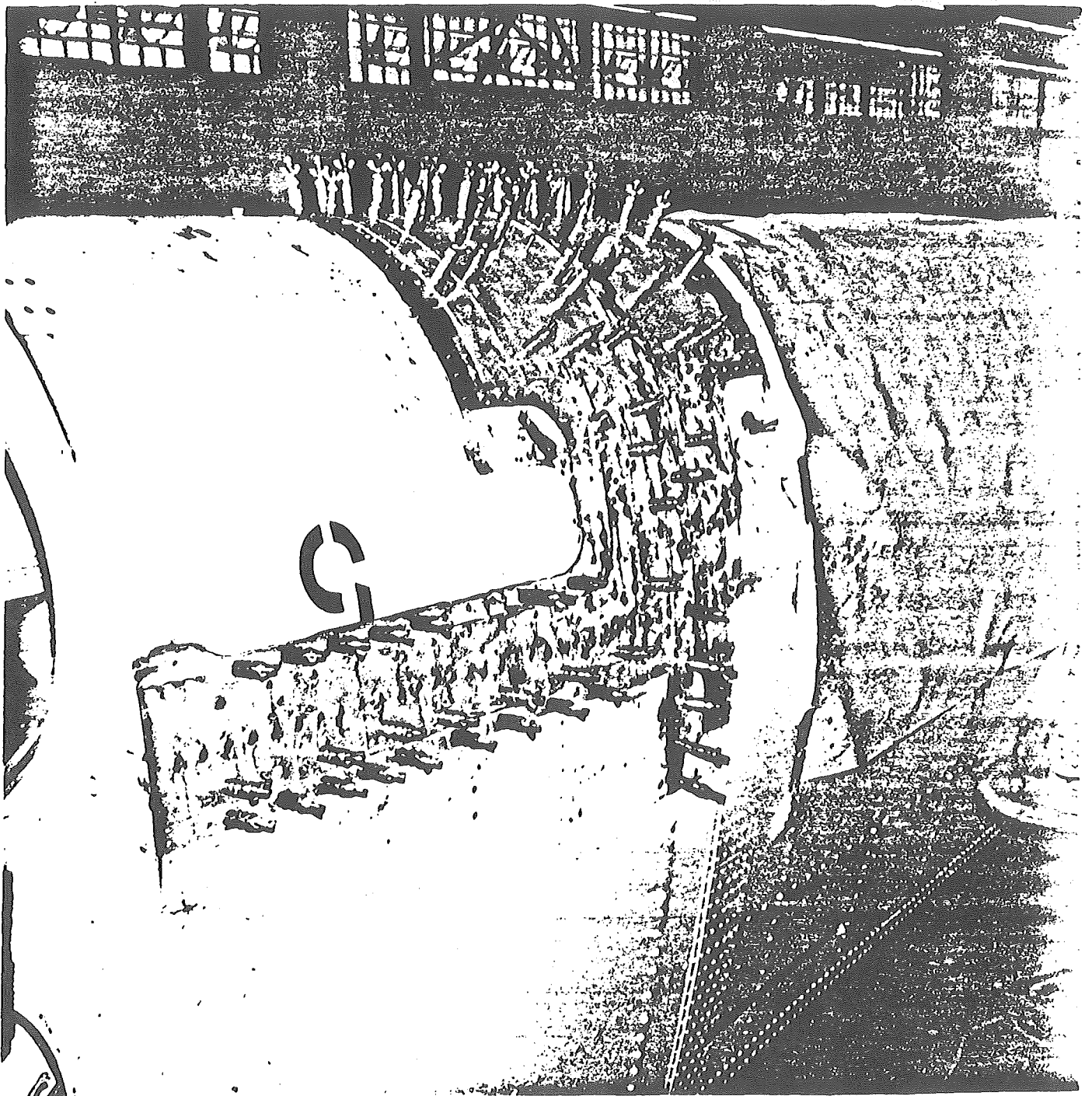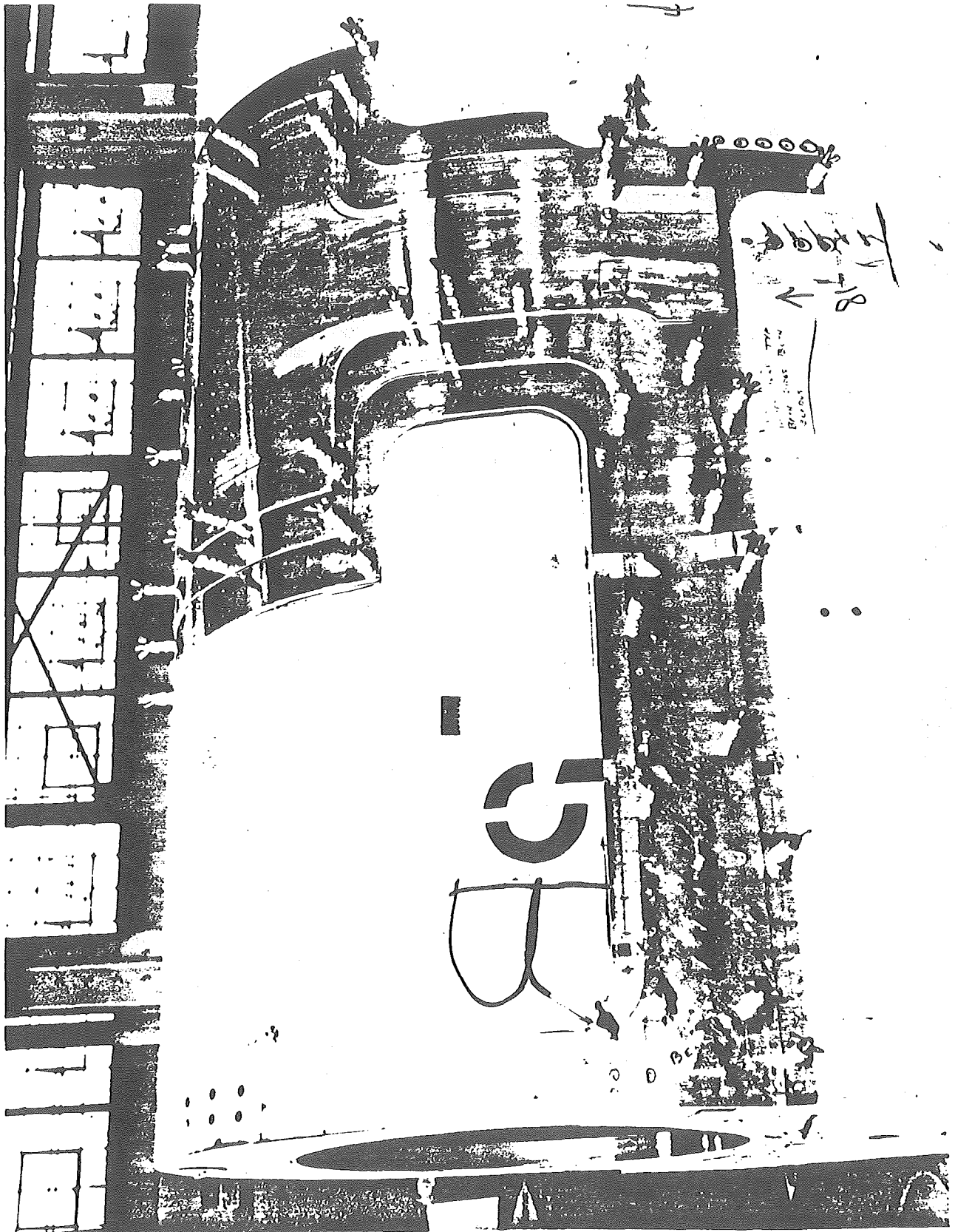
~0.250" LE Skin

~0.312" Side Skin

~0.125" TE Skin

Low Pressure Side

Steel Shank

~3¾"

~1½"

6-14-78
QS